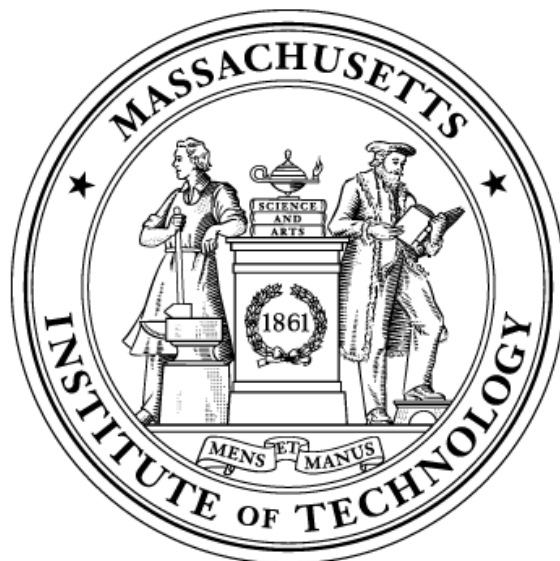# 8.13 Course Reader
(Dated: September 5, 2011)

This is the Course Reader for 8.13, MIT's advanced undergraduate experimental physics course. Each of the experiments, and the procedures for running them, are described in detail in this reader. Notes on laboratory safety, administrative guidelines and templates for written summaries, oral presentations and curve fitting are also detailed. This volume will be your constant companion in the laboratory. These materials are also available online at http://web.mit.edu/8.13.

Contents

Policies, Procedures and Safety Information

MIT Department of Physics
(Dated: September 5, 2011)

1. Overview of 8.13

The purposes of Junior Lab are to give you hands-on experience with some of the experimental bases of modern physics and, in the process, to deepen your understanding of the relations between experiment and theory, mainly in atomic and nuclear physics. You will do experiments on phenomena whose discoveries led to major advances in physics. The data you obtain will have inevitable systematic and random errors that obscure the relations between the macroscopic observables of our sensory experience and the physical laws that govern the submicroscopic world of atoms and nuclei. You will be challenged to learn how each of the experimental setups works, to master its manipulation so that you obtain the best possible data, and then to interpret the data in light of theory with a quantitative assessment of the errors. We believe you will find satisfaction in observing, measuring and understanding phenomena many of which would have won you the Nobel Prize if you had discovered them.

1.1. Section Organization

The Registrar has preassigned you to one of the sections listed in Table I, with further adjustments reflected on the 8.13 Stellar web page. If you cannot come to the assigned time, please email spatrick@mit.edu ahead of time to see if the section of your choice can be accommodated. Attempts are made to keep each section's enrollment less than or equal to 16 students, with 18 being a logistical maximum. If the course enrollment is especially large, you may not be able to have the section of your choice.

It is essential that you show up to the first session of at least one Junior Lab section in order to receive credit for mandatory radiation protection training.

Each section is run independently by one faculty member with the assistance of a graduate teaching assistant. The lab is also open on Fridays from 10AM to 4PM for additional lab time outside of your regularly scheduled section. Friday time reservations (3-hour block maximum, please) can be made through the Junior Lab online reservation tool.

You are expected to work in pairs, sharing as evenly as possible in the measurements, the analysis, and the interpretation of the data. The best choice for a lab partner may be someone who lives nearby and has a schedule that matches yours so you can get together outside of class to analyze and interpret your results. Most students find that they require the full 18 hours per week credited to

TABLE I: Junior Lab Section Instructors — Fall 2011

Section	Instructor
Monday-Wednesday 9-12am	Professor David Litster
Monday-Wednesday 2-5pm	Professor Gunther Roland
Tuesday-Thursday 9-12am	Professor June Matthews
Tuesday-Thursday 2-5pm	Professor Nergis Mavalvala

Junior Lab to do the work of the course.

1.2. Schedule Summary

The first few class sessions will familiarize you with the lab, giving everyone a common foundation in experimental techniques and data analysis. The first two sessions are dedicated to important organizational and administrative issues, plus important safety information and an introduction to the basics of statistics and data analysis. Next, one 3-hour session is scheduled for each of three short introductory experiments: 'Poisson Statistics', 'Transmission of Electromagnetic Pulses', and 'The Photoelectric Effect'. The preparatory questions and one written summary resulting from these preliminary experiments will be graded (to let you know how you're doing) but not recorded, so your final grade will be unaffected. Following this introductory period, students will plan and execute four longer experiments. The first will be executed in 5 sessions, while the last three will be done in 4 sessions each. The term culminates in a week-long series of public oral presentations given by students to peers, friends and faculty in an American Physical Society conference type event.

Throughout the term you will be required to keep a detailed laboratory notebook, which is provided to you by Junior Lab. This will be collected and graded 3 times during the semester: once after the introductory experiments (this grade is not recorded), once around midterm, and once at the end of the semester.

1.3. Attendance Requirements

You are required to attend your assigned lab session for the full three hour period. Any exception must be approved by the section teaching staff. The laboratories will be open every class day from 9AM–5PM and Friday from 10AM–4PM (except Institute holidays) with staff help available to discuss physics and maintain equipment. At

all other times the laboratories must be kept locked for security and safety. Junior Lab students may occasionally be permitted access to the lab outside of the normal hours, but only after consulting with their TA or faculty member. It is each student's responsibility to maintain security by making sure the doors are kept locked at all times outside of the regularly scheduled sessions. One should never work alone in a laboratory, especially if high voltages are involved. A partner or instructor must be in reach.

2. Ethics in Science and Education

When you read the report of a physics experiment in a reputable journal you can generally assume it represents an honest effort by the authors to describe exactly what they observed. You may doubt the interpretation or the theory they create to explain the results but at least you trust that if you repeat the manipulations as described, you will get essentially the same experimental results.

Nature is the ultimate enforcer of truth in science. If subsequent work proves a published measurement is wrong by substantially more than the estimated error limits, credibility is questioned. If fraud is involved, a career may be ruined. Thus most professional scientists are very careful about the records they maintain (see the Junior Lab notebook requirements in the next section of the reader) and the results they publish.

Junior Lab is designed to provide pre-professional training in the art and science of experimental physics. What you record in your lab book and report in your written and oral presentations must be exactly what you have observed *including date, time and name of experimenter.*

Sometimes you will get things wrong because of an error in manipulation, equipment malfunction, misunderstanding, or a miscalculation. Simply cross out errors using a diagonal line in your notebook and start again. The instructor's job is to help you figure out what went wrong so you can do better next time. If circumstances in an experiment are such that you cannot get your own data (e.g. broken equipment, bad weather), you may request your instructor's permission to use someone else's data, provided you acknowledge it.

Fabrication or falsification of data, using the results of another person's work without acknowledgement, and copying from "the files" are intellectual crimes as serious as plagiarism, and possible causes for dismissal from the Institute. This includes using someone else's data without your instructor's explicit permission.

The precaution regarding the acknowledgement of other people's data also applies to acknowledging other people's rhetoric. The appropriate way to incorporate an idea which you have learned from a textbook or other reference is to study the point until you understand it and then put the text aside and state the idea in your own words.

One often sees in a scientific journal, phrases such as "Following Albert Einstein ...". This means that the author is following the ideas or logic of Einstein not his exact words. If you quote material, it is not sufficient just to include it in the list of references at the end of your paper. You should use the following formatting:

> The quote should be indented on both sides or enclosed in quotes, and attribution must be given immediately in the form of a reference note.[1]

Importing text from a published work, from other student papers, or from the lab guide without proper attribution is a serious breach of ethics and will be dealt with by the Committee on Discipline.

Most Junior Lab experiments are concerned with data comparison measurements of well known fundamental constants such as $\hbar$, e, k_B, e/m, and c, or significant physical quantities such as the mean life of the muon or the cross section of an electron for scattering a photon. The purpose of these experiments is to give you hands-on experience with atomic and nuclear phenomena, a sense of the reality of the concepts and theories you have studied in books and courses, and the beginning of professional skill in obtaining and recognizing reliable data and extracting meaningful results from them.

There is nothing wrong with "peeking" in the CRC Handbook or any of the many relevant texts to see what your experiment should have yielded. In fact, in your conclusions, you should compare your values with the established ones — as you would in any of your later scientific publications. One way to get maximum benefit from your Junior Lab experience is to play it as a game in which you squeeze the most accurate measurement you can get out of the available equipment and the practical limits of analysis, make a rigorous estimate of the error, and then compare the results with the established value. If the established value is outside your error range, try to find out what went wrong, fix it, and try again. If the established value is in your error range, don't rest easy, but do whatever may be necessary to prove it isn't an accident. Repetition is the essential key to attaining confidence and meaningful errors for a result, whether of a single measurement or an entire experiment! But whatever the outcome of an experiment is, you must tell exactly what you observed or measured when you present your oral or written report, regardless of how "bad" the results may appear to be.

---

[1] A. Einstein: Personal communication. Footnotes may be placed either at the bottom of the page where referenced or at the end among the bibliography.

3. Required Texts

- Experimental Lab Guides, available for download from the Junior Lab web site.

- Data Reduction and Error Analysis for the Physical Sciences, 3rd Edition, by P.R. Bevington and D.K. Robinson (McGraw-Hill: 2003)

The Bevington and Robinson text contains a comprehensive treatment on error analysis and will be useful throughout your career.

3.1. Other Useful Texts

There are several other recommended textbooks on reserve in the Junior Lab Library.

- Experiments in Modern Physics by Adrian Melissinos (Academic Press: 1966 1st Edition & 2003 2nd Edition). Please consult these before and during your investigations. This text is only "Recommended" because the Junior Lab staff feel it is too expensive to "Require". *Material which is essential to the understanding of an experiment, and that can be found in the Melissinos text, is generally omitted from the Lab Guides.* Note that the Physics Reading Room has both editions which offer different material, you should consult them both!

- The Art of Experimental Physics by Daryl Preston and Eric Dietz (John Wiley: 1991)

- An Introduction to Error Analysis 2nd Edition, by John Taylor (University Science Books: 1997). This book covers much of the same material as Bevington and Robinson.

3.2. Reference Articles and Equipment Manuals

At this stage of your training as an experimentalist, you should realize that there is no "comprehensive" or perfect textbook. Much of the material you will need to dig into are the early journal papers which originally detailed many of these important discoveries. The Junior Lab web site has an electronic library containing many of these articles in PDF format and which is accessible using MIT certificates. Junior Lab also has numerous books on reserve in the Hayden Library Reserve Book Room (14N-132) and the Physics Reading Room (4-332). References and lending book resources are available through Barker and Hayden Libraries and students should become familiar with both of these Institute resources. Finally, there is a small Junior Lab Library in 4-361. These books may not by taken from the laboratory, but copies of a few pages may be made on the photocopier.

4. 8.13 Grading Policy

See Table II.

TABLE II: 8.13 grading policy

Attendance and Lab Performance	10%
Laboratory Notebooks (2 checks)	10%
Preparatory Questions & Homework (5)	10%
Oral Examinations (4)	30%
Final Public Oral Presentation	10%
4-Page Written Summaries (4)	30%

4.1. Attendance and Lab Performance — 10%

The regularity of your attendance will be a factor in determining your grade in the course. Also your preparedness for the measurements and alternating as the "lead" (with your partner), to carry them out. Lab instructors will be delighted to accommodate your improvements and corrections to the lab guides!

It is essential that you use efficiently all of the laboratory time assigned to you, and sometimes more. An experienced experimental physicist will be present in every scheduled session. He or she will be assisted by a graduate teaching assistant. In addition, the Junior Lab staff includes two technical instructors responsible for the maintenance of the equipment and the development of new experiments. We are ready and eager to help you make things work properly and answer questions. Call for help when you get stuck.

Failure to have a "dry run" of the final presentation with a Writing Program instructor (see below) will result in a 2% reduction of the lab participation grade.

4.2. Laboratory Notebooks — 10%

One critical objective of this course is to instill habits of record keeping that will serve you well in future research. To this end you will be given a standard experimental notebook in which the complete dated record of procedures, events, original data, calculations and results of every experiment is to be kept. **No other form of notebook is acceptable in this course.** Although you will generally work in pairs and are urged to collaborate in all aspects of carrying out the experiments and analysis, each student must keep a complete, dated record of each experiment and its analysis. The grid-lined paper in the notebook is convenient for formatting tabulations, for guiding line drawings, and for making rough plots. High resolution plots, photos, and photocopies of shared data should be glued or taped in place. You must write a sufficient narrative as the experiment

proceeds so that, years later, you could reproduce the results you obtained. Notes, tables, and graphs should be neat and compact, leaving as little empty space in the lab notebook as is compatible with clarity and the logic of organization. There should be no loose sheets or graphs in your notebook.

Analyze data in the lab in a preliminary way as you go along to check for reasonableness. If you are making a series of measurements of one quantity as you vary another, plot the results as you go along so that you can see the trend, catch blunders, and judge where you may need more or less data. **Repeat every measurement at least three times in as independent a manner as possible in order to establish a statistical basis for estimating random error and to reduce the chance of blunders.** If you get through all the manipulations and preliminary analysis of an experiment in less than the allotted time, take the opportunity to perfect part or all of the experiment so as to obtain the best possible data set.

Many experiments will require you to transfer your data to a computer and store them in files on disk. Obviously, it is not practical in these cases to print out all your data and paste them into your notebook. However, we expect to see in your lab notebook representative plots or tables. In addition, we expect a clear description and summary of the data files so that when you return to them days or weeks later, you are able to identify particular files with procedures you carried out in the lab.

Specific requirements for your notebooks are listed on the web at Junior Lab Notebook Guidelines.

Student notebooks will be evaluated three times during the fall term. The first will follow the Introductory Experiments and be "graded but not recorded" in order to help students learn what is expected. The second check will be around midterm for 5% of the grade. The final check will be at the end of the semester for 5% of the grade. Please talk with your section instructor before your notebook evaluation if you have any questions.

4.3. Preparatory Questions and Data Analysis Assignment — 10%

Each lab guide has a set of preparatory questions which point you to the essentials of the experiment. You are expected to work out the solutions to the preparatory problems and/or predictions in your notebook before starting the experiment. Make a photocopy of your solutions and deposit it in your TAs mailbox in 4-361. It will be collected shortly after the start of the first session of each new experiment. **Late solutions will not be accepted because you will need to know this material BEFORE the experiment: late solutions do not make sense.** Your solutions will be graded by the graduate teaching assistant and returned at the next session.

The Introductory Experiment preparatory questions will be graded for feedback but will not count towards your final course grade.

4.4. Oral Examinations (4 private) — 30%

A one hour total length (2 students $\times$ 30 minutes each) oral examination and discussion of each main experiment will be held between the pair of students and one or more of their instructors within 10 days of the last scheduled session for that experiment. Each student must bring his or her lab notebook to the exam session.

To familiarize you with the procedure, a one-hour oral will be held on ONE of the three Introductory Experiments of the students' choice. This oral will proceed identically as the others and will be scored but will **not count** towards the students final course grade. It is designed to give the student feedback on content, style and presentation without the pressure of a graded performance. Partners should choose different Introductory Experiments for this initial oral exam. Videos of these practice orals will be used along with guidance and advice from Lecturers from MIT's Program in Writing, Atissa Banuazizi and Lydia Volaitis. Students must schedule a 1-hour appointment with one of them within a week following their practice oral for feedback.

Each student should prepare a 15-minute oral report on the theoretical and experimental aspects of a single portion of the experiment. Fifteen minutes is a short time, so it is essential that you rehearse your presentation as you would if you were giving a 15-minute presentation at a meeting of the American Physical Society. Please review the Society guidelines at http://www.aps.org/meet/guidelines.cfm.

We suggest a maximum of ten slides and strongly suggest preparing your presentation electronically (e.g. LaTeX or MS PowerPoint) and using the LCD projector for the cleanest, most professional presentation possible. The Junior Lab website has detailed instructions and a template for generating your own presentations.

The theoretical section should demonstrate a mastery of some portion of theory relevant to understanding the significance of the experimental results. The experimental section should dominate and demonstrate an understanding of how the equipment works, what was measured, how the data were reduced, and how the random and systematic errors were estimated. **Each student must discuss different aspects of the motivating theory and experiment and furthermore it is not acceptable to discuss theory only or experiment only; every presentation should contain a balance! Full cooperation with lab partners and others in preparing for the oral reports is encouraged.** This latter aspect is particularly important to ensure that both partners report the same results!

The oral exam on the fourth main experiment is only required for students who wish to use that experiment for the final (public) presentation. (See below.) For stu-

dents who take the option to not present the fourth experiment, each of the remaining three oral exams still counts as 7.5% of the total grade, but the written summary (see below) for the fourth experiment will have its value doubled to 15%.

4.5. Final Public Oral Presentation — 10%

At the end of the term in December, each student will give a public oral presentation which will be attended by all students in the section and any other interested parties. This public oral is a major component of the CI-M requirement that 8.13 fulfills. This is in addition to the four jointly prepared oral presentations given to the section instructor. We have reserved the last two class sessions for this purpose. The public oral presentations should be given in the style of a paper presented at a conference, with careful attention paid to the preparation of material — usually in the form of an electronic presentation or transparencies — and to the clarity of the oral discussion. Questions from classmates and the audience are encouraged allowing for a general discussion of the experiment.

Each student is required to make a 1-hour appointment with a "Program in Writing" advisor to do a "dry run" and receive feedback at least four days prior to their public presentation. The dry run will not be graded, but, as mentioned above, failure to do it will result in a 2% reduction of the lab participation grade. Obviously, to present on an experiment in the public presentation, it must have previously been presented as an oral exam with the section instructor.

4.6. 4-Page Written Summaries — 30%

You must email a PDF copy of your **individually-prepared** written summary ($\leq$4 pages including figures) of the purpose, theory, and results of the experiment by midnight on the day you give your oral examination. The delay between oral exam and paper submission allows you to correct any egregious mistakes that were uncovered during the exam so as not to repeat them in your written work and receive a double penalty! **All your work on the experiment should be summarized, not just the part you chose for your oral presentation.** The individual summary you hand in should show evidence of your own mastery of the entire experiment, and possess a neat appearance with concise and correct English. Its organization and style should resemble that of an article in the Physical Review Letters (http://publish.aps.org/STYLE/). **The abstract is essential. It should briefly mention the motivation (purpose), the method (how measured) and most important, the quantitative result WITH uncertainties.** Based on those, a conclusion may be drawn. The report must be typeset in a form that would be suitable for submission as a manuscript. To aid you in this process we have produced a sample paper template written in LaTeX that we encourage you to study and use for your own submissions. The sample paper is downloadable from the Junior Lab site along with its associated .tex file.

The body of the summary should include a discussion of the theoretical issues addressed by the experiment, a description of the apparatus and procedures used, a presentation of the results (including errors!), a discussion of these results, and, finally, a section briefly presenting your conclusions. The total length (including figures) of your summaries should not exceed four pages in length. It is easiest to read if you include figures and plots inline within the text and the sample paper template shows you how this is easily done. However, do not inundate the reader with material; you should find a way to summarize your results in at most two or three plots or tables. The figures and tables must be properly captioned. Material and ideas drawn from the work of others must be properly cited, and a list of references should be attached to the summary.

Papers will be graded using the following criteria:

- Theoretical and/or experimental motivation: 15%

- Description of experiment: 35%

- Analysis of data and results: 35%

- Style and English: 15%

- Papers not submitted by midnight after the oral exam will be deducted 10% for each day they are late.

MIT has excellent resources for technical writing and oral presentations (including on-line writing consultations) at http://web.mit.edu/writing. Use them!

As mentioned above, students who take the option to not orally present the fourth experiment will have the value of the written summary for the fourth experiment doubled to 15% of the total grade.

5. Safety in Junior Lab

We are fortunate that there has never been a serious injury in Junior Lab. Prevention of injury is a matter of being aware of and having respect for pieces of equipment that are potentially dangerous. Nevertheless, since it is virtually impossible to set up a reasonably comprehensive and interesting set of experiments in modern physics without using equipment that has potential hazards, it is essential that students and staff be aware of the hazards, and exercise appropriate cautions.

5.1. Electrical Safety

The first rule is to never work alone. Some years ago a student was electrocuted in Building 4 by a laboratory power supply. Had he not been by himself, someone might have saved him.

All high voltage supplies are clearly marked as dangerous. Do not poke or probe into them. Turn off the supply if you need to change cable connections. The supply may be dangerous even when turned off if the capacitors have not discharged; always keep one hand in your pocket when testing any circuit in which there may be high voltages present so that if you get a shock, it will not be across your chest. Never go barefoot in the lab. Remember that it is current that kills. A good (e.g. sweaty) connection of 6 volts across your body can kill as well as a poor connection of 600 or 6000 volts.

5.2. Laser Safety

A laser beam may not seem very bright, but if it enters your eye it will be focused by the lens of your eye to a pinpoint spot on the retina where the intensity is sufficient to destroy retinal cells. It is wise to terminate a laser beam with a diffuse absorber so that the beam doesn't shine around the room. Never examine the performance of an optical system with a laser by viewing the beam directly with your eye or reflector.

5.3. Cryogenic Safety

When the cap on a liquid-helium Dewar is left off, air flows in and freezes in the neck, forming a strong cement. When a probe is inserted, it may be frozen in solid. Then pressure will build up until something explodes. During the superconductivity experiment, never leave the Dewar cap off for more than a few seconds. Always ream out the Dewar before you use it. Check periodically to see that the probe is free. If the probe should freeze in the Dewar, get help immediately from any of the Junior Lab staff or instructors.

Liquid nitrogen is chemically inert, but it can cause severe frostbite. Wear gloves and protective glasses when transferring or transporting liquid nitrogen.

5.4. Radiation Safety

Radiation safety at MIT is under the authority of the Radiation Protection Office (N52-496). Junior Lab is accountable to that office for the safe handling and accountability of the sources used in the experiments. During the first class session, Christopher Tavares, a member of the Radiation Protection Office, will instruct you in the safe use and handling of radioactive material. (See also Tables III and IV.) Attendance at this session is mandated by Massachusetts state law.

TABLE III: Precautions for Working with Radioactive Materials (ALARA)

1. Don't handle radioactive sources any more than you have to.

2. Work quickly when transferring or positioning radioactive sources.

3. Never take a source away from the Junior Lab, even temporarily. The senior staff are legally responsible for the sources and must periodically account for their presence and condition.

4. Replace sources in the lead storage cabinet when they are not in use and ensure that the cabinet is locked at all times.

5. Keep sources away from your body.

6. Never bring a radioactive source near your eyes because they are particularly sensitive to radiation.

7. Be aware of the sources being used in neighboring experiments.

8. Remember ALARA – *As Low as Reasonably Achievable*!

TABLE IV: A table showing the radioactive sources used in Junior Lab and their approximate activities.

Experiment	Isotope	$\sim$ Activity (mCi)
Compton Scattering	^{137}Cs	0.4
Mössbauer Spectroscopy	^{57}Co	7
Rutherford Scattering	^{241}Am	0.2
Alpha Decay	Uranium Ore	5×10^{-6}
Relativistic Dynamics	^{90}Sr	8
	^{133}Ba	0.08
X-Ray Physics	^{241}Am	10
	^{55}Fe	0.7
	^{90}Sr	0.6
	^{57}Co	0.02
Calibration Sources	^{133}Ba	0.005
	^{109}Cd	0.008
	^{137}Cs	0.007
	^{57}Co	0.0001
	^{60}Co	0.0005
	^{54}Mn	0.0002
	^{22}Na	0.002

Meticulous care must be taken by all students and staff to insure that every source signed out from the repository be returned immediately after its use and signed in.

Ionizing radiation damages tissue; any exposure should therefore be minimized. The unit of radiation exposure

is the rem (roentgen equivalent man). Your inescapable dosage from cosmic rays and other background sources is 360 mrem yr^{-1}, which works out to 4.2×10^{-2} mrem hr^{-1}. The recommended limit to controllable exposure for a member of the general public is 100 mrem yr^{-1}, averaged over any consecutive five years. If you follow the Junior Lab guidelines, your exposure will be only a small fraction of the dose you receive from the natural background. A meter is available in 4-361 for you to check the radiation levels yourself.

Radioactive sources emit three types of radiation: high energy helium nuclei (alpha rays), electrons (beta rays), or photons (gamma rays). Most of the sources in Junior Lab emit only gamma radiation. Of the sources which do emit alpha or beta particles, most are enclosed in plastic or metals, which prevent particulate radiation from escaping. The exceptions are the ^{90}Sr source in the e/m experiment and the ^{241}Am source in the Rutherford Scattering experiment; both sources are in an enclosed apparatus. These sources should never be handled. Handling of open alpha- or beta-emitters can result in dangerous dosages to the skin.

The strength of a radioactive source is measured in curies (Ci). A one-curie source has an activity of 3.7×10^{10} disintegrations s^{-1}. The "absorbed dose" is a quantity that measures the total energy absorbed per unit mass; it is measured in rads, where 1 rad = 100 erg g^{-1}. The "equivalent dose" is measured in the units discussed above, the rem. The equivalent dose is derived from the absorbed dose by multiplying by a "radiation weighting factor" which is a measure of how damaging a particular type of radiation is to biological tissue. For photons (gamma rays) and electrons and positrons (beta particles), the radiation weighting factor is unity; for helium nuclei (alpha particles), it is 20; for protons with energy greater than 2 MeV it is 5; and for neutrons it ranges from 5 to 20, depending on the energy. When you use the survey meter in the lab, the readings are in rads, and you must consider the type of particle when you work out the equivalent dose.

For gamma rays with energy greater than 1 MeV, a useful approximation is that the equivalent dose due to a source with an activity of C microcuries is $5.2 \times 10^{-4} C E_\gamma R^{-2}$ mrem hr^{-1}, where R is the distance from the source in meters and E_γ is the energy of the gamma ray in MeV. For gamma rays with energy less than 1 MeV, this formula is still approximately true for a full-body dose. However, low-energy gamma rays deposit their energy in a smaller mass of tissue than high-energy gamma rays and can cause high local doses. For example, the local dose to the hands from handling a 10 keV source can be up to 25 times the value given by the above formula; hands, however, have a higher tolerance to radiation than inner organs or eyes.

The protective value of shielding varies drastically with the energy of the photons. The intensity of a "soft" X-ray beam of < 1 keV can be reduced by many orders of magnitude with a millimeter of aluminum while 1.2 MeV gamma rays from ^{60}Co are attenuated by only a factor of 2 by a lead sheet one-half of an inch thick. The best way to keep your dosage down is to put distance between you and the source. If you stay a meter away from most sources in Junior Lab, you will be receiving, even without any lead shielding, a dose which is much less than your allowable background dose. If, however, you sit reading the write-up with a box of sources a few inches away, you may momentarily be receiving ten to a hundred times the background level.

The Photoelectric Effect

MIT Department of Physics
(Dated: September 5, 2011)

The objective of this experiment is to demonstrate the quantization of electromagnetic waves and to determine Planck's constant h. You measure the maximum kinetic energy of electrons ejected by the photoelectric effect from an alkali metal surface as a function of frequency. The constant "offset" is caused by the work function ϕ of the metal, e.g. the minimum energy needed to get an electron out of the specific metal.

1.   Preparatory Questions

1. If a certain metal with a work function of $\phi = 2.5$ eV is illuminated by monochromatic light of wavelength 3500 Å, what is the maximum kinetic energy of the electrons ejected in the photoelectric effect?

2. What are the principal lines in the spectrum of a mercury discharge lamp (see Reference [1], and Oriel high power mercury lamp specifcations)? Could you observe the photoelectric effect on a silver (as opposed to potassium) cathode?

3. How does a narrow-band optical interference filter work? See Optical Interference Filters [2].

4. Sketch the expected curves of current against retarding voltage when the cathode of the tube is illuminated with light of wavelengths 3650 Å, 4035 Å, 4360 Å, 5460 Å, and 5775 Å, respectively. Assume $I_0 = 1$ nA at 3650 Å.

2.   The Photoelectric Effect

A very accessible introduction to this material is in the American Institute of Physics's A Look Inside the Atom. In 1895 Heinrich Hertz observed that ultraviolet light from the sparks of his generator for radio waves he had recently discovered, falling on the negative electrode of his radio wave detector, induced the flow of electricity in the gap between the electrodes. Pursuing the phenomenon in detail, he discovered the photoelectric effect whereby light of sufficiently short wavelength causes the ejection of electrons from a metal surface. 1905 Nobel Laureate Philipp Lenard made improved measurements and demonstrated by determination of their charge to mass ratio that the ejected particles are identical with the electrons that had recently been discovered by 1906 Nobel Laureate J. J. Thomson in experiments with cathode rays.

Crude though the early data were, the qualitative fact of the dependence of the critical cutoff voltage on the wavelength of light emerged with sufficient clarity to induce the young Albert Einstein, working as a patent examiner in the Swiss Patent Office in 1905, to link the effect with the recent idea, introduced by Planck in 1900, that matter radiates its energy in quanta of energy $h\nu$. He postulated that light delivers its energy to an absorber in quanta with energy $h\nu$. Thus, if it takes an amount of energy ϕ to lift an electron out of the surface and away from its image charge, then the residual kinetic energy K of the ejected electron is

$$K = h\nu - \phi \qquad (2.1)$$

1921 Nobel Prize was awarded to Albert Einstein for his discovery of "the law of photoelectric effect". It was not until 1912 that the technical problems of making precision measurements of the photoelectric effect were overcome by 1928 Nobel Laureate Sir Owen Wilans Richardson and K. T. Compton (former MIT president) to the point where the Einstein photoelectric equation could be tested to high accuracy and used in precise determinations of Planck's Constant $h = 6.626 \times 10^{-34} J \cdot s = 4.135 \times 10^{-15} eV \cdot s$. In this experiment you will measure the photoelectric current from an alkali metal surface as a function of a retarding potential that opposes the escape of the electrons from the surface. From the data you will be able to derive the value of Plank's constant and the work function ϕ of the cathode material.

3.   Experimental Setup

The apparatus is depicted in Figure 1. Familiarize yourself with all of the components before turning anything on or making any signal connections.

The Agilent variable DC Power supply provides the retarding voltage between the anode and the cathode. Pay close attention to the grounding connections between the electrometer and the power supply! If the power supply meter does not have sufficient resolution, try using an external digital voltmeter.

3.1.   Light Source

The radiation source for this experiment is a high-power mercury discharge lamp Oriel 65130, or similar model. You should turn on the lamp as soon as you begin the lab to allow it to warm up. The spectral output of the lamp will change during the first $10 - 15$ minutes.
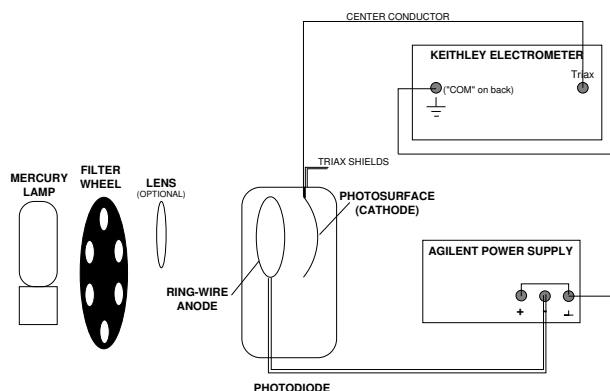
FIG. 1: Experimental arrangement for measuring the photoelectric effect. The lens focuses the light to avoid hitting the anode ring.
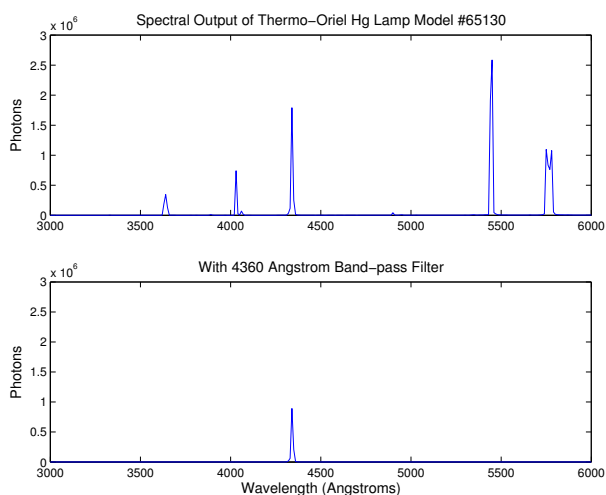

FIG. 2: Top Panel: Spectral output of the Thermo-Oriel 65130 Hg lamp after $\sim$ 20 minutes warmup. Bottom Panel: Shows the lamp output after passing through the 4360 Å filter.

Once the lamp has stabilized, the spectral output is similar to that shown in Figure 2.

The narrow band pass filters used to select individual mercury emission lines have a preferred orientation; point the highly-reflecting side (a silvery color) toward the lamp and the colored side towards the phototube cathode. **Be careful not to place the filters too close to the lamp! The heat can bleach the color of the filters, leading to undefined behavior! Monitor the heat of the filters as you perform the experiment.**

3.2. Connecting the Apparatus

Connect the phototube cathode to the Keithly electrometer (or similar model) operating as an ultra-sensitive ammeter. Note that the input connector to the electrometer requires a *triaxial* connector for double grounding and thus be certain that you insert a BNC–triax connector before connecting the BNC cable from the cathode. Turn on the power supply and reduce the retarding voltage to zero.

Illuminate the photocathode with light of the various spectral lines of mercury selected by the interference filters mounted on the filter wheel. You may want to start with the more energetic spectral lines. Rigorously convince yourself that the current you are measuring is a photoelectric current caused by the mercury lamp. With creative use of black tape and the open hole, one can correct for ambient light effects if necessary.

The cathode of the Leybold photocell is a very thin layer of potassium ($\phi_K = 2.3$ eV) deposited onto an oxidized silver coating electrically connected to the cylindrical brass cap on top of the cell. The potassium is the source of the photo-ejected electrons in this experiment. It is not possible to precisely determine the work function for removing an electron, because the cathode surface interacts with the remaining gases in the photocell as a getter, so that the surface characteristics change a little from the ideal case. The anode ring is made from platinum-rhodium alloy ($\phi_{Pt} = 5.7$ eV). Typical photoelectric currents are 100-1000 nA. It is important to note that the electronic work function W is a material constant which incorporates the different emission potentials of the cathode and anode. The former is a difficult quantity to estimate due to the manufacturing process which makes the cathode surface inhomogeneous. It is composed of a mixture of potassium, potassium oxide and oxidized silver. For this reason, you need to take care that the same area is always illuminated. The emission work function of the photoelectrons can vary locally!

1. The photocell consists of an evacuated glass bulb and is fragile!

2. Do not subject the photo cell to mechanical stresses.

3. Protect the photo cell from overheating

4. Protect the photo cell against excessive incident light (use filters if necessary!)

4. Procedure

Measure, tabulate, and plot the phototube current as a function of the the retarding voltage for each filter. Make sure to extend the measurements beyond $I = 0$ in order to measure the effects of "reverse" current. Repeat the series of measurements **at least five times** to obtain the data necessary for a reliable estimate of the random errors of measurement.

The following are practical problems with which you must contend:

1. Light striking the anode ring can produce photo-electrons that cause a reverse (negative) current in the electrometer and confuse the identification of the critical cutoff voltage. It is therefore important to focus the light beam so that it passes cleanly through the ring without illuminating it. Experiment with the location of the lens to produce the sharpest image possible at the aperture to the photocell holder.

2. Proper grounding of the apparatus is essential to obtaining reliable data. When the grounding is proper, the electrometer readings should be unaffected by touching or moving your hand near the equipment.

3. Because you are measuring such small currents (the currents you obtain with no retarding voltage should be on the order of hundreds of picoamps), the ammeter will be prone to pick up induced currents from ambient magnetic fields and your inducing charges while moving near the apparatus. You can avoid such interference by keeping the connecting wires as short and direct as possible and free of loops. For instance, you might want to use a short piece of copper wire to ground the positive terminal of the power supply as shown in Figure 1. You may also find it useful to twist some of the cables together.

4. Your measurement chain may or may not be sensitive to ambient light. Check to see if the current you are measuring is affected when you cover the experiment with black cloth.

4.1. Baking out the anode ring

Potassium can precipitate on the anode ring in very old photo cells in the course of storage at higher ambient temperatures or under illumination of the photocell at very high intensities, making it necessary to bake out the anode ring. **Bake out the anode ring only if the measurement cannot be improved by any other means, as the potassium atoms baked out of the anode ring can precipitate over the entire photocell. When the process is performed improperly, the potassium layer of the photocathode can be overheated, releasing more potassium and can irreparably damage the device!** Please do not attempt this procedure without first consulting a member of the technical staff!

5. Analysis

Determine the cutoff value of the retarding voltage for each of the filters, and assess the random and systematic errors of each determination. Plot the cutoff voltages
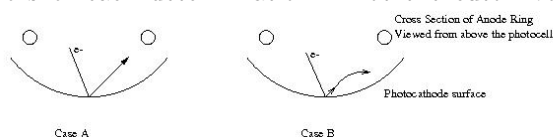
against the center frequency of the filter bandpass. Suggestion: You can probably make more reliable determinations of the change in cutoff voltage from one wavelength to the next if you normalize your current data so that the zero-voltage values are all the same. Plots of normalized current versus retarding voltage will then show clearly the effect of photon energy on the cutoff voltage. Compute h and ϕ from your plots and estimate the random and systematic errors, taking account of the effects of the errors in the cutoff determinations on your evaluation of the slope and intercept. One significant problem lies in the observation that the current decrease is not linear close to the cutoff voltage. Consider Figure 3 case (a) and (b) below for easy visualization.

Discuss in detail how the cutoff is determined.

If you can use two different methods, the difference in h and ϕ will give you a lower limit of the systematic errors.

5.1. Topics which may come up during oral exams

1. The wave-particle duality of photons and electrons.

2. The potential energy in eV of an electron as a function of distance from a smooth conducting plane.

3. Classically consider a metal atom ($d = 0.3$ nm) bathed in radiation of intensity 1 mW m^{-2}. How long does it take to accumulate enough energy to overcome $\phi = 4$ eV? How can you disprove the classical estimate?

6. Statistical Exercises

1. From your (hopefully) independent (what does that mean?) measurements, estimate the variance.

2. With these random errors, fit your plots of current I vs. retarding voltage V_r to the following functional form:

$$I_{fit}(V_r) = aV_r + b. \qquad (6.2)$$

for two cases: (a) the data as recorded by you and (b) after scaling the data and errors to $I_0 = 1$ nA.

FIG. 3: Figure (a): electrons will travel in a straight

[1] A. Melissinos, *Experiments in Modern Physics* (Academic Press, 1966).

[2] P. Baumeister and G. Pincus, Sci. Am. pp. 58–75 (????).

APPENDIX A: EQUIPMENT LIST

Manufacturer	Description	URL
Thermo Oriel	Low-Pressure Hg Lamp	oriel.com
Thermo Oriel	Hg Line Filters	oriel.com
Thor Labs	Optical Components	thorlabs.com
Leybold	Photocell	leybold-didactic.de

APPENDIX B: UV SAFETY

Ultraviolet radiation (UVR) is emitted from low pressure mercury vapour. The mercury vapor emits UVR when an electrical discharge is passed through it - most of the energy emitted is at a wavelength of 254 nm. This lies in the UVC portion of the spectrum (180 - 280 nm). In the case of fluorescent lighting, the 254 nm radiation is used to excite a phosphor which coats the inside of the glass envelope of the lamp. The phosphor will re-emit at visible wavelengths (different phosphors produce different colours), and any UVC which is not absorbed by the phosphor will be absorbed by the glass wall of the lamp. However, the mercury discharge will also emit at other wavelengths - notably at 365 nm, which lies in the UVA (315 - 400 nm). This UVA radiation may not be absorbed by the phosphor, and much of it will pass out through the lamp walls into the environment. For more information on UV radiation, see the Health Physics Society site at http://www.hps.org/hpspublications/articles/uv.html

Poisson Statistics

MIT Department of Physics
(Dated: September 5, 2011)

In this experiment you will explore the statistics of random, independent events in physical measurements. The random events used in this study will be pulses from a scintillation detector exposed to gamma rays from a radioactive source. The measurement will be compared to Poisson or Gaussian distributions which often govern the spread of physical data. A computer simulation using Monte-Carlo techniques will provide comparison for different numbers of events and give a demonstration of "normal" statistical fluctuations. This comparison technique is widely used in modern physics.

1.   Preparatory Questions

1. Describe how a scintillation counter works, starting from the entrance of an energetic charged particle or photon, and ending with an electrical pulse at the output of the photomultiplier. Why are subsequent signals independent?

2. Suppose the mean counting rate of a certain detector of random events is 2.1 counts per second. What is the probability of obtaining zero counts in a one-second counting interval? What is the most likely interval between successive pulses?

3. Given the formula for the Poisson distribution (Eqn. (2.2)), prove each of the following:

   - $\langle x \rangle = \mu$
   - $\langle x^2 \rangle = \mu(\mu + 1)$
   - $\langle (x - \mu)^2 \rangle = \mu$

   where $\langle x \rangle$ signifies the mean value of x.

4. Plot the frequency distribution of counts when the average counts per interval is 1.5.

5. Puzzler: Some experiments have painfully slow counting rates that try the experimenter's soul and make him or her question the performance of even the most reliable equipment. Suppose you are running an experiment that yields no counts in 11 hours and two counts in the 12th hour. Give a quantitative answer to the question: what is the likelihood that the equipment is malfunctioning?

2.   Theory of Poisson Statistics

A sequence of independent random events is one in which the occurrence of any event has no effect on the occurrence of any other. One example is simple radioactive decay such as the emission of 663 KeV photons by a sample of ^{137}Cs. In contrast, the fissions of nuclei in a critical mass of ^{235}U are correlated events in a "chain reaction" in which the outcome of each event, the number of neutrons released, affects the outcome of subsequent events.

A continuous random process is said to be "steady state with mean rate μ" if

$$\lim_{T \to \infty} \left(\frac{X}{T} \right) = \mu \qquad (2.1)$$

where X is the number of events accumulated in time T.

How can one judge whether a certain process does, indeed, have a rate that is steady on time scales of the experiment itself? The only way is to make repeated measurements of the number of counts x_i in time intervals t_i and determine whether there is a trend in the successive values of x_i/t_i. Since these ratios are certain to fluctuate, the question arises as to whether the observed fluctuations are within reasonable bounds for a fixed rate. Clearly, one needs to know the probability distribution of the numbers of counts in a fixed interval of time if the process does indeed have a steady rate. That distribution is known as the Poisson distribution and is defined by the equation:

$$P(x; \mu) = \frac{\mu^x e^{-\mu}}{x!} \qquad (2.2)$$

which is the probability of recording x counts (always an integer) when μ (generally not an integer) is the expected number, the mean rate times the counting time interval. It is easy to show that the standard deviation of the Poisson distribution is simply $\sqrt{\mu}$, that is, the square root of the mean. Derivations of the Poisson distribution and its standard deviation are given in References [1, 2]. You should study and understand binomial, Poisson and Gaussian distributions and their limits of application.

3.   Experiment

In the first part of this experiment you will set up a scintillation counter, expose it to gamma rays from a radioactive source (and ubiquitous cosmic rays), and record the frequency distribution of the numbers of counts in equal intervals of time. This will be repeated for four situations with widely different mean count rates, approximately 1, 5, 10, and 100 counts per second. You only know the "real" average rate at the end, but you should aim for these values within 25%. The experimental distributions and their standard deviations will
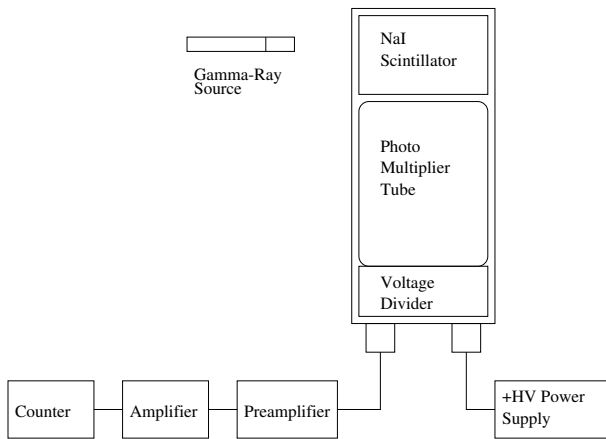
FIG. 1: The setup for measuring the number of counts
from a random process (radioactive decay) in a given
time interval. An oscilloscope (not shown) is used to
monitor the proper functioning of the system.

be compared with the theoretical distributions and their
standard deviations.

Later, you will generate Poisson distributions with a
Monte Carlo simulation and then compare them with the
ones produced by nature in your counting measurements.

3.1.   Setup to Measure Poisson Statistics

Set up the scintillation counter as shown in Figure 1.
Expose the detector to gamma rays from a ^{137}Cs or ^{60}Co
laboratory calibration source (a $1/2'' \times 5''$ plastic rod
with the source embedded in the colored end). The volt-
age applied to the photomultiplier should be $\sim +1000$
volts. Feed the output of the photomultiplier to the
"INPUT" connector on a charge-sensitive preamplifier.
(Some photomultiplier assemblies are provided with a
built-in preamplifier.) Use the oscilloscope to view the
output of the preamplifier and draw it in your lab note-
book. Note especially the rise and decay time of the
signal as well as the peak amplitude and polarity.

The output of the preamplifier is then connected to
the "INPUT" connector on the back or front of the am-
plifier. The amplified signal should be taken from the
"UNIPOLAR OUT" connector on the front of the ampli-
fier, and fed to the "POS IN(A)" connector on the scaler.
("Scaler" is another name for a "counter".) Set the am-
plifier to have a moderate gain and for positive pulses.
Again, note the pulse properties on the oscilloscope and
record them in your notebook. Start with the scaler's
discriminator set at its lowest value, usually about 0.1V.
Set the scaler to repeatedly acquire for about 5 seconds,
display the result, and then start again.

*Note: Throughout Junior Lab, you should pay close at-
tention to the polarities of applied and detected voltages.
Incorrectly setting the polarity on an oscilloscope trigger
can be very frustrating!*

3.2.   Procedure

Examine the output of the amplifier on the oscillo-
scope (sweep speed $\sim 1\mu$sec/division, vertical amplitude
~ 1 volt/division, or whatever settings allow you to best
observe the signal) to confirm the proper performance of
the measurement chain. Adjust the gain of the amplifier
to produce signal pulses of $\sim +3$ volts. If you trigger the
scope on the "rising edge" of the pulses and set the trigger
level to $\sim +3$ volts, you should see a signal which starts
on the left-hand side of the scope display at ~ 3 volts,
rises to a maximum of about ~ 5 volts, goes negative and
finally levels off at zero. If you also set the discriminator
on the counter to 3 volts, there should be an approxi-
mate one-to-one correspondence between pulses counted
and pulses displayed. Ask for assistance on this step if
you are unfamiliar with the operation of an oscilloscope.

Incidently, even without a "check source" nearby, you
should see signals due to "cosmic rays" at the rate of ~ 1
cm^{-2} min^{-1}.

You can control the counting rate by adjusting the dis-
tance of the source from the scintillator, by varying the
high voltage supplied to the photomultiplier, varying the
gain of the amplifier, or changing the threshold level of
the discriminator. Arrange things to yield four different
mean count rates of approximately 1 sec^{-1}, 4 sec^{-1}, 10
sec^{-1}, and 100 sec^{-1}.

**Record your instrumental settings and prepare
tables in your lab notebook for recording the
count data in a neat and compact form**[1].

At each of these four approximate rates, record the
counts for 100 repeated one-second intervals directly into
your lab notebook. Then, for each of these four approxi-
mate rates, also record the number of events in one con-
secutive run of 100 seconds.

3.3.   Analysis

The following analysis requires the use of repetitive
arithmetic on the collected data set. You could use either
Matlab or any other preferred tool on Athena.

a) For each of the four runs calculate and plot the cu-
mulative average, $r_c(j)$, of the rate as a function of
the sequence number, j, of the count. "Cumulative
average" means the quantity

$$r_c(j) = \frac{\sum_{i=1}^{i=j} x_i}{\sum_{i=1}^{i=j} t_i}. \tag{3.1}$$

---

[1] Whenever experimental conditions feasibly allow, it is desirable
to use your own mind and hands to record data, rather than an
automated data logger, as this process more readily engages the
senses and other mental pathways, bringing about a more active
awareness and understanding of the experiment.

where x_i is the number of counts detected in time t_i. For a process which is truly steady with mean rate μ, $r_c(j)$ should converge to μ in the asymptotic limit. Include error bars to demonstrate convergence.

b) Calculate the mean and standard deviation of each of the four 100-trial distributions, and compare the results with the mean and standard deviation of the corresponding 100-second run. Are they consistent?

c) Using the mean rate just determined, calculate the predicted Poisson frequency distribution (renormalized by multiplying by the total number of readings). Make a plot with "frequency bins" (counts per 1-second acquisition) on the horizontal axis and "number of events" (frequency of occurrence) for each bin on the vertical axis, as in Figure 2. Plot your data and calculated distribution on the same axes for ease of comparison. Be sure to include error bars on the data points.

d) For the observed distribution with the lowest mean rate ($\sim 1 \text{ sec}^{-1}$), take the highest deviation from that mean and test whether you might be justified in concluding that the counter was malfunctioning. Remember that there were 100 opportunities for such a deviation to occur.

e) For large values of μ you can use the Gaussian approximation to the Poisson formula as given by the relation

$$\lim_{\mu \to \infty} p(x; \mu) = \frac{1}{\sqrt{2\pi\mu}} e^{-(x-\mu)^2/2\mu}. \qquad (3.2)$$

Compare the Poisson and Gaussian distributions for both $\mu = 4$ and $\mu = 10$. Which is preferred? At what confidence level?

3.4. Simulating Poisson Statistics Using Matlab

You can run the suimulations on your own copy of Matlab (you can download the scripts from the experiment website) or the Athena version.

To access the scripts on Athena, add the Junior Lab Locker by typing

```
%> setup 8.13
```

Within Matlab type

```
>>addpath /mit/8.13/matlab
```

The two MATLAB scripts, `poisson.m` and `poissonsim.m`, can also be downloaded off the Junior Lab website and added into MATLAB's working directory.
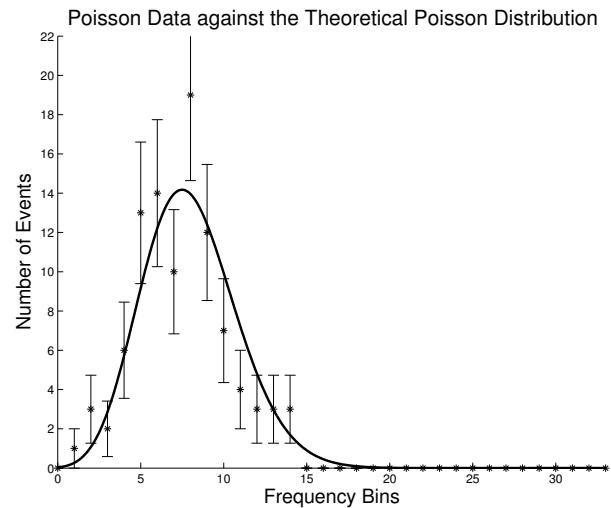

FIG. 2: A frequency distribution of observed numbers of counts. The renormalized Poisson distribution for the observed mean value is also plotted.

For information on how to use either one, type `help poissonsim` from within Matlab. For example type `poissonsim(3,20)` which will generate a 20 sample population with a mean of 3. The solid curve represents the theoretical poisson distribution while the red dots represent the simulated sample population. The `poissonsim` function will output two vectors: the frequency of each rate (i.e. the counts in each bin shown in the graph) and the count rates for all of the trials.

1. Generate 1000-trial distributions for your MEASURED mean rates ($\approx 1, 4, 10, 1000$).

2. Next, generate ten 100-trial distributions for each of the four mean counts you obtained in the experimental section using the scintillation counters. Record the mean values and standard deviations for each set of 10 distributions.

3. Compare the Monte Carlo-generated Poisson distributions with the experimental ones you obtained with the scintillation counter. The mean of the standard deviations should converge (within some statistical error) to the square root of the mean that is input to the Poisson generator.

4. Determine the error on μ and σ from the scatter of the ten distributions.

4. Statistical Exercise

The following questions are a subset of the full analysis discussed in Section 3.3.

1. For the 100 one-second measurements at ~ 4 Hz, evaluate the average and the variance and compare

the results with the mean and standard deviation of the long 100 second run. Are they consistent?

2. Plot the distributions of your measured data sets and compare to Poisson distributions of your experimental means. Are the variances in agreement with the theoretical expectation?

3. Fit the ∼4 Hz data set to both gaussian and poisson functions. Which is preferred? At what confidence level?

5.   Suggested Theoretical Topics for Oral Exam

1. The Poisson distribution, its origin from the binomial distribution and the limits of its application.

2. The Gaussian approximation to the Poisson distribution $P(x; \mu)$ for $x \gg 10$.

3. The differential distribution in the time lag between successive random pulses that occur at a fixed average rate.

[1] P. Bevington and D. Robinson, *Data Reduction and Error Analysis for the Physical Sciences* (McGraw-Hill, 2003), 3rd ed.
[2] A. Melissinos and J. Napolitano, *Experiments in Modern Physics* (Academic Press, 2003), 3rd ed.

APPENDIX A: MONTE CARLO GENERATION OF A RANDOM VARIABLE

Suppose we have a source of random numbers with a uniform distribution from 0 to 1. If we represent the uniform distribution by $q(y)$, so that $q(y')dy'$ is the probability that the random number y lies between y' and $y' + dy'$, then obviously $q(y') = 1$. The problem is how to convert a given random number y from this uniform distribution into a random variable x with a specified distribution $p(x')$ such that $p(x')dx'$ is the probability that the variable x will turn up with a value in the infinitesimal interval between x' and $x' + dx'$. We must find a relation between the distributions of y and x such that $p(x')dx' = q(y')dy' = dy'$.

To do this we compute, analytically if possible but otherwise numerically, the integral

$$P(x) = \int_{-\infty}^{x} p(x')dx' \qquad (A1)$$

which is the probability that the random variable will turn up with a value in the interval between $-\infty$ and x. From this definition is follows that

$$\lim_{x \to \infty} P(x) = 1 \qquad (A2)$$

since the probability that the random variable will turn up with some value is unity. Given the random number y, we set $y = P(x)$ and solve for x. To find the distribution of the resulting value of x we differentiate this expression,

using the rule for differentiating a definite integral with respect to its upper limit, and obtain $dy = dP(x) = p(x)dx$. Thus the distribution of x selected in this way is identical to the one specified.

Figure 3 shows how this works graphically. From the figure it is evident that a horizontal line at a random position y_i on the y-axis is more likely to intersect the $P(x)$ function where it is steeper than elsewhere; i.e., where the differential probability is larger than elsewhere.
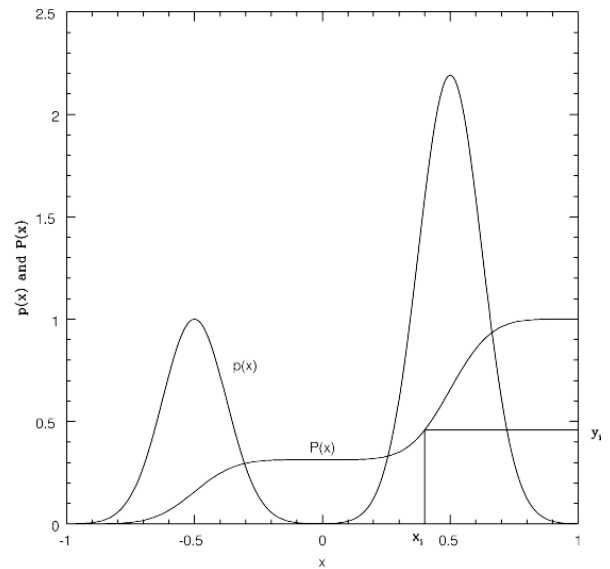

FIG. 3: Illustration of Monte Carlo selection of a random variable with a specified differential probability distribution is shown above. y_i is a random number between 0 and 1. x_i is the value of the variable for which the integral probability distribution equals y_i.

The Poisson probability, being a discontinuous func-

tion, is handled in a similar way, but with a summation rather than an integral. Given a value of $\mu < 88$ and a random number y, the Poisson Simulator find the smallest value of x for which $P(x; \mu) > y$, where P is defined by the formula

$$P(x; \mu) = \sum_{x'=0}^{x'=x} p(x'; \mu) \qquad \text{(A3)}$$

in which $p(x'; \mu)$ is the Poisson probability specified above. That value of x is the desired Poisson variate.

Inspect the Matlab `.m` files where the algorithm is described in more detail.

Transmission of Electromagnetic Pulses

MIT Department of Physics
(Dated: September 5, 2011)

The purpose of this experiment is to acquaint you with some of the principles involved in the manipulation of electrical pulses. You will study reflections and measure termination resistances and signal propagation velocities for different cables.

1.   Preparatory Problems

1. Derive an expression for the characteristic impedance of a coaxial cable with a central wire of radius a, a cylindrical sheath of radius b, and with the space between the inner and outer conductors filled by a non-conducting medium with a dielectric constant κ. See for example References [1–3].

2. A certain transmission line attenuates pulses at a rate of 2.5% per meter. Derive an exact formula for the pulse amplitude as a function of distance along the cable. Make a plot of the amplitude of a pulse as a function of position along the transmission line from 0 to 200 meters. (The formula is the solution of an elementary differential equation.)

3. Draw the predicted shape and amplitude of an ideal rectangular pulse of amplitude -1 volt and duration 10 nsec **after** it has traversed a coaxial cable 10 m long and returned following reflection from a shorted end.

2.   Introduction

Many experiments involve the production and measurement of electrical pulses. Depending on the length of the signals Δt, the approaches are very different:

- $\Delta t \geq 1$ms $\rightarrow$ do with your wires whatever you want. If the signals are small, you may want to use shielded cables.

- 1ms $\geq \Delta t \geq 0.1\mu$s $\rightarrow$ typical for computers. Use ribbon cable, "twisted pair," or cables without termination.

- 100ns $\geq \Delta t \geq 0.1$ns $\rightarrow$ region of interest for "fast" signals to be studied here. Cables must be terminated or undersirable reflections will occur. In Junior Lab, these types of signals are often present with photomultiplier signals but the subsequent amplifiers slow the signals into the middle category.

One may wish to measure a pulse's rate, distribution of amplitudes, the relation of their occurrence times relative to other pulses, etc. Such measurements are done with oscilloscopes, multichannel analyzers, amplifiers, discriminators, coincidence circuits, etc.[1], which may or may not be working properly. It is essential, therefore, to gain facility in the use of test equipment such as pulse generators and oscilloscopes so that the performance of a pulse-measuring apparatus can be checked, point by point. Electrical pulses are piped around a laboratory via transmission lines of one sort or another, with consequent delays, attenuations, and reflections. It is important to understand these effects and to know how to measure them. This experiment is a study of pulses in transmission lines. You will learn that you must terminate all transmission lines properly so as not to be deceived by false signals.

3.   EXPERIMENTS

3.1.   Reflection of electrical pulses from discontinuities in a transmission line

Connect a pulse generator to the input of a digital oscilloscope by means of a T-connector and attach a long RG58 cable to the third side of the T, as shown in Figure 1. Various terminating resistors will be connected to the far end of the long cable.

Use the fixed output on the pulse generator to produce pulses of amplitude ~5.0 V and the shortest possible duration (~4–30 nsec). Be careful to set the repetition rate slow enough that you are not confused by overlapping pulses. Set the oscilloscope controls so that you can observe the pulse produced by the pulse generator. Set the oscilloscope to whatever settings help you best visualize the signal of interest. For example, try setting the vertical amplifier control at 2 V/div, the sweep speed (commonly called the time base) at 50 nsec/div, and the trigger at internal, normal, and positive slope. Be sure to record to observed waveforms, including the settings used to view them, in your lab notebook.

---

[1] Oscilloscopes display the signals $V(t)$ vs. t as described in the Appendix. Multichannel analyzers (MCAs) sort signal events of different amplitudes into bins: that is, they make histograms. Amplifiers enlarge the signal but may also alter it's shape. Charge sensitive pre-amplifiers produce an output pulse proportional to the amount of charge generated in a detector. Discriminators emit a logical (square V(t)) signal if the input exceeds a certain threshold. Coincidence units produce a logical pulse if two (or more) inputs overlap in a certain window of time.
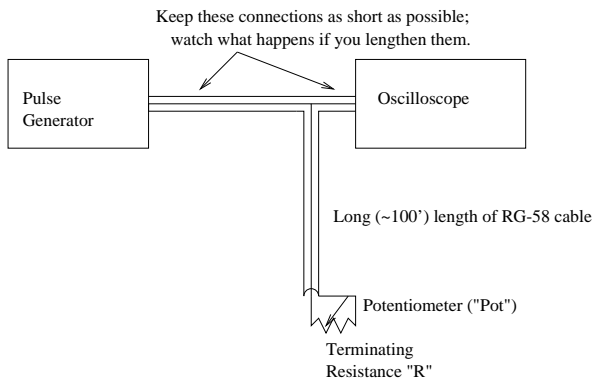
FIG. 1: Experimental setup to test the effect of various terminating resistances on the transmission and reflection of electrical pulses in coaxial cable.

Observe the primary pulse from the pulser and describe the pulse reflected from the end of the cable when the end is 1) open, 2) shorted, and 3) terminated with a variable resistor with values in the range from ∼10–200 Ohms. You will typically see one reflection[2]. Use the variable resistor to determine the characteristic impedance of RG58 cable, and then repeat the above steps RG59 cable. Take enough statistically independent measurements to find a mean and a variance of each characteristic impedance.

Connect another piece of cable to the end of the first cable by clip leads (i.e. a very bad connector) and observe the effects of the discontinuity in the transmission line. **Remember to graph the observed waveforms in your notebook and label both time and amplitude axes!**

3.2. Speed and attenuation of pulses in transmission lines.

Determine the velocity of pulses in the cable by measuring the difference in the arrival time of the direct and reflected pulses at the oscilloscope. Record sufficient data and other information to permit an accurate assessment of the random and systematic errors in your determinations. Compare the velocity in the cable to the velocity of light in vacuum, and explain the cause of the difference. Add at least three cables of known length to make a plot of time versus length.

Measure the attenuation of RG58 cable by comparing the amplitude of the pulse reflected from the open end of the cable with and without an additional length joined by a BNC connector[3]. Note that this strategy isolates the effect of the delay in the cable from possible compli-

cating effects of the discontinuities in the circuit at the connections to the oscilloscope and pulser.

3.3. Propagation of CW in a transmission line

Utilizing a function generator, explore the phenomena of a sinusoidal continuous wave (CW) propagating in a transmission line with various terminations and frequencies. Use two channels on the oscilloscope to measure the wave amplitudes V_{input} and V_{output}. Be sure the output is terminated. Why is this necessary?

Produce a graph of attenuation versus frequency for RG58 transmission line. Obtain attenuation values for frequencies ranging from 1 Hz to 10 MHz. Think about how this frequency dependence for CW signals explains the change in shape of pulsed signals observed in the previous section.

The function generator should default to a 1 kHz sine wave with an amplitude of 100 mV when you turn it on. Make sure you are using the `OUTPUT` terminal and not the `SYNC` terminal. To adjust the frequency, first press the `Freq` button. The current frequency will then be displayed. The flashing digit can be adjusted with the knob in the upper right hand corner. You can also enter the desired frequency by pressing `Enter Number`, entering the numeric value of the frequency and then pressing the the button for the appropriate units. For instance, you can hit the ∧ button for MHz.

A common means of expressing attenuation is in dB/100 ft where dB $= 20\log\left[V_{out}/V_{in}\right]$ when the cable termination is matched to its characteristic impedence. (e.g. -3 dB corresponds to an voltage ratio of 0.707.)

4. ANALYSIS

1. Determine the characteristic impedance Z for RG58 and for RG59 coaxial cables. Compare your values versus published values. Assess the random and systematic errors.

2. Determine V_{prop} for RG58 and RG59 coaxial cables. Compare your values versus published values. Assess the random and systematic errors.

3. Determine the attenuation in dB/m for RG58 and RG59 coaxial cables. Compare your coefficients versus published values. Assess the random and systematic errors.

5. Possible Topics for Oral Exam

1. The step function voltage on an open cable.

2. The partial differential equations for the voltage between the inner and outer elements of a coaxial transmission line carrying a signal.

---

[2] Why not $n + 1$? Hint: Pulse generators have an internal resistance, too (50Ω).

[3] Also observe how the shape of the pulse changes.

3. Estimate the attenuation at low frequencies (Ohm's law). Why does the attenuation grow rapidly at very high frequencies?

4. The fraction of the energy of a pulse reflected at the junction of two coaxial cables with different radii of the inner and outer conductors.

6. Statistical Exercise

1. With the setup described in Section 3.1, obtain 25 independent (explain how you ensure their in-dependence) measurements of the characteristic impedance for RG58 and RG59. Plot the two distributions and calculate their mean and variance.

2. Measure the speed of signals in RG58 by using at least 4 different cable lengths. Again, make sufficient measurements to obtain an estimate of the (random) error for the next step.

3. Plot delay vs. cable length and prove a linear relationship by fitting your data to a model.

[1] A. French, *Vibrations and Waves* (Norton, 1971).
[2] G. Bekefi and A. Barrett, *Electromagnetic Vibrations, Waves and Radiation* (MIT Press, 1977).
[3] W. Leo, *Techniques of Nuclear and Particle Experiments* (Springer, 1992).

APPENDIX A: VISUALIZATION OF ELECTRICAL SIGNALS BY OSCILLOSCOPES

A schematic of an analog oscilloscope is shown in Figure 2. A hot wire in the cathode ray tube emits electrons, which are accelerated by an annular anode by about 20 kV. Two pairs of crossed capacitors then deflect the electron beam (AA' horizontally, BB' vertically). The fluorescent screen emits green light when hit by the electron beam. By applying a linearly rising voltage to AA', a horizon line is produced on the screen (aa'). The (amplified or attenuated) signal applied to BB' produces a vertical deflection bb' for the time duration of $\Delta\tau$. This process is started by the trigger, which is initiated by a signal becoming larger than the threshold (adjusted by the knob control), which can be positive or negative.

computer is used to display the resulting data as a function of time, at various user-selectable voltage and time-scales. You may be using such a modern oscilloscope in this experiment. More information about the digital oscilloscopes used in Junior Lab is available in the online e-library.

APPENDIX B: EQUIPMENT LIST

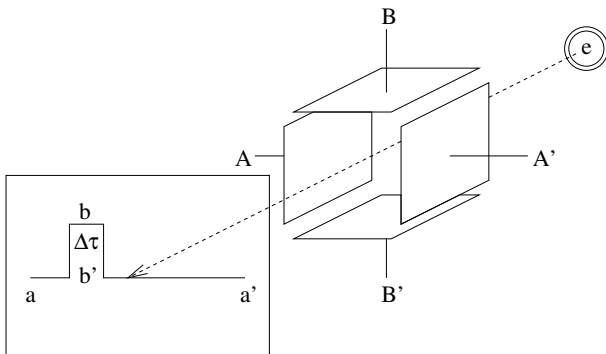| Manufacturer	Description	URL
HP-Agilent	100 MHz Scope	agilent.com
BNC	8010 Pulse Generator	berkeleynucleonics.com
Various	100' RG/58U Cable	
Various	100' RG/59U Cable	

FIG. 2: Schematic of how an analog oscilloscope works.

Modern digital oscilloscopes utilize a similar principle, but operate differently; they sample the incoming voltage periodically (after receiving a trigger event), then a

Compton Scattering

MIT Department of Physics
(Dated: September 5, 2011)

You will observe the scattering of 661.6 KeV photons by electrons and measure the energies of the scattered gamma rays as well as the energies of the recoil electrons. The results can be compared with the formulas for Compton scattering, considering the quantized photon like a particle.

1. PREPARATORY QUESTIONS

1. Describe four distinct ways in which 2 MeV photons can interact with matter.

2. Derive an expression for the final energy of a photon of initial energy E scattered from a free electron, initially at rest, at an angle θ from the forward direction, according to the Compton kinematics (see Reference [1]).

3. Sketch and explain the principle features of the pulse-height spectrum obtained from a NaI scintillation counter irradiated with 661.6 KeV photons (see Reference [2]). Give a qualitative reason for the scatter of energy values measured with these counters observing the 'line'. The pulse height spectrum from 661.2 keV gamma's into the counter will show a line and a continuum. Explain both features with a sketch and give keV values for the line and for the Compton edge.

Suggested schedule:

- Day 1 - Familiarize yourself with the equipment and do Section 4.1

- Day 2 - Repeat Section 4.1 and do Section 4.2. By the end of this session you should have verified that $E_{scat} + E_{recoil} \approx 662 keV$ for at least two angular positions.

- Day 3 - Perform Section 4.3

- Day 4 - Repeat portions of the experiment that need improvement.

2. INTRODUCTION

By 1920 the successes of the quantum theories of blackbody spectra (Planck, 1901), the photoelectric effect (Einstein, 1905) and the hydrogen spectrum (Bohr, 1913) had established the idea that interactions between electromagnetic radiation of frequency ν and matter occur through the emission or absorption of discrete quanta of energy $E = h\nu$. The next crucial step in the development of the modern concept of the photon as the particle of electromagnetic radiation was taken by Arthur Compton in the interpretation of experiments he initiated in 1920 to measure with precision the wavelengths of X rays scattered from electrons in materials of (low atomic number) [1, 3]. The phenomena of X-ray scattering had already been studied intensively. It was known that the penetrating power of X rays decreases with increasing wavelength and that X rays are less penetrating after being scattered than before, which indicated that the scattering process somehow increases their wavelength.

Compton's idea was to use the recently developed technique of high-resolution X-ray spectrometry, based on measurement of the angle of Bragg reflection of X-rays from crystals, to measure precisely the wavelengths of the scattered X-rays [4]. Irradiating a carbon target with an intense collimated beam of monochromatic molybdenum K_{α} X-rays and using an ionization chamber as the detector in his spectrometer, Compton found that the spectrum of scattered X rays had two distinct spectral lines, one at the wavelength of the incident X-rays and another at a wavelength that was longer by an amount that depends on the angle of scattering. The scattering without a wavelength shift was readily explained by the classical theory of coherent scattering of electromagnetic waves from electrons bound in atoms. However, the classical theory provided no explanation of the wavelength-shifting "incoherent" scattering process. The phenomenon of Bragg reflection used in Compton's measurements was a clear demonstration of the wavelike character of the X-rays. Nevertheless, Compton put forward the apparently contradictory idea that X-rays, known to be electromagnetic radiation of very short wavelength, interact with electrons like particles of zero rest mass so that their energy $E = h\nu = hc/\lambda$ and momentum p are related by the relativistic equation for particles of zero rest mass, namely $p = E/c$. He calculated according to relativistic mechanics the relations between the initial and final energies and momenta of an X-ray quantum and a free electron involved, like billiard balls, in an elastic collision. In this way he arrived at the formula for the "Compton shift" in the wavelength of incoherently scattered X-rays, namely (see [2], Appendix A)

$$\Delta\lambda = \frac{h}{mc}(1 - \cos\theta) \qquad (2.1)$$

where m is the mass of the electron, and θ is the angle between the trajectories of the incident and scattered photon.

The agreement between Compton's experimental results confronted physicists and philosophers with the con-

ceptual dilemma of the particle-wave duality of electromagnetic radiation. In particular, how was one to understand how each particle of light in a Young interference experiment goes simultaneously through two slits? The dilemma was further compounded when, in 1924, DeBroglie put forward the idea that material particles (i.e. electrons, protons, atoms, etc.) should exhibit wave-like properties characterized by a wavelength λ related to their momentum p by the same formula as that for light quanta, namely $\lambda = h/p$. In 1927 the wave-like properties of electrons were discovered by Davisson and Germer in experiments on the reflection of electrons from crystals. A particularly interesting account of these developments is given by Compton and Allison in their classic treatise [5].

2.1.   Experimental Goals

In this experiment you will measure:

1. The energies of Compton-scattered gamma-ray photons and recoil electrons,

2. The frequency of occurrence as a function of angle θ,

3. The total cross section of electrons for Compton scattering.

The results of 1.) will be compared with the predictions of Compton kinematics. The results of 2.) will be compared with the predictions of the classical (Thomson) theory of X-ray scattering and with the Klein-Nishina formula derived from relativistic quantum theory.

The experimental setup employs a radioactive source of 661.6 keV photons from ^{137}Cs, and two NaI scintillation counters. One counter serves as the scattering target and measures the energy of the recoil electrons; the other counter detects the scattered photons and measures the energy they deposit. Both the target and scatter counters have a scintillator consisting of a 2"x2" cylinder of Thallium-activated sodium iodide optically coupled to a photomultiplier. A 661.6 keV photon traversing sodium iodide has about equal probability of undergoing photoelectric absorption and Compton scattering. A photoelectric absorption event is a quantum mechanical transition from an initial state consisting of an incident photon of energy E and a neutral atom to a final state. This event therefore consists of an excited ion with a vacancy in one of its inner shells where the electron that was formerly bound and a free "photoelectron" with kinetic energy $E-W$, where W is the binding energy of the electron in the neutral atom. The energetic photoelectron loses its energy within a small fraction of a μsec by multiple coulomb interactions with electrons and nuclei in the sodium iodide crystal, and a certain fraction of the lost energy is converted into scintillation light. Meanwhile, the ion from which the photoelectron was ejected loses its energy of excitation through a cascade of transitions that fill the vacancy in its electronic structure and give rise to lower energy photons or electrons that, in turn, lose their energy in the crystal and generate additional scintillation light.

The total amount of scintillation light produced is closely proportional to the total amount of energy dissipated in all these processes. As a consequence the pulse height spectrum of a NaI scintillation counter exposed to monoenergetic gamma rays shows a distinct "photoelectric" peak which facilitates accurate calibration in terms of pulse height versus energy deposited. The counters can then be used to measure the energies of scattered photons and recoil electrons. The following background topics should be studied in [2, 6]:

1. Kinematics and theory of Compton scattering;

2. Properties of ^{137}Cs;

3. Scintillation counters and the interpretation of pulse height spectra (see preparatory question 3);

4. Radiation safety;

5. Parameter and error estimation [6].

3.   EXPERIMENTAL ARRANGEMENT

The experimental arrangement for the Compton experiment is shown schematically in Figure 1. The 2"x2" cylindrical "recoil electron" or "target" scintillator detector (Canberra Model 802-3/2007), is irradiated by a beam of 661.6 keV photons emitted by $\approx$ 100 μcuries ($\approx$ 1 μgram!) of ^{137}Cs located at the end of a hole in a large lead brick which acts as a gamma-ray "howitzer". If a photon entering the target scintillator scatters from a loosely bound, effectively free, electron, the resulting recoil electron may lose all of its energy in the target, causing a scintillation pulse with an amplitude proportional to the energy of the recoil electron. If the scattered photon emerges from the target scintillator without further interaction, and if its trajectory passes through the NaI crystal of the "scattered photon" detector, it will have a substantial probability of depositing all of its energy by a single photoelectric interaction or by a sequence of Compton scatterings and photoelectric interactions. This will produce a scintillation pulse that contributes to the "photopeak" of the pulse height spectrum. The median channel of the photopeak in the multichannel analyzer (MCA) display is a good measure of the median energy of the detected photons. If the scattered photon undergoes a Compton scattering in the scatter scintillator and then escapes from the scintillator, the resulting pulse, with a size proportional to the energy of the Compton recoil electron, will be registered in the *Compton recoil continuum* of the spectrum. Several experimental details are considered in [7–11].
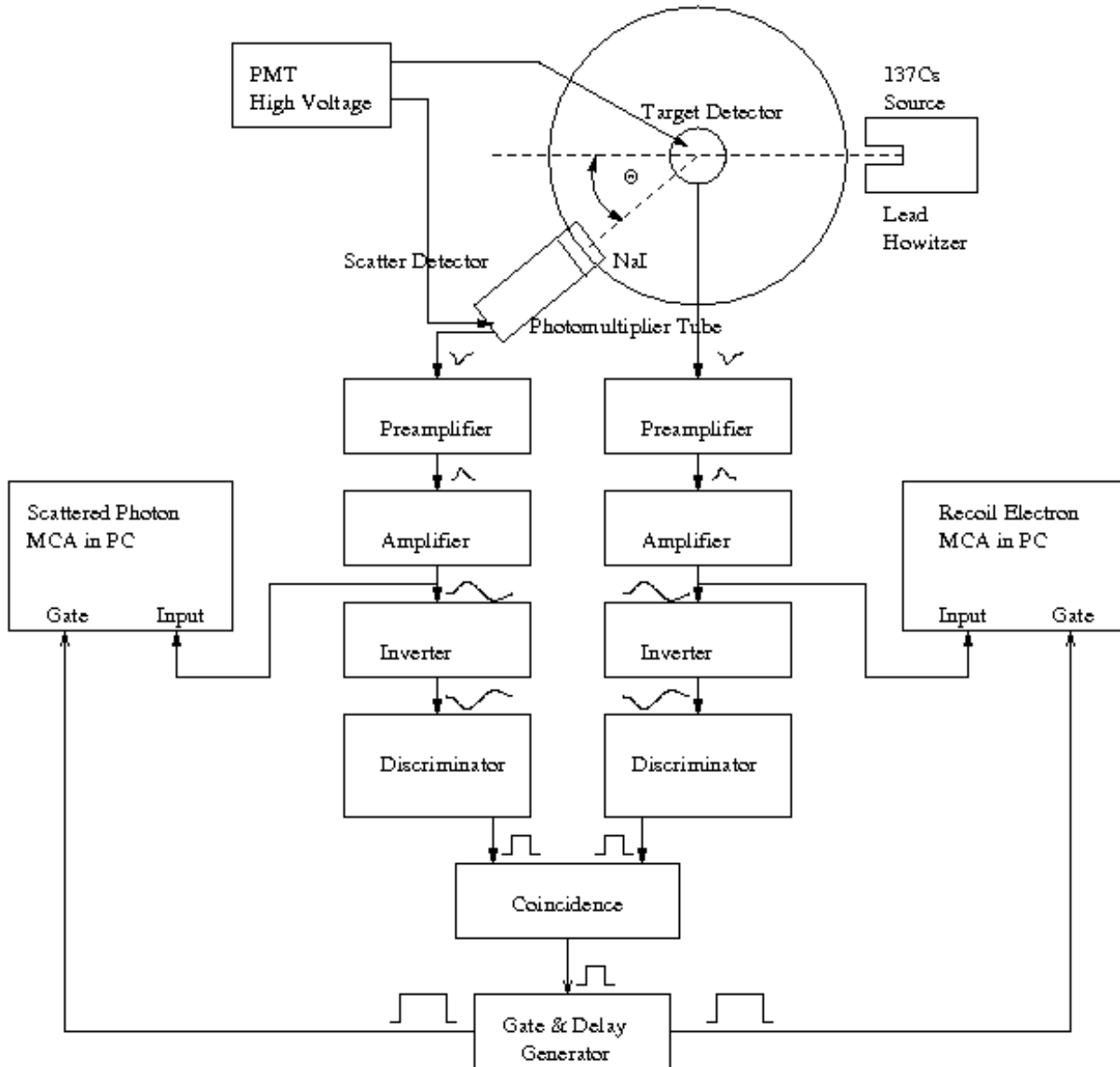
FIG. 1: Schematic diagram of the experimental arrangement for measuring Compton Scattering. Note that while most of the equipment (NIM Crate, NIM modules and detectors are on the lab bench, the two MCA cards are installed inside of the computer.

In the experimental arrangement described by [2] (p.256) the target is inert material (not a detector). The scatter counter suffers background due to gamma-ray photons leaking through the lead from the ^{137}Cs source, cosmic rays, and radioactive isotopes in the environment which is suppressed by the use of very heavy ($\approx$ 200 lb) lead shielding around the source and the scatter counter. Without such shielding and without any electronic tricks the pulses produced by Compton scattered photons would be buried in the background. In a better

way, the compton scattered signal can be discriminated from the background using time coincidence techniques, as described in the following paragraphs.

In our experiment (see Fig. 1) both the recoil electron detector and the scattered photon detector are scintillation detectors. Circuits are arranged so that a pulse from a detector is accepted for pulse height analysis by the multichannel analyzer (MCA) only if it is coincident (within a fraction of a μsec) with a pulse from the other detector. Coincident pulses occur when a gamma-ray

photon produces a Compton-recoil electron in the recoil electron detector, and the Compton-scattered photon is subsequently absorbed in the scattered photon detector. The two nearly simultaneous pulses produced in such an event are amplified and fed through inverters (Ortec Model 533) to constant fraction discriminators (CFD's) (Canberra Model 2126) whose threshold is user selectable between -50 mV and -1 V through a 10-turn potentiometer. (The inverters are required because the amplifiers are designed to put out positive pulses, whereas the CFDs are designed for negative input pulses.) CFD's employ a historically interesting method to achieve precise timing described in Appendix B. Your experiment does not require this accuracy, and it is superceded by modern electronics.

3.1. Coincidence Techniques

A true Compton event will produce coincident (within 2 μs) signals in both detectors. If the logic (square) discriminator outputs overlap, the coincidence ('AND') produces an output 'YES' signal to the gate generator, which in turn notifies the MCA in the computer to analyze the pulse heights generated by this event. Most likely it is a 'Compton Event', however there is a chance that two different (background) events accidently occured within the overlap time 2τ given by the discriminator outputs. From a scatter counter with rate n_s and target counter with rate n_t the accidental rate

$$n_a cc = 2\tau n_s n_t \qquad (3.1)$$

is small unless you have 'noise' increasing n_s or n_t. A good method to set up the coincidence uses a Na^{22} source placed in between the two detectors. But for Compton coincidences, consider that for small θ, the recoil (target) energy and hence signal are small. If the signals are below your discriminator threshold, you fail to see coincident Compton events at small θ.

3.2. Gating the MCA

In principle, the gate should tell the MCA 'ahead of time' that a good event is coming. With the present electronics, this is not possible so we try to catch the majority of the signal (see Fig. 2) including the peak.

The analog pulse shown is derived from the 'unipolar' output of the amplifier. The 'bipolar' has positive and negative peaks and is more tricky to use. Nuclear physicists use it at 'high' rates.

When you think you have everything working correctly, and before you commit to a long series of measurements, check the performance at the extreme values of θ, say 0° and 150°. At both positions the peaks in the spectra due to the scattered photons and the recoil electrons should stand out clearly. If they don't, then more adjustments
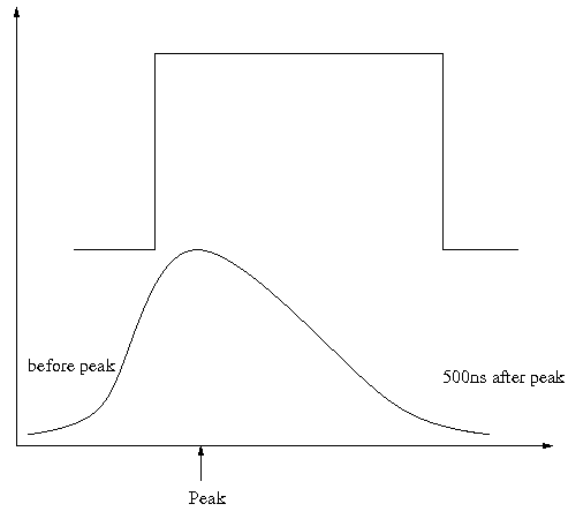

FIG. 2: Schematic representation of the proper time relation between the photomultiplier tube signal (amplified and inverted), whose pulse height is to be measured, and the coincident gate pulse produced by the Gate and Delay Generator NIM module. The coincident gate pulse needs to arrive before the peak of the pulse and persist for $\geq 0.5 \mu sec$ after the pulse peak.

must be made to achieve correct operation of the coincidence gate logic. In coincidence mode, the MCA histogram is not updated unless an appropriate gate pulse arrives at the gate input during the rise of the signal pulse. During the "dead time" required for each pulse height analysis ($\approx 8\mu sec$ for the MCA's used in Junior Lab) the input to the pulse height analyzer is held closed by a "disable gate" so that the arrival of a second pulse will not interfere with the current analysis. More details of the specific MCA's (Perkin-Elmer Model Trump-PCI) used in Junior Lab are available in the Junior Lab Filing Cabinet or in the online e-library.

4. Experimental Procedure

Keep the lead door of the gamma-ray howitzer closed when not in use. The purpose of the procedures described below is to acquaint you with the operation of the equipment, particularly the coincidence scheme which permits the experiment to achieve a good signal/background ratio with a minimum amount of shielding. The steps below suggest a sequence of tests and adjustments to achieve that purpose, but you should feel free to devise your own.

4.1. Experimental Calibration

Set up and test the experimental arrangement with 511 keV annihilation photons from a ^{22}Na calibration

source. ^{22}Na, a radioactive isotope of sodium, decays to an excited state of ^{22}Ne by emission of an anti-electron, i.e. a positron. The excited neon nucleus, in turn, decays quickly to its ground state by emission of a 1.27 MeV photon. Meanwhile, the positron comes to rest in the material in which the sodium isotope is embedded, combines with an electron to form an electrically neutral electronic atom called positronium (discovered at MIT in 1947 by Prof. Martin Deutsch). The latter lives about 10^{-7} s until the electron and positron annihilate yielding two 511 keV ($= m_e c^2$) photons traveling in opposite directions. Thus ^{22}Na is a handy source of pairs of monoenergetic photons traveling in opposite directions which can be used to test a coincidence detector system.

1. Set up the NaI recoil electron and scattered photon scintillation detectors as illustrated in Figure 1. Turn on the power to the NIM bin, HV supplies, MCA and oscilloscope. Keep the door on the ^{137}Cs source howitzer closed to reduce the intensity of 661.6 keV photons at the detectors.

2. Adjust the gain of the scattered photon detector and calibrate it. Apply high voltage to the scatter counter photomultiplier ($\approx +1000$ VDC). Using the Maestro-32 MCA software, turn off the coincidence gate requirement on the MCA. Place the ^{22}Na calibration source near the scattered photon detector and examine the output of the scattered photon amplifier signal (following the pre-amplifier AND the amplifier in series) with the oscilloscope. Adjust the gain so that the amplitude of the pulses produced by 511 KeV annihilation gamma rays is about $+7$ volts. (You might see that a few very high energy pulses saturate the amplifier resulting in 'square' peaked signals. Since the Compton scattering experiment will measure only energies < 662 KeV, it is okay to discriminate against these pulses.) Determine the gain setting of the primary amplifier at which non-linear response begins, as indicated by a flattening of the top of the pulse as viewed on the oscilloscope. Then reduce the primary amplifier gain sufficiently to assure a linear response up to energies safely above the 662 keV energy of the ^{137}Cs photons.

   Now feed the output pulses from the amplifier to the input of the MCA and acquire $\sim$30 seconds of pulse height data using the acquisition presets submenu. Examine the Energy spectrum/histogram of pulses from the scattered photon detector and adjust the gain of the amplifier so that the median channel of the photopeak for 511 keV photons is $\approx$ 2/3 of the full scale MCA range (check that this is set to 2048 channels). Calibrate the counter with other plastic rod calibration gamma-ray sources. A good set consists of ^{137}Cs (661.6 KeV), ^{22}Na (511 KeV), and ^{133}Ba (356, 302 and 81 KeV plus other lines) each of which produce easily identified photopeaks. Be aware that too high a counting rate

will spoil the spectrum by overlapping signals and amplifier saturation.

Write in your lab notebook a succinct description of what you are doing along with the data so that you can later recall exactly what you did and repeat it quickly. You will have to redo the calibration at the start of each lab session because other users will have changed the settings. When you have identified the photopeaks and are confident about the counting rates, measure the median channels of the photopeaks and plot the average median photopeak channel numbers versus the photon energies on millimeter graph paper to provide yourself with a calibration curve. The simplest way to estimate the random error in a measurement of the median is to repeat it five or more times and then evaluate the root mean square (rms) deviation of the successive measurements from their mean value.

3. Adjust and calibrate the recoil electron 'target' detector in the same way.

4. Send the amplified recoil electron and scattered photon signals to the Inverter module and then send the resultant negative polarity pulses into the two discriminators. Examine the positive output pulses generated by the units.

5. Send the two Discriminator outputs into Channels 1 and 2 of the Coincidence module and examine its output. (It's easiest if you temporarily use a single detector signal to trigger both discriminators for this test.)

6. Send the output from the Coincidence circuit into the Gate Generator Unit and explore its operation. Adjust the delay of the delay amplifier so the coincidence gate pulse arrives at the MCA gate input during the rise of the analog signal pulse (see Figure 2). A good way to verify the action of the gate pulse is to feed the pulses from one of the amplifiers to both CFD inputs. This will ensure that a coincidence pulse is generated at relatively high rates. (Students should play with the gate generator controls, specifically delay and width, to verify the operation of the MCA card coincidence circuitry as described in Figure 2).

7. Test the coincidence logic. Place the ^{22}Na source between the two scintillators so that pairs of annihilation photons traveling in precisely opposite directions can produce coincident pulses in the two counters. For this test it is interesting to reduce the gain by a factor of 2 so that the photopeak of the 1.27 MeV photons can be seen on the MCA spectrum display. Compare the spectrum with and without the coincidence requirement, and observe the effect of moving the source in and out of the straight line between the scintillators in order to observe hits by

a pair of annihilation photons. Take careful notes and be sure you understand what you observe. Do not hesitate to ask for help if you need it. **In each of the above steps it is very useful to sketch a picture (or generate a bitmap using the Agilent digital oscilloscopes) of the waveforms taking particular note of their amplitudes, rise and fall times and temporal relationships with other signals (e.g. gates)**

4.2.   Compton Scattering Using ^{137}Cs

This section details the measurement of the energies of the scattered gamma rays and the recoil electrons as functions of the scattering angle θ.

1. Align the primary gamma-ray beam from the ^{137}Cs source in the howitzer. Position the howitzer and the scatter counter so that the source (at the inside of the hole in the lead howitzer) and the scatter counter scintillator are at opposite ends of a diameter of the round platform, with the source $\approx$40 cm from the center of the scintillator. (Keep careful notes about the exact geometry you choose for the setup so you can return to it if necessary at a later time.) Open the door of the howitzer and measure the rate of pulses in the photopeak from the scatter counter as a function of its position angle. In other words, measure the "profile" of the beam and determine $\theta = 0$. Check that the beam profile is symmetric about a line from the source through the center of the turntable to insure that the target counter will be uniformly illuminated when it is placed at the center.

2. Adjust the discriminators of the CFDs to insure that they will generate coincident pulses whenever a Compton scattering occurs in the target scintillator with a scattering angle in the range you wish to cover. Position the NaI target counter over the center of the turntable at a height such that the axis of the beam intersects the mid-plane of the scintillator. For a preliminary test, connect the (inverted) output of the target amplifier to the inputs of both CFDs. Simultaneously connect the output of the target amplifier to the "INPUT" BNC connector on the MCA card in the PC. Connect the output of the coincidence circuit to the gate generator module and the output of the gate generator to the "GATE" BNC on the MCA card. Using the Maestro-32 software package, set the discriminators as low as possible without getting into the rapidly rising spectrum of photomultiplier noise such that the accidental coincidence rate would rival the true coincidence rate (see preparatory question 5 above). Start a spectrum accumulation and test the effects of changing the delay of the gate pulse with respect to the signal pulse.

3. **Measure the median energy E'_γ of scattered photons and the median energy E_e of recoil electrons as functions of the position angle θ' of the scattered photon detector.** With both the source in the howitzer and the scintillator of the scattered photon detector located $\approx$40 cm from the recoil electron detector, set the position angle of the scatter counter at 90°. With the coincidence requirement enabled, accumulate a spectrum of scattered photon detector pulses on the 'scatter' MCA and a spectrum of recoil electron detector pulses on the 'target' MCA and measure the median channel of the pulses in the photoelectric peaks. Repeat this dual measurement at several position angles from just outside the primary beam profile to as near to 180° as you can get. A good strategy is to take data at widely separated position angles, say 90°, 30°, 120°, 150° and then fill in when you have time. Plot the raw results (median energy against position angle) as you go along to guide your measurement strategy. It is wise to check the calibration between each measurement by switching the (software based) GATE setting to 'OFF' and recording in your notebook the median channels of the photopeaks produced by 661.6 KeV photons from the ^{137}Cs calibration source, the 511 KeV photons from ^{22}Na, and the 356 KeV and 81 KeV photons of ^{133}Ba.

Record the integration time of each measurement to find the rate as a function of θ to later compare with Thomson's classical prediction.

4.3.   Scattering Cross Section Measurements

In this part of the experiment, you will measure the total scattering cross section per electron in plastic. The plastic scintillator blocks used as absorbers in this measurement are made from polyvinyltoluene ($C_{10}H_{11}$, density = 1.032 g/cc, www.bicron.com) composed of almost equal numbers of carbon and hydrogen atoms. The most tightly bound electrons are in the K-shells of the carbon atoms where they are bound by 0.277 KeV, which is small compared to 662 KeV. In fact, many other materials can be used providing approximately 'free' electrons. This material resembles most modern plastic scintillators. You will determine their quantum efficiency, e.g. how often they 'see' γ-rays. Place the scatter counter at 0° and remove the target counter from the beam. Measure the counting rates in the 661.6 KeV photopeak of the NaI scatter counter with no absorber and with three or more different thicknesses of plastic scintillator placed just in front of the exit hole of the howitzer. Determine the thicknesses (in g cm^{-2}) of the scintillator blocks by measuring their dimensions and mass. Plot the natural logarithm of the measured rate as a function of the thickness and check the validity of your data by observing whether the data points fall along a straight line as

expected for exponential attenuation. Question: Why is it better to place the absorbers as near as possible to the source rather than just in front of the detector?

5. ANALYSIS

1. Plot $E_{target} + E_{scatter}$ vs. θ.

2. Compare your results on the angular dependence of energies of the scattered photons and the recoil electrons with the predictions of the Compton formula. Since the relation between the scattered photon energy E'_γ and the scattering angle θ, is non-linear, one can anticipate that a plot of the measured energy versus position angle could be fitted only by a curve. However, an easy manipulation of the Compton formula yields a linear relation between $1/E'_\gamma$ and 1-cos θ. Plot $1/E'_\gamma$ against $(1 - \cos\theta)$ with appropriate error estimates. On the same graph plot the calculated curve of $1/E'_\gamma$ against $(1 - \cos\theta)$ based on the Compton formula. Do a similar analysis of the recoil electron data on a separate graph. Plot $1/E_e$ against a function of θ such that the expected relation is linear. Comment on the degree of conformance of the prediction to your experimental results and discuss possible causes of any systematic differences.

3. Plot the measured 'rate' as a function of θ and compare to the classical Thomson prediction.

4. Compute the total interaction cross section per electron. The attenuation of a collimated beam of particles by interactions in a slab of material of thickness x (cm) is described by the formula

$$I(x) = I_0 e^{-\mu x} \tag{5.1}$$

where I_0 is the initial intensity and μ is the total linear attenuation coefficient (cm^{-1}). In plastic scintillator the attenuation of 661.6 keV photons is due almost entirely to Compton scattering. Under this circumstance the total attenuation coefficient is related to the Compton scattering cross section per electron, which we call σ_{total}, by the equation

$$\sigma_{total} = \frac{\mu}{n_e} \tag{5.2}$$

where n_e is the number of electrons/cm^{-3} of the material. To find μ from your data, you should fit an exponential directly to the data, determining the best-fit parameters and their errors. Alternatively, you may plot the natural log of the measured values of I/I_0 against x . Then determine the slope (and its error) of the straight line that best fits the data by linear regression. In either case, calculate the number of electrons cm^{-3} of scintillator $(CH)_n$, and find σ_{total}. Compare to the classical Thomson calculation and to the theoretical result of Klein-Nishina [12].

5.1. SUGGESTED THEORETICAL TOPICS

1. Relativistic mechanics and the Compton shift.

2. Derivation of the Thomson differential and total cross section for unpolarized photons.

3. Discuss the 'correct' Klein-Nishina prediction.

[1] A. Compton, Phys. Rev. **21**, 483 (1923), brother of K.T. Compton, MIT President.
[2] A. Melissinos and J. Napolitano, *Experiments in Modern Physics* (Academic Press, Orlando, 2003), 2nd ed.
[3] A. Compton, Phys. Rev. **22**, 409 (1923).
[4] A. Compton, Nobel Prize Lecture (1927).
[5] A. Compton and S. Allison, *X-Rays in Theory and Experiment* (Van Nostrand, Princeton, 1992), qA481.C738 Physics Department Reading Room.
[6] P. Bevington and D. Robinson, *Data Reduction and Error Analysis for the Physical Sciences* (McGraw-Hill, 2003), 3rd ed.
[7] G. Knoll, *Radiation Detection and Measurement* (John Wiley, Orlando, 1999), 3rd ed., ISBN 0471073385.
[8] R. D. N.H. Lazar and P. Bell, Nucleonics **14**, 52 (1956).
[9] R. Garner and K. Verghese, Nuclear Instruments and Methods **93**, 163 (1971).
[10] R. Hofstadter and J. McIntyre, Physical Review **78**, 619 (1950).
[11] J. Higbie, American Journal of Physics **42**, 642 (1974).
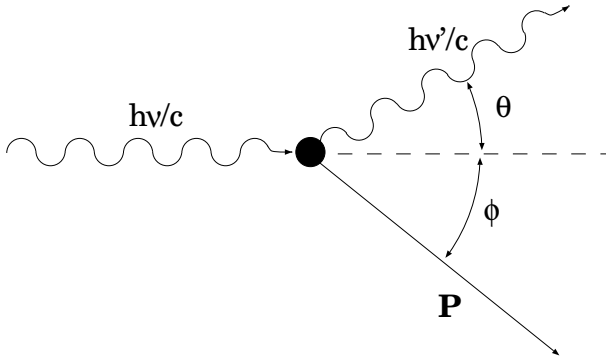[12] D. J. Griffiths, *Introduction to Quantum Mechanics* (Prentice-Hall, 1995).

FIG. 3: Schematic representation of Compton Scattering.

APPENDIX A: DERIVATION OF THE COMPTON SCATTERING FORMULA

Consider the interaction between a photon with momentum vector $\mathbf{p}_\gamma$ (and zero rest mass) and an electron initially at rest with rest mass m_e as depicted in Figure 3. Call $\mathbf{p}'_\gamma$ and $\mathbf{p}'_\mathbf{e}$ the momenta of the photon and the electron after the interaction, respectively. By conservation of momentum, the relation between the initial and final momenta is

$$\mathbf{p}_\gamma = \mathbf{p}'_\gamma + \mathbf{p}'_\mathbf{e} \qquad (A1)$$

Rearranging and squaring both sides we obtain

$$p_\gamma^2 + p'^2_\gamma - 2\mathbf{p}_\gamma \cdot \mathbf{p}'_\gamma = \mathbf{p}'^2_\mathbf{e} \qquad (A2)$$

The total relativistic energy E and momentum $\mathbf{p}$ of a particle are related to its rest mass m by the invariant relation $\mathbf{p} \cdot \mathbf{p}\mathbf{c^2} - \mathbf{E^2} = -\mathbf{m^2}\mathbf{c^4}$. By conservation of energy,

$$p_\gamma + m_e c = p'_\gamma + \sqrt{m_e^2 c^2 + p'^2_e} \qquad (A3)$$

Rearranging and squaring both sides, we obtain

$$p_\gamma^2 + p'^2_\gamma - 2p_\gamma p'_\gamma + 2m_e c(p_\gamma - p'_\gamma) + m_e^2 c^2 = m_e^2 c^2 + p'^2_e \quad (A4)$$

Subtraction of (2) from (4) and rearrangement yields

$$m_e c(p_\gamma - p'_\gamma) = p_\gamma p'_\gamma - \mathbf{p}_\gamma \cdot \mathbf{p}'_\gamma \qquad (A5)$$

Finally, dividing both sides by $m_e c p_\gamma p'_\gamma$, we obtain for the relation between the energies of the incident and the scattered photons the equation

$$\frac{1}{E'_\gamma} - \frac{1}{E_\gamma} = \frac{1}{m_e c^2}(1 - \cos\theta) \qquad (A6)$$

where θ is the angle between their final momentum vectors.

APPENDIX B: INTRODUCTION TO TIMING

A timing instrument marks or measures the precise occurrence of nuclear events. In practice, the release of electrons, which result from the detector's absorption of a particle's energy, occurs after the actual event; how long after is dependent upon the detector and how it is employed. The electronics processing this output further modifies its characteristics. All of these factors must be accounted for, in addition to the problem of noise, when making precise and highly resolved timing measurements.

Sharp timing ($2\,\tau$ overlap) reduces the number of 'accidentals'. The primary limitations in this (and other) experiments is the time slew. A pulse of lower amplitude reaches the threshold of the discriminator later. The coincidence time has to be enlarged to ensure overlap with the other 'normal' (earlier) signal. The time slew is large because the rise time our amplifiers is 'slow'. To overcome timing inaccuracies from 'slew' and differing pulse shapes, the constant fraction technique is used.
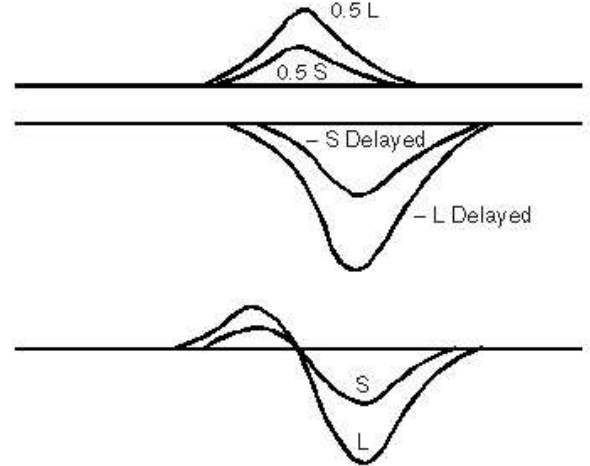

FIG. 4: Manipulation of input signal for constant fraction discrimination.

Constant fraction timing involves the inversion, delay and recombination of the signal to create a zero crossing mark. However, rather than adding the inverted and delayed signal to the original to achieve cancelation, some fractional part of the original is used to insure baseline crossover. As is evident in Figure 4, the crossover point is independent of amplitude of the input signal. The constant fraction discriminator (CFD) fixes its reference at this point.

1. Constant Fraction Discrimination

CFDs have an advantage over simple discriminators in experiments that require the detection of coincidences with high time resolution. A simple discriminator produces a logic output pulse that starts at some fixed time

after the voltage at the input rises above a set value. Therefore pulses of similar shape but different peak amplitudes trigger a simple discriminator at different times relative to the occurrence times of the events that generate the input pulses. A CFD also produces a logic output pulse if the voltage of the input pulse exceeds a set value; its special virtue is that the output pulse starts at a fixed time after the input pulse has risen to a certain constant fraction of its peak value, independent of the magnitude of that peak value. If the input pulses have a fixed shape, but different amplitudes, then the delay between the event that produces the input pulse and the logic output pulse from the CFD will be a constant, which can be adjusted by the "WALK" control. The positive +5VDC outputs of the CFDs are fed to a coincidence circuit that produces a logic pulse when all of its **enabled** inputs see input pulses within the selected **resolving time** (user selectable within two ranges: "fast coincidence" 10-100ns or "slow coincidence" 100-1000ns). The output pulses from the coincidence circuit are fed to a gate generator and delay module, after which, the suitably stretched and delayed gate signal is sent to the "gate" input of the MCA.

The amount of delay and the gate width in the delay module should be adjusted to meet the requirements of the coincident gate mode of the MCA. This requirement is that the gate pulse begin before the peak of the analog input signal and last for at least 0.5μsec beyond the peak. The coincidence gate requirement suppresses background events and makes the Compton scatter events stand out clearly in the resulting pulse height spectrum without the use of heavy shielding.

APPENDIX C: SCINTILLATION COUNTER EFFICIENCY CALCULATIONS

A significant complication in the analysis of the data on the differential cross section is the fact that the target is not "thin", i.e. the mean free paths of the incident and scattered photons suffer substantial attenuation as it passes through the target material, and the scattered photons suffer substantial attenuation in their passage out of the target. The effects of these attenuations on the counting rate obviously depend on the position of the detector. A count must therefore be taken of these thick target effects in order to derive accurate values of the differential cross section from the measured counting rates at various scattering angles.

As in all cross section measurements, the necessarily finite sizes of source, target and detector introduce into the analysis geometrical factors that require laborious multidimensional integrations for their evaluations. In our experiment we have a divergent beam of photons from a radioactive source of finite size that can interact at various depths in the target within certain ranges of solid angle to produce scattered photons that traverse the detector would be a convolution of the differential cross

section with geometrical and attenuation factors represented by a multiple integral over at least ten variables with hideous limits of integration. The only practical way around this kind of mess in particle physics experiments where the highest possible precision is required is the "Monte Carlo" technique in which the sequence of physical processes from emission to detection is sampled by use of appropriate distribution functions to represent the various possible processes, and random numbers to select the outcome of each process.

Here we outline an approximate analytical treatment of our problem based on several simplifying assumptions. The formulation is suitable for numerical computation on a modest computer. We will consider only single scattering events. We call R and H the radius and length, respectively, of the cylindrical scintillators which are the sensitive elements of the target and scatter counters. We assume that the source is so far from the target scintillator that the incident beam may be considered uniform and parallel (i.e unidirectional). We assume that the distance D of the scatter counter scintillator from the target is so large that the detected portion of the scattered radiation may be considered to comprise a parallel (but not uniform) beam.

Consider the scatterings that occur within a solid element of volume $rd\phi drdz$ at a position in the target scintillator with cylindrical coordinates r,ϕ,z. As can be deduced with the aid of Fig 5, the distance x of this element from the point of entry of the incident photons into the target scintillator is given by the expression

$$x = R\{[1 - (q\sin\phi)^2]^{\frac{1}{2}} - q\cos\phi\}, \qquad (C1)$$

where $q = r/R$. Similarly, for photons scattered from the point P at the angle θ, the distance y of the element from the point of exit is

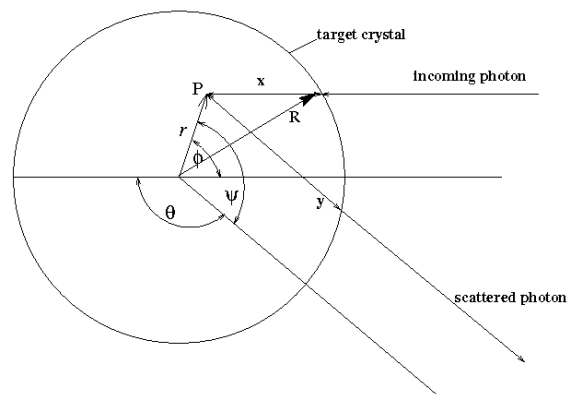$$y = R\{[1 - (q\sin\psi)^2]^{\frac{1}{2}} - q\cos\psi\}, \qquad (C2)$$

FIG. 5: Diagram of the Compton scattering geometry.

where $\psi = \pi - \theta + \phi$. We call α the total linear attenuation coefficient (units of cm^{-1}) of the target plastic

scintillator for the incident photons, $\beta(\theta)$ the total linear attenuation coefficient of the plastic for photons scattered at angle θ, and $\gamma(\theta)$ the total linear attenuation coefficient of the scatter counter NaI scintillator for those scattered photons. The efficiency for detection of scattering events that occur at a given position in the target scintillator is $\exp(-\beta y)[1 - \exp(-\gamma H)]$ which represents the probability that the scattered photon will escape from the target counter multiplied by the probability that the scattered photon interacts in the scatter counter.

We must now find the average of this efficiency over the target scintillator. Recalling the assumption that the incident beam is parallel and uniform, the weighting factor is $I_0 \exp(-\alpha x)$ which is the intensity of the incident beam at the point of interaction inside the target scintillator. We can now write for the average efficiency the expression

$$\eta(\theta) = \frac{\int \exp(-\alpha x) \exp(-\beta y)[1 - \exp(-\gamma H)]dV}{\int \exp(-\alpha x)dV} \quad \text{(C3)}$$

where the integrals are computed over the volume of the target scintillator. We note that $\eta \to 1$ as $\alpha \to 0, \beta \to 0$.

The total attenuation coefficients are functions of the energy of the scattered photon and the energy of the scattered photon is a function of the scattering angle. According to the Compton theory,

$$E_\gamma(\theta) = \frac{E_0}{1 + (E_0/mc^2)(1 - cos\theta)}. \quad \text{(C4)}$$

In the energy range from 0.2 to 0.7 MeV, the total attenuation coefficient in sodium iodide can be fairly represented by the formula

$$\mu = 0.514(\frac{E}{100keV})^{-0.368} + 5.51(\frac{E}{100keV})^{-2.78}cm^{-1}, \quad \text{(C5)}$$

and in plastic by the formula

$$\mu = 0.177(\frac{E}{100keV})^{-0.37}cm^{-1}. \quad \text{(C6)}$$

The quantity η can be evaluated as a function of θ by numerical integration.

The Franck-Hertz Experiment

MIT Department of Physics
(Dated: September 5, 2011)

These experiments measure two phenomena encountered in collisions between electrons and atoms: quantized excitation due to inelastic scattering, and ionization. The experiments also provide an opportunity to explore the thermionic emission of electrons and space charge limited current in a vacuum tube.

1.   PREPARATORY QUESTIONS

1. Considering that the energy of the first excited state of the mercury atom is about 5.0 eV above that of the ground state, what is the maximum amount of energy that an electron with 4.0 eV of kinetic energy can impart to a mercury atom with which it collides? Same question for a 6.0 eV electron.

2. Prepare a plot of the mean free path (in mm) of electrons in mercury vapor against the temperature (in degrees Celsius) of the tube in the region of interest. You should assume the following:

    - The cross section of a mercury atom-electron collision is geometrical (i.e. $\sigma = \pi R^2$, where R is the radius of the outer electronic shell of the mercury atom).

    - The mercury vapor in the tube is in thermo-dynamic equilibrium with liquid mercury. The vapor pressure of mercury is tabulated in [?].

3. Plot the expected curve of current against accelerating voltage in the Franck-Hertz experiment with mercury vapor, showing the positions of the peaks and valleys on an absolute voltage scale.

2.   Introduction

Franck and Hertz described the first observation of quantized excitation in 1914, one year after Bohr published his theory of the hydrogen atom with its concept of quantized energy states. They discovered that electrons moving through mercury vapor with an energy greater than or equal to a critical value near 4.9 eV can excite the 2536 Å line of the mercury spectrum. Electrons with less than the critical energy bounce elastically when they collide with mercury atoms and fail to excite any electromagnetic emission. The experiment provided crucial evidence in favor of the Bohr theory.

A version of the Franck-Hertz experiment, employing a mercury-filled vacuum tube with four electrodes made by the Leybold Company, is described in References [? ?] to which the reader is referred for a discussion of the physical principles and the measurement objectives of the Franck-Hertz experiment.

Experiments on the related Ramsauer-Townsend effect are described in Section 7.

3.   Apparatus

The present Junior Lab version of the experiment uses a different version of the equipment which consists of a mercury-filled triode and an oven with glass windows through which one can view the action. A power supply and control circuit built in the Junior Lab shop provides adjustable filament voltage for heating the cathode, adjustable accelerating grid voltage, and an adjustable retarding voltage. The same triode tube and power supply are used in the measurement of the ionization potential.

3.1.   Mercury Filled Triode

The experiments on the excitation and ionization of mercury atoms are carried out with a mercury-filled triode which is a sealed glass envelope containing three electrodes and a drop of mercury.[1] The experiments will be performed with the three configurations of the tube and associated circuits illustrated in Figure 1 and, in more detail, Figures 3, 4, and 7. The three electrodes are:

- a cathode which emits electrons when raised to a temperature of several hundred degrees by application of a voltage V_F to a heater filament,

- a perforated grid which is set at a positive potential V_{gc} relative to the cathode so that electrons emitted by the cathode are drawn toward it,

- an anode (counter electrode plate) which is connected to an ultra-sensitive Keithley electrometer for the measurement of the anode current I_a.

In the Junior Lab apparatus, the distance from the cathode to the perforated grid is 8mm while the distance between the grid and the anode is small (of order 1mm).

---

[1] Mercury is an ideal element for a study of excitation phenomena because its vapor is monatomic and its vapor pressure can be readily controlled over the range useful for this experiment by adjusting the temperature in the range from room temperature to 200°C.
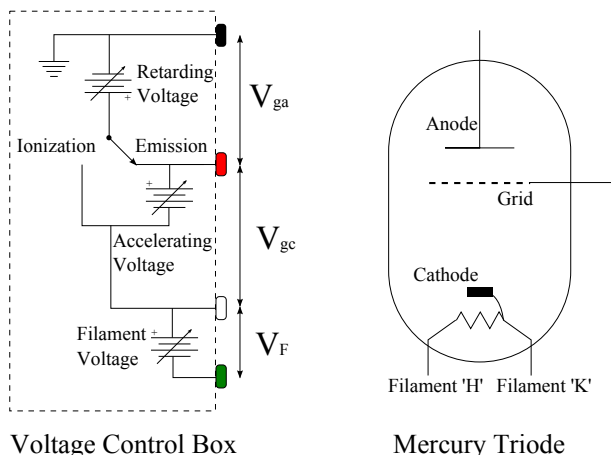
FIG. 1: Schematic illustrations of the mercury-filled triode and the voltage control box.

All of the measurements in these experiments can be made with total tube currents (i.e. cathode current = anode + grid current) of 1000 nA or less. To prolong the useful life of the tube care should be taken not to exceed 1000 nA.

3.2.   Voltage Control Box

The voltage control box, built by Junior Lab staff, is used to supply the desired voltages to the mercury-filled triode. The control box functions as three variable voltage supplies, shown in Figure 1:

- the filament voltage V_F, which controls the temperature of the cathode

- the accelerating voltage V_{gc}, between the grid and the cathode

- the retarding voltage V_{ga}, between the grid and the anode.

The values for the voltage supplies can be measured using the "Isolated D.C. Voltmeter" outputs. These outputs are designed for use with a voltmeter that does not have any connection to the wall or ground, i.e. a multimeter. See Section 3.4 for how to connect any of the circuit outputs to an oscilloscope.

It is wise to start each session by disassembling whatever wired-up circuit the previous users may have left. The only way to know for sure how a circuit is connected is to wire it yourself.

The control box has four circuit outputs which are color coded:

- Black is the common ground. It should be connected to the banana jack with the ground symbol near the anode connection on the oven chassis. This will establish a common ground.

- Red is connected to different points for different measurements during the experiment.

- White goes to the 'K' side of the filament, which determines the potential at the cathode. In our boxes, this is the banana jack on the right side.

- Green goes to the 'H' side of the filament, which determines the electrical power going through the filament (which has a fairly low resistance).

3.3.   Electrometer

An ultra-sensitive Keithley Model 614 electrometer is used to measure the current from anode to laboratory ground. (**Be sure to check the zero set**.) It is essential that the input cable be kept stationary during measurements. Flexing or moving even high quality cable may generate currents due to the triboelectric effect. Make current measurements as follows:

1. Turn the Model 614 on and allow one hour warm up.

2. Depress ZERO CHECK.

3. Select Volts function and the 0.2 V range. Adjust the voltage zero potentiometer with a small screwdriver to obtain a displayed reading of 0.00000. Adjustment on this range assures a proper zero on all other functions and ranges.

4. Select Current function, then appropriate units and range.

5. Apply input (be sure to use the BNC-Triaxial adapter!) and release ZERO CHECK.

6. Take measurement.

The electrometer has an analog output (2V full scale of display) in the back of its chassis which may be connected by a coaxial cable with grounded sheath to an oscilloscope or other voltmeter. The analog output can add noise to the signal which can be decreased using a low pass filter.

3.4.   Oscilloscope Setup

In this experiment you may wish to use an oscilloscope to measure a voltage difference where neither of the measurement points are at the ground potential (most notably, the accelerating voltage). This **cannot** be done using a banana-to-BNC connector from the voltage control box isolated voltmeter output, because the oscilloscope will make a connection between the negative output and ground. As neither of the outputs are supposed to be at the ground potential, this will have adverse effects on the circuit.

Instead, a floating voltage measurement may be set up using two oscilloscope probes:

1. Check that the oscilloscope probes are $10\times$ probes or that the probes are set to $10\times$. This is needed to increase the impedance of the probe-oscilloscope-ground connection and prevent the measurement from affecting the control box outputs.

2. On the oscilloscope, go to the Channel 1 menu and change the probe setting to $10\times$ or 10:1. Do the same for Channel 2. This tells the oscilloscope you are using $10\times$ probes.

3. Connect the probes to the voltage difference on the control box as shown in Figure 2. The probes can be connected to the actual circuit outputs or the isolated voltmeter outputs.

4. Use the math function built into the oscilloscope to subtract channel 1 from channel 2.

The math function displayed is the voltage difference. When saving data from the oscilloscope, the math function will not be saved. Make sure both channel 1 and 2 are saved so the math function can be reconstructed during analysis.

3.5. Oven

Several sections of this experiment require the mercury filled triode be heated above room temperature to increase the mercury vapor pressure. A ceramic heating element is situated below the triode and is used to heat the apparatus. Plug the oven electrical cord into the variable AC source (variac) and the variac into the wall outlet. The variac can then be used to set the oven temperature. **WARNING:** The heater should never receive more the 75 volts AC.
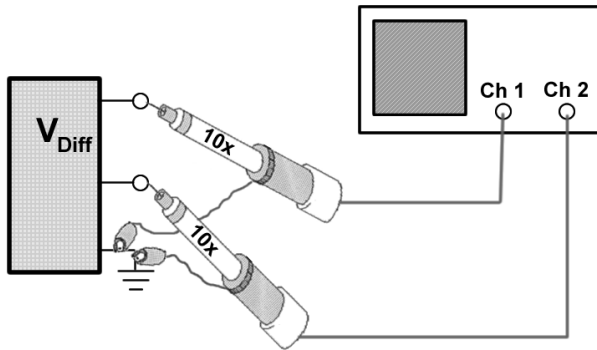

FIG. 2: The setup necessary to measure a floating voltage from the voltage control box with an oscilloscope.

3.6. Grounding

The electrometer and oscilloscope make connections between the negative input from the BNC cable and the ground of the electrical outlet. To prevent ground loops from affecting the experiment, **the voltage control box, electrometer, and oscilloscope must all share the same ground.** This is done by plugging all three boxes into the same wall circuit. The electrical outlets in lab are labeled with numbers indicating which circuit each outlet is on.

4. Thermionic Emission of Electrons and Space Charge Limited Current

Consider first the situation in the tube connected as shown in Figure 3. At room temperature the vapor pressure of the mercury is so low that the mean free path of electrons emitted by the cathode is large compared to the dimensions of the tube ($\sim$8 mm). When the cathode is heated by the filament, it emits electrons in a process called thermionic emission. In thermionic emission, electrons near the top of the Fermi distribution in the metal penetrate the potential barrier at the surface and escape. The kinetic energies of the emitted electrons roughly follow a Maxwell-Boltzmann distribution with a mean energy E_0 near kT, where T is the cathode temperature. In the steady state, with the grid at a positive potential relative to the cathode the emitted electrons form a cloud of negative charge over the surface of the cathode. This cloud changes the local electric field, suppressing electron emission by forcing lower energy electrons back to the cathode. This condition is known as space charge limited current. The physics of thermionic emission and space charge limited current is discussed in [**?**] for a tube with ideal cylindrical geometry. Our tube, designed for other purposes, has a different geometry that does not lend itself to a "clean" experiment in thermionic emission. Nevertheless the qualitative characteristics of space-charge limited current can be observed with it.

The first part of the experiment is an exploration of the dependence of the total tube current on two quantities: (1) the filament voltage which controls the temperature of the cathode and thus the emitted current density and (2) the accelerating potential between the electron emitting cathode and the grid. You will find a filament voltage which will be used throughout the rest of the experiment. The measurements are made at room temperature ($20 - 25°$C).

4.1. Procedure for Exploring Thermionic Emission

1. Connect the tube as shown in Figure 3. Set the toggle switch to 'emission'. Set the filament voltage V_F and the retarding voltage V_{ga} to their lowest values ($\sim$ 1.2 V and 0V, respectively).

2. In order to measure the TOTAL tube current, the grid and anode currents should be summed at the electrometer input with coaxial cables and a BNC 'T' connector. Use a two-prong banana plug-to-BNC adapter at the grid terminal on the triode tube, taking care as to which side of the banana plug adapter is connected to the grid's banana jack.

3. Set the accelerating voltage V_{gc} to its highest voltage, about 60V. Set the retarding voltage control so that $V_{ga} = 0$. Increase V_F in small steps until the total current is between 100 and 1000 nA. Tabulate and plot the total current (grid + anode) I_{ag} versus V_F as you proceed.

4. Set V_F at a value for which I_{ag} is in the range 100 - 1000 nA when $V_{gc} \approx 60$ V. Allow several minutes for the current to stabilize to ensure the current will remain in the desired range. Do not allow the current to remain above 1000nA, as that will shorten the life of the apparatus.

5. Now, tabulate and plot I_{ag} as a function of V_{gc} , shifting scales on the electrometer as needed. You may find that the current drifts substantially at any given setting of V_F and V_{gc}. Don't panic. **The purpose of this section is to obtain a rough idea of how the cathode current, i.e. the total tube current, is affected by the cathode temperature and the accelerating voltage. Don't spend a lot of time trying to perfect these particular data. Since the tube characteristics change significantly with usage, you should start each session with a similar rough check of I_{ag} versus V_F with V_{gc} set to ~60V and the oven at room temperature.**

5.   Ionization Potential of Mercury

In this next experiment the tube is connected as shown in Figure 4 so that the anode is maintained at a negative potential of a couple of volts with respect to the cathode. In this condition it is energetically impossible for any electrons to reach the anode. When the grid potential is made positive with respect to the cathode, electrons are accelerated to the grid. Some pass through the grid into the space between the grid and anode, but all are eventually pulled back and collected by the grid. However, if the electrons that enter the space between the grid and anode have sufficient energy to ionize the mercury atoms, then the resulting positive mercury ions are drawn to the anode and a positive current is registered by the electrometer. The experiment consists of measuring the anode current as a function of the grid-to-cathode potential difference. Analysis of the current-voltage relation yields a measure of the ionization potential.

The first task is to determine the optimum oven temperature for measurement of the ionization effect. If the
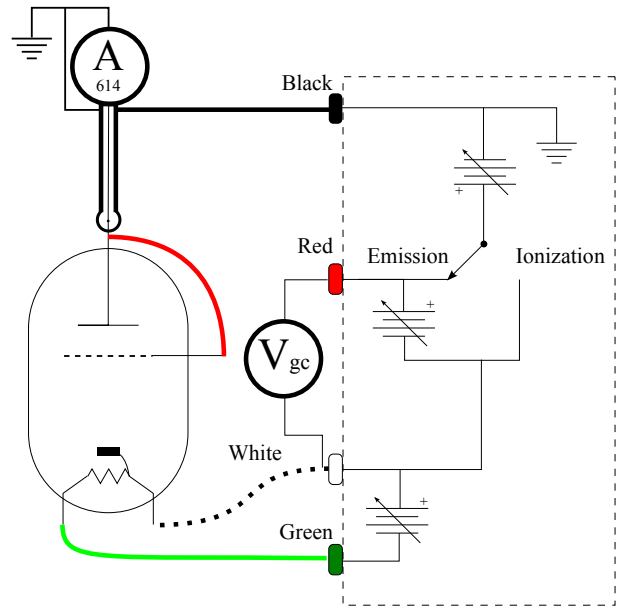

FIG. 3: Schematic diagram of the tube and circuit for measurements of space charge limited current from thermionic emission. The voltmeter labeled V_{gc} is the 'Isolated D.C. Voltmeter' outputs connected to a floating (non-grounded) voltmeter.

vapor pressure of the mercury is too low, then electrons entering the grid-to-anode region with sufficient energy to cause ionization will have a small probability of collision (long mean free path) and the ion current collected by the anode will be too small for accurate measurement. If the vapor pressure is too high, then electrons will suffer inelastic collisions in the space between the cathode and grid as soon as their energies slightly exceed the energy required to raise mercury atoms to their first excited (not ionized) state and will therefore never attain sufficient energies to cause ionization.

5.1.   Ionization Potential: Procedure

1. Connect the tube as shown in Figure 4. Make sure that you switch the toggle switch to 'ionization'.

2. Set the filament voltage at the value which gives a total tube current in the range 100–1000 nA when $V_{gc} \approx 60$ V, as determined in Section 4.

3. Set the accelerating voltage V_{gc} to 25 V (measure with the floating voltmeter connected between cathode and grid), which is a few volts above the ionization potential. You should see a blue glow from the cathode. This is lower-energy photon emission of the ionizing mercury in the visible spectrum. If you do not see this glow, raise V_{gc} or V_F until you see it, then return to your original settings.
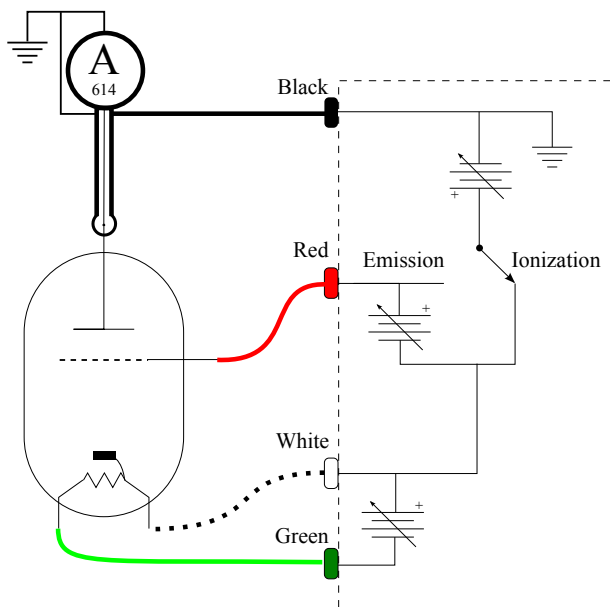
FIG. 4: Schematic diagram of the mercury-filled triode in the configuration for measurement of the ionization potential of mercury. After you complete the connections check all the potential differences in your setup with the floating Fluke voltmeter and verify that they are consistent with the instructions. Note that the mode-selecting toggle switch should be in the 'Ionization' position.

4. Set the retarding voltage so the cathode potential is 2 V above the anode potential.

5. Measure and plot the anode current as a function of oven temperature between 30 and 130 degrees Celsius in steps of 10 degrees and then repeat as it cools down back to room temperature. (**DO NOT EXCEED 200°C**). Explain what you observe in terms of the effect of temperature on the mean free path of the electrons. Discuss the time constants involved in the determination and setting of the desired operating temperature and how you might optimize this in future sessions. In light of your results, select an optimum temperature for the following measurement of the ionization potential and adjust the variac so as to maintain that temperature. When you repeat the experiment in later sessions, you might consider varying the oven temperature to measure its effect.

6. Set the variac at the optimal temperature setting and tabulate and plot the anode current I_a as a function of the accelerating voltage V_{gc}, using the picoampere and nanoampere scales. **To avoid damaging the tube by a runaway discharge do not exceed an accelerating voltage of 25 V in this part of the experiment.**

5.2.   Ionization Potential: Analysis

Estimate the value and uncertainty of V_{gc} when ionization just begins in the region between the grid and the anode. Using results from the subsequent experiment on the excitation potential, you will be able to correct your result for the effect of the contact potential.

6.   The Excitation Potential of Mercury

In the excitation potential experiment the tube is connected as shown in Figure 7 where the grid is at a higher potential then the cathode and anode. An idealized description of the excitation potential experiment can be made using the following assumptions (all inaccurate in varying degrees as the previous experiments have shown):

- All electrons emerge from the cathode with zero velocity.

- The number of electrons emerging from the cathode is unaffected by the accelerating field between the cathode and grid.

- The energy of an electron is unaffected by collisions with the mercury atoms as long as their energy is below that of the first excited state. Therefore all electrons at a given position between the cathode and grid have the same energy.

- All electrons that pass through the grid with energies less than the retarding potential between the grid and anode are pulled back and collected by the grid; all electrons with energy more than the retarding potential are collected by the anode.

- The inelastic cross section of mercury for electrons with energies above the critical value is so large that such electrons travel a negligible distance before suffering inelastic collision.

Were all these assumptions valid, a plot of anode current I_a against accelerating voltage V_{gc} would appear as shown in Figure 5. The separation between successive current increases (or decreases) is equal to the excitation potential of the first excited state of the Hg atom. The width of the minima in negative current is determined by the retarding potential between the grid and the anode. The difference between the accelerating voltage at the first drop and the excitation potential is the difference between the work functions of the cathode and grid metals, i.e. the contact potential between the two metals. In reality the I_a versus V_{gc} curve will depart considerably from the ideal for a variety of reasons.

Figure 6 illustrates the electric field with the voltages set for the measurement of the excitation potential in the idealized case of plane parallel electrodes. Also shown are the trajectories of two electrons, each interrupted by elastic and inelastic collisions. At gas pressures so low
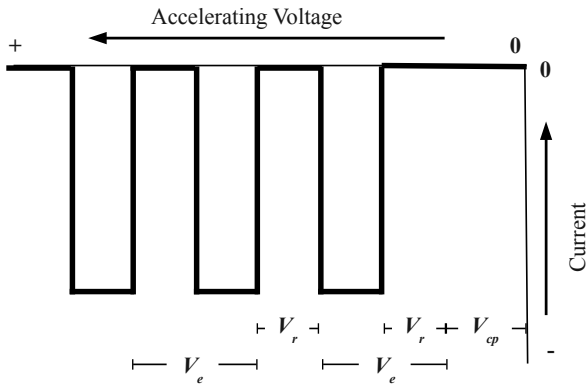
FIG. 5: Plot of anode current against accelerating voltage V_{gc} implied by set of idealized assumptions. V_{cp} is the contact potential.

that the mean free path of the electrons is large compared with all relevant distances, the motion is ballistic and the fraction of the electron current intercepted by the grid is approximately the fraction of area covered by the fine grid wires. At gas pressure so high that the mean free path is short compared with all dimensions, including the wire diameter, the electron orbits jitter along the field lines. Regardless of their energy, they are mostly intercepted by the grid since most of the field lines end there.
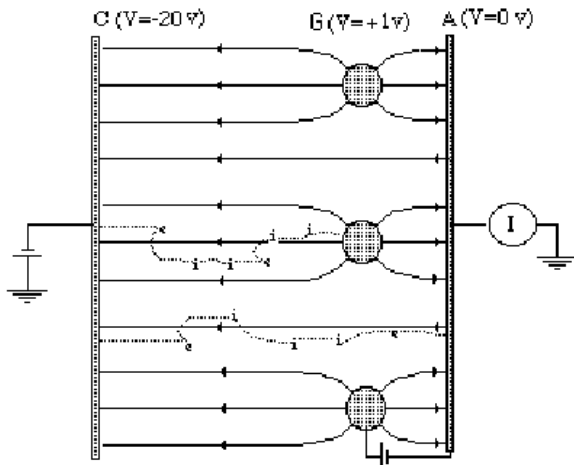

FIG. 6: Schematic illustration of the electric field lines in the measurement of the excitation potential. Two electron trajectories are illustrated. Elastic and inelastic scatterings are indicated by "e" and "i", respectively. One electron is caught by the grid G. The other makes it to the anode A.

Note that the lowest excited state of mercury is the 6^3P_0 state, which is metastable: a dipole transition to the ground state is forbidden. Its lifetime is $\sim 10^5$ times that of ordinary allowed transitions. As the electrons

accelerate toward the grid they acquire sufficient energies to excite a mercury atom in the ground state to the 6^3P_0 state. Because the excited atoms decay slowly, their number builds up to the point where most of the electron-mercury atom interactions become elastic collisions off of excited atoms. The 6^3P_1 state is not metastable and decays immediately by emission of a 2536 Å photon. Franck and Hertz detected these photons through a window in their tube. Having measured the threshold voltage V at which the photons appeared, they could derive a value for $h = Ve\lambda/c$. The agreement with the values obtained previously by Planck, Einstein, and Bohr from their theories of the blackbody spectrum, the photoelectric effect, and the hydrogen spectrum, respectively, was a striking and historic confirmation of the new quantum theory.

6.1.   Excitation Potential of Mercury: Procedure

1. For the excitation potential measurement connect the tube as shown in Figure 7. Check all the potentials with the floating voltmeter.

2. Set the oven temperature at so that the mean free path of the electrons is short compared to the cathode-grid distance.

3. Set the filament voltage to a value that would give a <u>total</u> tube saturation current (anode+grid) in the range 100–1000 nA <u>at room temperature</u>, as measured in Section 4.

4. Set the retarding voltage at a value between 0.1 and 2 volts. Electrons that pass through the grid with less than enough energy to overcome the retarding potential are turned back to be collected by the grid. Higher energy electrons reach the anode and are registered as a negative current by the Keithley electrometer.

5. By hand or by using the ramp function, sweep the accelerating voltage, V_{gc}, from 0 to 60 volts and note the occurrence of maxima and minima in the anode current I_a (probably best done on the picoampere scale). Measure and tabulate the values of V_{gc} at the maximum and minimum values of the current, and the corresponding maximum and minimum anode currents. In the measurement of the excitation potential, the accelerating voltage is between the cathode and grid. Neither of these electrodes is at ground potential. Therefor, if V_{gc} is measured on the oscilloscope, the measurement must be set up following Section 3.4.

6.2.   Excitation Potential: Analysis

Derive from your data the value and error of the excitation potential. Referring to the plot of I_a vs. V_{gc},
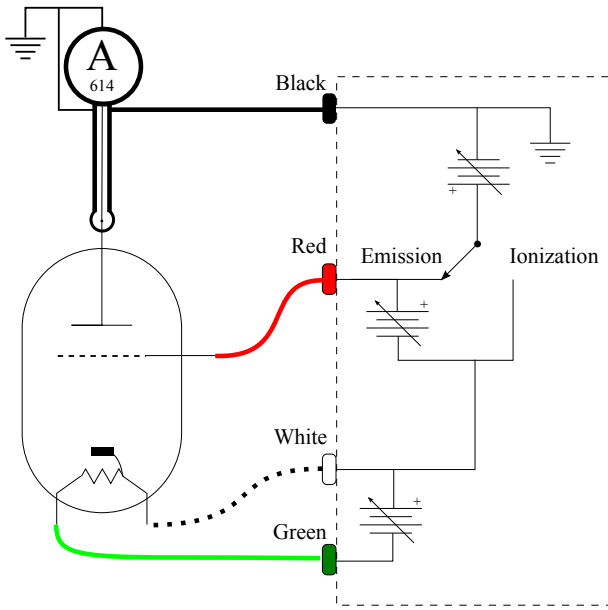
FIG. 7: Circuit arrangement for measurement of the critical excitation potential.

at what point between each successive pair of minima do you think the next set of excitation events begins? Derive an estimate of the value and error of the contact potential (see [? ?] for a discussion of the physics of contact potential) between the cathode and grid. You will need to correct the measurement of the ionization potential in section 5 by this quantity.

7.   The Ramsauer-Townsend Effect

   "The Ramsauer-Townsend effect may be thought of as a diffraction of the electron around the rare-gas atom, in which the wave function inside the atom is distorted in just such a way that it fits on smoothly to an undistorted wave function outside" [?].

The result is a near extinction of the scattered $\ell = 0$ partial wave (s-wave) and a consequent suppression of the scattering cross section. The effect can be observed only when it occurs at an energy below that of the first excited state of the scattering atom. Otherwise it is masked by inelastic scattering. Noble gases provide especially suitable targets because they are monatomic, their outer electrons are in a closed shell, excitation of their lowest excited state requires a comparatively large amount of energy, and they do not attach electrons to form negative ions.

The Ramsauer-Townsend effect was discovered in 1921, before the invention of wave mechanics in 1926 and the discovery of the electron diffraction by Davisson and Germer in 1927. Its explanation in terms of the scattering of matter waves — first suggested by Bohr and worked out in detail by Mott and Massey[?] and others on the basis of the Schrödinger equation — was one of the early successes of the new wave mechanics.

The theoretical treatment of the elastic scattering of an electron by a noble gas atom requires the solution of the three dimensional Schrödinger equation for a free electron incident on a spherically symmetric attractive potential. This can be done by the method of partial waves as explained in various intermediate texts on quantum mechanics (e.g. [? ? ? ?]).

The well-known model of a 1-dimensional scattering problem, solved in many elementary quantum mechanics texts, is often put forward as exhibiting the essential features of wave mechanical behavior that one observes in the Ramsauer-Townsend effect. The 1-D model bears a relation to the real 3-D scattering problem that is similar to the relation which the problem of the energy levels of a particle in a 1-D box bears to the 3-D problem of the hydrogen atom, i.e. suggestive, but fairly distant as far as numerical agreement is concerned. In the 1-D scattering problem, one finds the transmission coefficient has maxima at a series of discrete energies for both positive and negative potential wells, whereas in the 3-D case there is only one maximum, and that only for an attractive potential.

The present experiment is described in Reference [?]. A xenon-filled tube is commercially available in the form of a thyratron switch tube (2D21). The depression of the scattering cross section at the critical energy is indicated by the reduction in the intensity of an electron beam directed from the cathode to the anode.

7.1.   Ramsauer-Townsend: Apparatus

The apparatus and circuitry are illustrated schematically in Figure ??. Electrons emitted from the heated cathode are accelerated through a small potential difference toward the "grid" which is is actually a metal box inside of which there is no electric field. The electrons that enter the box "drift" through it, and those that emerge from the far end are collected by the anode and measured as a current by the Keithley electrometer. At high vacuum, when the xenon gas is condensed on the glass walls of the thyratron by cooling in liquid nitrogen, the fraction of atoms emitted by the cathode that reaches the anode depends only on the geometry of the electrodes. When the xenon is vaporized, the fraction reaching the anode is reduced by elastic scatterings which deflect electrons from the trajectories that would otherwise bring them to the anode. The amount of the reduction is a measure of the elastic scattering cross section of the xenon atoms. One obtains the required data by measuring the anode current as a function of the accelerating voltage both with and without the xenon vapor.

7.2. Ramsauer-Townsend: Procedure

1. With all voltages set to their minimum values, connect the circuit as shown in Figure ??, using the Keithley electrometer to measure the anode current and an isolated multimeter to measure the accelerating voltage.

2. Dip the tip of the thyrotron in liquid nitrogen to freeze out the xenon. **(To reduce the likelihood of cracking the tube by thermal shock the filament voltage should always be zero when the tube is dipped into the liquid nitrogen.)**

3. With an accelerating voltage of 5 volts increase the filament heater voltage until the anode current is 10 μA.

4. Leaving the filament voltage at the value just found, tabulate and plot the anode current (shifting to the nanoampere or picoampere scales where necessary) as a function of the accelerating voltage from 5V down to zero both with and without the xenon vapor frozen out, taking special care in the region between 0 and 2V where the interesting phenomenon occurs. It is wise to make your two sets of measurements at the same sequence of voltage values so that you can easily calculate the ratio of currents with and without the xenon frozen out. Compute and plot in your lab book the ratio against the accelerating voltage as you go along to monitor the trend of the data.
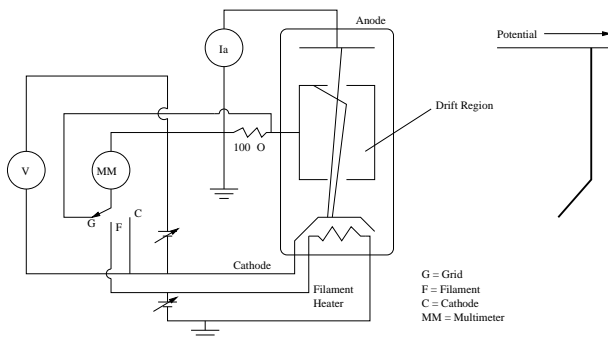

FIG. 8: Schematic diagram of the 2D21 thyratron and circuit used in the measurement of the xenon elastic scattering cross section using low energy electrons. The trajectories of two electrons are shown, one scattered by a Xenon atom and the other reaching the anode undeflected. Adjust the filament voltage so that the anode current measures $\approx 10\mu$A with an accelerating voltage of 5.0 V. The vapor pressure in the tube is approximately 0.05 Torr at room temperature (≈ 0.001 Torr at 77K) and the length of the scattering volume is 0.7cm.

The liquid nitrogen needed to freeze out the xenon is available in a 240L dewar in the lab. **Handle it care-**

fully and wear goggles! Do not fill the Dewar flask to the brim. The tube need only be partially immersed to bring the xenon below its boiling point.

7.3. Ramsauer-Townsend: Analysis

The discussion of the experiment's interpretation by Kukolich [**?**] may be a little obscure. The following remarks may help. Call $I_0(V)$ the measured current with the xenon frozen out when the accelerating potential is V, and $I(V)$ the measured current at the same accelerating voltage with the xenon gas free in the tube. If every electron scattered by a xenon atom were effectively removed from the beam, then these two measurements would be related by the equation

$$I(V) = I_0(V)e^{[-n\sigma(V)l]}, \qquad (7.1)$$

where n is the number of xenon atoms cm^{-3}, $\sigma(V)$ is the cross section of the xenon atoms for inelastic scattering the electrons of energy eV, and l is the path length from cathode to anode. The desired measure of the cross section would then be

$$\sigma(V) = \frac{1}{nl} \ln\left[\frac{I_0(V)}{I(V)}\right] \qquad (7.2)$$

Actually, not every scattered electron is removed from the beam due to the poor geometry of the thyratron tube in this particular application. Therefore the value of the cross section derived from the simple analysis of the present experiment, assuming the quantity nl were accurately known, is somewhat less than the true value of the total inelastic scattering cross section.

Plot $\ln\left[\frac{I_0(V)}{I(V)}\right]$ against V. Discuss the sources and magnitudes of the errors and indicate your error estimates on the plot. Comment on the position of the minimum and its relation to the size of the xenon atom.

8. Possible Theoretical Topics for Oral Exam

- Richardson's law

- Child's law

- Distribution in energy of electrons emitted by a hot metal

- Propagation of electrons through Hg vapor

- Transmission of electrons through a rectangular potential well

- Partial-wave scattering theory of the Ramsauer-Townsend effect

Relativistic Dynamics

MIT Department of Physics
(Dated: September 5, 2011)

This experiment is a study of the relations between energy, momentum and velocity of relativistic electrons. Using a spherical magnet generating a uniformly vertical magnetic field to accelerate electrons around a circular path and into a narrow slit, you will be able to predict relationships between properties of high velocity electrons. The experiment's goal is to compare your data with the models predicted by classical and relativistic dynamics. Additionally you will be able to determine the value of the electron charge to mass ratio, the electron mass, and subsequently the electron charge.

1.   Preparatory Questions

1. Compare the classical and relativistic relations between energy, momentum and velocity.

2. The source of high-energy electrons used in this experiment is the radioactive isotope ^{90}Sr and its decay product ^{90}Y. Describe the decay process of these isotopes and the energy spectra of the electrons (beta rays) they emit.

3. How does a semi-conductor diode detector work? Estimate the charge of the signal from a 280 keV electron in Si (0.5 eV per pair)

4. How good a vacuum is necessary for the experiment?

5. Compute the voltage required to cancel the magnetic force on the electrons in the velocity selector when the magnetic field is 110 Gauss. Assume the dimensions of the apparatus given in Figure 1, the book value of e/m, and the validity of relativistic mechanics. (The result will be a clue to where in the selector-voltage range you should search for the maxima in the counting rate for a typical magnetic field.)

6. A velocity selector is made of two parallel plates separated by a distance $d = 0.180 \pm 0.003$ cm. Using the same parameters of the previous problem, a) What is the spread in momentum of electrons that can enter the selector? b) What ΔV do you need to pass the highest and lowest momentum?

1.1.   Units in this lab guide

This lab guide uses Gaussian units in which the force on a moving charge in a static field is

$$\vec{F} = q\vec{E} + \frac{q}{c}(\vec{v} \times \vec{B}).$$

The units are:
 F—dyne
 q—statcoulomb (esu)
 B—gauss
 E—statvolts cm^{-1}
v,c—cm sec^{-1}
  Some useful constants:

$$e = 4.80298 \times 10^{-10} \text{ statcoulombs}$$
$$mc^2 = 511 \text{ keV} = 8.18727 \times 10^{-7} \text{ ergs}$$
$$1 \text{ volt} = 3.336 \times 10^{-3} \text{ statvolts}$$

1.2.   Suggested Progress Check at end of 2nd Session

With the spectrometer magnetic field set to 100 gauss, plot the electron count rate at the detector versus velocity selector voltage (converted to units of β). Also, plot at least three data points of various kinematic energies versus β.

2.   Introduction

Between 1900 and 1910 the relation between the energy, momentum and velocity of charged particles moving at high speeds was a central problem of physics. The fundamental contradictions between Newtonian mechanics and the Maxwell theory of the electromagnetic field, revealed most dramatically in the failures of the Michelson-Morley experiment to detect absolute motion of the earth through the "aether", barred the way to a logically consistent understanding of the deflection of a charged particle by electric and magnetic fields when the particle is moving at a velocity approaching the velocity of electromagnetic waves. Various formulas were derived by Abraham, Lorentz, and Poincare. In 1901 Kaufmann, using the new vacuum techniques pioneered by Thomson, determined the "apparent mass of the electron" by measuring the deflections of the recently discovered β rays from radioactive substances. There was considerable confusion as to whether the experimental results confirmed or contradicted one or another of the

formulas. Then Albert Einstein, at the time an obscure 25-year-old examiner in the Swiss patent office, provided a clear and compelling theory of "the electrodynamics of moving bodies" which came to be called the special theory of relativity. Among its remarkable predictions was the slowing of clocks moving at high speed (demonstrated in the Junior Lab experiment on muon decay), and the non-classical relations between momentum, energy and velocity that are demonstrated in the present experiment [?].

In classical dynamics a particle acted on by a force $\vec{F}$ for a time dt over a displacement $\vec{dr}$ gains momentum $\vec{dp} = \vec{F}dt$ and kinetic energy $dK = \vec{F} \cdot \vec{dr}$.

According to Newtonian dynamics the kinetic energy K, momentum $\vec{p}$, and velocity $\vec{v}$ of a particle are related by the equations

$$\vec{p} = m\vec{v} \tag{2.1}$$

and

$$K = p^2/2m \tag{2.2}$$

where $p^2 = \vec{p} \cdot \vec{p}$ and m is the inertial mass of the particle. In classical mechanics there is no limit on the magnitude of $\vec{v}$.

According to relativistic dynamics (see [?], or other text on special relativity), these quantities are related by the equations

$$\vec{p} = m\gamma\vec{v} \tag{2.3}$$

and

$$E^2 = p^2c^2 + m^2c^4, \tag{2.4}$$

where $E = K + mc^2 = \gamma mc^2$ is the "total relativistic energy." The quantity m is a relativistic invariant and identical with the classical inertial mass, and γ is the Lorentz factor defined by the equation

$$\gamma = (1 - \beta^2)^{-1/2}, \tag{2.5}$$

where $\beta = |\vec{v}|/c$. Solving equation (2.4) for the kinetic energy one obtains

$$K = mc^2 \left(\left[1 + \left(\frac{p}{mc} \right)^2 \right]^{1/2} - 1 \right). \tag{2.6}$$

In the limit of high velocities where $p \gg mc$, equation (2.6) approaches

$$K = pc, \tag{2.7}$$

which is the exact relation between the energy and momentum of massless particles such as photons and neutrinos. For $p < mc$ equation (2.6), expanded by the binomial theorem, becomes

$$K = \frac{p^2}{2m} \left[1 - \frac{1}{4} \left(\frac{p}{mc} \right)^2 + \cdots \right]. \tag{2.8}$$

In the limit of low velocities ($|\vec{v}| \ll c$) where $p \ll mc$, equation (2.8) reduces to the classical relation expressed by equation (2.2).

The electromagnetic force on a charged particle is

$$\vec{F} = q \left[\vec{E} + \left(\frac{\vec{v}}{c} \right) \times \vec{B} \right], \tag{2.9}$$

where q is the invariant charge, $\vec{E}$ and $\vec{B}$ are the electric and magnetic field intensities, respectively, and c is the invariant speed of light. This force law is valid in both classical and relativistic dynamics. In this experiment you will measure the effects of electromagnetic force on the motion of electrons with velocities up to about $0.8c$, and measure directly the relations between $\vec{v}$, $\vec{p}$, and K.

Some useful references related to beta-decay, beta-spectroscopy and this experiment in particular are given in [? ? ? ? ? ?].

3.   Experimental Setup

The apparatus for the present experiment, shown schematically in Figure 1, is contained in a vacuum chamber inside a spherical magnet that maintains a uniform field in the vertical direction. Inside the vacuum chamber are 1) a source of energetic electrons (a minute quantity of ^{90}Sr which emits electrons with a spectrum of energies up to 0.546 MeV yielding a decay product ^{90}Y which emits electrons with a spectrum of energies up to 2.27 MeV), 2) baffles that reduce background counts due to scattered electrons that bounce around the vacuum chamber, 3) a narrow slit in the baffles at the 90-degree position around a circular path from the source, 4) a narrow slit that defines the radius of curvature of the electrons that enter the velocity selector, and 5) a solid state PIN diode detector. The velocity selector has a length of 10 cm and the plate separation in the velocity selector is 0.180±0.003 cm. An electron, emitted with a momentum in a narrow range of magnitude and direction, traverses a helical path of fixed radius in the magnetic field and enters the gap between the velocity-selector plates. The distance from the source to the velocity selector, which is also the diameter of the electron's path, is 40.6 ± 0.4 cm. If the voltage, V, between the plates is adjusted so that the electric force cancels the magnetic force, then the electron passes through the "velocity selector" in a nearly straight trajectory and strikes the PIN diode in which a number of silicon valence electrons proportional to the energy deposited are promoted to the conduction band of the semiconductor and collected as a pulse of charge. The latter is converted by a low-noise preamplifier and precision amplifier into a voltage pulse with an amplitude proportional to the deposited energy which is measured by a multi-channel pulse height analyzer (MCA).

For each of several settings of the magnet current one measures 1) the magnetic field, 2) the voltage across the selector plates that yields the maximum counting rate of

Velocity Selector
Plate Separation = 0.180 ± 0.003 cm
Length = 10 cm

Digital Voltmeter
Flake 8012A

VS   PIN

Preamp
Canberra Mo. 2003BT

Velocity Selector
HV Supply: 0-5000 V
Canberra Mo. 2003BT

Bias Voltage
Supply: 70 V
EG&G Ortec 428

$\otimes \vec{B}$

40.6 ± 0.4 cm

Oscilloscope

Amplifier
Ortec 471

Multi-Channel
Analyzer

^{90}Sr/^{90}Y Source
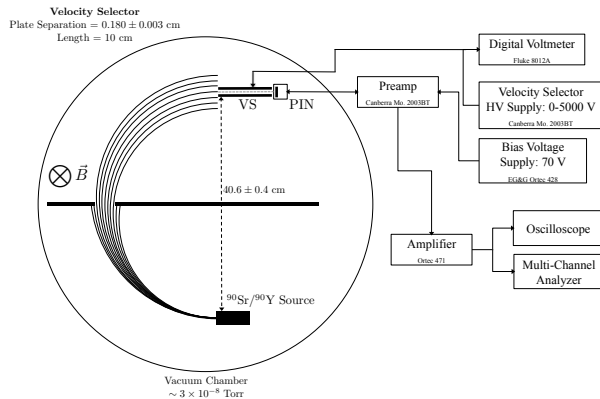
Vacuum Chamber
$\sim 3 \times 10^{-8}$ Torr

FIG. 1: Schematic diagram of the electron trajectory in the apparatus, the particle spectrometer and associated circuitry. The velocity selector is labeled VS, and the diode detector PIN.

pulses in the narrow range of pulse height channels of the MCA corresponding to the energy range of the detected electrons, and 3) the median channel of the pulse height distribution. Given these data, the dimensions of the apparatus, and the energy calibration of the PIN detector one can determine the momentum, energy, and velocity of electrons and estimate the values of e/m, m, and e.

4.   Theory of the Experiment

In the region between the source and the velocity selector, where only a magnetic field exists, the motion is described by the equation

$$\frac{e|\vec{v}|B}{c} = \left|\frac{d\vec{p}}{dt}\right| = \omega|\vec{p}| = \frac{|\vec{v}|p}{\rho}, \qquad (4.1)$$

so

$$B = \left(\frac{c}{e\rho}\right)p, \qquad (4.2)$$

where ρ is the radius of curvature of the particle trajectory under the influence of the magnetic force. Placement of the source, the collimator, and the aperture of the velocity selector on a circle of radius ρ allows only particles with a momentum in a narrow range around $Be\rho/c$ to enter the velocity selector. In the region between the velocity selector plates $\vec{E}$, $\vec{B}$, and $\vec{v}$ are perpendicular to each other so one can write for particles that experience zero deflecting force and go exactly parallel to the plates the relation

$$eE - \frac{evB}{c} = 0. \qquad (4.3)$$

The voltage between the velocity selector plates is known from Faraday's law,

$$V = \oint \vec{E} \cdot d\vec{\ell}, \qquad (4.4)$$

and therefore $E = V/d$. Hence

$$\beta = |\vec{v}|/c = E/B. \qquad (4.5)$$

Thus, for any combination of E and B such that $E < B$, the velocity selector transmits particles with velocities near E/B in a narrow range of magnitudes whose width depends on the geometry of the gap between the plates.

A plot of measured values of B against the ratio E/B reveals the relation between momentum and velocity. According to the classical equation (2.1), the plot would be fit by a straight line with a slope of $(mc^2)/(e\rho)$. Deviation from a straight line as $E/B \to 1$ indicates the failure of the classical relation between momentum and velocity as the velocity approaches c. According to the relativity equation (2.3), a plot of B against $(E/B)[1-(E/B)^2]^{-1/2}$ should be fit by a straight line with a slope of $(mc^2)/(e\rho)$. From the slope and knowledge of the values of c and ρ one can estimate the invariant quantity e/m.

In the experiment it is a good idea to set the magnetic field and then determine the voltage between the selector plates that gives the highest rate of counts of electrons that traverse the circular path and pass between the velocity selector plates to strike the PIN diode detector.

Note that measurements of E and B alone yield a determination of e/m but neither e nor m separately. This is characteristic of all experiments involving only electromagnetic forces. Why is this so? Consider the analogy to the problem of determining the ratio of gravitational to inertial mass of a body moving under the influence of gravity. (Incidentally, the Johnson Shot Noise experiment in Junior Lab yields the measurement of e.)

The PIN diode detector combines the virtues of an ultra-thin entrance window and surface dead layer with a total sensitive thickness sufficient to stop electrons with several hundred keV of kinetic energy. Thus, with appropriate calibration, the PIN diode provides a measure of the kinetic energy of the detected electrons. Plots of the kinetic energy against E/B or against $[1-(E/B)^2]^{-1/2}$ reveal the relation between energy and velocity; the slope of the latter plot yields a value of m (or more conveniently mc^2 expressed in units of keV in terms of which the energies of the calibration X and gamma-ray photons are expressed). A plot of energy against B reveals the deviation of the energy-momentum relation from the classical quadratic form $E = p^2/(2m)$ toward the linear form $E = pc$ valid for a particle moving with a velocity close to c.

5.   Apparatus Details

The magnet consists of a stack of circular air-core coils enclosing a spherical volume and connected in series so as to produce a current distribution over the surface of the sphere which is approximately equal to the ideal smooth distribution required to produce a uniform field inside the sphere. It turns out that the required distribution of
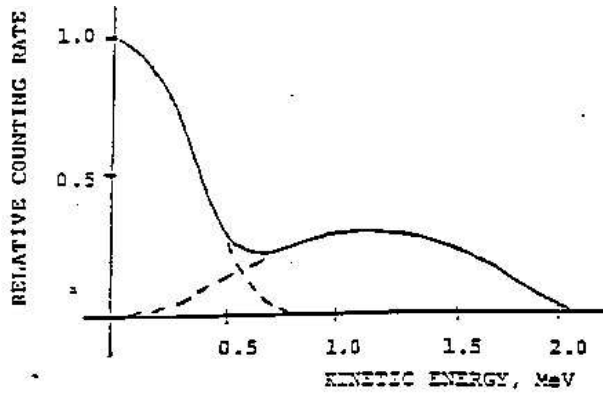
FIG. 2: The β-ray Spectra of ^{90}Sr and ^{90}Y. The actual energy spectrum of the electrons in this experiment will be distorted by energy loss of the electrons in the material of the source and in the thin metal covering over the source.

FIG. 3: Photon detection efficiencies in silicon.

surface current density is

$$J(\theta, \phi) = J_0 \sin \theta, \tag{5.1}$$

where J_0 is related to the magnitude $B_i = |\vec{B}_i|$ of the uniform field inside by an equation that is left for the reader to derive (for hints see Appendix A).

The current for the magnet is provided by a stabilized supply whose output can be as high as 200 volts at low impedance, which means that it can deliver a lethal shock. **Be careful! Turn off the power supply before touching the magnet. Be sure the cooling fan is turned on whenever the current exceeds 3 amperes.**

The coil assembly is split at its equator. The upper hemisphere can be lifted with the block and tackle for access to the spectrometer assembly which is located inside the vacuum vessel under a heavy plastic plate.

The β-ray source, ^{90}Sr, decays with a half life of 28 yrs to ^{90}Y with emission of an electron with a maximum energy of 0.546 MeV. The yttrium nucleus in turn decays with a half life of 64 hrs to ^{90}Zr with emission of an electron with a maximum energy of 2.27 MeV. In each of these steps, a neutron in the nucleus is transformed into a proton with the simultaneous emission of an electron and an antineutrino. Since the two particles emitted in the β-decay process can share the available energy with the recoiling nucleus in any proportion consistent with the conservation of momentum, the energy spectra of the electrons are continuous from zero to the specified maxima (for details see [?]). A sketch of the energy spectrum of electrons emitted by a thin ^{90}Sr source is displayed in Figure 2.

A narrow slit located at the 90-degree position defines the circular trajectory. The velocity selector consists of two aluminum blocks mounted with their faces precisely parallel to each other and tangent to the central electron path at 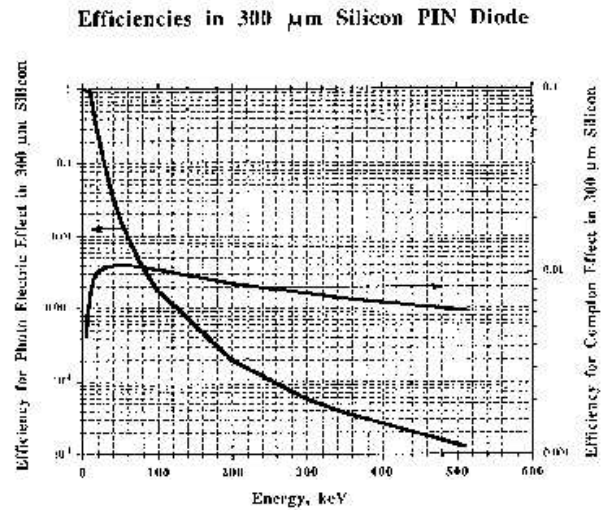the entrance to the gap. The voltage for the velocity selector is provided by a high-impedance high-voltage power supply supplemented by a high-voltage battery.

The detector is a PIN diode shielded from light by a thin film of aluminized Mylar. The PIN diode should be operated with a positive bias of 50 volts (**caution: voltage above 70 volts will destroy it**). A graph of various interaction efficiencies for photons in silicon is shown in Figure 3.

6. Experiment

Check that the vacuum is better than 10^{-4} torr. A good vacuum is essential because multiple small angle scattering of the electrons by residual gas will distort the trajectories. The rms angle of scattering can be estimated by the following approximate formula:

$$\sqrt{\langle \theta^2 \rangle} = \frac{15 \text{ MeV}/c}{p} \sqrt{\frac{X}{X_0}}, \tag{6.1}$$

where p is the momentum measured in MeV/c (1 MeV/c = 5.34×10^{-17} dyne-sec), X is the amount of material in the path measured in gm cm^{-2}, and X_0 is a constant, called the "radiation length" and characteristic of the material. The radiation length of air is 37 gm cm^{-2}.

Set up the pulse height measurement chain, and check the performance at each stage with the oscilloscope.

The magnetic field is measured with a Hall effect magnetometer. **Before every use of the magnetometer check the calibration and the zero setting.** The Hall sensor, fragile and expensive, is a thin wafer of semiconductor attached to the signal leads (see Figure 4). The wafer and its attached wires should be carefully inserted in the protective aluminum tube and the tube inserted in the plastic block that can be placed on top of the plastic cover
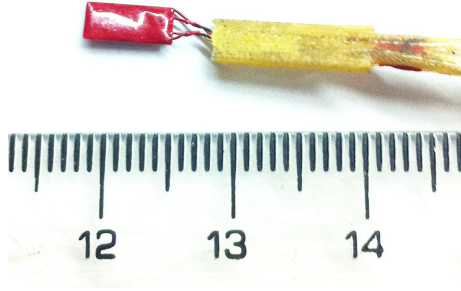
FIG. 4: Hall effect sensor. It is found in at the end of the Hall probe housing.
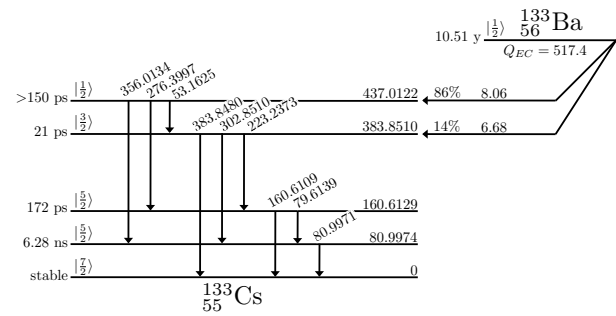

FIG. 5: Decay of Ba-133 to Cs-133 with associated energy levels. The time on the left is the half-life of the state, next to it is the state's spin, and on the right is the energy in KeV. The arrows denote the transitions between energy levels in Cs-133, with energies in KeV. Data taken from the Table of Radioactive Isotopes.

of the vacuum chamber. To measure accurately the vertical component of the magnetic field the plane of the semiconductor wafer must be exactly horizontal. To achieve this condition raise the top hemisphere of the magnet just enough to allow you to place the plastic block with the Hall sensor flat inside the aluminum tube in the middle of the vacuum cover where you can assume the field will be almost exactly vertical. Turn on the magnet current to 5 amperes. Rock the plastic block to find the orientation that yields the maximum magnitude of the field. Then rotate the aluminum tube containing the Hall sensor so that the maximum reading is obtained with the plastic block lying flat on the vacuum cover.

Explore the operation of the experiment, and survey the ranges of the measurements before starting a definitive sequence of measurements:

1. With the magnet current set to give a field of approximately 100 gauss, measure the precise values of the field at several positions above the circular trajectory from source to PIN diode with the magnet closed to ascertain the degree of uniformity of the field and estimate error in the field measurement due to non-uniformity.

2. Calibrate the measurement chain with the X-ray and gamma-ray emissions of the laboratory calibration sources. Be aware of the possibility of a zero offset, i.e., of the 0 channel corresponding to some positive energy. Specially useful for the calibration is the ^{133}Ba source stored in the lead container under the spherical magnet (^{133}Ba decays by electron capture, so in addition to the gamma rays of several energies emitted by the daughter nucleus, the daughter atom, Cs, also emits a K X-ray). You can find the gamma-ray energies by examination of Figure 5 taken from http://ie.lbl.gov/toi.html. The K-shell X-ray energies can be found in various X-ray tables (e.g. CRC handbook).

The cross section for photoelectric interaction of high-energy photons of energy E in matter of atomic number Z varies approximately as ZE. In the energy range from ~ 20 to 100 keV monoenergetic photons interacting in the silicon PIN diode produce a pulse-height spectrum with a prominent photoelectric peak. Above 200 keV the photoelectric interaction cross section is small relative to the Compton scattering cross section. However, you can use the high end (Compton edge) of the distribution of pulse heights produced by recoil electrons from Compton scattering of the photons as a calibration point. In the text of Melissinos you can find a discussion of Compton scattering, and the relevant information for calculating the energy corresponding to the Compton edge of the distribution of pulse heights produced by electrons that recoil from the scattering events. **The first day you should acquire a 2-3 hour (or overnight if possible) calibration in order to generate sufficient events at higher energies for a multipoint calibration.** On subsequent days, a 10-15 minute calibration should suffice at the start of each lab session. Plot as many calibration energies as possible against the median MCA channels of the corresponding spectrum features (photopeak or Compton edge). To help correctly identify the relevant peaks and Compton edges consult references [?] and [?]. The resultant calibration should be very linear if you have accurately recognized all the features.

3. With the magnet field at approximately 100 gauss, vary the voltage applied to the velocity selector around 4.5 kV while looking for evidence of pulses accumulating in a narrow distribution in the spectrum of pulse heights displayed on the MCA screen. Increase the energy of the selected electrons step by step by increasing B and V, and adjust the measurement chain so that the pulses recorded with the highest attainable energies accumulate near the high end of the spectrum displayed on the MCA.

4. For each of many (~ 10) values of B spread over as wide a range as possible, measure the voltage V that yields the maximum counting rate. The best procedure is to measure the counting rate as a function of V around V and at enough values of V to permit a gaussian fit to the data. Tabulate B, V, and the kinetic energy corresponding to the median channel number of the pulse-height distribution. Estimate the errors in each of these measurements so that you have the necessary data for error analysis of your results. (Note: the error of a voltage determination is not the FWHM of the measured curve of V vs count rate.)

7.   Analysis

For each value of B and $E = V_0/d$ calculate $\beta = E/B$. Then plot β on the Y axis against B on the X axis. On the same plot draw curves that show the relations between these quantities predicted by classical and relativity dynamics.

For each value of B, calculate e/m according to the classical and the relativity formulas and plot the results with error bars against B.

Discuss the effect of the spread in the trajectories of the detected electrons on the errors in the determinations of e/m.

Derive a final best value of e/m with a probable error using the techniques in [**?**].

Plot your measured values of K against p, and draw the curves predicted by classical and relativity mechanics.

7.1.   Possible Theoretical Topics

1. The surface current distribution required to produce a uniform field inside the spherical magnet.

2. Relativistic dynamics—-i.e., the relation between v, p, and E.

3. Compton scattering and the photoelectric effect at gamma-ray energies.

4. PIN diodes as particle detectors.

5. Resolution of the velocity selector.

6. Multiple Coulomb scattering of the electrons by the residual air in the vacuum chamber.

APPENDIX A: THE SPHERICAL UNIFORM-FIELD MAGNET

The magnet is an arrangement of currents in coaxial coils distributed over the surface of a sphere in such a way as to produce a uniform magnetic field B_i inside the sphere. The design problem is to find the distribution of surface current density $J(\theta, \phi)$ that achieves this condition.

Everywhere but on the surface of the sphere $\nabla \times B = j = 0$. It follows that $B = -\nabla \phi_m$, where ϕ_m is the magnetic potential function, i.e. a solution of Laplace's equation $\nabla \times (\nabla \phi_m) = \nabla^2 \phi_m = 0$. Potential theory says that a solution of Laplace's equation that satisfies a particular set of boundary conditions, such as the distribution of currents on the surface of our sphere, is unique except for an additive constant. Thus if you can cook up a solution of Laplace's equation that does, indeed, satisfy the boundary conditions, you can be sure you have got the one and only solution to the problem.

If the field is to be uniform inside the sphere, then

$$\phi_m(r, \theta, \phi) = -B_i z = -B_i r \cos \theta. \qquad r < R \qquad (A1)$$

Outside at large distances it is certainly true that

$$\phi_m = \frac{m \cos \theta}{r^2} \qquad r \gg R \qquad (A2)$$

i.e. the potential must have the form of a dipole potential at large distances since the field is the sum of contributions from many coaxial circular current loops. The problem boils down to that of matching an outside dipole field to the inside uniform field B_i by proper adjustment of the surface current distribution in such a way as to satisfy the continuity requirements on the radial and tangential components of $\vec{B}$. The continuity conditions follow directly from the two Maxwell equations governing the magnetostatic field, namely

$$\vec{\nabla} \cdot \vec{B} = 0,$$
$$\vec{\nabla} \times \vec{B} = \left(\frac{4\pi}{c}\right) \vec{j}.$$

(Note: $\vec{j}$ is the volume current density with dimensions of statamps cm^{-2} , whereas what we seek is the surface current density with dimensions statamps cm^{-1}.)

The rest of the solution is left to the reader.

For the general approach to the solution of such boundary condition problems see, e.g., Jackson [**?**] or Griffiths [**?**].

APPENDIX B: EQUIPMENT LIST

Manufacturer	Description	URL
Agilent	Oscilloscope	agilent.com
Sorenson	0-5A Power Supply	
RFL	Gaussmeter	
Bertran	7.5kV Velocity Selector PS	
Canberra 2006	Charged Particle Preamp	
Hamamatsu	PIN Diode	
Ortec	Amplifier	ortec-online.com

Manufacturer	Description	URL
Agilent	Oscilloscope	agilent.com

Pulsed-Nuclear Magnetic Resonance

MIT Department of Physics
(Dated: September 5, 2011)

In this experiment, the phenomenon of Nuclear Magnetic Resonance(NMR) is used to determine the magnetic moments of the proton and the fluorine nucleus. The spin-lattice and spin-spin relaxation times are determined from the measurements of free-induction signals and spin echoes. The variation of relaxation constants with viscosity and concentration of paramagnetic ions is studied.

1. PREPARATORY QUESTIONS

1. Show that a particle with angular momentum $\vec{I}$ and magnetic moment $\vec{\mu} = \gamma \vec{I}$ placed in a uniform magnetic field $\vec{B_0}$ precesses with angular frequency $\vec{\omega_0}$ (called the Larmor angular frequency) that is independent of the angle between $\vec{\mu}$ and $\vec{B_0}$, given by

$$\vec{\omega_0} = -\gamma \vec{B_0} \equiv -(g\mu_N/\hbar)\vec{B_0}. \qquad (1.1)$$

   Here g is the counterpart of the Landé g-factor in atomic spectroscopy and μ_N is the nuclear magneton, $e\hbar/2m_p$.

   For protons, $g = 5.58$, so $\gamma = 26.8 \times 10^3$ radians sec^{-1} gauss^{-1}, which corresponds to a Larmor frequency of 4.26 MHz at 1 kGauss magnetic field. Note that 1 Gauss $= 10^{-4}$ Tesla.

2. Derive the classical expression for the potential energy of a magnetic dipole in a magnetic field.

3. According to quantum mechanics the component of angular momentum in a given direction, e.g. the direction of $\vec{B_0}$, is an integer or half-integer multiple of $\hbar$. Write an expression for the energies U_m of all the possible states of a nucleus with total angular momentum quantum number I in a magnetic field. Draw on a single diagram the variation of all U_m's with B_0 over the range 0 to 10,000 Gauss for the proton and the fluorine nucleus.

4. Show on the above diagrams the frequencies of photons which would cause transitions among the various levels at $B_0 = 1770$ Gauss. Confirm that the photon frequencies are the same as the corresponding Larmor frequencies.

5. The samples used in the NMR measurements contain very large numbers of the dipoles being studied. These interact with one another and are in thermal equilibrium at room temperature. The relative populations of their allowed energy states therefore follow the Boltzmann distribution, namely $N \propto e^{-E/kT}$. Calculate the fractional difference in the populations of the magnetic states of the proton, that is, $(n_+ - n_-)/(n_+ + n_-)$, in a sample at room temperature in a magnetic field of 1770 Gauss.

2. Progress Check

By the end of your 2nd session in lab you should have a determination of the nuclear magnetic moment of fluorine. You should also have a preliminary value of T_2 for 100% glycerine.

3. Theory of NMR

The NMR method for measuring nuclear magnetic moments was conceived independently in the late 1940's by Felix Bloch and Edward Purcell [1–3]. Both investigators, applying somewhat different techniques, developed methods for determining the magnetic moments of nuclei in solid and liquid samples by measuring the frequencies of oscillating electromagnetic fields that induced transitions among their magnetic substates resulting in the transfer of energy between the sample and the measuring device. Although the amounts of energy transferred are extremely small, the fact that the energy transfer is a resonance phenomenon enabled it to be measured. Bloch and Purcell both irradiated their samples with a continuous wave (CW) of constant frequency while simultaneously sweeping the magnetic field through the resonance condition. CW methods are rarely used in modern NMR experiments. Radiofrequency (rf) energy is usually applied in the form of short bursts of radiation (pulsed NMR) and the effects of the induced energy level transitions are observed in the time between bursts. It is experimentally much easier to detect the extremely small effects of the transitions if this detection phase is separated in time from the rf burst phase. More importantly, as we shall see, it is much easier to sort out the various relaxation effects in pulse nmr experiments. The present experiment demonstrates the essential process common to all NMR techniques: the detection and interpretation of the effects of a known perturbation on a system of magnetic dipoles embedded in a solid or liquid. In addition, the effects of perturbations caused by the embedding material yield interesting information about the structure of the material.

3.1. Classical Motion of a Single Spin

One can describe the dynamics of a particle with spin in a magnetic field by drawing an analogy with a gyro-

scope in a gravitational field. The spin vector precesses about the field direction and then, as energy is transferred to or from the particle, the angle between its spin axis and the field axis gradually changes. This latter motion is called nutation.

The trouble with the gyroscope analogy would appear to be that an individual spin which obeys quantum mechanics cannot nutate continuously, since its projection on the field direction is quantized. Bloch, in 1956, proposed a vector model in which he showed that although nuclear spins obey quantum laws, the ensemble average taken over a large number of spins behaves like a classical system, obeying the familiar laws of classical mechanics. Thus one can gain significant insight by a classical analysis of a spinning rigid magnetized body in a magnetic field.

Following the discussion given by [4], we consider the motion of a nucleus with angular momentum $\vec{I}$ and magnetic moment $\vec{\mu} = \gamma \vec{I}$ in a magnetic field $\vec{B} = \vec{B_0} + \vec{B_1}$ composed of a strong steady component $B_0 \hat{k}$ and a weak oscillating component $B_1 \sin(\omega t)\hat{\imath}$ perpendicular to B_0. Here $\hat{\imath}, \hat{\jmath}, \hat{k}$ are the unit vectors in the laboratory reference frame x, y, z. The quantity γ is called the gyromagnetic ratio. (In the present experiment, the strong steady field has a magnitude of several kiloGauss; the weak oscillating field is the field inside a small solenoid 2 cm long, wound with 10 turns, and connected to a crystal-controlled fixed-frequency generator and wide-band power amplifier producing an rf alternating current with a peak amplitude of ~ 1 mA at 5.00×10^6 Hz. A simple calculation will confirm that under such conditions $B_1 \ll B_0$). The equation of motion of the particle is

$$\frac{d\vec{I}}{dt} = \gamma \vec{I} \times \vec{B}. \tag{3.1}$$

If $B_1 = 0$, the motion in a reference frame fixed in the laboratory is a rapid precession of the angular momentum about the direction of $\vec{B_0}$ (the z-axis) with the Larmor precession frequency γB_0, as shown in one of the preparatory questions. To understand the perturbing effects of the small-amplitude oscillating field on the motion we first represent it as the vector sum $\vec{B_1} = \vec{B_r} + \vec{B_l}$ of two counter-rotating circularly polarized components given by the equations

$$\begin{aligned}\vec{B_r} &= \tfrac{1}{2}(B_1 \cos \omega t \ \hat{\imath} + B_1 \sin \omega t \ \hat{\jmath}) \\ \vec{B_l} &= \tfrac{1}{2}(B_1 \cos \omega t \ \hat{\imath} - B_1 \sin \omega t \ \hat{\jmath}),\end{aligned} \tag{3.2}$$

where the subscript l denotes the component rotating in the direction of rapid precession (the proton precesses in the left hand direction as can be seen by solving Eq. 3.1), and r denotes the component rotating in the opposite direction.

Next we consider the situation from the point of view of an observer in a reference frame x', y', z' rotating in the direction of precession with angular velocity ω and unit vectors:

$$\begin{aligned}\hat{\imath}' &= \cos \omega t \ \hat{\imath} + \sin \omega t \ \hat{\jmath} \\ \hat{\jmath}' &= -\sin \omega t \ \hat{\imath} + \cos \omega t \ \hat{\jmath} \\ \hat{k}' &= \hat{k}.\end{aligned} \tag{3.3}$$

In this rotating frame $\vec{B_r}$ is a constant vector $(B_1/2)\hat{\imath}'$, $\vec{B_l}$ is rotating with angular velocity -2ω, and the rapid precession will have angular frequency $\gamma(B_0 - \omega/\gamma)$, as though the particle were in a field whose z-component is B_0 plus a fictitious field in the opposite direction of magnitude ω/γ. Suppose now that ω is adjusted so that $\omega = \gamma B_0$. Then the rapid precession will vanish, i.e. its frequency in the rotating frame will be zero, and the particle will precess slowly about the direction of the steady field $(B_1/2)\hat{\imath}'$ with angular velocity $\gamma B_1/2$, with only a tiny flutter averaging to zero due to the counter-rotating component. If $\vec{I}$ is initially parallel to B_0, then in time $\pi/(\gamma B_1)$ the spin direction will precess by $90°$, putting $\vec{I}$ in the $x'y'$ plane, perpendicular to B_0. If the oscillating field is now turned off, the particle will be left with its magnetic moment in the $x'y'$ plane and, from the point of view of an observer in the laboratory frame, it will be rotating in the xy-plane with angular frequency γB_0 about the z-direction.

3.2. Dynamics of an Ensemble of Spins

According to the Bloch theorem, this classical treatment of a single magnetized spinning body is actually valid for an ensemble of quantized magnetic moments.

Consider such a sample containing protons placed between the poles of the magnet. According to the Boltzmann distribution law, if the sample is in thermal equilibrium at temperature T, then the ratio of the number of protons n_+ with z components of spin up to the number with z components down is

$$n_+/n_- = e^{(-E_+ + E_-)/kT} = e^{\mu_p B_0/kT}, \tag{3.4}$$

where μ_p is the magnetic moment of the proton. At room temperature in a field of several kilogauss this ratio is only slightly greater than one, which means that the magnetization due to alignment of the proton moments in the z-direction is very slight.

Now, if the ensemble is rotated $90°$ by application of an rf field under the conditions described above for the correct amount of time (a "$90°$ rf burst"), then the nuclear magnetization will end up in the plane perpendicular to B_0 and precess with angular velocity γB_0 about the z direction. The precessing magnetization creates an alternating magnetic flux in the solenoid which, according to Faraday's law, induces an rf voltage. This rf voltage can be readily detected after the rf burst has been terminated, thereby proving that the resonance condition was achieved and that the applied frequency was equal to or very close to the precession frequency of the protons. Knowledge of the field strength and the resonance

frequency allows the determination of the gyromagnetic ratio of the proton, which is a measurement of fundamental importance in nuclear physics.

To detect the nuclear-induced rf signal of angular frequency γB_0 that appears across the terminals of the solenoid immediately after the 90° rf burst, it is mixed with a steady signal of frequency ω from the fixed oscillator to produce a beat signal of comparatively low frequency $|\gamma B_0 - \omega|$ which can be observed directly on an oscilloscope. The 90° rotation of magnetization still works even if ω is slightly off resonance.

However, the precession of spins in the transverse plane does not last forever. It decays because of three distinct effects:

1. The field of the magnet is not perfectly uniform so that the protons in different parts of the sample precess at slightly different frequencies and get out of phase with one another, thereby gradually decreasing the net magnetization of the sample. This effect, although physically the least interesting, is always the dominant effect.

2. Protons in any given substance are generally located in several different molecular environments in each of which the precession frequency will be perturbed in a slightly different amount by magnetic dipole interactions. As in 1) the result is a gradual loss of phase coherence and a decay of the resultant magnetization.

3. Electromagnetic interactions between the protons and the surrounding particles cause transitions between the spin up and spin down states whose coherent combination is manifested as magnetization rotating in the xy-plane. The result is a gradual decay of these coherent combinations and a return to the state of thermal equilibrium in which the magnetization is in the z-direction and therefore no longer capable of inducing a signal in the solenoid.

The oscillatory induced signal modulated by a decaying exponential (Figure 1) is referred as the Free Induction Decay (FID.) An excellent reference describing these relaxation effects is given in [5] and is available from the Junior Lab e-library.

3.3. Spin-Lattice Relaxation Time, T_1

Application of rf pulses and the consequent rotation of the spins from the z-axis to the xy-plane is a disruption of the thermal equilibrium of the spins. Effect number 3 described above is called thermal relaxation, that is, the approach to thermal equilibrium after being disturbed by the rf pulse.

How fast the spins regain equilibrium is a measure of the coupling of the protons to their environment. The approach to equilibrium is exponential and is characterized
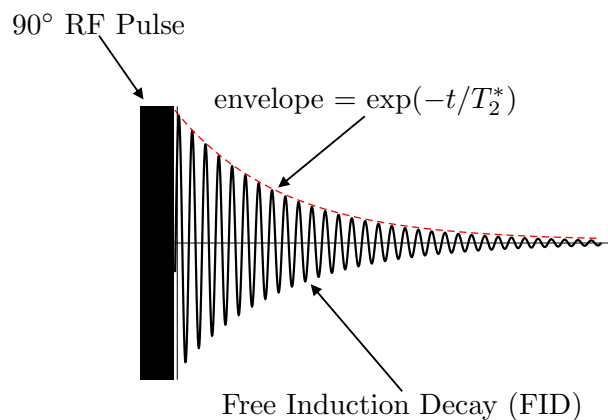

FIG. 1: The Free Induction Decay.

by a time constant denoted by T_1, called the spin-lattice or the longitudinal relaxation time. We can write

$$M_z(t) = M_z^{eq} + (M_z(0) - M_z^{eq})e^{-t/T_1},$$

where $M_z(t)$ is the z-magnetization at time t and M_z^{eq} is the value of z-magnetization at thermal equilibrium. The process of thermal relaxation is governed by the ease with which the nuclei are able to exchange energy with their surroundings. Transfer of energy from the spins to the lattice requires that there be a fluctuating magnetic field with Fourier components vibrating near the Larmor precession frequency in order to induce NMR transitions. The field originates from magnetic dipoles which are in thermal agitation.

3.4. Spin-Spin Relaxation Time, T_2

The time constant T_1 described in the previous section measures the regaining of longitudinal magnetization. However, there is another process that happens. With the passage of time after the rf pulse puts the spins in the transverse plane, the magnetic moments interact with one another and lose their phase coherence in the xy-plane (this is effect number 2 described above). This loss of transverse magnetization is characterized by the time constant T_2, called the spin-spin or the transverse relaxation time.

T_2^* is the name given to the observed value of the decay constant. This observed time constant consists of two components

$$1/T_2^* = 1/T_2 + \gamma \Delta H_0, \qquad (3.5)$$

where T_2 is the spin-spin, or the transverse relaxation time and ΔH_0 is the inhomogeneity of the magnetic field over the sample volume. The second term on the right is always larger than $1/T_2$ and is sometimes referred to in the literature as $1/T_2'$.

The measurement of T_2 is the basis for the powerful method of pulsed NMR chemical analysis based on measurement of the various perturbed precession frequencies

due to the various locations of the protons within the molecule. Given the spectrum of these frequencies for a new complex organic compound, an expert can practically write out the chemical formula.

In many cases, the same physical mechanisms determine T_1 and T_2 so that they are equal. The cases of interest are those where there are additional mechanisms for spin-spin relaxation such that T_2 is shorter than T_1. After a 90° pulse all phase coherence may be lost before any substantial z-magnetization is recovered. The transverse magnetization, and thus also the rf voltage induced in the sample coil, fall off as the phase coherence is lost. The dominant effect of magnet inhomogeneity, which could be fatal for such precision measurements, can be virtually eliminated by the remarkable invention of Hahn who discovered the phenomenon of "spin echoes" [6, 7]. Fig. 1 shows an FID (Free Induction Decay).

4.   Measurement Techniques

4.1.   The Measurement of T_2: Spin Echoes

To see how a spin echo is produced, consider a typical sample which has an enormous number of protons, of the order of 10^{23}. They can be divided into millions of ensembles, each one of which consists of a still enormous number of protons in a region where the external field has values within a very narrow range. Each ensemble will have a certain net magnetization which contributes to the total magnetization, but each such magnetization will precess with a slightly different frequency and therefore gradually get out of phase with respect to the others.

Suppose that after a sufficiently long time interval τ, a second transverse rf burst of double duration, i.e. a 180° burst, is applied to the sample.

The magnetization of each ensemble will be flipped by 180° about the direction of the applied pulse. This puts the magnetization back in the xy-plane where it will resume its precession motion. But now the accumulated phase differences between the various ensembles are all precisely reversed. Those that were ahead of the average are now behind by the same amount, and as the precession proceeds, the dephasing of the ensembles is gradually reversed. After precisely the same time interval τ all the ensembles are back in phase, the total magnetization reaches a maximum, and a "spin echo" signal is induced in the solenoid.

The amplitude of the echo is usually smaller than that of the original FID. There will be some loss in magnitude of the magnetization due to thermal relaxation and the effects of random fluctuations in the local fields that perturb the precession of the nuclear moments and it is precisely the relaxation time of this loss that we wish to measure. The spin-echo method enables one to eliminate the otherwise dominant effects of the nonuniformity of the magnetic field. If the two-pulse sequence is repeated for several different values of τ, the height of the echo
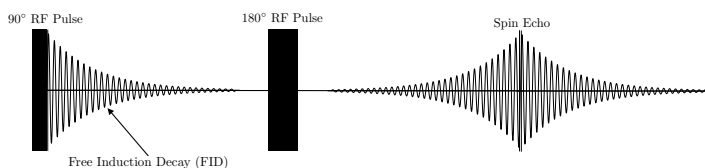

FIG. 2: The NMR signal observed when the applied rf frequency is offset slightly from the Larmor frequency. The fast oscillations corresponds to the beat between the two frequencies.

should vary as $\exp(-t/T_2)$.

A necessary assumption implied in the spin-echo technique is that a particular spin feels the same constant magnetic field before and after the "refocusing" 180° pulse. If, because of Brownian motion, a spin has diffused to a different region of magnetic field before the echo, then that spin will not be refocused by the 180° pulse. This is often the case for non-viscous liquids and will result in a decay of echoes which is not quite exponential and somewhat faster than that observed in viscous liquids. The **Carr-Purcell** technique, described in [8, 9] and summarized below, elegantly addresses this difficulty. The section of this lab guide entitled "measurements" will ask you to take data to measure the apparent T_2 for two samples (e.g. a viscous sample such as glycerine and a non-viscous one such as H_2O containing Fe^{3+}) to compare with later measurements taken from the same samples by the Carr-Purcell technique.

4.2.   The Measurement of T_1

We describe three methods of measuring T_1.

4.2.1.   90° − 90°

As mentioned above, the spin-lattice relaxation time (T_1) can be measured by examining the time dependence of the z-magnetization after equilibrium is disturbed. This can be done by saturating the spins with a 90° pulse, so that the z magnetization is zero. Immediately after the first pulse one should be able to observe a free induction decay (as in Fig.1) whose amplitude is proportional to the z-magnetization just before the pulse. One then waits a measured amount of time, τ, so that some magnetization has been reestablished, and then applies a 90° pulse to the recovering system. The second 90° pulse will rotate any z magnetization into the xy plane, where it will produce a FID signal proportional to the recovered magnitude it had just before the second pulse. If the two-pulse sequence is repeated for different values of τ, the amplitude of the FID as a function of t will give the value of T_1.
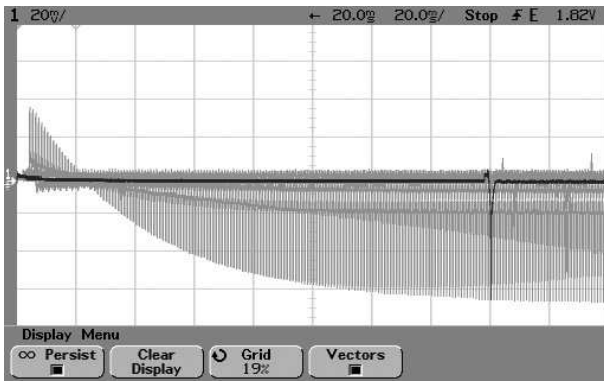
FIG. 3: An example data set using the "Three-Pulse" technique with the oscilloscope set to infinite-persist.

4.2.2. $180° - 90°$

Another sequence, the $180° - \tau - 90°$, is also used. A $180°$ pulse is applied to the equilibrium system, causing the population of the states to be precisely inverted, and thus leaving the xy-magnetization at zero. In this case, there should be little or no FID immediately after the first pulse. The system is then allowed to approach equilibrium for a specified delay, after which a $90°$ pulse is applied to rotate the partially recovered z-magnetization into the xy-plane. The magnitude of the FID gives a measure of the size of the magnetization, which can be plotted against the delay to give the exponential time constant. In this case, the magnetization actually reverses, going through zero at time $T_1 \ln 2$.

4.2.3. $180° - \tau - 90° \ 180°$

It was mentioned earlier that it is experimentally much easier to detect the extremely small effects of transitions if they are separated in time from the multi-watt rf bursts. Unfortunately, the usual "Inversion Recovery" method requires observation of the FID immediately after the second rf pulse. This problem was addressed several years ago by two Junior Lab students[1], who proposed the "Three-Pulse" sequence [10]. See Figure 3 for a sample data set using this technique.

The first pulse ($180°$) inverts the population along the z axis as in the normal Inversion-Recovery method. After a delay of τ, the second and third pulses can be understood as a normal $180° - \tau - 90°$ sequence, which is used to measure the fraction of spins which are in the $|+z\rangle$ state at the moment that the pulses are applied. The time between the second and third pulses is kept

———

[1] Both of these students, Rahul Sarpeshkar and Isaac Chuang, are now M.I.T. professors. Creativity in Junior Lab is one indicator of future success in science!

small to minimize T_2 effects. The amplitude of the echo is therefore related to the amount of T_1 decay (or recovery) for a given value of τ. Varying τ will have the form $A(1 - 2\exp(-\tau/T_1))$.

The three experiments mentioned so far, (i.e. the spin-echo, the $90° - 90°$ and the $180° - 90°$ sequences) have each been performed successfully many times in this lab. However, each has its intrinsic difficulties leading to various modifications which will be discussed.

5.   Experimental Apparatus

This experiment uses a permanent magnet whose field is ~ 1770 Gauss (0.177 Tesla). Care should be taken to avoid bringing any magnetizable material (such as iron or steel) near the magnet as this may be pulled in and damage the magnet.

The experimental apparatus, shown in Figure 4 consists of a gated rf pulse generator with variable pulse widths and spacings, a probe circuit that delivers rf power to the sample and picks up the signal from the sample, a preamp that amplifies the signal, and a phase detector which outputs an audio signal whose frequency corresponds to the difference between the Larmor frequency and the frequency of the signal generator. Details of how to design and build NMR probes can be found in [11].

The rf pulse generating system is made up of a 15 MHz frequency synthesizer (Agilent 33120A), a digital pulse programmer based on a STAMP micro-controller, a double-balanced mixer used as an rf switch (Mini-Circuits ZAS-3), a variable attenuator, and an rf power amplifier capable of 2 watts output.

The frequency synthesizer feeds a +10dBm rf sine wave to the power splitter. The power splitter keeps all impedances appropriately matched while feeding one half of the rf power to a double-balanced mixer (DBM) used as a gate for the rf. The other half is used as a reference signal in the phase detector. The gate is opened and closed by TTL pulses provided by the digital pulse programmer. After the switching stage, the rf pulses pass into a constant-gain (+33 dBm) rf power amplifier. The power amplifier feeds the amplified pulsed rf into the probe circuit.

The signal out of the sample, as well as a considerable amount of leakage during pulses, comes from the probe circuit, and is amplified by a sensitive preamp (Tron-Tech W110F). The signal then goes into a phase detector (Mini-Circuits ZRPD-1), where it is mixed with the reference signal coming out of the other port of the power splitter. Since the NMR signal is, in general, not precisely at the frequency of the transmitter, when the two signals are mixed, a signal is produced at the difference frequency of the resonance signal and the applied rf. Since we are looking at NMR signals in the vicinity of 1-8 MHz, mixing this down to a lower frequency makes it easier to see the structure of the signal.
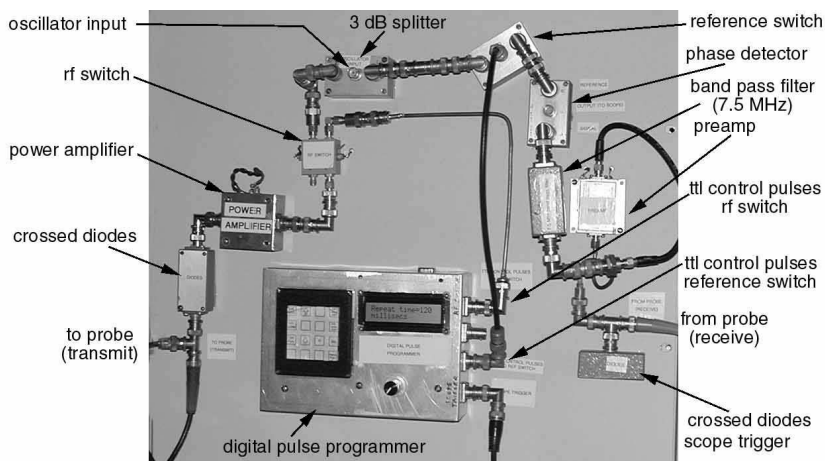
FIG. 4: The Experimental Setup. The magnet and the probe circuit are not shown

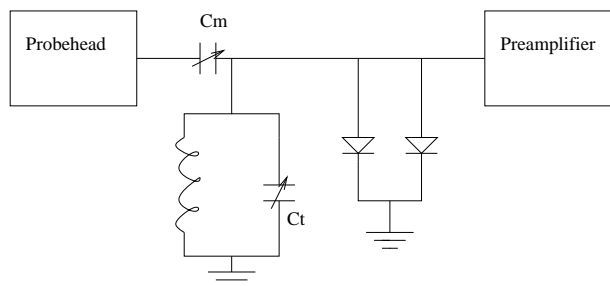## 5.1.   The probe circuit

FIG. 5: Schematic of the probehead circuit.

The probe circuit is a tuned LC circuit, impedance matched to 50 ohms at the resonant frequency for efficient power transmission to the sample. The inductor L in the circuit is the sample coil, a ten turn coil of #18 copper wire wound to accommodate a standard 10mm NMR sample tube. The coil is connected to ground at each end through tunable capacitors C_m and C_t, to allow frequency and impedance matching. Power in and signal out pass through the same point on the resonant circuit, so that both the power amplifier and the signal preamp have a properly matched load. Between the power amplifier and the sample is a pair of crossed diodes, in series with the probe circuit from the point of view of the power amplifier. By becoming non-conducting at low applied voltages, these serve to isolate the probe circuit and preamp from the power amplifier between pulses, reducing the problems associated with power amplifier noise. The crossed diodes however, will pass the high rf voltages that arrive when the transmitter is on. The signal out of the probe circuit passes through a quarter-wavelength line to reach another pair of grounded crossed diodes at the input of the preamp. The diodes short the preamp end of the cable when the transmitter is on, causing that end of the cable to act like a short circuit. This helps to protect the delicate preamp from the high rf power put out by the power amplifier. Any quarter-wave transmission line transforms impedance according to the following relation:

$$Z_{in} = Z_0^2/Z_{out} \tag{5.1}$$

where Z_0 is the characteristic impedance of the line.

Therefore during the rf pulse, the preamp circuit with the quarter-wave line looks like an open circuit to the probe and does not load it down. Between pulses, the voltage across the diodes is too small to turn them on, and they act like an open circuit, allowing the small NMR signal to pass undiminished to the preamp.

6.   Experimental Procedure

Although it is the policy in Junior Lab to discourage the use of pre-wired experiments, there are two reasons why the present set-up should not be (lightly) changed. Several of the components, particularly the double-balanced mixers (DBM) and the low-level TRON-TECH pre-amplifier, are easily damaged if the rf power level they are exposed to exceeds their specified limit. Furthermore, the lengths of some of the cables have been specifically selected to fix the relative phase relationship of different signals.

Most of the controls that you will manipulate are on the digital pulse programmer, the oscilloscope or the function generator. The keypad of the Digital Pulse Programmer is shown in Figure 6. Press any of the four buttons on the right to select a parameter (First Pulse Width (PW1), Second Pulse Width (PW2), Tau (τ), or Repeat Time). Then use the arrow buttons to set the corresponding time for that parameter. The default times are: PW1 = 24μs, PW2 = 48μs, τ = 2ms, and Repeat Time = 100ms. The top two buttons on the left determine whether a two-pulse sequence occurs only once
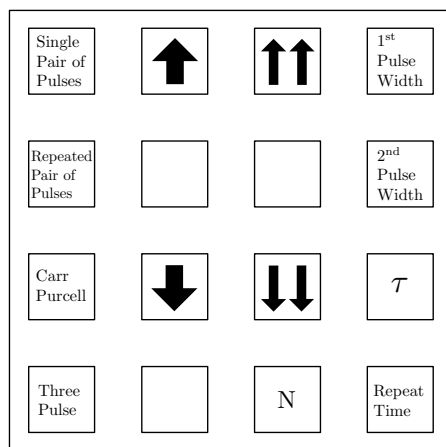
FIG. 6: The Pulse Programmer Interface.

(the Single Pair of Pulses buttom), or repeats continuously (the Repeated Pairs of Pulses button) with a pause between sequences of a length set by the Repeat Time parameter. The third button, labeled "Carr-Purcell," will create a series of pulses corresponding to the Carr-Purcell technique described in Section 6.3. Finally, the fourth button, "Three Pulse," outputs $180°\ -\tau-\ 90°\ 180°$ pulses for a measurement.

Set the delay, τ, to the minimum position and observe the amplified rf pulses from the port marked "transmitter" on channel 2 of the oscilloscope. The pulses should be approximately 20-30 volts peak-to-peak. Choose the slowest possible sweep speed; this will enable both pulses to be viewed simultaneously. A good starting pair of pulse-widths might be 24 μs and 48 μs, corresponding to approximately 90° and 180°. Now switch to channel 1, which displays the output of the phase detector (through the low-pass filter). Incidentally, there is another low-pass filter which is part of the scope itself. On the Tektronix analog scope there is a button marked "BW limit 20 MHz", which limits the allowed bandwidth. This button should be pressed in (active). On the HP digital scope the BW limit is set by one of the soft keys. On an Agilent scope, this is set in the channel 1 or channel 2 menu. Set the y-sensitivity to about 10 mV/div at first. Channel 1 will display the NMR signal. Place the glycerine vial in the probe and place the probe in the magnet. Now the fun begins!

Refer to Figure 2, which is a highly stylized version of the signals you might obtain. The form of the voltage displayed during the two bursts is unimportant. You will be focusing your attention on the FID signals that appear after each burst, and on the echo. For five or ten microseconds after the rf pulse the amplifier is still in the recovery phase, so this part of the signal should be ignored.

6.1. Free Induction Decay (FID)

As mentioned above, the oscillations following the first pulse represent a beat between the applied rf frequency and the Larmor frequency. Since the latter is proportional to B_0, you should see high-frequency oscillations as you raise ω from below the resonance condition. They will spread out in time, pass through a zero-beat condition and then begin to increase in frequency again as the field continues to increase. These oscillations with their exponentially decaying envelope is referred to as the Free Induction Decay (FID).

6.2. Setting Pulse Widths

It is sometimes easiest to set the pulse widths with the magnetic field slightly off resonance so that the FID is well displayed. The size of the FID should be maximum after a 90° or 270° pulse, minimum or zero after a 180° pulse. It is usually easiest to set the pulse-width to 180° by minimizing the FID. Then, if you want a 90° pulse, halve the pulse-width.

You have four or more degrees of freedom, including the widths of each of the two pulses, the delay between the pulses, and the frequency of the applied current. Experiment with all of them. Look for FID's; vary the FID so that you get varying amounts of oscillations (beats), and try to explain the beats. Once you find oscillatory FID's, move the probe slightly between the pole pieces of the magnet in a direction perpendicular to the magnetic field. Explain the changes you see. Use these changes to find the most homogeneous position in the field, then leave the probe there for the remainder of the experiment. Measure T_2^*. Using various combinations of 90° and 180° rf pulses, obtain data from which you can determine T_1 and T_2 in several samples (see Section 7.)

6.3. The Carr-Purcell Experiment

The Carr-Purcell experiment is a technique used to measure T_2. As mentioned above, if diffusion causes nuclei to move from one point of an inhomogeneous magnetic field to another in a time less than 2τ, the echo amplitude is reduced. It can be shown that the echo amplitude for a pulse separation τ is

$$E(2\tau) = E(0)\exp\left[-\frac{2\tau}{T_2} - \frac{2}{3}\gamma^2 G^2 D\tau^3\right], \qquad (6.1)$$

where G is the gradient of the inhomogeneous field and D is the diffusion constant. Because of the τ^3 dependence, the effects of diffusion are pronounced for large values of t and thus affect the measurement of long T_2's. Carr and Purcell [8] introduced a pulse sequence which can be described as follows: $\pi/2, \tau, \pi, 2\tau, \pi, 2\tau, \pi, 2\tau...$ (i.e. 90 deg pulse at time 0, followed by 180 deg pulses at times
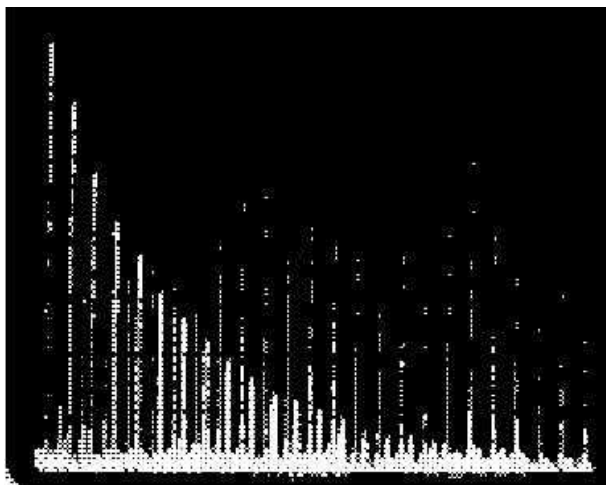
FIG. 7: The Carr-Purcell pulse and echo sequence

$\tau, 3\tau, 5\tau$, etc.) Echoes will be observed at times $2\tau, 4\tau, 6\tau$, etc.

When you are ready to do a Carr-Purcell, set up the pulse width and magnetic field first with a two-pulse spin echo and then switch to the Carr-Purcell mode using the pulse programmer. The scope readout should resemble Figure 7.

7. MEASUREMENTS

7.1. Magnetic Moments of Hydrogen and Fluorine

With this apparatus, we can measure the magnetic moments of two nuclei: the proton ^1H and the Fluorine nucleus ^{19}F. One of the strongest signals you can detect is due to hydrogen in glycerine. Once you have obtained a good resonance, remove the sample and replace it with the transverse probe of the Hall Gaussmeter. From the magnetic field strength ($\sim$ 1770 Gauss) and the measured frequency you can calculate the magnetic moment. Repeat the measurement for fluorine using the trifluoric acetic acid sample or the hexafluorobenzene (you may wish to consult the CRC or another source to get an idea of what resonant frequency you are looking for). The former is a strong acid and should be handled with extreme care. Before looking for the fluorine resonance, move the knob on the probe circuit in the magnet to point to "F". Also note that the T_1 relaxation time for our fluorine sample is long and if you use the default (100 ms) repetition rate of the pulse sequence, the observed signal will be small! Finally, be creative with the pulse programmer. For example, by setting pw2 $= 1\mu s$ you can effectively create a one pulse sequence.

7.2. Relaxation Constants for Water

In the case of water, the relaxation times (T_1 equals T_2 for most non-viscous liquids) are of the order of several seconds. The measurement of T_2 is quite difficult but the equivalent measurement of T_1 can be done as follows:

Set up a $90° - 180°$ echo sequence with the shortest possible delay between pulses. As mentioned above, one must usually wait at least 5 times T_1 between successive repeats of this pulse sequence to allow sufficient time for equilibrium to be re-established. If less time is taken, the echo signal is diminished. Taking advantage of this fact, one can vary the repeat rate and plot the echo height against the repeat time. For times less than about 3 sec, you can read this repeat time from the small numerical display on the scope (push the button marked "per"). For slower rates switch to the manual ("one-shot") mode and use your watch to wait a specified amount of time in between pulses. Repeat the measurement for both tap-water and distilled water.

The first measurements of T_1 in distilled water stood for about thirty years. Since then careful measurements have produced a number which is about 50% higher. The difference is due to the effect of dissolved oxygen in the water (O_2 is paramagnetic). As an optional experiment, you might try to carefully remove the dissolved oxygen from a sample of distilled water. Bubbling pure nitrogen through the water will work as will other methods in the literature. A challenging question which you might discuss in your oral examination is why O_2 is paramagnetic while N_2 is diamagnetic.

7.3. Effects of Paramagnetic Ions

An extremely small amount of any substance with unpaired electron spins has a very dramatic effect of reducing T_1. There is a bottle of $FeCl_3.6H_2O$ in the lab. The standard starting solution has a molarity of 0.166M corresponding to approximately 10^{20} Fe^{+++} ions/cc. There are 15 serial dilutions made from the standard solution with which measurements of both T_1 and T_2 should be taken. Repeat your measurements across the dilutions several times to ensure accuracy and precision. Plot the relaxation times versus concentration on a log-log scale.

7.4. Effect of Viscosity

It has been shown that the major contribution to both T_1 and T_2 processes comes from the fluctuating dipolar fields of other nuclear (and unpaired electron) spins in the immediate region. Only those fluctuations which have a sizeable Fourier component at the Larmor frequency can affect T_1, but spin-spin relaxation is also sensitive to fluctuations near zero frequency. It is for this reason that viscous liquids (whose fluctuations have a sizeable low-frequency component) exhibit a T_2 less than

Viscosity of Aqueous Glycerine Solutions in Centipoises/mPa s

Glycerine per cent weight	Temperature (° C)										
	0	10	20	30	40	50	60	70	80	90	100
0 [1]	1.792	1.308	1.005	0.8007	0.6560	0.5494	0.4688	0.4061	0.3565	0.3165	0.2838
10	2.44	1.74	1.31	1.03	0.826	0.680	0.575	0.500	–	–	–
20	3.44	2.41	1.76	1.35	1.07	0.879	0.731	0.635	–	–	–
30	5.14	3.49	2.50	1.87	1.46	1.16	0.956	0.816	0.690	–	–
40	8.25	5.37	3.72	2.72	2.07	1.62	1.30	1.09	0.918	0.763	0.668
50	14.6	9.01	6.00	4.21	3.10	2.37	1.86	1.53	1.25	1.05	0.910
60	29.9	17.4	10.8	7.19	5.08	3.76	2.85	2.29	1.84	1.52	1.28
65	45.7	25.3	15.2	9.85	6.80	4.89	3.66	2.91	2.28	1.86	1.55
67	55.5	29.9	17.7	11.3	7.73	5.50	4.09	3.23	2.50	2.03	1.68
70	76	38.8	22.5	14.1	9.40	6.61	4.86	3.78	2.90	2.34	1.93
75	132	65.2	35.5	21.2	13.6	9.25	6.61	5.01	3.80	3.00	2.43
80	255	116	60.1	33.9	20.8	13.6	9.42	6.94	5.13	4.03	3.18
85	540	223	109	58	33.5	21.2	14.2	10.0	7.28	5.52	4.24
90	1310	498	219	109	60.0	35.5	22.5	15.5	11.0	7.93	6.00
91	1590	592	259	127	68.1	39.8	25.1	17.1	11.9	8.62	6.40
92	1950	729	310	147	78.3	44.8	28.0	19.0	13.1	9.46	6.82
93	2400	860	367	172	89	51.5	31.6	21.2	14.4	10.3	7.54
94	2930	1040	437	202	105	58.4	35.4	23.6	15.8	11.2	8.19
95	3690	1270	523	237	121	67.0	39.9	26.4	17.5	12.4	9.08
96	4600	1580	624	281	142	77.8	45.4	29.7	19.6	13.6	10.1
97	5770	1950	765	340	166	88.9	51.9	33.6	21.9	15.1	10.9
98	7370	2460	939	409	196	104	59.8	38.5	24.8	17.0	12.2
99	9420	3090	1150	500	235	122	69.1	43.6	27.8	19.0	13.3
100	12070	3900	1410	612	284	142	81.3	50.6	31.9	21.3	14.8

[1]Viscosity of water taken from "Properties of Ordinary Water-Substance." N.E. Dorsey, p. 184. New York (1940)

FIG. 8: The viscocity of water-glycerine mixtures. Taken from http://www.dow.com/glycerine/resources/table18.htm

T_1. You will find a series of samples of glycerine-water mixtures in different ratios. Each will be marked with its viscosity[2] Measure T_2 by the Carr-Purcell method and T_1 by the $180° - 90°$ method, the three-pulse method or the method suggested in Subsection 7.2. With the aid of Figure 8, compare your results with those found in the extraordinary thesis of Bloembergen [12] started in the year that NMR was discovered.

8. Supplemental Questions

Each of the magnetic moments in a sample is influenced by the magnetic fields of other moments in its neighborhood. These differ from location to location in the sample, depending on the relative distance and orientation of neighbor moments to one another. An approximate measure of the magnetic field variation experienced by the proton moments in the water molecule is the range corresponding to parallel alignment of two interacting protons at one extreme to opposite alignment at the other.

1. Using μ/r^3 for the field of the neighbor moment, show that the half-range in the Larmor precession frequencies is given by $\Delta\omega \approx (g\mu_n)^2/hr^3$.

2. The return to normal of the transverse distribution of the protons following resonance occurs as moments with different precession frequencies become more and more randomly orientated in the precession angle. Estimate the transverse relaxation time T_2 for the water sample by finding the time required for two moments, differing by the average $\Delta\omega$ calculated in part a., to move from in-phase to π-out-of-phase positions.

As you've probably guessed, this lab is merely a stepping off point for an incredibly varied set of potential investigations. Some good general references for this lab (beyond the ones already cited in the text) are [13–19].

[1] F. Bloch, Phys. Rev. **70**, 460 (1946).
[2] N. Bloembergen, E. Purcell, and R. Pound, Phys. Rev. **73**, 679 (1948).
[3] *Nobel Lecture for Felix Bloch and Edward Mills Purcell* (1952).
[4] A. Abragam, *Principles of Nuclear Magnetism* (Oxford University Press, 1961), ISBN QC762.A158, physics Department Reading Room.
[5] Derome, Mod. NMR Technique. For Chem. Research (1987).
[6] E. Hahn, Phys.Rev. **80**, 580 (1950).
[7] E. Hahn, Phys Today **Nov. 1953**, 4 (1953).
[8] H. Carr and E. Purcell, Phys. Rev **94**, 630 (1954).
[9] S. Meiboom and D. Gill, Rev. Sci. Inst. **29**, 668 (1958), a short paper with a major modification of the Carr-Purcell sequence. Without such a modification, it is not possible to generate a long train of echoes. This is an early application of a complex multiple-pulse sequence with phase shifts which have become routine.
[10] I. Chuang, Junior Lab Paper (1990).
[11] R. Ernst and W. Anderson, Rev. Sci. Instrum. **37**, 93 (1966).
[12] N. Bloembergen, *Nuclear Magnetic Relaxation* (W.A. Benjamin, 1961), ISBN QC173.B652, physics Department Reading Room.
[13] G. Pake, American Journal of Physics **18**, 438 (1950).
[14] T. Farrar and E. Becker, *Pulse and FT NMR* (Acad. Press, 1971), ISBN QC454.F244, physics Department Reading Room.
[15] Feynman, Leighton, and Sands, *Lectures on Physics*, vol. Volume II, Chapter 35 (Addison-Wesley, 1965), ISBN QC23.F435, interesting discussions of angular momentum, the Stern-Gerlach Experiment and NMR, Physics Department Reading Room.
[16] E. Fukushima and S. Roeder, *Experimental Pulse NMR* (Addison-Wesley, 1981), ISBN QC762.F85, an excellent practical reference, Science Library Stacks.
[17] R. Freeman, *A Handbook of Nuclear Magnetic Resonance* (Farragut Press, 1997), 2nd ed., ISBN QD96.N8.F74, spin-Lattice Relaxation, Science Library Stacks.
[18] G. Pake, Annual Review of Nuclear Science **19**, 33 (1954).
[19] G. Pake, Sci. Amer. **Aug.** (1958), an excellent introduction, Science Library Journal Collection.

APPENDIX A: QUANTUM MECHANICAL DESCRIPTION OF NMR

Recall that for all spin-1/2 particles (protons, neutrons, electrons, quarks, leptons), there are just two eigenstates, spin up: $|S, S_z\rangle = |\frac{1}{2}, \frac{1}{2}\rangle \rightarrow |0\rangle$ and spin down: $|S, S_z\rangle = |\frac{1}{2}, \frac{-1}{2}\rangle \rightarrow |1\rangle$. Using these as basis vectors, the general state of a spin-1/2 particle can be expressed as a two-element column matrix called a **spinor**:

$$|\psi\rangle = u|0\rangle + d|1\rangle = \begin{bmatrix} u \\ d \end{bmatrix}. \tag{A1}$$

Normalization imposes the constraint $|u|^2 + |d|^2 = 1$.

The system is governed by the Schrödinger equation:

$$i\hbar \frac{d}{dt}|\psi\rangle = H|\psi\rangle \tag{A2}$$

which has the solution $|\psi(t)\rangle = U|\psi(0)\rangle$, where $U = e^{-iHt/\hbar}$ is unitary. In pulsed NMR, the Hamiltonian

$$H = -\vec{\mu} \cdot \vec{B} = -\mu[\sigma_x B_x + \sigma_y B_y + \sigma_z B_z] \tag{A3}$$

is the potential energy of a magnetic moment placed in an external magnetic field. The σ's are the Pauli spin matrices,

$$\sigma_x \equiv \begin{bmatrix} 0 & 1 \\ 1 & 0 \end{bmatrix}, \quad \sigma_y \equiv \begin{bmatrix} 0 & -i \\ i & 0 \end{bmatrix}, \quad \sigma_z \equiv \begin{bmatrix} 1 & 0 \\ 0 & -1 \end{bmatrix}. \tag{A4}$$

Inserting (A4),(A1) and (A3) into (A2), we get:

$$\dot{u} = \mu[iB_x + B_y]d + i\mu B_z u \tag{A5}$$
$$\dot{d} = \mu[iB_x - B_y]u - i\mu B_z d \tag{A6}$$

If $B_x = B_y = 0$ and the equations reduce to

$$\dot{u} = i\mu B_z u, \quad \dot{d} = -i\mu B_z d. \tag{A7}$$

Integrating with respect to time yields

$$u = u_0 e^{i\mu B_z t} = u_0 e^{i\omega_0 t}, \quad d = d_0 e^{-i\mu B_z t} = d_0 e^{-i\omega_0 t} \tag{A8}$$

where $\omega_0 = \mu B_z/\hbar$ is the **Larmor Precession Frequency**. If an atom undergoes a spin-flip transition from the 'spin-up' state to the 'spin-down' state, the emitted photon has energy $E = 2\omega_0\hbar$.

Now let's add a small external magnetic field B_x but still keeping $B_y = 0$ and such that $B_x \ll B_z$. Equations A5 and A6 become:

$$\dot{u} = i\mu B_x d/\hbar - i\mu B_z u/\hbar \tag{A9}$$
$$\dot{d} = i\mu B_x u/\hbar + i\mu B_z d/\hbar \tag{A10}$$

For a time varying magnetic field of the type produced by an 'RF-Burst' as in pulsed NMR, $B_x = B_{x0} \cos\omega t = B_{x0} \left(e^{i\omega t} + e^{-i\omega t}\right)/2$. Define $\omega_x = \mu B_x/\hbar$. We see that

$$\dot{u} = -i\omega_0 u + i\omega_x \left(e^{i\omega t} + e^{-i\omega t}\right) d/2 \tag{A11}$$
$$\dot{d} = i\omega_0 d + i\omega_x \left(e^{i\omega t} + e^{-i\omega t}\right) u/2 \tag{A12}$$

Using $\omega_x \ll \omega_0$ since $B_x \ll B_0$, we can try for a solution of the form

$$u = C_u(t)e^{-i\omega_0 t}, \quad d = C_d(t)e^{i\omega_0 t} \tag{A13}$$

Inserting them into the differential equations for u and d, we get

$$\dot{C}_u = \frac{i\omega_x}{2}C_d \left[e^{i(\omega - 2\omega_0)t} + e^{-i(\omega - 2\omega_0)t}\right] \tag{A14}$$
$$\dot{C}_d = \frac{i\omega_x}{2}C_u \left[e^{i(\omega - 2\omega_0)t} + e^{-i(\omega + 2\omega_0)t}\right] \tag{A15}$$

Now we use the approximation $\omega \ll \omega_0$ to show that the leading terms are very small. If we run at **resonance** ($\omega = 2\omega_0$):

$$\dot{C}_u = \frac{i\omega_x}{2}C_d, \quad \dot{C}_d = \frac{i\omega_x}{2}C_u \tag{A16}$$

Taking the derivatives of these equations, we see that these coefficients act like harmonic oscillators of frequency $\omega_x/2$. These have the general solution

$$C_u = a\cos(\omega_x t/2) + b\sin(\omega_x t/2) \tag{A17}$$
$$C_d = ia\sin(\omega_x t/2) - ib\cos(\omega_x t/2) \tag{A18}$$

Putting these in A13, we get the solution for u and d. These are called **Rabi Oscillations**, valid for $\omega_x \ll \omega_0$.

APPENDIX B: BLOCH SPHERE REPRESENTATION

A single qubit in the state $a|0\rangle + b|1\rangle$ can be visualized as a point (θ, ϕ) on the unit sphere, where $a = \cos(\theta/2)$, $b = e^{i\phi}\sin(\theta/2)$, and a can be taken to be real because the overall phase of the state is unobservable. This is called the Bloch sphere representation, and the vector $(\cos\phi\sin\theta, \sin\phi\sin\theta, \cos\theta)$ is called the Bloch vector.

The Pauli matrices give rise to three useful classes of unitary matrices when they are exponentiated, the *rotation operators* about the $\hat{x}$, $\hat{y}$, and $\hat{z}$ axes, defined by the equations:

$$R_x(\theta) \equiv e^{-i\theta X/2} = \cos\frac{\theta}{2}I - i\sin\frac{\theta}{2}X$$
$$= \begin{bmatrix} \cos\frac{\theta}{2} & -i\sin\frac{\theta}{2} \\ -i\sin\frac{\theta}{2} & \cos\frac{\theta}{2} \end{bmatrix} \tag{B1}$$

$$R_y(\theta) \equiv e^{-i\theta Y/2} = \cos\frac{\theta}{2}I - i\sin\frac{\theta}{2}Y$$
$$= \begin{bmatrix} \cos\frac{\theta}{2} & -\sin\frac{\theta}{2} \\ \sin\frac{\theta}{2} & \cos\frac{\theta}{2} \end{bmatrix} \tag{B2}$$

$$R_z(\theta) \equiv e^{-i\theta Z/2} = \cos\frac{\theta}{2}I - i\sin\frac{\theta}{2}Z$$
$$= \begin{bmatrix} e^{-i\theta/2} & 0 \\ 0 & e^{i\theta/2} \end{bmatrix}. \tag{B3}$$

One reason why the $R_{\hat{n}}(\theta)$ operators are referred to as rotation operators is the following fact. Suppose a single qubit has a state represented by the Bloch vector $\vec{\lambda}$. Then the effect of the rotation $R_{\hat{n}}(\theta)$ on the state is to rotate it by an angle θ about the $\hat{n}$ axis of the Bloch sphere.

An arbitrary unitary operator on a single qubit can be written in many ways as a combination of rotations, together with global phase shifts on the qubit. A useful theorem to remember is the following: Suppose U is a unitary operation on a single qubit. Then there exist real numbers α, β, γ and δ such that

$$U = e^{i\alpha} R_x(\beta) R_y(\gamma) R_x(\delta) \,. \qquad \text{(B4)}$$

APPENDIX C: FUNDAMENTAL EQUATIONS OF MAGNETIC RESONANCE

The magnetic interaction of a classical electromagnetic field with a two-state spin is described by the Hamiltonian $H = -\vec{\mu} \cdot \vec{B}$, where $\vec{\mu}$ is the spin, and $B = B_0 \hat{z} + B_1(\hat{x}\cos\omega t + \hat{y}\sin\omega t)$ is a typical applied magnetic field. B_0 is static and very large, and B_1 is usually time varying and several orders of magnitude smaller than B_0 in strength, so that perturbation theory is traditionally employed to study this system. However, the Schrödinger equation for this system can be solved straightforwardly without perturbation theory, in terms of which the Hamiltonian can be written as

$$H = \frac{\omega_0}{2} Z + g(X\cos\omega t + Y\sin\omega t) \,, \qquad \text{(C1)}$$

where g is related to the strength of the B_1 field, and ω_0 to B_0, and X, Y, Z are the Pauli matrices as usual. Define $|\phi(t)\rangle = e^{i\omega t Z/2}|\chi(t)\rangle$, such that the Schrödinger equation

$$i\partial_t |\chi(t)\rangle = H|\chi(t)\rangle \qquad \text{(C2)}$$

can be re-expressed as

$$i\partial_t |\phi(t)\rangle = \left[e^{i\omega Z t/2} H e^{-i\omega Z t/2} - \frac{\omega}{2} Z \right] |\phi(t)\rangle \,. \qquad \text{(C3)}$$

Since

$$e^{i\omega Z t/2} X e^{-i\omega Z t/2} = (X\cos\omega t - Y\sin\omega t) \,, \qquad \text{(C4)}$$

(C3) simplifies to become

$$i\partial_t |\phi(t)\rangle = \left[\frac{\omega_0 - \omega}{2} Z + gX \right] |\phi(t)\rangle \,, \qquad \text{(C5)}$$

where the terms on the right multiplying the state can be identified as the effective 'rotating frame' Hamiltonian. The solution to this equation is

$$|\phi(t)\rangle = e^{i\left[\frac{\omega_0 - \omega}{2} Z + gX \right] t} |\phi(0)\rangle \,. \qquad \text{(C6)}$$

The concept of *resonance* arises from the behavior of this solution, which can be understood to be a single qubit rotation about the axis

$$\hat{n} = \frac{\hat{z} + \frac{2g}{\omega_0 - \omega}\hat{x}}{\sqrt{1 + \left(\frac{2g}{\omega_0 - \omega}\right)^2}} \qquad \text{(C7)}$$

by an angle

$$|\vec{n}| = t\sqrt{\left(\frac{\omega_0 - \omega}{2}\right)^2 + g^2} \,. \qquad \text{(C8)}$$

When ω is far from ω_0, the spin is negligibly affected by the B_1 field; the axis of its rotation is nearly parallel with $\hat{z}$, and its time evolution is nearly exactly that of the free B_0 Hamiltonian. On the other hand, when $\omega_0 \approx \omega$, the B_0 contribution becomes negligible, and a small B_1 field can cause large changes in the state, corresponding to rotations about the $\hat{x}$ axis. The enormous effect a small perturbation can have on the spin system, when tuned to the appropriate frequency, is responsible for the 'resonance' in nuclear magnetic resonance.

In general, when $\omega = \omega_0$, the single spin rotating frame Hamiltonian can be written as

$$H = g_1(t) X + g_2(t) Y \,, \qquad \text{(C9)}$$

where g_1 and g_2 are functions of the applied transverse RF fields.

APPENDIX D: MODELING THE NMR PROBE

The material in this appendix was provided by Professor Isaac Chuang. A tuned circuit is typically used to efficiently irradiate a sample with electromagnetic fields in the radiofrequency of microwave regime. This circuit allows power to be transferred from a source with minimal reflection, while at the same time creating a large electric of magnetic field around the sample, which is typically placed within a coil that is part of it.
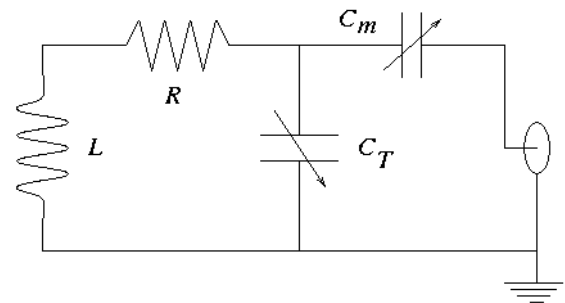

FIG. 9: Schematatic diagram of NMR probe circuit. The connector on the right goes off to the source and any detection circuitry.

1.   Circuit and Input Impedance

A typical probe circuit, as shown in Figure 7, consists of an inductor L, its parasitic coil resistance R, a tuning capacitor C_T, and an impedance matching capacitor C_m. We can analyze the behavior of this circuit using the method of complex impedances, in which the capacitors have impedance $Z_C = 1/i\omega C$, inductors $Z_L = i\omega L$, and resistors $Z_R = R$, with $\omega = 2\pi f$ being the frequency in rad/sec. The input impedance is thus

$$
\begin{aligned}
Z &= Z_{C_m} + \left[\frac{1}{Z_{C_T}} + \frac{1}{R + Z_L} \right]^{-1} \\
&= \frac{1}{i\omega C_m} + \left[i\omega C_T + \frac{1}{R + i\omega L} \right]^{-1} \\
&= \frac{1 + i\omega R(C_T + C_m) - \omega^2 L(C_T + C_m)}{i\omega C_m(1 + iR\omega C_T - \omega^2 LC_T)}. \quad \text{(D1)}
\end{aligned}
$$

2.   Tune and Match Conditions

The resonant frequency of this circuit is set by

$$
\omega_*^2 = \frac{1}{L(C_T + C_m)}, \quad \text{(D2)}
$$

and at this frequency, the input impedance is

$$
Z_0 = \frac{R(C_T + C_m)}{C_m(1 + iR\omega_* C_T - \omega_*^2 LC_T)}. \quad \text{(D3)}
$$

We would like this impedance to be 50 ohms, because that is the typical impedance expected by RF or microwave sources and the coaxial cable which carries in the signal. Setting $Z_0 = 50$ we obtain:

$$
\frac{50}{R} = \frac{(C_T + C_m)^2}{C_m \left[C_m + iR\omega_* C_T(C_T + C_m) \right]}. \quad \text{(D4)}
$$

To good approximation, the $iR\omega_* C_T(C_T + C_m)$ term in the denominator may be neglected, giving

$$
\frac{50}{R} = \left(1 + \frac{C_T}{C_m} \right)^2. \quad \text{(D5)}
$$

When these conditions are satisfied, almost all the source power goes into the tuned resonator at the resonant frequency, thus creating the strongest possible oscillating magnetic field inside the coil L.

The Speed and Mean-Life of Cosmic-Ray Muons

MIT Department of Physics
(Dated: September 5, 2011)

The purpose of this experiment is to demonstrate 1) the existence of a speed limit on the motion of particles by measuring the speed of cosmic-ray muons, and 2) the relativistic dilation of time by comparing the mean life of muons at rest and in high speed motion.

1.   PREPARATORY QUESTIONS

1. What are muons, how are they produced in the atmosphere, and why are they particularly penetrating particles (as opposed to electrons or protons)?

2. Starting from the Lorentz transformation equations, derive an expression for the mean life measured in the laboratory of unstable particles traveling with kinetic energy K. Their rest mass is m_0, and their mean life at rest is τ_0 . Assuming that the most likely momentum for the muon is approximately 1 GeV/c (see Appendix B), calculate β, γ and the flight time for a trip of 3 meters (approximate flight path in this apparatus.)

3. A singly charged particle traveling in matter at nearly the velocity of light loses energy by Coulomb interactions with the atoms of matter at a rate of approximately $2 MeV/(\mathrm{gm/cm}^2)^{-1}$ (the denominator is an "area density" and is equal to the volume density times the thickness). How much energy is lost by a relativistic particle ($v \approx c$) particle in vertically traversing the entire atmosphere?

4. Describe how a scintillation counter works, starting with the entrance of an energetic charged particle into a scintillator, and ending with an electrical pulse at the output of the photomultiplier.

5. How many "accidentals" (i.e. pulses from unrelated particles) will you observe from two scintillation counters with rates $n_1 = 10^4 s^{-1}$ and $n_2 = 2 \cdot 10^4 s^{-1}$ if you measure for 1 hour? Assume the time window for determining coincidence to be 100ns. How will these accidentals be distributed in your spectrum of "counts vs. time"?

6. The weight of the cylinder of plastic scintillator used in the measurement of the muon mean life is 20.3 kg. Predict the rate of muon decay events in the cylinder. (See Appendix A).

2.   WHAT YOU WILL MEASURE

1. According to classical mechanics the speed of a particle is proportional to the square root of its kinetic energy. Since there is no limit, in principle, on the kinetic energy of a body, there is no classical speed limit. According to the theory of relativity there is a speed limit. In the first of these experiments you will measure the velocity distribution of high energy muons that are generated high in the atmosphere through the interactions of primary cosmic ray nuclei and pass through the lab from ceiling to floor.

2. In the second experiment you will measure the decay curve of muons that have come to rest in a scintillator and determine their mean life. Given your measured values of the speed limit and the mean life, and given the fact that most of the muons are produced at altitudes above 10 km, you will confront the fact that the muons that traverse the scintillator paddles survived much longer than the mean life of muons at rest in the laboratory. How is that possible?

2.1.   Suggested Progress Check for end of 2nd Session

Using your measured MCA distributions of muon time of flights for two different paddle positions, calculate the speed of the cosmic-ray muons to zeroth order.

3.   INTRODUCTION

Webster's Ninth New Collegiate dictionary defines kinematics as "a branch of dynamics that deals with aspects of motion apart from considerations of mass and force." Relativistic kinematics deals with motion at speeds approaching that of light. These experiments are concerned with phenomena of high speed kinematics - the distribution in speed of very high energy particles, and the comparative rates of clocks at rest and in high speed motion.

Common sense, based on experience with comparatively slow motions, is a poor guide to an understanding of high speed phenomena. For example, in classical kinematics velocities add linearly in accordance with the Galilean transformation, which implies no limit, in principle, to the relative velocities of two bodies. On the other hand, Maxwell's equations have solutions in the form of waves that travel in vacuum with the universal velocity c, without regard to the motion of the source or observer of the waves. Thus, until Einstein straightened things out in 1905 in his special theory of relativity, there

was a fundamental contradiction lurking in the kinematical foundations of physics, as embodied in Newtonian mechanics and the Maxwell theory of electromagnetism [?].

This contradiction was laid bare in interferometry experiments begun by Michelson in 1881, which demonstrated the absence of any detectable effect of the motion of an observer on the velocity of light. Apparently without knowing about the Michelson experiment, Einstein took this crucial fact for granted when he began to think about the problem in 1895 at the age of sixteen (Pais, 1982). Ten years later he discovered the way to fix the contradiction; keep Maxwell's equations intact and modify Galilean kinematics and Newtonian dynamics. The fundamental problem of kinematics is to find the relations between measurements of space, time and motion in different reference frames moving with respect to one another. An excellent reference on special relativity can be found in French (1968)[?].

Consider, for example, two events (think of two flash bombs, or the creation and decay of a muon) that occur on the common x-axes of two mutually aligned inertial coordinate systems A and B in uniform motion relative to one another in the direction of their x-axes. Each event is characterized by its four coordinates of position and time, which will, in general, be different in the two frames. Let x_a, y_a, z_a, t_a represent the differences between the coordinates of the two events in the A frame, i.e., the components of the 4-displacement. Similarly, x_b, y_b, z_b, t_b are the components of the 4-displacement in the B frame. According to the Galilean transformation of classical mechanics, the components of the 4-displacement in A and B are related by the simple equations

$$x_b = x_a - vt_a, \ \ y_b = y_a, \ \ z_b = z_a, \ \ t_b = t_a \qquad (3.1)$$

and their inverse

$$x_a = x_b + vt_b, \ \ y_a = y_b, \ \ z_a = z_b, \ \ t_a = t_b \qquad (3.2)$$

where v is the velocity of frame B relative to frame A. If the two events are, in fact, two flash bombs detonated at a particular location in a third coordinate system (think of a rocket ship carrying the bombs) traveling in the x-direction with velocity u relative to B, then

$$\frac{x_b}{t_b} = u \text{ and } \frac{x_a}{t_a} = u + v \qquad (3.3)$$

i.e., the velocity of the rocket ship relative to A is the sum of its velocity relative to B and the velocity of B relative to A. This simple result accords with common sense based on experience with velocities that are small compared to c , the speed of light. Clearly, it implies no limit on the velocity of one body relative to another and assigns no special significance to any particular velocity. For example, if $u = 0.9c$ and $v = 0.9c$, then $x_a/t_a = 1.8c$. According to the special theory of relativity such a "superluminal" velocity is impossible because kinematics

is actually governed by the transformation equations

$$
\begin{aligned}
x_b &= \gamma(x_a - \beta ct_a), \\
y_b &= y_a, \\
z_b &= z_a, \\
ct_b &= \gamma(ct_a - \beta x_a),
\end{aligned}
\qquad (3.4)
$$

and their inverse,

$$
\begin{aligned}
x_a &= \gamma(x_b + \beta ct_b), \\
y_a &= y_b, \\
z_a &= z_b, \\
ct_a &= \gamma(ct_b + \beta x_b),
\end{aligned}
\qquad (3.5)
$$

where $\beta = v/c$ and $\gamma = 1/\sqrt{(1-\beta^2)}$. We obtain the addition equation for velocities, as before, by dividing the equations for x_a and t_a. Thus

$$\frac{x_a}{t_a} = \frac{u+v}{1+\frac{uv}{c^2}} \qquad (3.6)$$

Now, if $u = 0.9c$ and $v = 0.9c$, then $x_a/t_a = 0.9945c$. No compounding of velocities less than c can yield a relative velocity of two bodies that exceeds c. Moreover, any entity that propagates with velocity c (i.e., massless particles such as photons, gravitons, and probably neutrinos) relative to one inertial reference frame will propagate with velocity c relative to every other inertial frame regardless of the motions of the frames relative to one another. Thus the velocity of light in vacuum is raised to the status of a universal constant - the absolute speed limit of the universe. The first experiment will demonstrate the consequences of this fact of relativity for the distribution in velocity of high-energy cosmic-ray muons.

Consider what these equations imply about different observations of the time interval between two events such as that between two flash bombs, or between the birth and death of a particle or person. Suppose a rocket ship carrying two flash bombs is at rest in frame B so that the bombs go off at the same position in B ($x_b = 0$) with a separation in time of t_b. Then $t_a = \gamma t_b$; i.e., as measured in frame A, the time interval between the two events is longer by the Lorentz factor γ. This is the relativistic dilation of time.

3.1. Cosmic Rays

Much of the material in this section is taken from the classic works by Bruno Rossi[? ? ?]. Interstellar space is populated with extremely rarefied neutral and ionized gas ($\approx 10^{-3}$ to 10^3 atoms cm^{-3}), dust ($\approx$ 1-10% of gas), photons, neutrinos, and high-energy charged particles consisting of electrons and bare nuclei with energies per particle ranging up to 10^{21} eV. The latter, called cosmic rays, constitute a relativistic gas that pervades the galaxy and significantly affects its chemical and physical evolution. The elemental composition of cosmic-ray

nuclei resembles that of the sun, but with certain peculiarities that are clues to their origins. Most cosmic rays are generated in our galaxy, primarily in supernova explosions, and are confined to the galaxy by a pervasive galactic magnetic field of several microgauss. It is an interesting and significant fact that the average energy densities of cosmic rays, the interstellar magnetic field, and turbulent motion of the interstellar gas are all of the order of 1 eV cm^{-3}.

When a primary cosmic ray (90% of which are protons, 9% helium nuclei, 1% other) impinges on the Earth's atmosphere it interacts with an air nucleus, generally above an altitude of 15 km. Such an interaction initiates a cascade of high-energy nuclear and electromagnetic interactions that produce an "air shower" of energetic particles spreading outward in a cylindrically symmetric pattern around a dense core. (See Figure 1.) As the shower propagates downward through the atmosphere the energy of the incident and secondary hadrons (nucleons, antinucleons, pions, kaons, etc.) is gradually transferred to leptons (weakly interacting muons, electrons and neutrinos) and gamma rays (high-energy photons) so that at sea level the latter are the principal components of "secondary" cosmic rays. Typical events in such a cascade are represented by the reactions shown in Figure 1. High altitude observations show that most of the muons that arrive at sea level are created above 15 km. At the speed of light their trip takes ≈ 50 μsec.

In 1932, Bruno Rossi, using Geiger tubes and his own invention, the triode coincidence circuit (the first practical AND circuit), discovered the presence of highly penetrating and ionizing (i.e. charged) particles in cosmic rays. They were shown in 1936 by Anderson and Nedermeyer to have a mass intermediate between the masses of the electron and the proton. In 1940, Rossi showed that these particles, now called muons, decay in flight through the atmosphere with a mean life in their rest frame of about 2 microseconds. Three years later, using another electronic device of his invention, the time to pulse-height converter (TAC), he measured the mean life of muons at rest in an experiment resembling the present one in Junior Lab, but with Geiger tubes instead of a scintillation detector.

In an ironic twist of history, these particles were believed to be Yukawa type (pions) until 1947 when they were found by Powell to be muons from $\pi^+ \to \mu^+ + \nu_\mu$.

Cosmic rays are a convenient and free source of energetic particles for high energy physics experiments. They suffer the disadvantage of being a mixed bag of uncollimated particles of various kinds with low intensity and a very broad range of energies. Nevertheless, the highest energy of a cosmic-ray primary measured so far, $\approx 10^{21}$ eV, exceeds by many orders of magnitude the practical limit of any existing or conceivable man-made accelerator. Cosmic rays will therefore always be the only source of particles for the study of interactions at the highest observable energies. In the present experiment they will be used to explore relativistic kinematics at the comparatively modest energies of a few GeV (1 GeV= 10^9 eV), which are the typical energies of the muons detected at sea level.

3.2. The Speed Distribution of Cosmic-Ray Muons

According to Newtonian mechanics the velocity of a particle is related to its energy and mass by the equation

$$v = \sqrt{\frac{2E}{m}} = c\sqrt{\frac{2E}{mc^2}}. \qquad (3.7)$$

For the muon the value of mc^2 is 105.7 MeV. Thus, the Newtonian prediction for the velocity of a 1 GeV muon is approximately $4.3c$. According to relativistic mechanics, the higher the energy of a particle, the closer its speed approaches c. Thus an observation of the distribution in speed of high-energy cosmic-ray muons provides a dramatic test of the relation between energy and velocity. The experiment consists of a measurement of the difference in the time of flight of muons between two detectors in the form of plastic scintillator "paddles" when they are close together and far apart. The 2nd Edition of Melissinos (2003) describes this experiment in some detail [**?**].

The setup is shown in Figure 2. The signal from the top detector generates the start pulse for the time-to-amplitude converter (TAC). The pulse from the bottom detector, after an appropriate delay in a long cable, generates the STOP pulse. A multi-channel analyzer (MCA) records the amplitude of the positive output pulse of the TAC; that amplitude is proportional to the time interval between the input start and stop pulses. The median value of this interval for many events changes when the bottom detector is moved from the top to the bottom position. The change in the median value is a measure of the median time of flight of the detected muons and, given the distance between the top and bottom positions of the bottom paddle, of the median velocity.

4.   MEASURING THE SPEED OF COSMIC-RAY MUONS

4.1.   Procedure

Throughout the setup procedure it is essential to use the fast (200 MHz) Tektronix oscilloscope to check the signs, amplitudes, occurrence rates and timing relationships of the pulses into and out of each component of the electronic system. Please note that the BNC inputs to the scope are relatively weakly connected to its internal circuit board and thus are susceptible to damage when attaching and removing cables. Short leads have been 'permanently' attached to the inputs on channels 1 and 2. Please do not remove the leads, but rather just connect your cables to the ends of these 'pig-tails'.
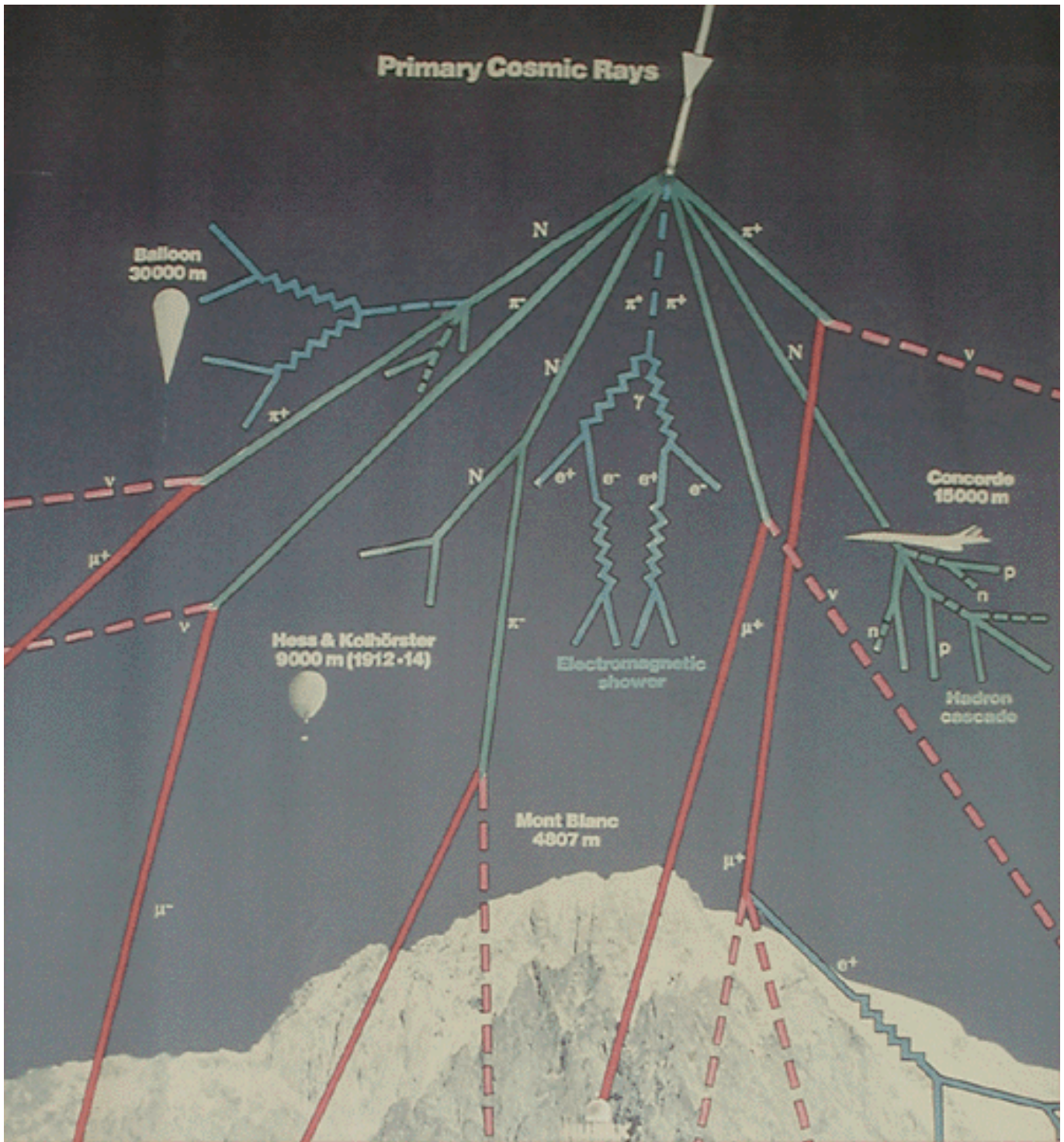
FIG. 1: (a) Production and decay of pions and muons in a representative high energy interaction of a cosmic-ray proton with a neutron in the nucleus of an air atom. (b) Masses and lifetimes of pions and muons.

Since you are aiming to measure time differences of the order of the travel time of light from the ceiling to the floor (≈ 10 nanosec), all the circuits up to the MCA must have "rise times" substantially shorter, which means that you must use very high sweep speeds on the oscilloscope in order to perceive whether things are behaving properly. To avoid confusing reflections from the ends of cables, it is essential that all cables carrying fast pulses be terminated at their outputs by their characteristic impedance of 50 ohms, either with a terminating plug
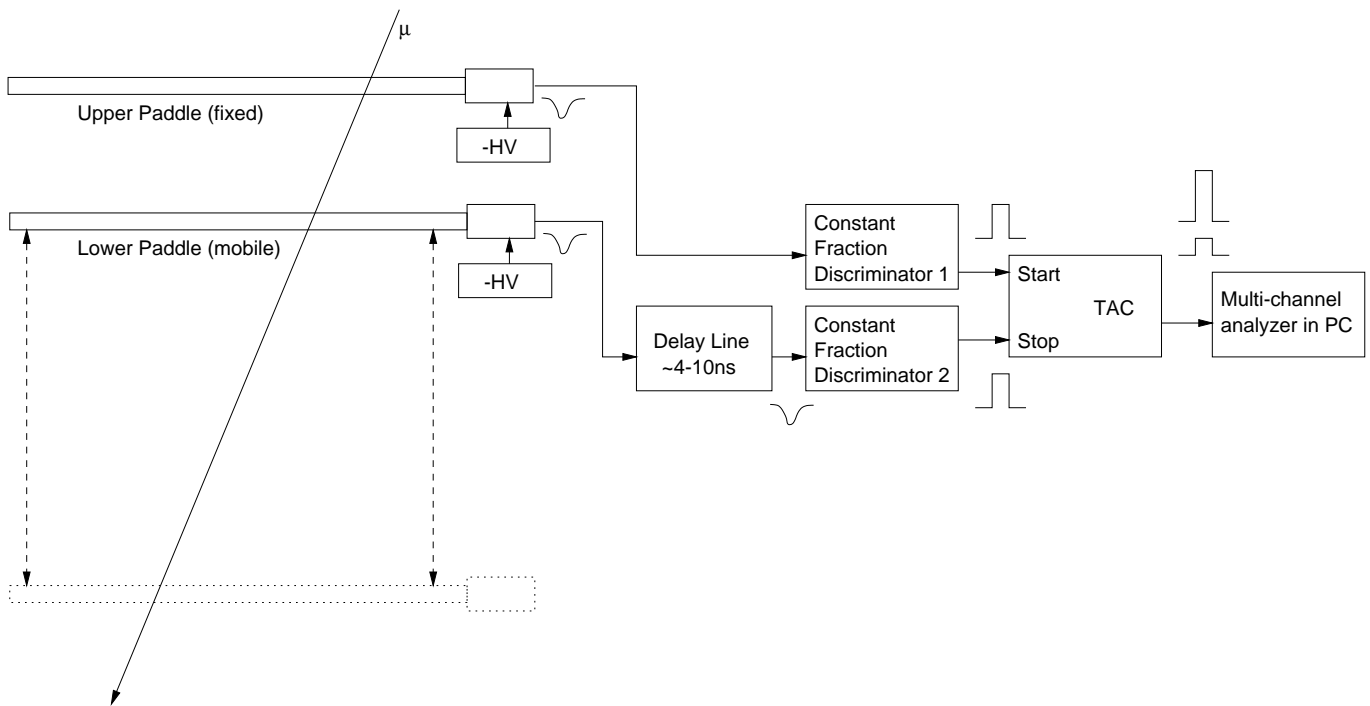
FIG. 2: (a) Arrangement for measuring the speed of cosmic-ray muons.

on a T-connector, or by an internal termination at the input of a circuit.

Check the reasonableness of the arrival rates of single pulses by measuring the size of the scintillator and estimate the total rate of muons R traversing it. You can use the following empirical formula that provides a good fit to measurements of the intensity of penetrating particles at sea level as a function of the zenith angle:

$$I(\phi) = I_v cos^2(\phi), \qquad (4.1)$$

where $I_v = 0.83 \times 10^{-2}$ cm^{-2} s^{-1} str^{-1}, and ϕ is the zenith angle (Rossi 1948). $I(\phi)d\Omega dA dt$ represents the number of particles incident upon an element of area dA during the time dt within the element of solid angle dΩ from the direction perpendicular to dA. By integrating this function over the appropriate solid angle you can estimate the expected counting rates of the detectors due to the total flux of penetrating particles from all directions, and the expected rate of coincident counts due to particles that arrive within the restricted solid angle defined by the telescope (See Appendix C). **The rates of single events and coincidences for τ_μ are very important calculations and you should not proceed until you have determined these values!**

The Lecroy constant fraction discriminators (CFD's) or the Canberra CFD's should be used for this portion of the experiment. Their thresholds are nominally set to 30mV by adjusting a small trim potentiometer recessed in the front panel of the module. *O*ptional: Its value can be checked by using a function generator to generate signals above and below the threshold. **After confirming**

a 30mV level, please do not adjust the threshold levels further, so as to extend the life of the delicate potentiometers. Adjust the high voltages supplied to the photomultiplier tubes (PMT's) of each of the detectors so that the rate of pulses from the discriminators is about $4R$ counts/s, but not more than 1kHz as checked by the scaler (not more than 1700V for each PMT). This will achieve a high detection efficiency for muon pulses, including those buried in the background of events due to local radioactivity.

Explore the operation of the TAC and the MCA with the aid of the time calibrator (TC). The TC produces pairs of fast negative pulses separated by multiples of a precise interval. When these pulses are fed to the START and STOP inputs of the TAC, the TAC produces output pulses with amplitudes proportional to the time intervals between the input pulses. The amplitudes are measured by the MCA.

With the aid of the TC, set the controls of the TAC and MCA so that the calibration of the system is approximately 20 MCA channels per nanosecond. Test the linearity of the time-to-height conversion. Calibrate the system so that you can relate accurately the difference between the numbers of any two channels on the MCA display to a change in the time interval between START and STOP pulses at the TAC. Check this calibration by adding a known length of 50Ω RG-58 cable just before the STOP input at the TAC.

Now feed the negative gate pulses from CFD1 and CFD2 to the start and stop inputs of the TAC, making sure you have them in the right order so that the

stop pulse arrives at the stop input after the start pulse arrives at the start input, taking account of both the time of flight and the pulse transmission times in the cables. Connect the output of the TAC to the input of the MCA operating in the PHA mode. Adjust the delays and set the controls of the TAC and MCA so that the timing events generated by the muons are recorded around the middle channel of the MCA's input range.

Acquire distributions of the time intervals between the START and STOP pulses for a variety of paddle positions. Integration times should range from about 10 minutes (bottom paddle in its highest position) to about 45 minutes (bottom paddle in its lowest position). How much do you gain by making longer runs?

Calibrate the time base with the TC. Do not alter any of the cabling or electronic settings between any pair of top and bottom measurements. Even a small change in a high voltage or the triggering level of a discriminator can change the timing by enough to introduce a large systematic error in a velocity determination.

4.2.   ANALYSIS

4.3.   Analysis: Speed of Cosmic-Ray Muons

Keep in mind the fact that the measured quantities are not actual times of flight of muons between the up and down positions of the middle detector. Rather, they are differences in arrival times of pulses from the top and middle detectors generated by flashes of scintillation light that have originated in various places within each scintillator paddle and have diffused at the speed of light in plastic to the photomultiplier window. Each event yields a quantity t_i which can be expressed as

$$t_i = t_0 + \frac{d_i}{v_i} + \Delta t_i, \tag{4.2}$$

where t_0 is a constant of the apparatus, d_i is the slant distance traveled by the ith muon between the top and middle detectors, v_i is the velocity of the muon, and Δt_i is the error in this particular measurement due to the difference in the diffusion times of the scintillation light to the two photomultipliers and other instrumental effects. (In this measurement it is reasonable to assume that the systematic error due to the timing calibration is negligible. Therefore we can deal directly with the t_i's as the measured quantities rather than with the channel numbers of the events registered on the MCA.) Suppose we call T_u and T_d the mean values of the t_i's in the up and down positions respectively. The simplest assumption is that

$$\Delta T = T_d - T_u = \frac{D}{v}, \tag{4.3}$$

where D is the difference in the mean **slant distance** traveled by the muons from the top to the middle paddle

in the down and up positions, and v is the mean velocity of cosmic ray muons at sea level. Implicit in this is the assumption that $(\Delta t_i)_{av}$ is constant in both the up and down positions. Then v can be evaluated as

$$v = \frac{D}{(T_d - T_u)}, \tag{4.4}$$

and the random error can be derived from the error in the means (i.e. in T_d and T_u) which can be figured according to the usual methods of error propagation. (The error of a mean is the standard deviation divided by the square root of the number of events.) Good statistics are needed because of the width of the timing curve. This width is of the same order of magnitude as the muon flight time in the apparatus for several reasons (you should produce estimates of the sizes of each of these effects):

1. The time of flight between the two counters is given by Eq. (4.3), $\Delta T = T_d - T_u = D/v$. The cosmic ray muons have a momentum distribution given in Figure 11 in Appendix B. Using the experimental points in this figure, estimate the dispersion in ΔT due to this effect.

2. The cosmic ray muons have a distribution of angles given by Eq. (4.1). This causes the distribution of distribution of flight paths D to differ in the "close" and "far" position. Estimate the dispersion in ΔT due to this effect. Take into account the dimensions of the detectors.

3. The cosmic ray muons hit the scintillators approximately uniformly. However, the phototube is placed at one end of the scintillator. There is a dispersion in the time that a light pulse, created in the scintillator from the passage of the muons, hits the phototube. Estimate the dispersion in ΔT due to this effect, assuming that the index of refraction of the scintillator is $n \approx 1.5$.

5.   MEASUREMENT OF THE MEAN LIFE OF MUONS AT REST

Muons were the first elementary particles to be found unstable, i.e. subject to decay into other particles. At the time of Rossi's pioneering experiments on muon decay, the only other "fundamental" particles known were photons, electrons and their antiparticles (positrons), protons, neutrons, and neutrinos. Since then dozens of particles and antiparticles have been discovered, and most of them are unstable. In fact, of all the particles that have been observed as isolated entities, the only ones that live longer than muons are photons, electrons, protons, neutrons, neutrinos and their antiparticles. Even neutrons, when free, suffer beta (e^-) decay with a half life of ~ 15 minutes, in the decay process

$$n \to p + e^- + \bar{\nu}_e.$$
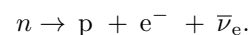
Similarly, muons decay through the process

$$\mu^- \to e^- + \bar{\nu}_e + \nu_\mu$$

with a lifetime of $\tau^{-1} = \frac{G_F^2 m_\mu^5}{192\pi^3}$ in the Fermi β-decay theory, based on Figure 3(a). This has become better understood in the modern electroweak theory where the decay is mediated by heavy force carriers W.

(a) Fermi
Interaction

(b)
Emission
of a W
boson

FIG. 3: Feynman diagrams of the muon decay process, in which the time axis is directed to the right. Figure (a) represents Fermi's original theory of interaction, while figure (b) reflects a modern understanding of the electroweak interaction. Note an arrow to the right indicates a particle travelling forward in time, while an arrow to the left indicates an antiparticle travelling forward in time.

Muons can serve as clocks with which one can study the temporal aspects of kinematics at velocities approaching c, where the strange consequences of relativity are encountered. Each muon clock, after its creation, yields one tick – its decay. The idea of this experiment is, in effect, to compare the mean time from the creation event to the decay event (i.e. the mean life) of muons at rest with the mean time for muons in motion. Suppose that a given muon at rest lasts for a time t_b. Equation 3.5 predicts that its life in a reference frame (See Figure 3 (a)) with respect to which it is moving with velocity v, is γt_b, i.e. greater than its rest life by the Lorentz factor γ. This is the effect called relativistic time dilation. (According to relativistic dynamics, γ is the ratio of the total energy of a particle to its rest mass energy).

In this experiment you will observe the radioactive decay of muons and measure their decay curve (distribution in lifetime) after they have come to rest in a large block of plastic scintillator, and determine their mean life. From your previous measurement of the mean velocity of cosmic-ray muons at sea level and the known variation with altitude of their flux, you can infer a lower limit on the mean life of the muons in motion. A comparison of the inferred lower limit with the measured mean life at rest provides a vivid demonstration of relativistic time dilation. During the period from 1940 to 1950, observations of muons stopped in cloud chambers and nuclear emulsions demonstrated that the muon decays into an electron and that the energy of the resulting electron, may have any value from zero to approximately half the rest energy of the muon, namely $\approx$ 50 MeV. From this it was concluded that in addition to an electron the decay products must include at least two other particles, both

neutral and of very small or zero rest mass (why?). The decay schemes are shown in Figure (1).

The experimental arrangement is illustrated in Figure 5. According to the range-energy relation for muons (see Rossi 1952, p40), a muon that comes to rest in 10 cm of plastic scintillator ($[CH_2]_n$ with a density of ≈ 1.2 g cm^{-3}) loses about 50 MeV along its path. The average energy deposited by the muon-decay electrons in the plastic is about 20 MeV. We want both START and STOP pulses for the TAC to be triggered by scintillation pulses large enough to be good candidates for muon-stopping and muon-decay events, and well above the flood of < 1 MeV events caused mostly by gamma rays and the "after" pulses that often occur in a photomultiplier after a strong pulse.

The success of the measurement depends critically on a proper choice of the discrimination levels set by the combination of the HV and the CFD settings. If they are too low, and the rate of accidental coincidences into the TAC is correspondingly too high, then the relatively rare muon decay events will be lost in a swamp of accidental delayed coincidences between random pulses. If the discrimination levels are too high, you will miss most of the real muon decay events. To arrive at a decision, review your prediction of the rate of decay events in the plastic cylinder. The answer to Preparatory Problem 5 tells you (implicitly) how to estimate the rate of accidental delayed coincidence events in which a random start pulse is followed by a random stop pulse within a time interval equal to, say, five muon mean lives. You want this rate of accidental events to be small compared to the rate of muon stoppings, allowing for reasonable inefficiency in the detection of the muon decay events due to the variability of the conditions under which the muons stop and the decay electrons are ejected.

It is important that pulses from the same event do not trigger the TAC to both start and stop the timing sequence. To avoid this, the pulse from a single event to the START input must be delayed by a sufficient length of coaxial cable to ensure that the identical pulse at the STOP input does not interfere with the timing sequence initiated by that same event. In this way the first STOP pulse is ignored, whereas the corresponding delayed START pulse begins the TAC timing sequence. The next pulse at the STOP input (arising from a *different* event) stops the TAC, provided it occurs before the end of the TAC timing ramp. See figure 4 for an illustration of the correct timing of the pulses. What effect
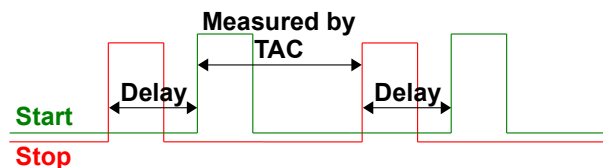
FIG. 4: Arrival times of pulses along the STOP input (red) and the START input (green) of the TAC.
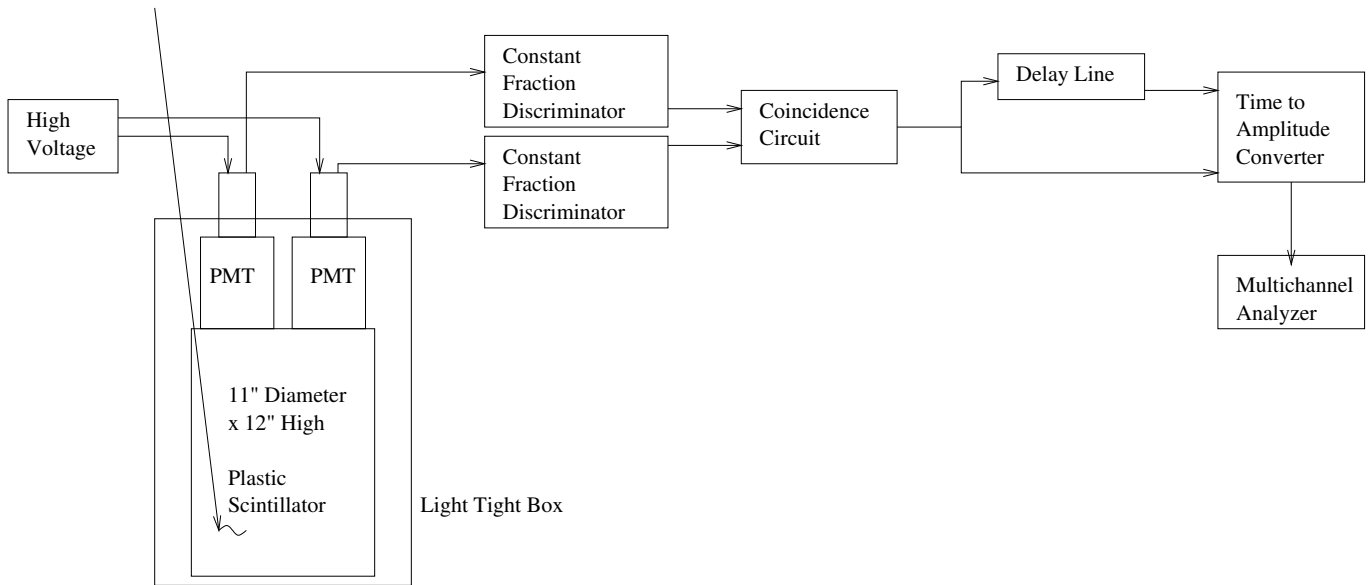
FIG. 5: Arrangement for measuring the mean life of muons

does this necessary delay of the start pulse and the consequent loss of short-lived events have on the mean life measurement?

A potential complication in this measurement is the fact that roughly half of the stopped muons are negative, and therefore subject to capture in tightly bound orbits in the atoms of the scintillator. If the atom is carbon, then the probability density inside the atomic nucleus for a muon in a 1s state is sufficiently high that nuclear absorption can occur by the process (see Rossi, "High Energy Particles", p 186)

$$\mu^- + p \rightarrow n + \nu, \tag{5.1}$$
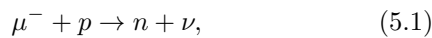
which competes with decay in destroying the muon. (Note the analogy with K-electron capture, which can compete with positron emission in the radioactive decay of certain nuclei. Here, however, it is the radioactive decay of the muon with which the muon capture process competes.) The apparent mean life of the negative stopped muons is therefore shorter than that of the positive muons. Consequently, the distribution in duration of the decay times of the combined sample of positive and negative muons is, in principle, the sum of two exponentials. Fortunately, the nuclear absorption rate in carbon is low, so that its effect on the combined decay distribution is small.

5.1. Why muon decay is so very interesting

We now know that there are two oppositely charged muons and that they decay according to the following three body decay schemes:

$$\mu^- \rightarrow e^- + \bar{\nu}_e + \nu_\mu \tag{5.2a}$$

$$\mu^+ \rightarrow e^+ + \nu_e + \bar{\nu}_\mu \tag{5.2b}$$
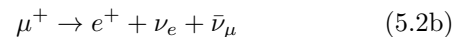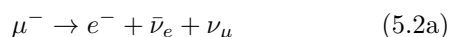
Rossi's particle was falsely believed to be the one demanded by Yukawa, which in 1947 was found to be the pion at 140 MeV. However, the charged pion decays[1] into muons via

$$\pi^- \rightarrow \mu^- + \bar{\nu}_\mu, \tag{5.3}$$

a two-body decay! We learned from this the following three things:

1. **The existence of a new kind of neutrino, ν_μ.** The energies of the decay electron in the pion and muon decay schemes look very different:

   Fig. 6 shows schematic spectra: on the left is a 2-body decay, the right must be a three body decay and from the peculiar shape, experts know that the 3rd body must have a spin=1/2. The 1988 Nobel Prize in Phyiscs was awarded[2] for work in which a ν_μ beam was generated from π decays with all muons being swept away by a B field. ν_μ only created muons, never electrons!

2. **Parity Violation.** The muons from pion decay are polarized anti-parallel to the flight direction and retain their polarization when stopping. The number of decay electrons emitted in the forward hemisphere of the former flight direction is different from the one into the backward hemisphere, thus violating parity (here, mirror symmetry).

---

[1] The decay $\pi \rightarrow e^- + \bar{\nu}_e$ is of course also possible but is suppressed by spin helicity.

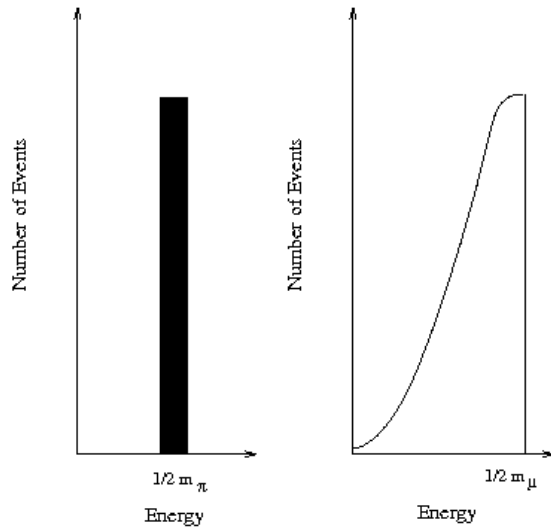[2] http://nobelprize.org/physics/laureates/1988/index.html

FIG. 6: Typical energy spectra resulting from two (left figure) and three (right figure) body decays.
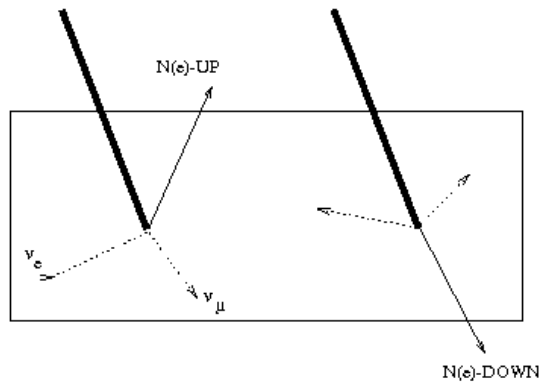

FIG. 7: Schematic of polarized muon decay demonstrating parity violation, i.e.
$$N(e)_{UP} \neq N(e)_{DOWN}$$

3. **Muon decay can be calculated exactly.** Enrico Fermi explained all beta decays (a weak interaction) as the decay of neutrons bound differently in their isotopic nuclei. Free neutrons decay slowly (mean lifetime 886 seconds) into a proton, an electron, and an electron neutrino. Since this is governed by weak interactions, all β-decays are characterized by the small coupling constant

$$G_F = 1.16 \times 10^{-5} (\hbar c)^3 / GeV^2. \qquad (5.4)$$

This was then superseded by the Electroweak Unified Theory (GWS, Nobel Prize in 1979), in which the interaction is mediated by the 81 GeV W-meson. This is an enormous energy; according to the uncertainty, this should occur only very sel-

dom, causing the "weak" appearance at low energies ($\ll M_W$). Now we can say

$$G_F = \frac{\sqrt{2}}{8} \left(\frac{g_W}{M_W c^2} \right)^2 (\hbar c)^3. \qquad (5.5)$$

Comparing the dimensionless constants, $g_W = 1/29 \gg \alpha = 1/137$, indicating the weak interaction is stonger than the electromagnetic interaction at high energies. Using the numerical value of G_F from Equation 5.4 in Equation 5.5, the muon lifetime can be calculated exactly to be [**?**]

$$\tau = \frac{192\pi^3 \hbar^7}{G_F^2 m_\mu^5 c^4}. \qquad (5.6)$$

Therefore, since we know G_F from beta decays, measuring τ allows us to find m_μ.

5.2.   Procedure: Measuring the Mean Life of Muons

Examine the outputs of the high gain photomultipliers with the oscilloscope. Adjust the high voltage supplies so that negative pulses with amplitudes of 1 volt or larger occur at a rate of the order expected for muon traversals (use your own calculations to check this). Do not exceed 1850 V to keep the noise tolerable. Feed the pulses to the coincidence circuit. Examine the output of the coincidence circuit on the oscilloscope with the sweep speed set at 1 μsec cm^{-1}, and be patient. You should occasionally see a decay pulse occurring somewhere in the range from 0 to 4 or so μsec, and squeezed into a vertical line by the slow sweep speed. Now feed the negative output of the coincidence circuit directly to the STOP input and through an appropriate length of cable (to achieve the necessary delay as explained above) to the START input of the TAC. A suitable range setting of the TAC is 20.0 μsec, obtained with the range control on 0.2 μsec and the multiplier control on 100. Connect the TAC output to the MCA. Verify that most of the events are piling up on the left side of the display within a timing interval of a few muon lifetimes. Let some events accumulate and check that the median lifetime of the accumulated events is reasonably close to the half-life of muon. Calibrate the setup with the time calibrator.

Commence your measurement of muon decays. To record a sufficient number of events for good statistical accuracy, you may have to run overnight or over a weekend. Be sure to plan your run in conjunction with the groups in the other sections to ensure that all have an opportunity to obtain muon lifetime measurements. When taking an overnight dataset, leave a note on the experiment with your name, phone number, email and what the file is to be saved as.

If you have recorded a sufficient number of events, say several thousand, and if the background counts are a small fraction of the muon decay events near $t = 0$ then the pattern on the MCA screen should look like that

shown in Figure (8). You should refer to Preparatory Question #5 for help in determining the rate of 'background' events but be careful in your selection of the value for τ.
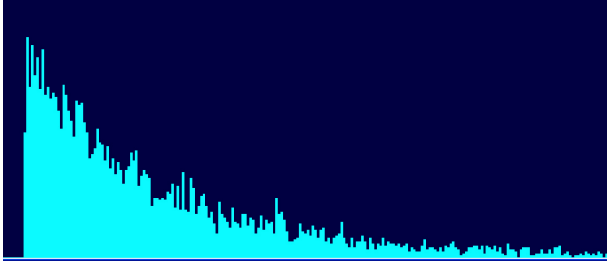

FIG. 8: Typical appearance on the MCA of the distribution in time of muon decays after about 10 hours of integration.

There is a potential pitfall in the analysis. The distribution in duration of intervals between successive random pulses is itself an exponential function of the duration, with a characteristic "decay" time equal to the reciprocal of the mean rate. If this characteristic time is not much larger than the muon lifetime, then the muon decay curve will be distorted and a simple analysis will give a wrong result. If the average time between events is much larger than the mean decay time, then you may assume that the probability of occurrence of such events is constant over the short intervals measured in this experiment, provided the triggering level is independent of the time since the last pulse. Under this condition, the observed distribution is a sum of a constant plus an exponential function of the time interval between the start and stop pulse. The constant, which is proportional to the rate of background events, is the asymptotic value of the observed distribution for large values of t. If this constant is subtracted from the distribution readout of the MCA, then the remainder should fit a simple exponential function, the logarithmic derivative of which is the reciprocal of the mean life.

5.3.   Analysis: Calculating the Mean Life of Muons

You can derive a value of the muon mean life by first determining the background rate from the data at large times and subtracting it from the data. Then plot the logarithms of the corrected numbers of counts in sucessive equal time bins versus the mean decay time in that interval, and fit a straight line. You should also use a non-linear fitting algorithm to fit the 3-parameter function

$$n_i = a \, e^{(-t_i/\tau)} + b \qquad (5.7)$$

to your data by adjusting a, b, and τ by the method of least squares, i.e. by minimizing the quantity

$$\chi^2 = \sum (n_i - m_i)^2/m_i, \qquad (5.8)$$

where m_i is the observed number of events in the ith time interval. (Watch out for faulty data in the first few tenths of a μsec due to resolution smearing after pulsing of the photomultiplier, and the decay of negative muons that suffer loss by nuclear absorption.) Consult Melissinos (1966) for advice on error estimation. Finally, compare your fit value for b to the expected number of 'accidentals'.

Evaluate:

1. How long does it take a typical high energy cosmic-ray muon to get to sea level from its point of production? What would its survival probability be if its life expectancy were the same as that of a muon at rest?

2. Given their observed intensity at sea level, what would be the vertical intensity of muons at an altitude of 10 km if all cosmic ray muons were produced at altitudes above 10 km and time dilation were not true? How does this value compare with the actual value measured in balloon experiments? (See Appendix B for data on the flux versus atmospheric depth.)

3. Calculate a typical value of the Lorentz factor γ at production of a muon that makes it to sea level and into the plastic scintillator.

To think about: Suppose your twin engineered for you a solo round trip to Alpha Centauri (4 light years away) in which you felt a 11.0 g acceleration or deceleration all the way out and back (could you get out of your seat?). How much older would each of you be when you returned?

5.4.   Possible Theoretical Topics

1. The Special Theory of Relativity.

2. Energy loss of charged particles in matter.

3. Fate of negative muons that stop in matter.

4. Violation of parity conservation in muon decay.

Beyond the primary references already cited in the labguide, useful secondary references include [? ? ? ?].

APPENDIX A: PROPERTIES OF THE FLUX OF COSMIC-RAY MUONS

The differential flux $I_v = dN(dAdtd\Omega)$ is given in Fig. 10 for vertical (ϕ=0) incidences as a function of atmospheric depth. Sea level is $\approx$1000 g cm^{-2} areal density. There the momentum distribution peaks at 1GeV/c (see Fig. 11). Each momentum corresponds to a penetration depth differentially given in Fig. 12 for light elements (e.g. air, scintillators, etc.)
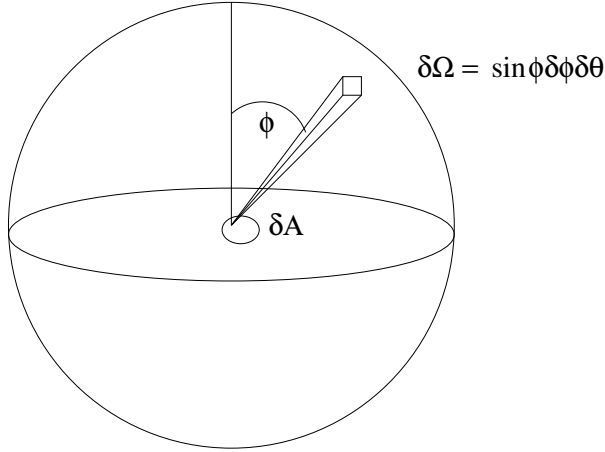

FIG. 9: Differential element of the flux of cosmic-ray muons.

The distributions at other zenith angles can be represented fairly well by the empirical formula $I(R,\varphi) = I(R,0)\cos^2\varphi$. The stopping material in the experiment is a cylinder of scintillator plastic. Call its height b, its top area A, and its density ρ. Consider an infinitesimal plug of area dA in an infinitesimally thin horizontal slice of thickness (measured in $g\ cm^{-2}$) $dR = \rho dx$ of the cylinder. The stopping rate of muons arriving from zenith angles near φ in $d\varphi$ in the element of solid angle $d\Omega$ in that small volume $dA\,dx$ can be expressed as

$$ds = I(R',0)\cos^2\varphi(\cos\varphi dA)(\rho dx/\cos\varphi)d\Omega \quad (A1)$$

where ($\cos\varphi\,dA$) is the projected area of the plug in the direction of arrival, ($dx/\cos\varphi$) is the slant thickness of the plug, and R' is the residual range of muons that arrive from the vertical direction with just sufficient energy to penetrate through the overlying plastic to the elemental volume under consideration. The total rate S of muon stoppings in the cylinder can now be expressed as the multiple integral

$$S = 2\pi\rho \int\limits_0^A dA \int\limits_0^b I(R',0)dx \int\limits_0^{\pi/2} \cos^2\varphi\sin\varphi d\varphi \quad (A2)$$

in which we have replaced $d\Omega$ by $2\pi sin\varphi d\varphi$ under the assumption of azimuthal symmetry of the muon intensity. Looking at Figure 12, we see that the muon range

spectrum is nearly constant out to energies much greater than necessary to penetrate the building and the plastic. So we can approximate the quantity $I(R',0)$ by the constant $I(R,0)$. Performing the integrations and calling $m = Ab\rho$ the mass of the entire cylinder, one readily finds for the total rate of muons stopping in the cylinder the expression

$$S = \frac{2\pi}{3}mI(R_{av},0). \quad (A3)$$

APPENDIX B: REFERENCE FIGURES: OBSERVED PROPERTIES OF COSMIC-RAY MUONS

Several plots of empirical data concerning cosmic-ray muon behavior, for reference purposes.

From B. Rossi, Rev. Mod. Phys., **20**, 537 (1948)
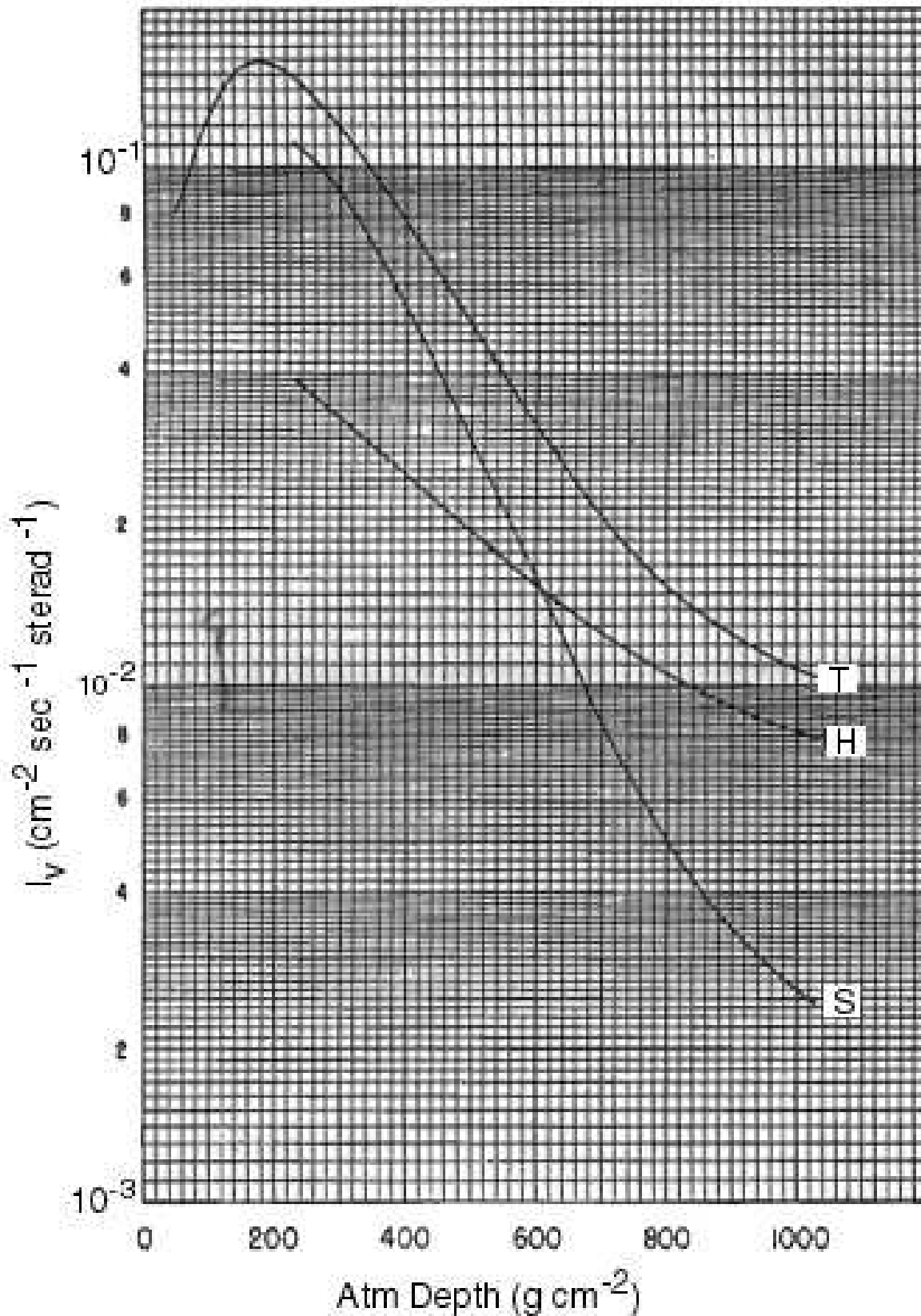
FIG. 10: The vertical intensities of the hard component (H), of the soft component (S), and of the total corpuscular radiation as a function of atmospheric depth near the geomagnetic equator.
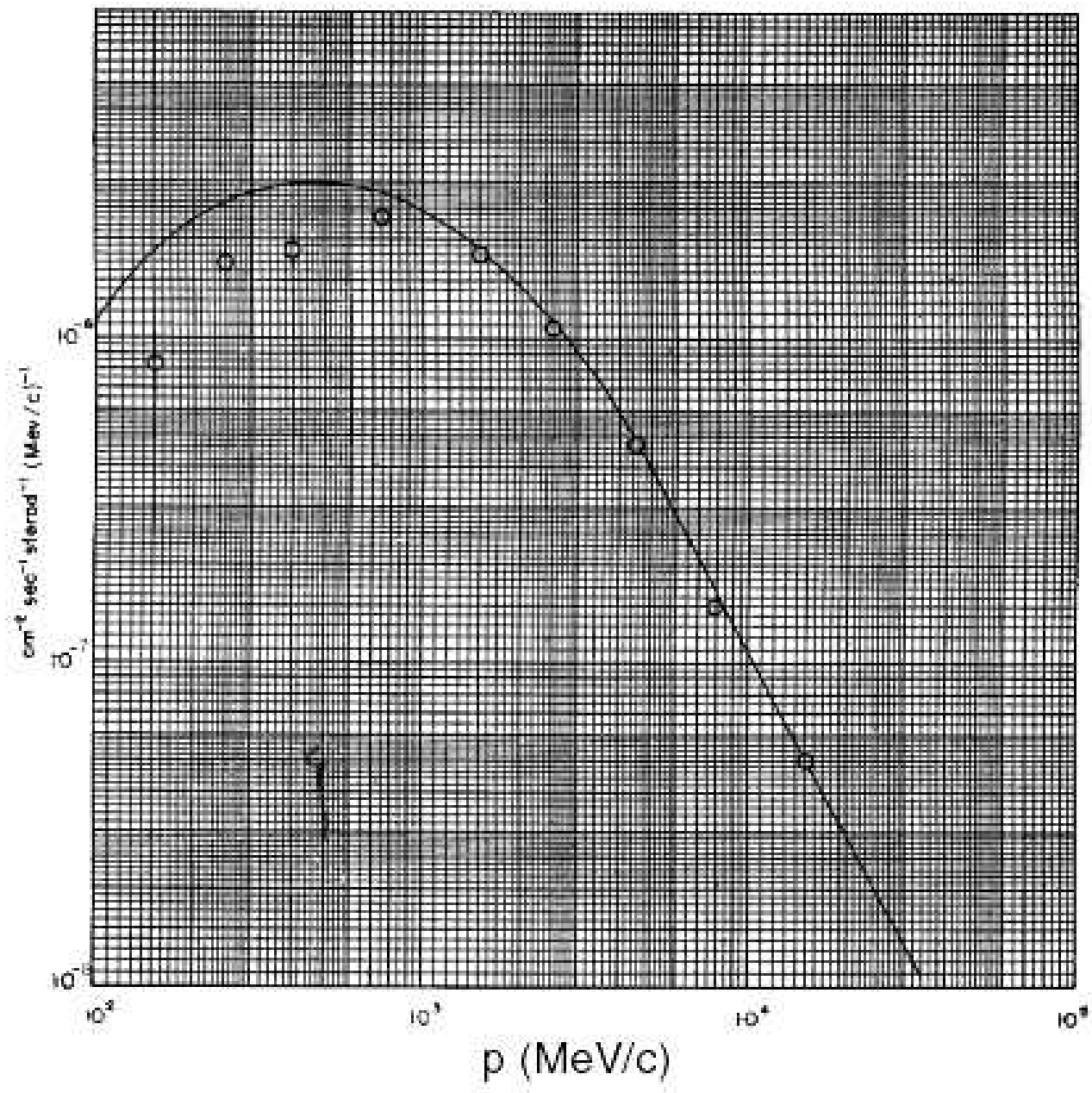
FIG. 11: Differential momentum spectrum of muons at sea level. The x-axis ranges from 10^2 to 10^5
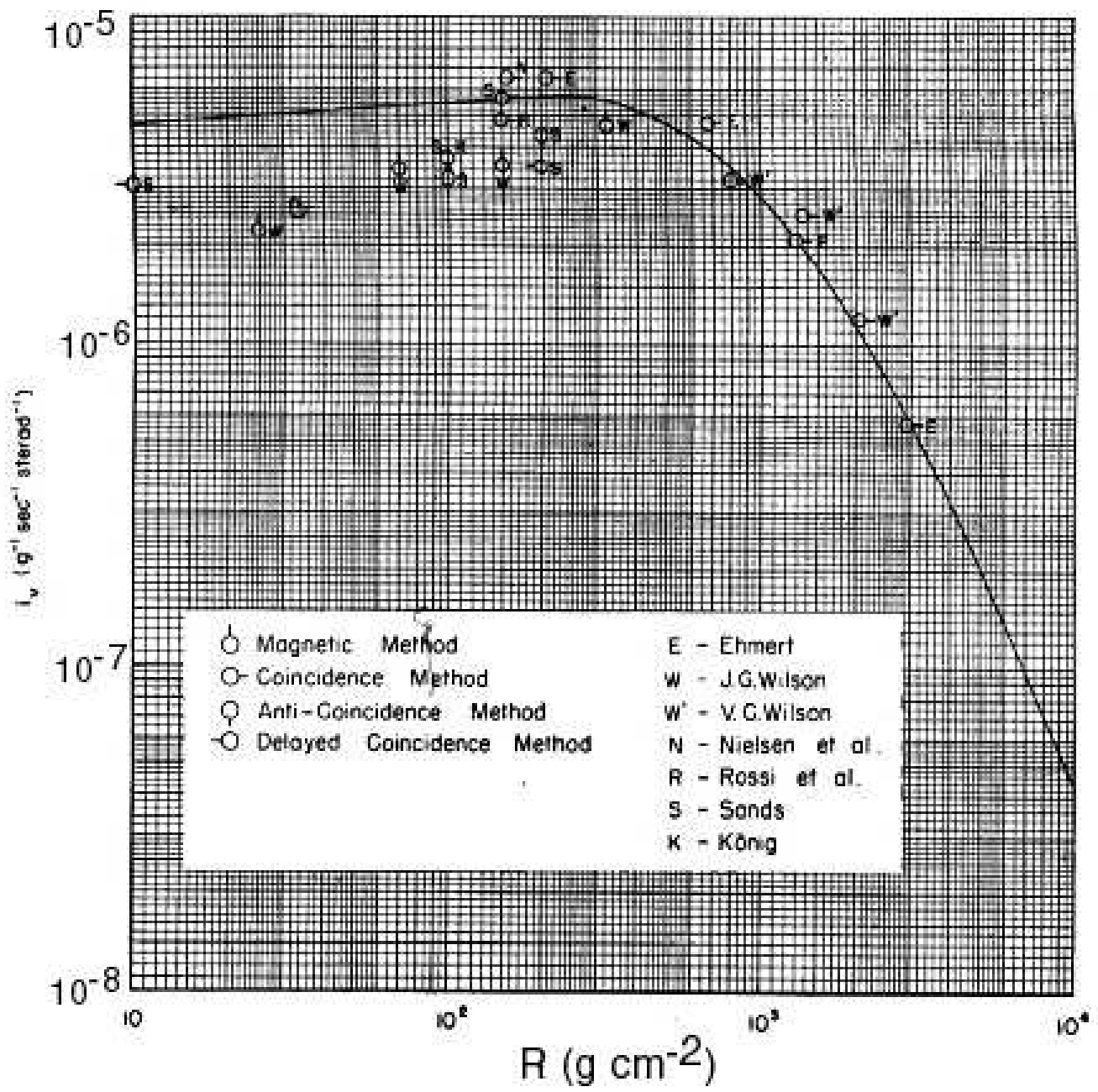
FIG. 12: Differential range spectrum of muons at sea level. The range is measured in gm cm^{-2} of air. The x-axis ranges from 10 to 10,000

APPENDIX C: DISTRIBUTION OF DECAY TIMES

The fundamental law of radioactive decay is that an unstable particle of a given kind that exists at time t will decay during the subsequent infinitesimal interval dt with a probability rdt, where r is a constant characteristic of the kind of the particle and independent of its age. Call $P(t)$ the probability that a given particle that exists at $t = 0$ will survive till t. Then the probability that the particle will survive till $t + dt$ is given by the rule for compounding probabilities,

$$P(t + dt) = P(t)[1 - rdt]. \quad\quad (C1)$$

Thus

$$dP = -Prdt, \quad\quad (C2)$$

from which it follows that

$$P(t) = e^{-rt}. \quad\quad (C3)$$

To find the differential distribution of decay times $n(t)$, which is the distribution measured in the muon decay experiment with the TAC and MCA, we multiply the negative derivative of P by the product of the rate S at which muons stop in the scintillator by the total time T of the run. Thus

$$n(t) = (ST)(-dP/dt) = (ST)re^{-rt}. \quad\quad (C4)$$

Identical reasoning can be applied to the problem of finding the distribution in duration of the intervals between random events that occur at a constant average rate s, like the background events in the muon decay experiment. In this case each random event that starts a timing operation, in effect, creates an 'unstable' interval (=particle) that terminates (=decays) at the rate s. Thus the distribution is a function of exactly the same form, namely

$$m(t) = (sT)s\ e^{-st}, \quad\quad (C5)$$

where (sT) is the expected total number of events in the time T. Note that the number of background events is proportional to s^2. This suggests a limit on how low the discriminator can be set in an effort to catch all of the muon stopping events. At some point the ratio of muon decay events to background events will begin to decrease as s^2.

Rutherford Scattering

MIT Department of Physics
(Dated: September 5, 2011)

This is an experiment which studies scattering alpha particles on atomic nuclei. You will shoot alpha particles, emitted by ^{241}Am, at thin metal foils and measure the scattering cross section of the target atoms as a function of the scattering angle, the alpha particle energy, and the nuclear charge. You will then measure the intensity of alpha particles scattered by thin metal foils as a function of the scattering angle for several elements of very different atomic number.

1. Preparatory Questions

1. What is the closest possible distance of approach of a 5.5 MeV alpha particle to a gold nucleus, and how does that distance compare to the radius of the nucleus?

2. Define the differential scattering cross section.

3. Sketch the expected curve of counting rate as a function of the scattering angle for the gold foil.

4. Describe in words how charged particles lose energy in traversing matter. How does the rate of energy loss depend on the velocity of a particle?

5. How much energy does an alpha particle emitted by ^{241}Am lose in traversing 1 cm of air at STP?

6. How does the solid-state detector used in this experiment work? See References [1, 2].

2. Introduction

Little was known about the structure of atoms when Geiger and Marsden began their experiments scattering alpha particles on thin metal foils in 1909 at the Cavendish Laboratory. A decade earlier at the Cavendish, J. J. Thomson had discovered the electron and determined the ratio of its charge to its mass by measuring the deflections of electron beams (cathode rays) by electric and magnetic fields. In 1909, Millikan measured the charge of the electron in the oil drop experiment. Thus by 1909 both the charge and mass of the electron were known with considerable accuracy. Furthermore, Thomson's interpretation of X-ray scattering from carbon and other light elements had established that the number of electrons per atom of a given element was equal not to its atomic weight, but to its atomic number, determined by its position in the periodic table. Since the mass of an electron is much less than the mass of the lightest atom, hydrogen, it was clear that most of the mass in any atom is associated with the positive charge. The central problem was to figure out how the positive and negative parts of an atom are held together, in such a way as to produce optical emission spectra with the regularities expressed by the Balmer formula (discovered by Johann Balmer in 1885) for hydrogen and the combination rules and series limits for the complex spectra of multielectron atoms.

Thinking within the limitations of Newtonian mechanics and Maxwell's electromagnetic theory, Thomson imagined the atom as a sphere of positive charge within which the electrons occupy certain positions of equilibrium, like raisins in a pudding. Set in motion, the electrons should vibrate harmonically, radiating electromagnetic energy with characteristic sharp frequencies that would be in the optical range if the radii of the atomic spheres were of the order of 10^{-8} cm. However, the "raisin pudding" model yielded no explanation of the numerical regularities of optical spectra, e.g. the Balmer formula for the hydrogen spectrum and the Ritz combination principle[3] for spectra in general.

At this point, Ernest Rutherford got the idea that the structure of atoms could be probed by observing the scattering of alpha particles. He had recently demonstrated the emanation of positively charged radioactive substances from certain sources; known as alpha particles, they are also bare helium nuclei. The positively charged emanation of radioactive substances that he had recently demonstrated were helium ions. According to the raisin pudding model, an alpha particle traversing a thin gold film should experience many small angle deflections as it passes close to or through the positive spheres of the gold atoms. Rutherford showed [4] that the fraction of particles scattered in this way through an angle θ or greater should decrease exponentially according to the equation

$$F_\theta \approx \exp(-\theta^2/\theta_m^2), \qquad (2.1)$$

where θ_m is the mean multiple scattering angle. For a typical foil of gold leaf, $\theta_m \sim 1°$. Thus at $\theta = 30°$, one finds F_θ on the order of $\exp(-30)$ or 10^{-13}.

Rutherford's formula turned out to be correct for very small angles of scattering. Evidently there was substantial truth in the idea of multiple scattering. But in experiments initiated at Rutherford's direction, Geiger and Marsden (1909) found that 1 in 8000 alpha particles passing through a thin film of platinum was scattered through more than 90°! It was as though bullets fired at a bale of cotton could occasionally ricochet backward. Such an observation might lead one to suspect rocks in the cotton.

At this point Rutherford (1911) advanced the hypoth-

esis that the positive charge and most of the mass of an atom is concentrated in a "nucleus" with dimensions of the order of 10^{-12} cm (10,000 times smaller than the atom as a whole) with the electrons in some sort of configuration around it. Applying the principles of classical mechanics, he calculated the trajectories of alpha particles passing near such nuclei, and derived an expression for the differential scattering cross section which accounted accurately for the scattering data, thereby validating the hypothesis of the nuclear atom.

The Rutherford scattering differential cross section *per target atom* for any target atom is

$$\frac{d\sigma}{d\Omega} = \left(\frac{ZZ'e^2}{4E}\right)^2 \frac{1}{\sin^4(\theta/2)} \qquad (2.2)$$

where θ is the scattering angle, Ze is the charge of the target nuclei, $Z'e$ is the charge of the alpha particles and E is their kinetic energy. (For a derivation, see Reference [5].) Further excruciatingly tedious experiments by Geiger and Marsden confirmed the validity of the formula within the statistical errors of their measurements. Geiger hadn't invented the Geiger counter yet, and electronic detection methods were still 20 years in the future. They used a low power microscope to observe and count by eye the scintillations produced by the alpha particles when they impinged on a screen lightly coated with zinc sulfide dust.

References [5, 6] present the Rutherford theory and discuss the interpretation of data from a scattering experiment that is quite similar to that in the Junior Lab, with the exception of the specific detector and circuit arrangement. We will confine our discussion to the features of the experimental setup and procedures that are peculiar to our setup.

3.   Apparatus

Figure 1 is a schematic drawing of the apparatus in the vacuum chamber. The source, ^{241}Am, emits alpha particles of various discrete energies, the most frequent of which are 5.486 MeV (86%), 5.443 MeV (12.7%), and 5.391 MeV (1.4%). All these decays lead to excited states of ^{237}Np. The half-life of ^{241}Am is 458 years. The source, deposited on a thin metal disk with the highest activity of ^{241}Am per unit area commercially available (~ 1.5 millicuries per square inch) and sealed with an evaporated gold coating 1.5 microns thick, is covered by a metal washer with a 0.64 cm diameter hole and enclosed in a "howitzer" with a 0.64 cm diameter aperture in its snout. Due to the gold coating, the alpha particles' initial energies are reduced to valuea closer to 4.8 eV. Under near-vacuum, a collimated beam of alpha particles emerges from the snout (the range of 5.5 MeV alpha particles in air at atmospheric pressure is only ~ 4 cm).

If the setup is under vacuum turn the bias voltage on the detector slowly down to zero, close the vacuum valve
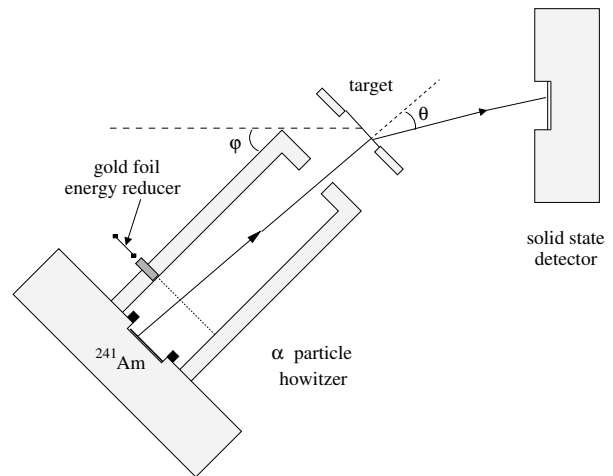
FIG. 1: Schematic of the howitzer, target, and detector in the vacuum chamber.

between the pump and the chamber, and slowly open the vacuum release valve, leaving the pump running. Place the black hood on a table where it can serve as a cushion for the plastic cover. Lift the cover off the steel cylinder and place it flat on the hood, being careful not to damage the underside of the plastic cover. Find out how you can adjust the relative positions of the howitzer and detector with respect to the target, and how you can turn, raise and lower the target with the control rod that protrudes from the bottom of the chamber. Note how you can simultaneously rotate the howitzer and the target about a vertical axis through the target with the lever attached to the outer cylinder under the chamber. This feature enables you to maintain a fixed relative orientation of incident beam and target while you vary the scattering angles of the detected alpha particles.

Two warnings: **Do not remove the black cover while the detector is still on.** The lights in the lab are far stronger than what the detector is designed to absorb. Exposure to the background light in the lab may fry the detector. **Do not release the vacuum too quickly.** A rapid change in pressure can cause the delicate foil targets to rupture.

3.1.   Calibrate the Measurement Chain

Move the howitzer support arm so that the howitzer points directly at the detector through the empty target hole. Pump the system down with the bias voltage off. If necessary, a good way to apply the necessary pressure to initially 'seal' the O-ring and gasket is by weighting the plexiglass cover with $6-8$ lead bricks available next to the experiment. Also, there is vacuum grease available, but don't overuse it! A pea-sized amount is more than enough for the surface of the O-ring. Using an oscilloscope, you can watch the pulses from the unbiased detector appear and gradually grow in amplitude as the

amount of air between the source and detector diminishes. The pressure should reach 200 microns in 10 to 15 minutes. If it doesn't, you probably have leak a around the O-ring seal under the plastic cover or around the gasket under the stainless-steel cylinder. It can be remedied by placing a 'perimeter' of lead bricks around the edge of the cover to help weight the edges and initiate the vacuum. When the pressure is below 200 microns leave the bias voltage supply switch on its lowest position and turn the continuous bias voltage control. Connect a voltmeter to the small aluminum box that is situated between the voltage supply and preamp for the detector. Slowly increase the voltage until the meter reads +50 volts. Adjust the gain so that the alpha-particle (bipolar) pulses have an amplitude of about +7 volts. The bipolar amplifier output is better for handling high count rate detection such as the case with no foil. Observe the pulse size distribution with the MCA and readjust the gains so that the peak of the alpha-particle pulse-size distribution lies at a convenient position within the full range of the multichannel analyzer. You can assume that the amplitude of a detector pulse is proportional to the energy lost by the particle in the silicon detector. Thus a linear plot of the channel number versus energy, scaled to match the energy of the alpha-particles coming straight from the source, should be an accurate plot for the interpretation of the pulse sizes you will be measuring.

3.2. Adjust the Position of the Target

Accurate vertical positioning of the target holder is essential to assure that the particle beam passes cleanly through one or another of the holes in the aluminum sheet that supports the foils, without touching the edge of the hole. Either you or your partner can manipulate the target holder from under the table while the other judges its position.

With the target holder in the open hole position, measure the counting rate as a function of the howitzer position angle from $\sim$ -10° to $\sim$ +10° relative to the nominal center position. **Plot the data as you proceed on a log scale. Log graph paper is available if desired.** Determine the exact pointer readings of the center position and at the positions of zero counting rate intercepts on either side of the center to determine the beam center and its total width.

3.3. Measure the Effects of Target Foils on the Pulse-Height Spectrum of Alpha-Particles

Using the preset accumulation time feature of the MCA accumulate a size spectrum of the pulses produced by unscattered alpha particles with the howitzer position angle set at the center position. To characterize the width of the distribution, place the start and stop cursors on either edge of the distribution at the positions

where the counting rate is half the maximum value, and note the channel numbers. Measure the channel number of the peak counting rate. Compare the results with no foil, the two gold foils, and the titanium foil, and figure out the most probable energy lost by the alpha particles in traversing each of the films. Describe and explain the changes in the shape of the size spectrum when a target foil is in the beam.

Determine the thicknesses of the target by reference to the range-energy data available on the web at [7]. Be sure to use the "projected range" data and not the CSDA range data. To interpolate this table plot the tabulated range versus energy. Call c_1 and c_2 the median channels of the pulse before and after passage through a target. You can assume with some confidence that the median channel number is proportional to the particle energy. From your range energy plot, read the range of the incident alpha particles E_0 and the range of particles with energy $(c_2/c_1) E_0$. The difference in range is the thickness of the target in $mg \cdot cm^{-2}$. Does your data fit better using $E_0 = 5.48$ MeV ot using a reduced value accounting for the 1.5 μm gold coating on the source?

3.4. Plan and Make Your Scattering Measurements

Your data from this experiment should consist of **at least** the results of the following operations:

1. Determine the essential characteristics of the experimental setup.

    (a) Measure the counting rate as a function of howitzer position angle with the open hole.

    (b) Measure the loss in energy of the alpha particles in traversing each of the three targets and determine the thicknesses of the targets from the data.

2. Measure the angular dependence of the scattering cross section of gold. Measure the counting rate with a gold target for the full energy alpha particle beam as a function of howitzer position angle out to the largest angles that counting statistics and time limitations allow.

3. Determine the total cross section σ. Measure the intensity of the beam that emerges from the howitzer. Note that the howitzer is designed so that the entire emergent beam irradiates the target foils; i.e., the beam is sufficiently narrow to pass through the foils without intercepting the target holder.

4. Measure the Z-dependence of the Rutherford cross-section. Compare your results from the gold targets to counting rates measured using the provided targets containing other elements.

At large scattering angles the counting rates are very low, so the accuracy of your data will be severely limited by the (Poisson) statistical accuracy you can achieve. Your best strategy will be to make a complete set of measurements with short integrating times (10 – 30 minutes) in each configuration you plan to use, and to carry out a preliminary analysis of the resulting data during the first session. Then, in the light of what you have learned about the counting rates and the problems of analysis, you can make a run plan allotting enough time to each configuration to obtain enough counts to insure good statistical accuracy. Obviously, you cannot afford to measure the counting rates at 2° intervals of the howitzer angle. You may decide, for example, to settle for measurements of good statistical accuracy of the angular dependence of the counting rate with one target only at howitzer angles of, say, 20°, 30°, 40° and 60°, and measurements of the Z and E dependence at only one howitzer angle, say 20°.

You will probably want to attain at least 2 – 20% (> 4 – 400 counts) statistical accuracy in each of your measured rates. If you occupy the first lab sessions getting acquainted with the experiment, then you will have a total of about 9 hours in the next three sessions to get your definitive scattering data plus a possible overnight run at a very large scattering angle to observe the amazing phenomenon of atomic bullets ricocheting nearly straight back. Clearly you cannot afford to creep along the curve of rate versus position angle at one-degree intervals. Rather, you must take large steps in position angle to define the general shape of the curve, and then fill in to refine your data as time permits.

3.5. Suggested Progress Check at End of Session 2

Plot the rate of alpha particle observations for 10° and 30° vs. $1/\sin^4(\theta/2)$. Comment on the agreement.

3.6. Challenge Experiment for Session 4: Cross-Section Energy Dependence

To measure the energy dependence of the cross section you can reduce the incident energy by inserting into the slot in the howitzer the titanium foil in the holder provided. You should make your measurement of the energy dependence of the differential cross section at a position angle large enough (say 20°) to reduce the complications caused by multiple small-angle Rutherford scattering. Your analysis will be simpler if you maintain the same geometrical relation between the howitzer and the scattering foil. This is feasible for measurements at position angles from 0° to $\approx 60°$.

4.   Analysis and Interpretation

Some additional references that you may find useful include [7–10].

1. Using a log plot, plot the gold-foil counting rates against $\sin^{-4}(\theta/2)$, where θ is the howitzer position angle, and compare the result with the theoretical expectation based on the Rutherford formula. Compare also with the results given in [5]. Be sure to also complete a full error analysis.

   To make an accurate comparison between the data plot and the predictions of the Rutherford theory, you should take into account the spread in the angular response of the apparatus. The inescapable fact of any scattering measurement is that events with a range of scattering angles contribute to the counting rate at any given position angle of the detector. Ideally one would like that range to be very small so that a plot of counting rate against position angle would be, in effect, a plot of counting rate against scattering angle. But then the counting rate would be impractically small. Thus, in designing a scattering experiment, one must strike a compromise between angular resolution and counting rate. To achieve acceptable counting rates in the present experiment, it was necessary to design it with a broad angular acceptance.

   Consequently, your plot of counting rate against position angle should be compared to a convolution of the Rutherford cross section with the angular response function of the apparatus. This may be approached in one of several ways of differing sophistication. To see how this can be done, call $g(\theta, \phi)$ the angular response function such that $g(\theta, \phi)d\theta$ is the probability that a particle scattered at an angle between θ and $\theta + d\theta$ will be detected when the howitzer is at position angle ϕ. Then the expected counting rate at ϕ is

$$C(\phi) = C_0 \int_0^\pi g(\phi, \theta) \sin^{-4}(\theta/2)d\theta, \qquad (4.1)$$

   where C_0 is a constant that includes the solid angle subtended by the detector at the point of scattering. For a crude approximation one might represent g by a triangular function defined by

$$g(\phi, \theta) = \begin{cases} (1 - \frac{|\theta - \phi|}{\theta_0}), & |\theta - \phi| < \theta_0 \\ 0, & |\theta - \phi| > \theta_0 \end{cases}, \qquad (4.2)$$

   where θ_0 is the half-width of the base of a triangular function. The value of θ_0 can be estimated by analysis of Figure ??, which is a scale drawing of the howitzer, target holder and detector. One might
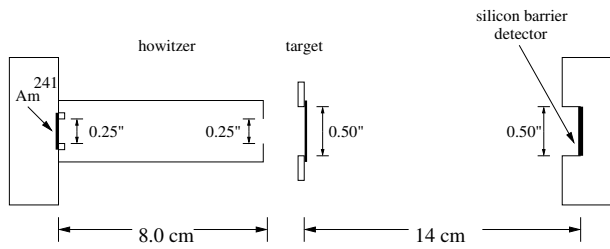
FIG. 2: Dimensioned drawing of the alpha-particle howitzer, target foil, and detector geometry. Dimensions which are easily verified by the user should be done so.

set $2\theta_0$ equal to the difference between the extreme angles of scattering that detected particles can undergo when $\phi = 0$. The convolution should yield a curve of counting rate versus position angle that conforms more closely to the data than the function $\sin^{-4}(\phi/2)$ of the Rutherford cross section.

A second approximation may be made simply by using the beam profile obtained in Section 3.2.

A little thought will convince you that it is a formidable job of geometrical analysis to construct an exact analytical expression for g. A more practical approach is to write a "Monte Carlo" program that simulates the experiment by following individual particles through the system, choosing positions and directions of emission and scattering with random numbers according to appropriate probability distributions, among which is the Rutherford scat-

tering probability distribution to be tested. If you are an experienced programmer you may want to try this approach, which is also not a trivial job. You can probably get advice on how to proceed from one of your instructors.

2. Determine the differential scattering cross section per gold atom at an angle (say $30°$) large enough to reduce substantially the problems of interpretation caused by multiple scattering.

3. There is a substatial problem with Rutherford's distribution that should by now be very apparent: equations of the form $1/\sin^4(\theta)$ approach ∞ in the limit $\theta = 0$. However, you will not observe an infinite number of particles emitted from the target when it is at the center position. Try to come up with an explanation to reconcile the Rutherford model with what you observe. A few things to think about: multiple scattering; the nature of scattering cross sections; quantum mechanics.

4.1. Possible Theoretical Topics

- The Rutherford scattering cross section.

- Energy loss of charged particles in matter.
- Multiple Coulomb scattering.

- Silicon barrier detector.

[1] A. Melissinos, *Experiments in Modern Physics: Solid-State Detectors* (Academic Press, 2003), chap. 8.5, pp. 344–354, 2nd ed.
[2] G. F. Knoll, *Radiation Detection and Measurement: Semiconductor Diode Detectors* (John Wiley and Sons, 2000), chap. 11, pp. 353–404, 3rd ed., covers solid state detectors at a higher level of detail than Melissinos.
[3] W. Ritz, Astrophysical Journal **28**, 237 (1908).
[4] E. Rutherford, Philisophical Magazine **21**, 669 (1911).
[5] A. Melissinos, *Experiments in Modern Physics: Rutherford Scattering* (Academic Press, 1966), chap. 6, pp. 226–252.
[6] A. Melissinos, *Experiments in Modern Physics: Interaction of Charged Particles with Matter* (Academic Press, 1966), chap. 5, pp. 152–165.
[7] J. C. M.J. Berger and M. Zucker, Tech. Rep., NIST, Gaithersburg, MD (1999-2002), URL http://physics.nist.gov/PhysRefData/Star/Text.
[8] P. Bevington and D. Robinson, *Data Reduction and Error Analysis for the Physical Sciences* (McGraw-Hil, 1992), 3rd ed.
[9] S. Gasiorowicz, *Quantum Physics* (Wiley, 1974), 2nd ed.
[10] E. Serge, *Nuclei and Particles* (Benjamin, 1977), chap. 2.

APPENDIX A: EQUIPMENT LIST

Manufacturer	Description	URL
Canberra	PIPS α-particle detector	canberra.com
Canberra 2006	Charged Particle preamplifier	canberra.com
Canberra	Amplifier	canberra.com
Ortec	Multi-Channel Analyzer	ortec-online.com

Optical Spectroscopy of Hydrogenic Atoms

MIT Department of Physics
(Dated: September 5, 2011)

This experiment uses optical spectroscopy to study the spectra of "hydrogenic" atoms, atoms with one "optical" electron in the valence electron shell. Measurements include finding the Balmer lines of atomic hydrogen and the fine structure of sodium lines and the determination of the mass of the deuteron from the isotope shift. A high-resolution scanning monochromator is used to study the Balmer lines of hydrogen and the more complex hydrogenic spectrum of sodium, using the mercury spectrum as the wavelength calibrator. The measured Balmer wavelengths are compared with the quantum theory of the hydrogen spectrum, and a value of the Rydberg constant is derived. The transitions responsible for the sodium spectrum are identified, and the regularities in the fine structure and adherence to the selection rules are observed. A measurement of the isotope shift between the Balmer lines of hydrogen and deuterium is made from which the ratio of the deuteron mass to the proton mass is derived.

1. PREPARATORY QUESTIONS

1. Construct as complete an energy level diagram of atomic hydrogen as you can, and show the transitions that give rise to the Balmer lines. (Incidentally, just exactly what is a spectral "line"?)

2. Define the following terms and, where applicable, calculate them for the two optical systems used in this experiment: *grating equation, diffraction orders, angular dispersion, linear dispersion, resolving power, spectral resolution, bandpass, focal length, f/#, and free-spectral range.* (See [1, 2])

3. Suppose perfectly monochromatic light of wavelength 4500 Å enters a Czerny-Turner monochromator with the input slit width set at 10.0 μm, and suppose the beam fully illuminates the concave grating which is a 10 cm x 10 cm square with 3600 lines mm^{-1}. Make a plot with properly scaled axes of the light intensity versus angular displacement in the focal plane of the spectrograph in the first order diffracted image of the slit. Show quantitatively the salient features of the multiple slit diffraction pattern. (see [2])

4. Throughout this experiment the tabulated wavelengths of the mercury spectrum will be used as the calibration reference. Suppose, however, you had to start from scratch with no reference wavelengths. How would you establish an absolute scale of wavelengths?

5. Predict the isotope shift in wavelength (i.e., the difference in wavelength $\Delta\lambda = \lambda_H - \lambda_D$) of the first 3 Balmer lines of hydrogen and deuterium. (see [3])

2. INTRODUCTION

The study of the optical spectra of hydrogen and other atoms having a single "optically active" electron in a spherically symmetric potential was specially important in the development of modern physics because of the simplicity of the spectra and the clarity with which their features could be understood in terms of the developing theories of quantum electrodynamics and atomic structure. The purpose of this experiment is to acquaint you with some of these features and with some of the methods of optical spectroscopy through an investigation of the spectra of hydrogen, deuterium, and the alkali metals.

Bohr's theory of the optical spectrum of hydrogen, published in 1913, opened the door to the modern theory of atomic structure. In 1912 Bohr had come to Rutherford's Laboratory at Manchester University where the concept of the atomic nucleus had been invented the previous year by Rutherford in his theory of the scattering of alpha particles by thin metal foils. Bohr immediately began to wrestle with the problem of how electrons in orbit about a nucleus can constitute a stable system when the classical laws of electromagnetism imply they must radiate their orbital energy and spiral into the nucleus. Bohr concluded that new, non-classical physical principles must govern atomic phenomena. By the summer of 1912 he arrived at his central idea that some form of quantization restricts the orbits of electrons inside atoms. He had in mind the quantum idea introduced by Planck in 1900 in his theory of the spectrum of blackbody radiation and invoked by Einstein in 1905 to explain the photoelectric effect. Then somebody brought to Bohr's attention the simple regularities of the hydrogen spectrum, expressed in the formula discovered by Balmer in 1885. Afterward he said, "As soon as I saw Balmer's formula the whole thing was immediately clear to me" (Rhodes 1986 [4]).

The Balmer spectrum of atomic hydrogen is readily produced by an electrical discharge in molecular hydrogen (H$_2$) at low pressure. The resulting collisions of mildly energetic electrons with hydrogen molecules cause dissociations of the molecules and excitations of the resulting atoms to states which decay in transitions that yield the Balmer lines in the visible region of the spectrum, as well as the Lyman lines in the ultraviolet, and other series of lines in the infrared. **Measurement of**

the Balmer lines, verification of the Balmer/Bohr formula for their wavelengths, and determination of the Rydberg constant are the first objectives of this experiment.

Interesting variations on the theme of the hydrogen spectrum are found in the spectra of other single-electron atoms such as deuterium, tritium, singly ionized helium, doubly ionized lithium, all the way up to 25-times ionized iron. One expects the spectra of these atoms to be similar to that of hydrogen except for the effects of changes in the reduced mass, the nuclear charge, and the hyperfine interactions between the electronic and nuclear magnetic moments. In the laboratory it is difficult to produce a sufficient density of excited, multiply-ionized helium or lithium to yield a detectable spectrum of their single-electron ion species. As for hydrogen-like iron, it has only been seen in the radiation from solar flares, neutron stars in accreting binary systems, and the hot intergalactic gas in clusters of galaxies. But the effect on the spectrum of a change in the reduced mass of the nucleus-electron system is readily observed in deuterium. **Measurement of this "isotope" shift in the Balmer lines and determination of the ratio of the mass of the deuteron to the mass of the proton is another objective of this experiment.**

Another kind of "hydrogenic" spectrum is produced by atoms with one electron outside of "closed" shells. Examples are the alkali metals, singly-ionized alkaline earth metals, doubly-ionized elements in the third column of the periodic chart, etc. In such an atom or ion a single "optical" electron moves in the spherically symmetric potential of the nucleus and the closed shells of the inner electrons, and the eigenstates and energy eigenvalues of the atom can be calculated, in principle, as perturbed solutions of the Schrödinger equation for a hydrogen-like atom with a perturbation potential that represents the distortion of the simple 1/r potential of a point nucleus by the inner electrons. One effect of this shielding is to enhance the splitting of the levels with angular momentum quantum numbers $L > 0$ due to the spin-orbit interaction. Measurements of the doublet separations provide clues to the identity of the states involved in the transitions that give rise to the lines. **A third objective of this experiment is the measurement of the doublet separations of the spectral lines of sodium and the identification of the quantum transitions responsible for the lines.**

Most of the theoretical background you need for understanding the atomic spectra to be measured in this experiment is the Appendices and in Melissinos (2003) [5]. More thorough treatments can be found in your texts for 8.04 and 8.05, e.g. [3, 6]. Another useful and classic reference is *Introduction to Atomic Spectra* by C. F. White (1934) [7]. Here we will concentrate on describing the features of the equipment and procedures peculiar to the setups in Junior Lab. Excellent discussions of the optics of monochromators and spectrometers is given in Jobin Yvon's Tutorial *The Optics of Spectroscopy* by J.M. Lerner and A. Thevenon [1] and, more rigorously, in *Optics* by E. Hecht (2002) [2]

3. EXPERIMENTAL APPARATUS

The instrument used to perform this experiment is the research grade high-resolution (0.03Å) scanning **monochromator** (Jobin Yvon 1250M) shown in Fig. 2 which has a maximum resolving capacity $R_{max} = \lambda/\Delta\lambda \approx 10^4$.

The monochromator has been painstakingly aligned. Please do not alter the arrangement of the optical components between the entrance and exit slits. You may adjust the other parts of the equipment, i.e. the slits themselves and the input optics which couple the light source to the input slit. If you suspect misalignment of the internal parts of the monochromator, ask for help.

The monochromator utilizes what is known as a Czerny-Turner mount. In this configuration, light from a source is focused onto an input slit through which it expands to fill a concave spherical mirror at a distance equal to the focal length of the instrument. The collimated light then is reflected onto a plane reflection grating which can be rotated by a precision stepping motor. Light reflected (and dispersed) from the grating is sent to a second spherical concave mirror which refocuses the light in the focal plane of the exit aperture where the photons are detected and integrated using a photomultiplier tube.

4. High-Resolution Monochromator

The monochromator is interfaced to a PC running Microsoft Windows and National Instruments LabVIEW software over a GPIB connection. A schematic of the instrument is shown in Figure 2.

The basic steps for using the instrument follow:

1. Note the position of the grating's mechanical counter on the side of the monochromator. If it is not close to zero, please seek help from the technical staff. At the end of your session, return the monochromator's grating to the zero position before shutting off the motor controller unit. Failure to do so will frustrate the calibration of the next group.

2. Turn on the mercury discharge lamp and place it so that its emission falls upon the input slit.

3. Remove the small lid on the top of the monochromator to verify groove density of the installed gratings. The turret holds two gratings, either of which may be selected in software: Grating position '0' has 1800 groves mm^{-1} at a blaze wavelength of

400nm while grating position '1' has 3600 grooves mm^{-1} with a blaze wavelength of 300nm.

It is recommended that you start with the coarse 1800 groove mm^{-1} grating in order to survey the broadest portion of the spectrum and explore the operation of the instrument before making your final measurements.

4. Turn on the Ministep Driver Unit (MSD-2) using the power switch on the back panel. You should hear a small clunk as the gear motor is engaged. Power cycling once or twice is sometimes necessary.

5. The LabVIEW monochromator control program is shown in Figure 1. After the program is loaded, run the code by clicking on the white arrow in the upper left corner of the window. The main drop down menu bar contains various operations for controlling the monochromator.

6. Select the desired grating ('1800 lpmm' or '3600 lpmm') and then 'Change Turret Position' from the drop down menu bar. Wait for the menu bar to revert back to 'Waiting for next command' before proceeding. You should execute this step even if the display 'reads' the correct position, as it needs to retrieve information about the grating's groove density. The two gratings installed on the turret have groove densities of 1800 and 3600 gpmm.

7. Examine the mechanical counter on the side of the monochromator to see that it reads exactly 0.0. This counter can be used to determine the current wavelength setting according to $\lambda = counter \times \frac{X(lpmm)}{1200lpmm}$ where X is either 1800 or 3600 depending on the position the grating turret. If not, select 'Move grating to zero position' from the menu bar.

8. Replace the lid with 4 screws above the turret grating assembly.

9. **Double check that the top of the monochromator is covered before turning on the high voltage to the photomultiplier tube as ambient light levels can damage a PMT biased at high voltages.** Set the high voltage to +950 VDC.

10. The input and output slits are controlled by micrometers. They can be set from 3 μm to 3mm. Set the width of both slits initially to be 100μm. **Do not attempt to adjust the micrometers to a width $< 3\mu$m. This can damage the sensitive slits!** The height of the input slit is controlled by a sliding blade and should be set initially at 2mm.

11. The light 'acceptance cone' of the instrument is set by the size of the grating (110x100mm) and the focal length of the first spherical mirror (1250mm). For this instrument, the $F\# = 11$. If you find that you are photon limited, try using a short focal length lens to form an image of the lamp at the entrance slit which is it F# matched to the monochromator (so as not to under-full or overfill the first spherical mirror).

The wavelength range of the monochromator is 0-15,000 units as displayed by the mechanical counter. The gratings are rotated by a spring-loaded lever set against the grating mount which is attached to a turret inside the instrument. **Please do not attempt to change the turrets yourself since a slip may damage the very expensive gratings.**

4.1. MERCURY CALIBRATION SPECTRUM

Your first task is to examine the instruments' calibration. Measure several lines in the mercury spectrum (using the CRC handbooks for reference data) and make a graph of wavelength vs. mechanical counter reading.

Explore the effects of input and output slit widths, grating line density, and integration time on spectral intensity, spectral resolution, and spectral bandpass. There is a LabVIEW program 'Model Instrumental Profile' in the same library as the main control program which can be used to model the effect of different slit widths. The acquired spectrum will probably show a profusion of lines - many more than the prominent yellow, green, blue and purple lines of the famous mercury spectrum. Several of the lines are, in fact, ultraviolet lines in the second-order spectrum, superimposed on the visible lines of the first-order spectrum. Your first job is to identify all the lines with the aid of the mercury spectrum table in the CRC handbook. Later you will use the mercury spectrum as your calibration for measurements of the hydrogen and sodium spectra.

Identify the lines by means of a bootstrap operation in which you first latch onto several of the most prominent lines, establish a tentative wavelength-position relation, and then see if the other fainter lines fall in place. The yellow doublet (5789.7 Å and 5769.6 Å), the green line (5460.74 Å) and the purple line (4358.33 Å) are particularly useful landmarks within the mercury spectrum. It will help to make a plot of wavelength versus position. Look out for second order UV lines superposed on the first order visible spectrum (e.g. a 2500 Å line in second order would fall at exactly the same position as a 5000 Å line in first order).

Label as many of the transitions as you can with the aid of Figure 2.13 of Melissinos (in the figure caption "hydrogen" should be "mercury"). Note in particular the lines due to the interesting transitions $6^3D \to 6^1P$ for which $\Delta S=1$, and the 2536.5 Å line which is due to decay of the first excited state that is involved in the Franck-Hertz experiment. Check the validity of the dipole radiation selection rules.

Determine the number of lines mm^{-1} in the grating by measuring the linear separation of two identified lines of
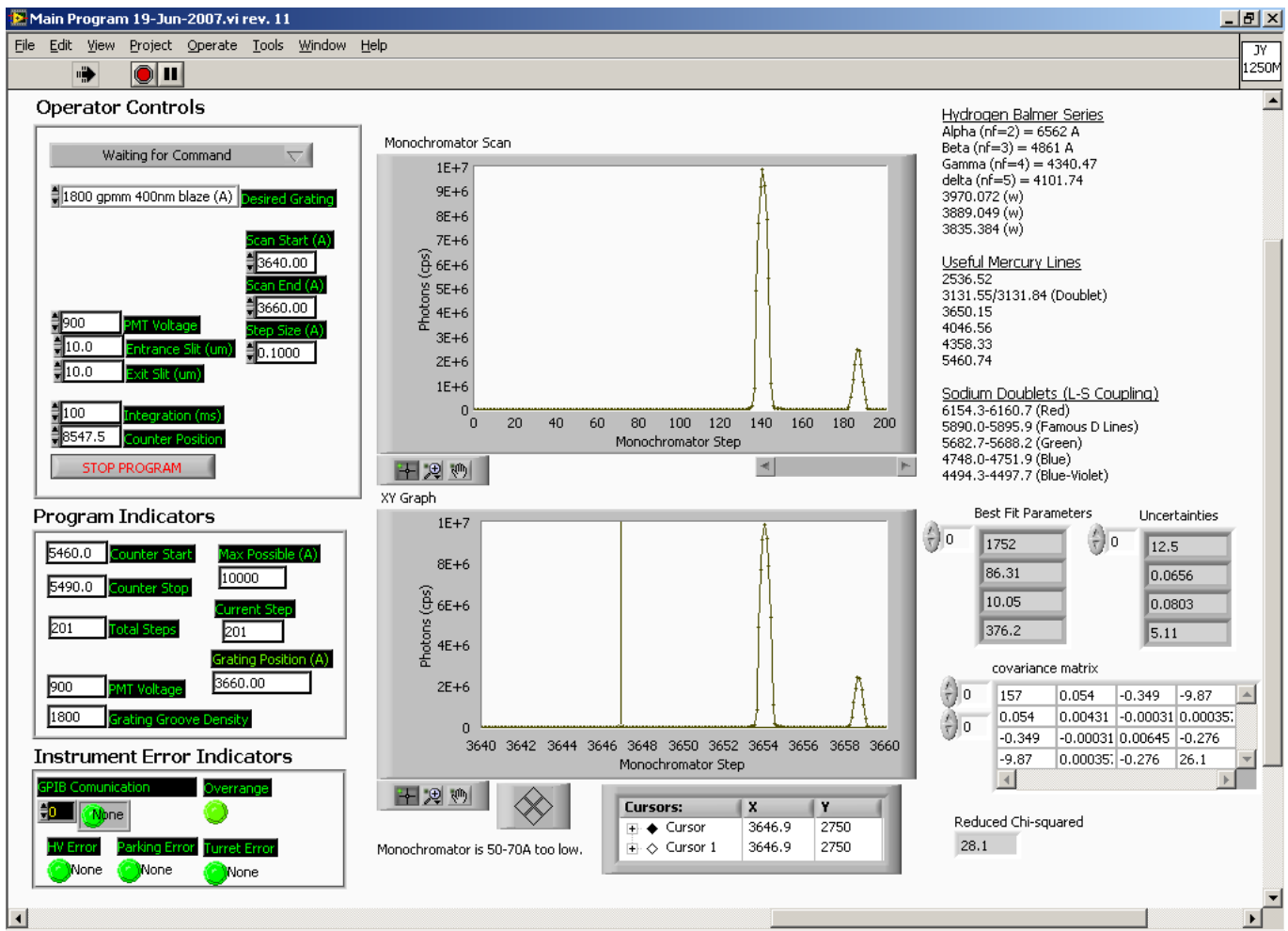
FIG. 1: The LabVIEW software interface to the Jobin-Yvon 1250M monochromator. Note that the user should always enter spectral units of Å while the 'counter' indicator will display the mechanical counter positions necessary to scan this portion of the spectrum. The limits of the instrument are 0 to 15,000 in mechanical counter units. **Be very careful not to drive the grating beyond this limit!**

known wavelength on the acquired spectrum and applying the grating equation (see Appendix A).

4.2. HYDROGEN SPECTRUM – THE BALMER SERIES

The goals of this part of the experiment are:

1. to record the hydrogen spectrum at low and high resolutions together with a mercury calibration spectrum;

2. to identify and measure the wavelengths of the Balmer lines using a calibration based on mercury;

3. to compare the measured wavelengths with the Balmer formula, namely

$$\frac{1}{\lambda} = R_H \left(\frac{1}{n_f^2} - \frac{1}{n_i^2} \right) \qquad (4.1)$$

where $n_f = 1,2,3,...$ and $n_i > n_f$. $n_f = 2$ corresponds to the Balmer series in the visible while $n_f = 1$ corresponds to the Lyman series in the UV.

4. to determine the value of the Rydberg constant, $R_H = \frac{M}{M+m} R_\infty = 1.096776 \times 10^7 m^{-1}$

Acquire a series of hydrogen spectra with superimposed mercury calibration spectra, experimenting with resolution changes and integration times. Take care not to disturb the instrument between the hydrogen exposure and the mercury calibration exposure. Identify and measure as many of the Balmer lines as you can, comparing the wavelengths with those predicted by Equation 4.1. One way to do this is to compute a value of λ_0 for each
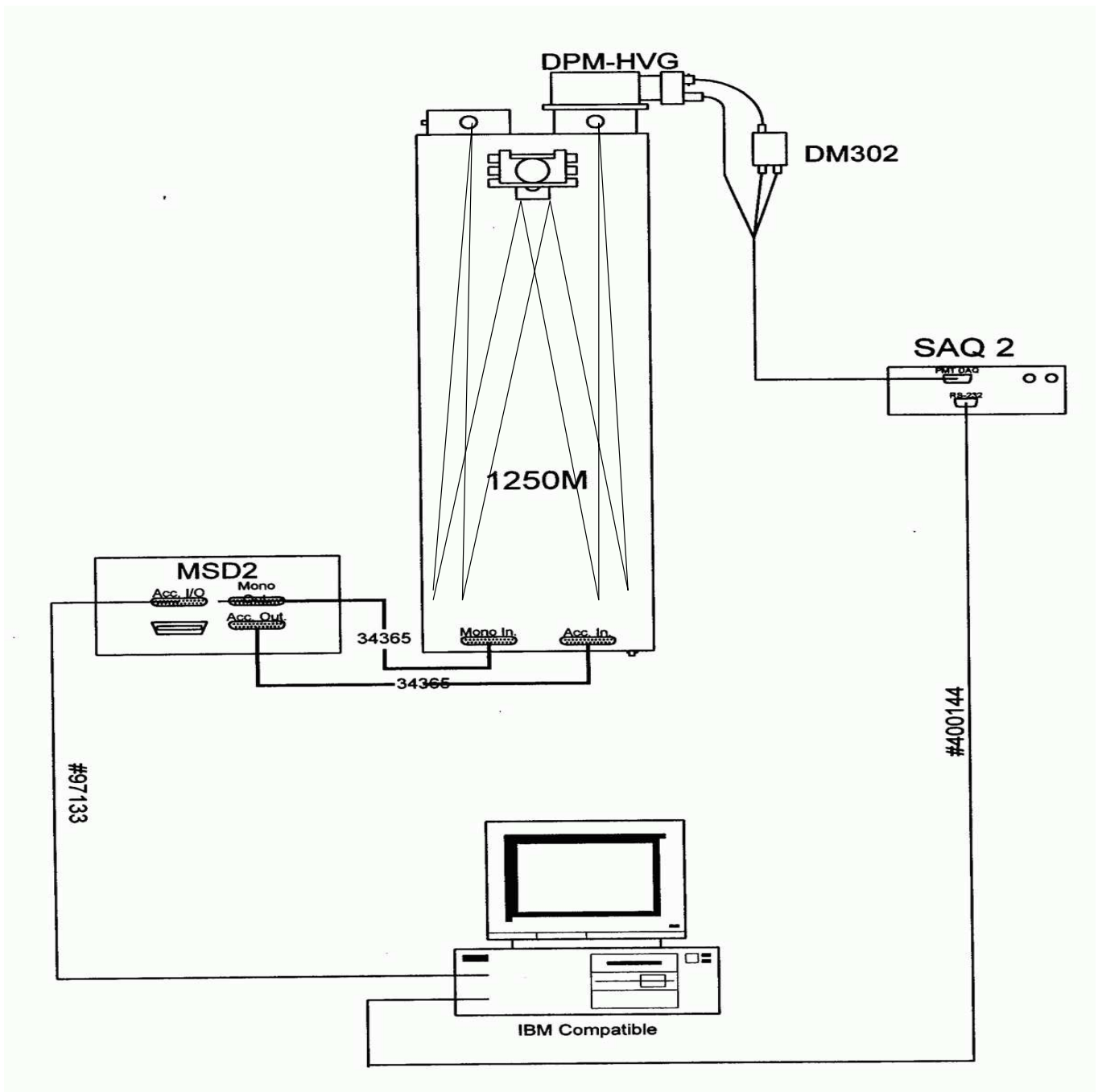
FIG. 2: Schematic of the Jobin Yvon 1250M monochromator.

of your measured Balmer lines, using in each case the appropriate values of n_f and n_i. From these data, determine a value and error for the Rydberg constant. You will probably observe other fainter features in the spectrum of the hydrogen discharge tube. Try to identify them.

4.3. SODIUM SPECTRUM– FINE STRUCTURE

The goals of this part of the experiment are:

1. to obtain a calibrated spectrum of sodium;

2. to measure the wavelengths of the lines and to measure their doublet separations;

3. to identify the transitions that give rise to the observed lines;

4. to determine the maximum energy of excitation of the sodium in the lamp.

The distortion of the $1/r$ field of the nucleus by the inner electrons has a substantial effect on the fine structure splittings of the $l > 0$ states that arise from the interaction between the magnetic moments associated with the spin and orbital angular moments of the optical electron. Where the fine structure splitting in hydrogen is very small and difficult to detect (0.08 Å in H_β), it is readily observed and measured in the alkali atoms. It decreases with n and l approximately as $1/[n^3 l(1 + l)]$, and so is most prominent in the P states. The splitting of the levels gives rise to a corresponding "doublet" structure of the spectral lines, with the most conspicuous effects occurring in the lines due to transitions to and from the P $(l = 1)$ states. Doublets due to transitions that begin or end at a common state have identical energy separations. In the early days these separations provided important clues for identifying the transitions and deducing the level structure from observed spectra. See Melissinos for an energy level digram for sodium.

Obtain various sodium spectra of varying integration times with a superposed short mercury calibration spectrum, both with and without the UV filter. Determine the wavelengths of all the features of the spectrum.

Identify as many of the sodium lines as you can together with the initial and final atomic states of the transitions. Group them according to common final states and within each group compare the wavelengths with those expected from energy levels given by the Rydberg formula

$$E = E_\infty - \frac{hcR}{(m + \mu)^2} \qquad (4.2)$$

where m is an integer, and E and μ are constants.

Determine the fine-structure splittings of the ^2P levels involved in the transitions responsible for the various doublets. Check whether the doublets originating from and terminating at the same ^2P level have the same separation (in wave numbers). Determine the ratio of the doublet separations of the $3P$ and $4P$ levels, and compare with the semi-empirical rule that the ratio is proportional to $1/n^3$. Approach these measurements as an exercise in experimental accuracy and error estimation, and their interpretation as a challenge to your understanding of atomic structure. Note that in spectroscopic notation, the upper left superscript is equal to $2S+1$ and the lower right subscript is the total angular momentum 'j'.

You may find there are lines you cannot identify using only the sodium lines listed in the CRC Tables. Try to identify them, i.e. figure out what other element(s) may be in the lamp.

4.4. Measuring Isotopic Shifts in the Balmer Lines

In this part of the experiment you will determine the ratio of the deuteron mass to the proton mass by measuring the isotope shifts of the Balmer lines. Most of the differences in the energy levels of the hydrogen isotopes (hydrogen, deuterium, and tritium) arise from the differences in the reduced mass that occurs in the simple Bohr theory that explains the Balmer formula. (The differences due to interactions involving the nuclear magnetic moments are very much smaller in magnitude and not detectable with our instruments). With a little algebra the ratio of the deuteron mass to the proton mass can be expressed in terms of the wavelength λ of a Balmer line and its shift $\Delta\lambda$ between hydrogen and deuterium.

5. ANALYSIS

Compute the value of m_d/m_p and an error estimate from the measured separations of the hydrogen and deuterium Balmer lines, using the mercury calibration data. Compare the results with the known ratio of the atomic weights of deuterium and hydrogen.

5.1. Possible Theoretical Topics

1. Derivation of the grating equation.

2. Bohr theory of the hydrogen atom and the isotope shift.

3. Schrödinger theory of the hydrogen atom.

4. Fine structure.

5. The correspondence principle.

[1] J. Lerner and A. Thevenon, *The Optics of Spectroscopy* (Jobin-Yvon, 2000).

[2] E. Hecht, *Optics* (Addison Wesley, 2002).

[3] A.P.French and E. Taylor, *An Introduction to Quantum Physics* (Norton, 1978).

[4] R. Rhodes, *The Making of the Atomic Bomb* (Simon and Schuster, 1986).

[5] A. Melissinos, *Experiments in Modern Physics* (Academic Press, 2003), 2nd ed.

[6] S. Gasiorowicz, *Quantum Physics* (Wiley, 1996), 2nd ed.

[7] C. White, *Introduction to Atomic Spectra* (McGraw-Hill, 1934).

APPENDIX A: GRATING PHYSICS

Figure 2 shows the optical layout in the monochromator. Note that the "source" for both this system is a narrow slit upon which an external light source is focused. To understand the optics of any spectrograph or monochromator it is essential to realize that a narrow spectral "line" is actually a monochromatic image of the slit. Widen or lengthen the slit and you widen or lengthen the resulting spectral line. The width of a line depends on the width of the slit, the sharpness of the focus, and the intrinsic spectral width of the line, and the number of reflecting grooves of the grating that contribute to the total amplitude of the optical disturbance at the focal plane.

To understand the physics of a monochromator, envision spherical monochromatic light waves (i.e. "Huygens wavelets") diverging from any given point at the slit and which are reflected by the collimating mirror into plane waves traveling toward the grating. Reflections from the grooves in the gratings form cylindrical wavelets which interfere constructively only in certain narrow ranges of directions so as to comprise, in effect, a set of plane waves each traveling in one of those directions.

A second mirror focuses the incident plane waves to a diffracted image of the original slit at the focal plane of the monochromator where it then passes through an exit slit and onto the photocathode of a sensitive photomultiplier tube. The spectrum appears as monochromatic slit images spread out in the direction of dispersion of the grating. The bandpass spectrum is adjusted by rotating the grating about a vertical axis.

The gratings used in the monochromator are plane reflection gratings.

The most general form of the plane reflection grating is shown in Figure 3. Each "tread" or "riser" of the staircase reflects a narrow rectangular piece of an incident plane wave, and this piece spreads about the specular reflection direction according to the principles of Fraunhofer diffraction. The resulting cylindrical wavelets may be thought of as combining at some distance to form diffracted plane waves with maximum intensities in directions such that the differences in path length along the reflected rays from successive grooves is an integral number of wavelengths. This condition is expressed by the grating equation

$$m\lambda = d(\sin\alpha + \sin\beta) \qquad (A1)$$

where α and β are the angles between the grating normal GN and the directions of incidence and reflection, respectively, d is the distance between grooves, and m is an integer called the "order" of the interference.

The angular dispersion produced by this grating is defined by the differential relation

$$\frac{d\beta}{d\lambda} = \frac{1}{d\lambda/d\beta} = \frac{m}{d\cos\beta} = \frac{\sin\alpha + \sin\beta}{\lambda\cos\beta} \qquad (A2)$$
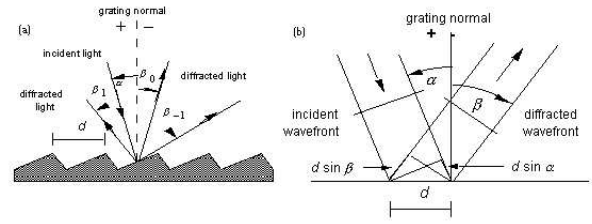
FIG. 3: Reflection Grating Geometry: (a) A beam of monochromatic light of wavelength λ is incident on a grating and diffracted along several discrete paths. (b) For planar wavefronts, The terms in the path difference, $d\sin\alpha$ and $d\sin\beta$, are shown. (From Thermo RGL Handbook)

For a given diffracted wavelength λ in order m (corresponding to an angle of diffraction β), it is convenient to characterize the reciprocal linear dispersion or plate factor P, usually measured in nm mm^{-1}

$$P = \frac{d\cos\beta}{mf} \qquad (A3)$$

where f is the effective focal length of the instrument.

In the monochromator the grating is used in a Littrow Configuration where $\alpha = \beta$, and under these conditions Equation A1 simplifies to

$$m\lambda = 2d\sin\beta \qquad (A4)$$

Furthermore, Equation A2 becomes

$$D = \frac{d\beta}{d\lambda} = \frac{2}{\lambda}\tan\beta \qquad (A5)$$

When $|\beta|$ increases from 10° to 63° in Littrow use, the angular dispersion increases by a factor of ten, regardless of the spectral order or wavelength under consideration. Once β has been determined, the choice must be made whether a fine-pitch grating (small d) should be used in a low order or a coarse-pitch grating (large d), such as an echelle grating, should be used in a higher order. In this experiment, the former solution was chosen to provide a much larger free spectral range (see below).

At 4358 Å in first order (corresponding to $\beta = 31.5°$ by Equation A4), the grating in our monochromator has dispersion of 2.8×10^{-4} radians Å^{-1} using Equation A5. With a focusing mirror of focal length 1250mm following the grating, the linear dispersion would be 0.35 mm Å^{-1}.

The grating used in the Hydrogenic Spectroscopy experiment is ruled with 2400 (as well as 1800 and 3600) lines mm^{-1} (d=4167 Å). From Equation A4, light at 4358 Å will be refracted in first order at $\beta = 31.5°$ and at 63.0° in 2nd order. Light emitted at this latter angle will miss the focusing mirror and thus we are dealing with essentially just 1st order diffraction.

Finally, from Equation A4 we find that the difference between two wavelengths diffracted at the same angle in successive orders, called the free spectral range, is given by the equation

$$\lambda_1 + \Delta\lambda = \frac{m+1}{m}\lambda_1 \qquad (A6)$$

from which

$$F_\lambda = \Delta\lambda = \frac{\lambda_1}{m} \qquad (A7)$$

APPENDIX B: EQUIPMENT LIST

Item	Model	Contact
1" UV Filter	6057	oriel.com
1" PCX Lenses	Various	thorlabs.com
Monochromator	1250M	jobinyvon.com
Photomultiplier Tube	R928	usa.hamamatsu.com/hcpdf/R928.pdf
H-D Spectral Lamps	Custom	electrotechnicalproduct.com
Spectral Lamps	Various	edmundscientific.com
LabVIEW		ni.com

Neutron Physics

MIT Department of Physics
(Dated: September 5, 2011)

The three main parts of the experiment are; the Maxwell-Boltzmann distribution, Bragg scattering of thermalized neutrons and finally the DeBroglie relation with neutron absorption cross sections. The technique of time-of-flight spectroscopy with a mechanical beam chopper is used to study the properties of thermal neutrons in a beam emerging from the MIT research reactor. First, the distribution in velocity of the neutrons is measured, and the results are compared with the Maxwell Boltzmann distribution for the temperature of the reactor. Second, the DeBroglie relation between wavelength and momentum of neutrons is determined from measurements of the angle of Bragg reflection of the beam from a copper crystal as a function of the velocity measured by time-of-flight. Third, the absorption cross sections of several elements are measured, and the $1/v$ dependence of the boron cross section is observed.

—REQUIRED—

- GERT Training

- Reactor Practicum attendance

- Peruse MIT-NRL website and experiment setup: http://web.mit.edu/nrl/www/index.html

PREPARATORY QUESTIONS

1. Compute the average velocity, $\sqrt{<v^2>}$, of neutrons in a beam emerging from a reactor operating at 50°C.

2. Describe how a proportional counter containing boron trifluoride (BF_3) works to detect neutrons. Why is a low efficiency detector used for the measurement of the velocity distribution of the thermal neutrons?

3. Compute the angles of first order Bragg diffraction of 0.025 eV neutrons from the (200) and (111) planes of crystalline copper. Could you diffract 0.0025 eV neutrons from a copper crystal?

4. Suppose a measurement shows that a sheet of linear thickness x of a particular element of atomic weight A and density ρ reduces the intensity of a beam of monoenergetic neutrons by the ratio I/I_0. Derive a formula for the cross section σ of the element for absorption of neutrons in terms of these defined quantities.

SUGGESTED PROGRESS CHECK FOR END OF 2ND SESSION

Using MCS distributions of neutron time of flights at the near and far detector positions, calculate the velocity of the particles to zeroth order.

1. Experimentation at the MIT Research Reactor (MITR): Radiation Protection and Security

This experiment was developed for Junior Lab by Professor Clifford Shull [1]. It employs a rather intense beam of low energy neutrons produced at the MIT Research Reactor located in Building NW12 on the edge of the campus at 138 Albany Street. The MIT reactor has been operating for 30 years and has served as a base for countless investigations by faculty, graduate and undergraduate thesis students, UROP and other undergraduate student projects. Use of its facilities is perfectly safe, providing reasonable and common-sense guidelines and procedures are followed. To insure that you are familiar with these procedures, a certain amount of indoctrination is required. This involves some advance study of material, followed by a briefing by staff from the Radiation Protection Office and from the Reactor Operations Group. Following completion of this procedure, you are "cleared" to perform the experiment at the reactor in the presence of "badged" reactor escort. In keeping with the spirit of the Junior Lab, you will operate all the equipment yourself and after two sessions at the reactor you will able to run the experiment remotely in Junior Lab.

Access to the reactor building is restricted in keeping with regulations at this and every other nuclear reactor facility in this country (or anywhere for that matter). You will be required to take a practicum at the reactor, complete radiation safety training and be escorted at all times in accordance with federal regulations. For the purpose of Junior Laboratory experimentation, the following steps should be taken in order to have access to the reactor:

1. Download the web-based training instructions from http://web.mit.edu/8.13/www/38.shtml. Follow these instructions to successfully complete your General Employee Radiological Training (GERT). Altogether this will take about two hours, and can be done at home.**YOU MUST COMPLETE THE GERT BEFORE CONTINUING TO THE NEXT STEP!**

2. Next, you must attend a scheduled briefing session

(normally held on the 2nd and 3rd Fridays of the fall term) at the reactor to discuss the material and to complete any required forms. Following this discussion, you will be taken on an Inspection Tour of the reactor by the operating staff. The discussion period and tour will take about 1.5 hours. You will notice that entry into the reactor building is through a locked gate which may be opened with a magnetically-coded identification card.

The equipment is reserved for your use at the scheduled time. To operate the experiment remotely you must contact the reactor operator 24-hours in advance to have the neutron-shutter opened for you. You should also clear any proposed changes to your scheduled attendance with your section instructor.
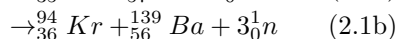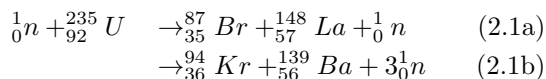
3. During your first scheduled period, Dr. Robinson (ext 3-5082,), a technical instructor, or a TA will be present to show you the apparatus and procedures. Please contact Dr. Robinson in advance if a conflict or change of schedule interferes with this important introductory session.

2.   Nuclear Reactors

2.1.   Operational Physics Of The Nuclear Reactor

The nuclear reactor is a chain-reacting system which bears resemblance in operational principle to a coal fire, with nuclear reactions being the source of heat rather than chemical reactions. In a coal fire, some carbon atoms are excited by thermal "starting" so that they combine with oxygen (burn). The heat released in this exothermic chemical reaction activates other carbon atoms to do the same, thereby forming a chain reaction without further need of "starting". The fire grows in intensity until an equilibrium level is reached, wherein heat losses from the system limit the thermal power available for further steps in the chain reacting process.

In a nuclear reactor, the counterpart to the carbon fuel is the nuclear fuel (most commonly the fissionable isotope of uranium, $^{235}_{92}U$), and neutrons serve as the communicative thermal energy counterpart. In 1939 Hahn and Strassman discovered that neutrons react with uranium nuclei to cause fission in which the heavy nucleus splits into two smaller and not necessarily equal nuclei plus "debris" such as neutrons, gamma-rays, electrons, etc. The fragmentation can proceed in many different ways. Typical reactions are shown in Equation 2.1.

$$\begin{aligned} ^{1}_{0}n + ^{235}_{92}U \quad &\rightarrow ^{87}_{35}Br + ^{148}_{57}La + ^{1}_{0}n && (2.1\mathrm{a}) \\ &\rightarrow ^{94}_{36}Kr + ^{139}_{56}Ba + 3^{1}_{0}n && (2.1\mathrm{b}) \end{aligned}$$

Notice that the above reaction equations are written as balanced equations in both numbers of nucleons and charge. However, if you look in a table of precise mass

values, you will find for the nuclear masses of the entries in the first reaction:

$$\mathrm{M}(^{235}_{92}U) \ = 235.11240$$
$$\mathrm{M}(^{87}_{35}Br) \ = 86.95722$$
$$\mathrm{M}(^{148}_{57}La) = 147.98930$$

These values imply a mass loss of 0.16588 mass units in the reaction. Using the Einstein mass-energy equivalence, this calculates to 155 MeV of energy which, according to the energy conservation principle, must show up as kinetic energy distributed among the reaction fragments. This is a very large amount of energy when compared with that of ordinary nuclear processes such as alpha, beta or gamma decay (1–10 MeV), and especially when compared to chemical reactions ($\sim$5 eV).

A second notable feature of fission reactions is that neutrons are released as debris. Shortly after the discovery of fission, careful measurements in several laboratories proved that the average number of neutrons released per fission is more than one. It was then apparent that under appropriate circumstances these neutrons could initiate fission of other $^{235}_{92}U$ nuclei and that the physical basis for a nuclear chain reaction exists. The possibilities for practical nuclear power generation and bombs were immediately recognized by experts all over the world, and a race began. The first controlled nuclear chain reaction was achieved in 1941 at the University of Chicago by a team under the direction of Enrico Fermi, and the first bomb was exploded in 1945.

Nuclide	ν, Per Thermal N Induced Fission	η, Per Thermal N Absorbed	η, Per Fast N Absorbed
$^{233}_{92}U$	2.50	2.27	2.60
$^{235}_{92}U$	2.43	2.06	2.18
$^{239}_{94}Pu$	2.90	2.10	2.74

TABLE I: Number of Neutrons Liberated per Neutron Capture in Fissile Material.

Table I lists the average numbers of neutrons released in various fissile materials. In this table, the differences between ν and η (defined therein) arises because neutrons are sometimes captured without producing fissioning.

For technical reasons of efficiency and control most nuclear reacting systems operate so that the neutrons which produce the fissioning are "slow", i.e. have very low kinetic energy. On the other hand, the neutrons which are released in the fission process are "fast" neutrons with relatively high kinetic energy, on the average about 1.5 MeV. Thus they must be slowed down (or moderated) to a low energy. This can be done by elastic scattering of the neutrons from light atoms in a cool *moderator*. Each scattering reduces the energy of a neutron until its energy approaches the mean energy of the moderator atoms in accordance with the equipartition theorem of statistical physics. Carbon in the form of graphite was used as the moderator in Fermi's first reactor. Light water (H_2O) is
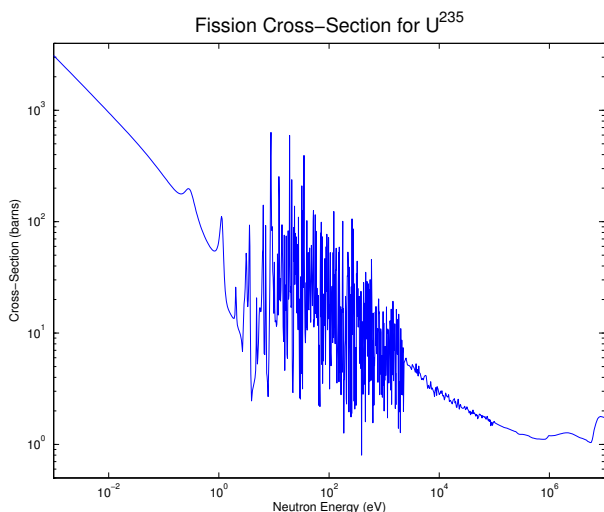
FIG. 1: Schematic Fission Cross-Section for $^{235}_{92}U$. Data from atom.kaeri.re.kr/ton.

Nuclide	Fission (barns)	Capture (barns)	Capture/Fission ratio
$^{232}_{90}Th$	—	7.4	—
$^{233}_{92}U$	527	54.	0.102
$^{235}_{92}U$	577	106.	0.184
$^{238}_{92}U$	—	2.7	—
$^{239}_{94}Pu$	742	287.	0.387

TABLE II: Thermal Neutron Cross-Sections for Nuclear Materials.

now commonly used (as in the MIT reactor). Analysis shows that, on the average, one needs about 18 scattering events with hydrogen nuclei (protons) to reduce the neutron energy from 1.5 MeV to a typical thermal energy of 1/40 eV at which point further scattering events can raise as well as lower the neutron energy. The thermal equilibrium is characterized by the physical temperature of the moderator (about 50°C at MIT, but much higher in a power-producing reactor).

The efficiency of neutrons in producing fission depends upon the neutron energy and is conventionally described in terms of the *fission cross section*, or effective target area of the fissioning nucleus, expressed in *barns* (a picturesque name for 10^{-24} cm^2). The dependence of this upon neutron energy for the case of $^{235}_{92}U$ is shown in Figure 1 which displays a nice distinction between commonly-designated neutron groups: slow or thermal (< 0.1 eV), resonance (0.1–1000 eV), and fast ($> 10,000$ eV). Note particularly the much higher fission cross section for thermal neutrons. Neutron physics is sometimes studied in regimes beyond the above classes, in particular as cold or ultra-cold ($\approx 10^{-7}$ eV). Ultra-cold neutrons (UCN) exhibit very interesting properties. For example, they cannot penetrate surfaces and can be contained in a "bottle"!

An important quantity for reactor design purposes is the fission cross section at the thermal energy which is attained by most of the neutrons after moderation. For a moderator kept at temperature T (absolute Kelvin), the thermal energy is kT and at room temperature this is about 1/40 eV. The cross sections for fissionable nuclei are listed in Table II.

2.2. Design Features of a Nuclear Reactor

In the preceding section, we have surveyed some of the physical concepts and parameters that are of significance in thinking about a nuclear chain reaction. Of course, this is far removed from answering the question, "how to make it work?". Many different reactor designs have evolved, each one aimed at achieving certain objectives. *Research reactors* produce radiation, radionuclides or other products useful in scientific and medical studies; *power reactors* produce energy for practical use; *production reactors* use excess neutrons to transmute the abundant non-fissionable isotope of uranium, $^{238}_{92}U$, into fissionable plutonium, $^{239}_{94}Pu$ for bombs.

Components of a reactor that are common to all designs include:

1. **Fuel Elements -** Either natural uranium or uranium enriched in the isotope $^{235}_{92}U$, usually in the form of uranium oxide or alloyed with aluminum and sealed in aluminum tubes or plates.

2. **Moderator -** Frequently light or heavy water, but in some cases graphite or beryllium.

3. **Thermal Heat Transfer System -** Removes the heat generated by conversion of the kinetic energy of the fission fragments. The latter are entirely retained in the fuel elements.

4. **Control Elements -** Neutron absorbing elements such as cadmium are used to control the neutron flux density and hence the rate of the chain reaction and power output of the reactor.

5. **Surrounding Radiation Shield -** Intense neutron and gamma radiation, produced by the fission process and the radioactive decay of fission fragments, must be contained by shielding.

The simplest spatial configuration of these components would be many small fuel elements positioned in a spatial lattice and immersed in a liquid moderator which is circulated through an external heat exchanger to dissipate or utilize the heat generated by the process. To maintain the desired power level thermometers and/or radiation
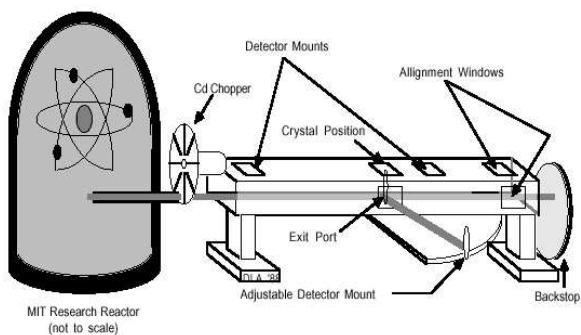
FIG. 2: Experimental setup for time-of-flight spectroscopy at the MIT Nuclear Reactor.

FIG. 3: Schematic diagram of the time of flight spectrometer showing the beam chopper and the BF$_3$ detector.

monitors would be connected to servo-mechanisms to adjust automatically the positions of cadmium control rods inserted into the lattice. Details of the particular features of the MIT Reactor will be provided to you at the time of your briefing. Useful references on nuclear engineering and reactors include [2–4].

3. Part I: Study of the Maxwell-Boltzmann Distribution of Neutrons in the Nuclear Reactor

In all of the present experimentation we shall use a pulsed, collimated beam of neutrons emerging from the reactor in a setup shown schematically in Figure 2. The distribution in energy of the neutrons in the beam reflects the equilibrium spectrum of the moderated neutrons in the reactor. In accordance with the principles of statistical physics, we anticipate that this spectrum is the Maxwell-Boltzmann spectrum characterized by a temperature that is the same as the physical temperature of the moderating agent in the reactor (normal water in the case of our reactor), providing complete moderation of the neutrons has occurred. Thus we can think of the neutrons in the reactor as constituting a neutron gas in thermal equilibrium with the moderator, with a certain density and temperature. We will examine the velocity spectrum of the neutrons by letting some escape as a collimated beam through a small opening in the reactor shield.

We will measure the velocity spectrum by timing the flight of individual neutrons over a laboratory distance of about 1.5 meters. We do this by "chopping" the beam as it emerges from the reactor to produce periodic short bursts of neutron intensity. After traveling the flight distance the neutrons are detected with a small neutron counting tube, and the occurrence times of the individual counting pulses relative to the starting time of the burst are recorded with a multichannel scaling (MCS) card.
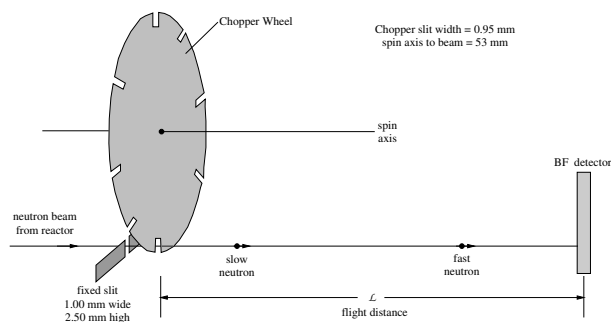
3.1. The Neutron Chopper

The chopper is a slotted disk of neutron-absorbing cadmium which rotates about an axis above and parallel to the neutron beam line, as illustrated in Figure 3. Cadmium is very absorptive to neutrons of energy less than about 0.40 eV (speed of 8760 m/sec), and serves as a good shutter for thermal neutrons. The cadmium disk of thickness 1 mm is sandwiched between two aluminum disks for mechanical stability. Around the periphery of the disk assembly, eight radial slots have been cut. The width of each slot is 0.95 mm. Immediately upstream of the chopper disk is a fixed slit opening made of neutron absorbing material (boron containing plastic) with width 1.00 mm and height 2.5 mm. This serves to define the beam size entering the chopper assembly. The axis of rotation is located 53 mm above the geometrical center of the defined neutron beam. A small speed-controlled synchronous motor rotates the disk. Every time a radial slit passes the fixed slit a burst of neutrons is admitted to the flight line. Since the slit widths are nearly equal the time structure of intensity in this burst (which may contain several hundred neutrons) is triangular, with a full width at half maximum (FWHM) determined by the slit width and rotational speed. You should convince yourself of this feature. Also, consider what it would be for the case of unequal slits.

The rotational speed of the synchronous driving motor is fixed by the power line frequency and is seen as a digital display of the rotational speed in RPM or the neutron burst repetition rate in Hertz. This frequency will be 240 Hz throughout the experiment.

It is necessary to establish a reference time for the origin of each of the neutron bursts. This is done by the periodic interruption of a light beam passing parallel to the neutron beam line between a tiny photodiode and photodetector which is positioned about 90° around the disk from the neutron beam. The geometry is arranged so that a light signal occurs a short time before each neutron burst. The light signal sets the time origin of the MCS used to measure the neutron flight time. Thus the actual neutron burst origin time is slightly later than the

MCS origin time by a certain fixed delay which must be determined as a part of the experiment.

3.2. The Neutron Detector

Small gas proportional counters are used as neutron detectors. For this part of the experiment, the counter of choice contains BF$_3$ gas in a sealed aluminum tube of diameter 0.5 inch and length 3 inches. The neutron beam is located near the bottom (vertically) center (horizontally) of the BF$_3$ detecor's range of motion. High voltage (**bias the BF$_3$ detector at +1000 VDC and the He-3 detector at +1600 VDC**) is applied between the metal tube and a fine center wire. The resulting electric field collects the charges produced by gas ionization caused by the energetic nuclei from the reaction $^1_0n + ^{10}_5B \rightarrow ^7_3Li + ^4_2He$. The $^{10}_5B$ isotope forming 18.8% of natural boron captures neutrons with a large cross section that varies as $1/v$, where v is the neutron speed. Many nuclei, such as ^1_1H , ^6_3Li, ^3_2He, and $^{197}_{79}Au$ exhibit this "$1/v$ law" capture of slow neutrons (see the plot of the $^{235}_{92}U$ fission cross section in Figure 1).

Our counter contains BF$_3$ gas at a pressure of 40 cm Hg; a typical neutron passing along a diameter will be detected with an efficiency of about 1%. It is purposely selected to be "thin" (low efficiency) so that a simple analytical correction can be applied in the analysis of the spectral data. Electrical pulses from the counter are amplified in a preamplifier and in a main-line amplifier, selected by a single channel "window" analyzer, and counted by a scaler. Thereafter they are sent to an oscilloscope for observation, and to a MCS for arrival time sorting. The output pulses from the amplifier are about 5 μs in duration. Operating details concerning the counter high-voltage, amplifier settings and MCS operating conditions are posted at the experiment location.

3.3. Thermal Spectrum Theory

The Maxwell-Boltzmann (M-B) distribution law describes the distribution in speed (or kinetic energy or momentum) of atoms in a gas in a state of thermal equilibrium. Neutrons within the reactor can be expected to obey a similar distribution law, namely

$$n(v)dv = \frac{4N}{\sqrt{\pi}}\left(\frac{v^2}{v_0^3}\right)\exp\left(-\frac{v^2}{v_0^2}\right)dv, \qquad (3.1)$$

where v is the neutron speed (m/sec), v_0 is the most probable speed (i.e. the peak of the speed spectrum), N is volume density of all neutrons (neutrons/m^3), $n(v)dv$ is the neutron density for those with speeds falling in the speed interval between v and $v + dv$ (see texts on gas kinetic theory, e.g. Reference [5, 6]).

This can be recast in terms of other kinetic parameters such as kinetic energy E for which we have

$$E = \frac{1}{2}mv^2 \qquad \text{and} \qquad dE = mvdv, \qquad (3.2)$$

yielding

$$n(E)dE \propto \left(\frac{E}{E_0}\right)^{1/2}\exp\left(-\frac{E}{E_0}\right)dE, \qquad (3.3)$$

with

$$E_0 = \frac{1}{2}mv_0^2 = kT, \qquad (3.4)$$

where m is the neutron mass.

The corresponding flux density in the collimated beam, i.e. the number of neutrons per unit area per unit time with velocity between v and $v+dv$ passing a given point, is

$$\begin{aligned} j(v)dv &= vn(v)dv \\ &= J_0v^3\exp\left(-\frac{v^2}{v_0^2}\right)dv. \end{aligned} \qquad (3.5)$$

As mentioned above, the neutron detector is a "thin" counter for which the efficiency e varies with neutron speed as $1/v$. Thus

$$e = A(1/v), \qquad (3.6)$$

with A = some constant. If we now call $j'(v)dv$ the number of *detected* neutrons per unit area of detector per unit time with velocity between v and $v + dv$, then

$$j'(v)dv = Bv^2\exp\left(-\frac{v^2}{v_0^2}\right)dv, \qquad (3.7)$$

with B is a constant. Can you figure out the reason for using a "thin" counter rather than using one with higher efficiency of say 50%, aside from the fact that we don't need the higher efficiency because the measured intensity is adequately high?

The quantity actually measured by the apparatus in each event is the time interval between the fiducial signal from the photodetector and the detection of a neutron by the BF$_3$ counter (rather than the velocity). The accumulated data in the MCS is the number N_i of neutrons detected in the i-th MCS-time channel corresponding, after appropriate calibration and zero-time correction, to a flight time t_i . Since $L = vt$, we have

$$N_i = D\left(\frac{1}{t_i^4}\right)\exp\left(-\frac{L^2}{v_0^2t_i^2}\right)\Delta t, \qquad (3.8)$$

where Δt is the finite and constant width of the MCS-time channels, and t_i is a flight time within the i-th interval, and D is a constant.

We note that

$$\ln(t_i^4 N_i) = -\left(\frac{L}{v_0}\right)^2\left(\frac{1}{t_i}\right)^2 + \text{constant}, \qquad (3.9)$$

or, equivalently, that

$$\ln\left(\frac{N_i}{v_i^4}\right) = Q - \frac{v_i^2}{v_0^2}, \qquad (3.10)$$

where Q is a constant. Thus a display of the quantity (N_i/v_i^4) against v_i^2 on semi-log graph paper should be a straight line with negative slope $(1/v_0^2)$. It will be convenient to display the data in this way to check the validity of the Maxwell-Boltzmann distribution and to evaluate v_0 and T.

3.4. Experiment Procedure—Part I

1. Examine the apparatus and, with the aid of an instructor, identify the components and their functions.

2. Activate the chopper motor and wait until it settles to the rotational speed corresponding to a neutron burst frequency of 240 Hz.

3. Place the BF$_3$ counter (already mounted in a small shield box) at the location point very close to the chopper and set the counter voltage and amplifier conditions at the prescribed levels. Instructions for this will be posted locally.

4. Open the shutter to admit the neutron beam to the apparatus—a yellow "beam-condition" warning light will be activated. The neutron beam is fully exposed until it is finally absorbed in a beam stop at the end of the flight path. **The beam is of high intensity and exposure of any part of the body to it must be avoided**. In addition to the thermal neutrons used in this experiment, there are also gamma-rays and unmoderated fast neutrons which are damaging to tissue.

5. Examine the neutron detection pulses from the amplifier on the oscilloscope screen, noting their time width.

6. The Multi-Channel Scaler (MCS) that you will be using is a board plugged into the PC. The presets should be set as follows:
   a) Dwell time   2 μs
   b) Pass Length 1000
   c) Pass Count   432,000

   The dwell time (s ch^{-1}) multiplied by the pass length (ch) must be less than the time interval between consecutive neutron bursts (see note 2 above). Instructions for using the MCS software can be found on-line from the "Help" Menu and in the software the manual in the top desk drawer. Don't forget to EXPORT the data files into a text readable format after saving them to the default Perkin Elmer format. This latter format is not readable from computers that do not have the MCS software installed.

7. Set the MCS into operation and note the build-up of neutron counts in early time channels of the MCS time display. Since the flight distance is so small (only about 5 cm), neutrons of different speed do not have a chance to spread apart before detection. Collect data over a recorded time interval, stop the collection, and save the data to a file in your personal directory. Only a short collection time will be needed for this, as you see the quick build-up on the MCS display.

8. While you have the counter at the front position just behind the chopper, you can measure the intensity of the beam coming through the stopped, open slit. From this intensity and the known geometry of the collimator tube in the reactor shield, you can calculate an approximate value for the neutron flux inside the reactor. With the chopper stopped, adjust its angular position to get the maximum intensity as seen in the 5-second counting intervals on the scaler digital display. Record a number of these counts for averaging. Do the same with the chopper oriented so the beam is obstructed by the cadmium in the chopper. The difference between these average values divided by the detector efficiency gives the thermal neutron intensity expressed in neutrons per second. Using the formulae given in Appendix B, along with the known geometrical factors, you can calculate the neutron flux and the neutron density inside the reactor.

9. Move the BF$_3$ counter to the back position along the flight channel. Again, note the build-up of neutron counts on the MCS display. Neutrons are now found in later time channels distributed over a time spectrum. Collect data for a recorded time interval. This will take about 30 minutes to get statistically meaningful numbers because the neutron counts are now spread over many channels. (The electronic cut-off of high channels is purposely introduced to eliminate overlap from one burst to another.)

10. Close the neutron beam shutter. Measure the distance from the cadmium in the chopper disk to the counter tube center for both positions. Always take these measurements in centimeters with an accuracy to about one millimeter. Record this measurements along with rotational speed, the MCS channel width, and the collection time. Double check your distance measurements, since an error here will affect all of your later analysis.

3.5.   Data Analysis

The procedures detailed in this section are readily accomplished using Matlab on Athena or some other mathematical package of your choice.

1)   Plot your data for the small distance case, neutron counts vs. channel number, and determine the center position and uncertainty. Is the shape what you expect, and does the FWHM agree with what you calculate? Remember that the neutrons have had little chance to spread out. On the other hand, the finite flight time over your small distance has shifted this peak by a small amount relative to the neutron burst origin time. You can correct for this shift by making use of the observed travel time of the peak in the MCS display for neutrons going from L_1 (the short flight distance) to L_2 (the long flight distance). Thus the correction is

$$\frac{L_1}{(L_2 - L_1)}(C_{2p} - C_{1p}), \qquad (3.11)$$

and the neutron time origin channel C_0 becomes

$$C_0 = C_{1p} - \frac{L_1}{(L_2 - L_1)}(C_{2p} - C_{1p}). \qquad (3.12)$$

Here, C_{1p} is the MCS channel of the center of the approximately triangular distribution obtained when the detector is at the near position; C_{2p} is the MCS channel position for the peak of the distribution recorded when the detector is at the far position which is at a distance L_2 and correspondingly for C_{1p}. It is interesting to note that the speed of the neutrons in the peak in the MCS time distribution

$$N_i = C\left(\frac{1}{t_i^4}\right)\exp\left(-\frac{L^2}{v_0^2 t_i^2}\right)\Delta t, \qquad (3.13)$$

becomes $\sqrt{2}v_0$, as you can establish by setting its time derivative to zero, thereby obtaining t_{peak}, and looking at this dependence on L. This can be compared to the peak in the velocity distribution which is v_0.

Note that the channel spread about the peak centered at C_0 (in the data taken at the small distance position) is a direct representation of the time resolution of the system. All later measurements are smeared by this limiting time resolution.

2)   Plot a spectrum of your data as taken at the back counter position. Identify on your graph the neutron origin channel position C_0—all flight times are now established relative to this.

Create a plot of all the data points and an interpolated line. We expect that the spectrum will approach equal asymptotic levels at the two extremes of the spectrum, and that this is a background level by which all observed spectral intensity values should be corrected. Are the deviations of individual points from your smooth curve meaningful on statistical grounds? Remember that the collection of N statistically distributed events in a measurement means that there is 68% probability that the value N will fall within $\langle N\rangle$ of the true value as established by many repetitive measurements.

Since the expected M-B spectrum approaches zero asymptotically at both extremes of the spectrum (because of the t^{-4} dependence at the high channel (low energy) end and the exponential dependence at the low channel end), the residual or base level that is observed represents a background intensity level arising from leakage neutron events not associated with opening or closing the chopper. Thus all observed intensities should be corrected by subtracting this background level. In assessing this background level for your data, you should note that $t \to 0$ for channels just above C_0 so the intensity level for channels just above C_0 should represent the base level. On the other hand, at the other extreme, near the electronic cut-off level of about channel 1000 (or whatever the number of channels has been set to in the MCS software), the M-B spectrum has not completely collapsed to zero and the observed intensity may be somewhat higher that it would be for even lower channels. We can correct for this residual M-B intensity in high channels by noting that its value, relative to the peak intensity depends upon v_0. **Previous experimentation has determined v_0, and calculation has shown that the ratio of this residual intensity in channels above 950 to that at the peak is 0.013.** Using this ratio value, determine the background base value which is most consistent with the observed intensity pattern at both ends of the spectrum. Pay no attention to intensity values corresponding to negative channel numbers (below C_0) since they are associated with transparency of the Cd in the chopper and with other leakage neutrons.

3)   Create data vectors of $N_{\text{observed}} - N_{\text{base level}}$ and corresponding $C_{\text{observed channel}} - C_0$. Follow with calculated values of the speed v using your measured flight distance and the individual channel time. Carry a number of significant figures that is consistent with the measurement precision.

Finally, tabulate values of $N_{\text{corrected}}/v^4$ and v^2. Make a semi-log plot covering about 3 log cycles of these quantities. According to our M-B theory, these points should fall on a straight line whose slope is $1/v_0^2$. Graphical trick: to make full use of 3-cycle log paper, adjust your intensity data by an arbitrary multiplicative factor—this will not affect the slope.

4)   You will probably find that the high-velocity data points (> 5000 m/sec) in this semi-log display fall above a straight line fitted to the low-velocity data. Two effects contribute to such discrepancies: (a) The finite duration of the pulses of neutrons that emerge from the chopper causes a smearing of the observed velocity distribution

so that it differs significantly from the true flight time distribution (see if you can estimate the effect of this on your data); (b) High energy neutrons generated in the fission process and encountering the relatively cold moderator, are continually diffusing in "velocity space" toward lower velocity with the diffusion driven by an excess at high velocities over the equilibrium Maxwell-Boltzmann distribution.

Deviations from linearity of the plot may also occur at low velocities (< 1000 m/sec) for various reasons such as the high absorption cross sections of reactor materials for slow neutrons. It must be recognized, also, that the background intensity makes up a larger portion of the observed counting rates at the low and high-velocity ends of the data.

In any event, when fitting a straight line to the data, remember both effects and pay special attention to the main center region of the range. Since your physical judgment must establish the range of linearity, it is hardly worthwhile to use a least-squares fitting of the points to a straight line. Use your best judgment in this and estimate the uncertainty in the slope of the line. Don't hesitate to calculate values and plot additional points beyond your initial sampling of your smoothed spectral curve in assessing the best line fit. If you find gaps in your selected point distribution, analyze additional intermediate ones which will help in recognizing the linear range.

5)   Evaluate the slope of your best straight line (be very careful in this—students frequently have much trouble with the slope of a line on semi-log display) and calculate v_0, $E_0 = 1/2mv_0^2$, and T from $kT = 1/2mv_0^2$, and justify this relation. Recall in gases $E_{\text{kinetic}} = \frac{3}{2}m\bar{v}^2$. Does your neutron temperature T agree with that of the moderator? Does the peak position in the observed spectrum agree with that expected from your fitted parameters? From the uncertainty in the slope of the line, what are the uncertainties in these quantities?

6)   Calculate the neutron flux and neutron density in the reactor from your data obtained in Sections 3.4, 7 and the analysis in Appendix B. If we think of these neutrons as being confined in a walled container, what pressure would they exert on the walls?

4.   Part II: Bragg Diffraction of Neutrons and the De Broglie Relation

See Bragg (1915) [7].

In the early years of the twentieth century, physicists were faced with the wave-particle dilemma in describing the properties of the electromagnetic field and how it interacts with matter. Young's interference experiments with visible light (1801), Hertz's experiments with radio waves (1887), and von Laue's discovery of X-ray diffraction (1912) showed wave interference and provided measures of wavelength for electromagnetic radiation from radio to X-rays. On the other hand, Planck's theory of the black-body spectrum (1901), and Einstein's theory of the photoelectric effect (1905) showed that electromagnetic radiation is *absorbed* at a surface in discrete amounts of energy (quanta) and not as a continuous flow. Bohr's theory of the hydrogen atom (1913) showed that electromagnetic energy is *emitted* in discrete quanta. And, finally, Compton's interpretation of his own experiments on the incoherent scattering of X-rays (1923) showed that X-rays of wavelength λ interact with free electrons like particles with energy hc/λ and momentum h/λ. A composite picture was thus formed in which electromagnetic radiation is characterized by the seemingly contradictory concepts of wave frequency and wavelength, and particle momentum and energy.

Recognizing this interrelation for photons between wave and dynamical properties, De Broglie suggested in 1924 (in his PhD thesis) that similar properties should characterize all particles of matter. At that period, matter was considered to be made up of electrons and protons. This meant that electrons and protons (or any composite of them like an atom, a baseball or the earth) in motion should possess a wave character. De Broglie proposed a relation between the wavelength (λ) and momentum (mv):

$$\lambda = \frac{h}{mv}, \tag{4.1}$$

where h is Planck's constant. This relation is the same as for photons, with, however, the recognition that photon momentum $p = E/c$ (with the photon energy $E = h\nu$ and ν the wave frequency of the electromagnetic photon).

Although not taken too seriously at first (it is reported that Einstein himself was incredulous initially), De Broglie's suggestion was given full acceptance with the discovery of electron diffraction by G. P. Thompson and by Davison and Germer in 1927. They drew upon the fact that atoms in a crystal are positioned relative to each other in a very regular way, and that their spacing is a few Angstroms ($1\text{Å} = 10^{-10}$ m) in scale. Their experiments on the reflection of electron beams from metal crystals demonstrated that wave interference effects were obtained with electrons of an energy such that their De Broglie wavelength is comparable to the separation of the crystal planes, a result completely analogous to that previously observed with X-ray photons (which certainly were endowed with a wavelength) and interpreted by Laue and Bragg. Since that time, further confirmation of the wave-particle duality has come for other types of particles (waves) such as alpha particles, atoms, neutrons and mesons. We shall see this duality in full display in Section 4 of this experiment, where we shall again directly measure the velocity of a group of neutrons and at the same time observe the diffraction of these same neutrons by a crystal, thereby establishing their De Broglie wavelength.
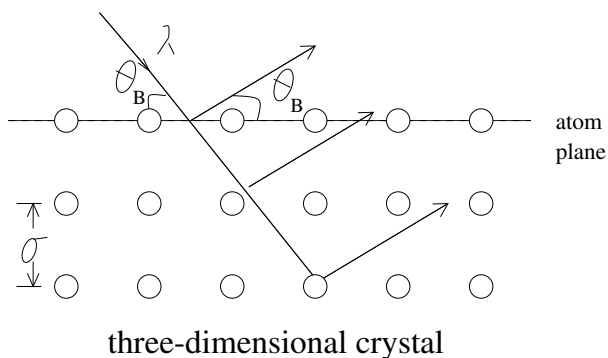
FIG. 4: Schematic representation of a crystal with rows of atoms extending into the page.
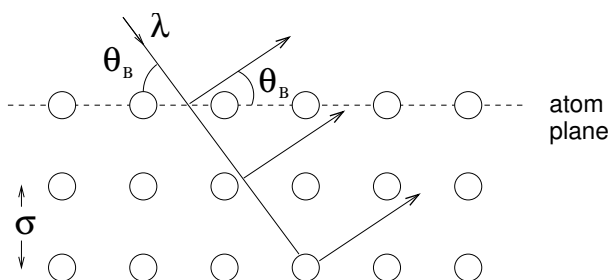

FIG. 5: Schematic representation of a diffraction grating as a one-dimensional set of scattering centers.

We shall first need to know some things about crystals and the wave interference effects that may be observed with them. As mentioned above, a crystal represents a collection of many atoms bound together by inter-atomic forces to form a three-dimensional solid (however, two-dimensional cases and liquid crystals are known to exist). In a perfect crystal, the atoms are positioned in a spatial array (or lattice) with precision, this being determined by the symmetry and balancing of inter-atomic forces on each atom. With this regularity of position, illustrated schematically in Figure 4, it is easy to envision the overall crystal as being made up of parallel sheets (or planes) of atoms which can serve to provide wave interference between the components of radiation scattered by individual atoms. Almost any textbook on general or modern physics (e.g., reference [8, 9]) will have an elementary derivation of the conditions necessary for constructive interference of radiation scattered from atoms in a crystal plane. These conditions are expressed by Bragg's Law,

$$n\lambda = 2d \sin\theta_B, \qquad (4.2)$$

where n = order of diffraction $(1, 2, 3, \ldots)$, λ is the wavelength, d is the interplanar spacing, and θ_B, called the Bragg angle, is the grazing angle of incidence and reflection. It is deceptively similar in appearance to the law describing constructive interference from a one-dimensional set of scattering centers (e.g. a grating), and it is worth pointing out the difference.

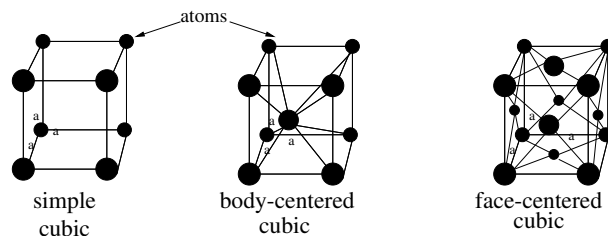In the one-dimensional case, illustrated in Figure 5,

FIG. 6: The three forms of cubic crystals.

the approach angle θ_1 may have any value, and the exiting angle θ_2 for constructive interference is then defined by the interference equation with θ_2 not necessarily equal to θ_1. For reasons not so obvious, this generality is not present in three-dimensional diffraction where $\theta_1 = \theta_2 = \theta_B$. In fact, diffraction from a crystal always occurs in symmetrical fashion from atom planes with both incident and emergent angles being equal to θ_B. (This subtle distinction is discussed in [10] and in various texts on crystallography, e.g., X-Ray Crystallography, M. Wolfson, Cambridge 1970.) A given set of atom planes of spacing d will reflect radiation of wavelength λ with intensity concentrated in a narrow range of angles (typically within 10^{-5} radians) with a maximum at the Bragg angle θ_B defined above. This is not true for the one-dimensional grating where, for any incident angle θ_1, diffraction maxima occur at angles θ_2 given by the formula in the figure, provided $d > \lambda$.

A crystal may be considered as being made up of an infinite number of different atom plane layers, each set with a different interplanar spacing and different orientation. Bragg diffraction can occur from any of these sets as long as the Bragg Law is satisfied. What we need at this point is a shorthand method of classifying these different sets of planes, which we now develop. Since nature causes atoms to pack together in different ways (but always in a given way for a given species of atoms or molecules; a change of external conditions such as the temperature, pressure, or magnetic field application can invoke a change of structure, a phase transition), it is apparent that many different forms of crystal structure may be encountered. These are classified according to symmetry characteristics: cubic, hexagonal, ortho-rhombic, etc. Common to all forms is the concept of the unit cell which represents the smallest collection of atoms (or molecules) which, when repeated along the three axes, make up the whole crystal. Thus cubic crystals have cubic unit cells and the size of the unit cell a_0 is set by one dimension. However, cubic cells may contain any one of three different atom configurations as shown in Figure 6.

For the general case, the unit cell can be defined by three vectors a, b, and c directed parallel to the unit cell edges and of magnitude equal to the size in that direction. Furthermore, we can identify the orientation of any plane of atoms in the crystal by the intersections of this plane with the three axes of the unit cell. It is a great convenience to do this in terms of the Miller indices
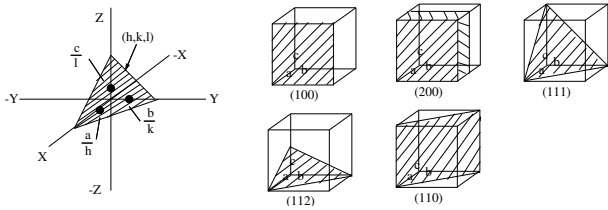
FIG. 7: Diagrams showing how Miller indices are used to define crystal planes.

FIG. 8: Illustration of Bragg reflection from a fcc crystal in which destructive interference between reflections from adjacent (001) planes occurs.

FIG. 9: Schematic diagram of the neutron beam diffracted from the copper crystal. The distance from the chopper to the crystal is 33.63 ± 0.06 inches. The distance from the crystal to the detector is 20.00 ± 0.06 inches.

h, k, and l (small integers) with a/h, b/k, c/l being the intersection points of the plane with the respective axes, as illustrated in Figure 7.

We label a particular set of atomic planes as being (hkl) planes according to these Miller indices. A little geometry will show, for the case of a cubic crystal, that the interplanar spacing d_{hkl} will be given simply by

$$d_{hkl} = \frac{a_0}{(h^2 + k^2 + l^2)^{1/2}}. \qquad (4.3)$$

In our experiment, we shall be using a metal crystal of pure copper which has a face centered cubic structure (four unique atoms per unit cell) with unit cell size $a_0 = 3.6147$ Å. Note that this value of a_0 may be calculated from the measured density $\rho = 8.939$ gcm^{-3}, Avogadro's number 6.0221×10^{23} atoms per mole, the molecular weight 63.57gXF, and the number of atoms per unit cell. Check that this is so. Also calculate interplanar spacing values for planes (200), (220), and (111) which you will be using in the experiment. You should identify, in the above figure of cubic unit cells, just which atoms are unique to the unit cell—there are four for face centered cubic (how many are there for the other cells?). Incidentally, among some common elements, Fe, Cr, Na, and Mo crystallize as body centered cubic (bcc) and Cu, Al, Au, and Pb as face centered cubic (fcc). No element is known to exist in simple cubic form.

Before leaving our crystallographic considerations, we should investigate whether there are restrictions on the appearance of Bragg diffraction from the many (hkl) sets of planes. To illustrate this for our fcc case, a view of the unit cell normal to a face shows atoms and atom planes as shown in Figure 8. There are sheets of atoms separated by the fundamental distance d (002) = $a_0/2$, with common atomic density in all sheets. If we were to attempt to observe (001) diffraction as prescribed by Bragg's Law, we would find reflected rays (A) and (C) to be in phase, as would (B) and (D), but the two groups would be out of phase with respect to each other, and hence overall destructive interference would occur. Thus zero intensity in (001) diffraction is expected, but finite intensity in (002) diffraction. Without going into detail, **the general rule for an fcc structure is that the Miller indices must be either all even integers or all odd integers in order for constructive interference to occur**. Thus there will be no (100), (110), (221) diffraction occurring, but there can be (020), (111),
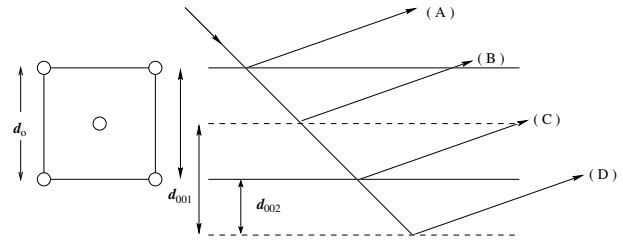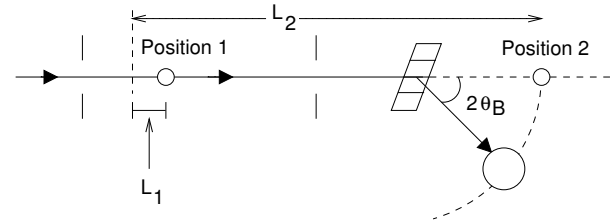
(022), (311) for fcc. Other crystal structures would have different selection rules. Miller indices can be taken negative as well as positive, and a negative index is written as a bar over the index. Thus $(11\bar{1})$ would designate an allowed set of planes in the fcc structure Bragg diffraction.

4.1.   Experiment Arrangement and Procedure

We shall use the same neutron beam as in Section 3. As we have seen, it is a full spectrum beam with all neutron speeds (or as De Broglie asserted, all wavelengths). However, before detecting it on its normal straight flight line, we shall interrupt it with a diffracting crystal of copper. After repositioning the detector, we can detect the Bragg diffracted beam in the direction that makes an angle of $2\theta_B$ with the incident beam, as shown in Figure 9.

The copper crystal will be positioned along the neutron flight line, somewhat in front of the position where you placed the detector for the Section 3 spectrum measurement. Notice that there is a fixed slit opening (of width 3.0 mm) just before (upstream from) the crystal position, and this serves to further define the direction of neutron ray trajectories (along with the fixed slit in front of the chopper disk shown in Figure 3) that can hit the crystal. It was there during your spectrum measurement, but served no particular purpose, since we were interested only in flight distance to the detector and not
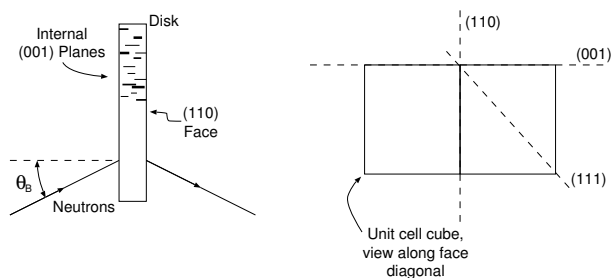
FIG. 10: Illustration of the orientation of the crystal planes in relation to the geometrical shape of the crystal.

the direction of rays.

If a particular set of crystal planes (hkl) is oriented at an angle θ_B from the incident beam direction, neutrons with wavelengths in a narrow band will satisfy Bragg's Law and hence be diffracted at angles in a narrow range around $2\theta_B$ from the incident beam direction. We can detect this diffracted beam by placing our detecting counter at the appropriate angular position. In our experiment, we shall select various orientation positions of the crystal (thereby selecting θ_B) and simultaneously measure the flight time of the diffracted neutrons which arrive at the detector. This provides both the wavelength λ (from the Bragg Law) and the velocity v of the diffracted neutrons. By changing the crystal orientation (and the detector position), we can scan over a range of λ and v and test the De Broglie relation in a very direct way.

4.1.1.   The Crystal

The copper crystal has been grown and cut in the form of a small disk of diameter about 15 mm and thickness about 2.3 mm. Copper metal exists usually in polycrystalline form, i.e., it is made up of many microscopic crystallites (perhaps about 1 μm in size) oriented at random. Our single crystal has been prepared in a special way (called the Bridgman method): the metal was melted in a crucible of special shape, and the temperature was very slowly reduced through the freezing temperature with a controlled temperature gradient. This permits a single crystal to grow to a size limited only by the crucible dimensions (if the conditions are right!). Our crystal disk has been cut from such a grain after establishment of the grain orientation by diffraction techniques (neutrons, of course!). The flat faces of the disk have been cut and surface polished to high precision—they are parallel to (110) crystallographic planes within 1 arc minute. Looking down on the crystal disk, we see the unit cell as illustrated in Figure 10.

In testing the De Broglie relation, we shall use diffraction from the (002) planes which are accurately perpendicular to the (110) faces. Thus we shall be using the disk in transmission orientation, i.e., the neutrons will

pass symmetrically through the disk. Copper is relatively transparent to neutron radiation with an absorption cross section of 3.69 barns for thermal radiation of speed 2200 m/sec. You should calculate the intensity loss this implies.

The crystal disk has been attached to a support plate with our (002) planes vertical.

4.1.2.   The Detector

Instead of using the low efficiency, thin BF_3 counter that was used in the Section 3 spectrum measurement, it will be helpful to use a high efficiency (about 90%) counter with ^3_2He gas. This is similar in operation to the BF_3 counter, but it contains isotopic ^3_2He gas at high pressure, about 40 atmospheres. ^3_2He is the very rare and expensive isotope of elemental helium. As with boron, ^3_2He also exhibits a $1/v$ absorption cross section for neutrons. The same counting circuit will be used, but different counter voltage and amplifier gain setting will be needed—these conditions will be posted locally.

4.1.3.   Crystal Diffraction Measurements

a) Set the crystal orientation so that the (002) planes have $\theta_B = 20°$ as closely as you can read the vernier. Leave the chopper motor off and put the chopper slot in the open position.

b) Open the neutron beam shutter so that a steady neutron beam falls on the crystal.

c) Without disturbing the crystal orientation, move the counter in angle position around $2\theta = 40°$— there is a crude angle scale on the table and a paper vernier scale on the counter box. With Bragg diffraction occurring at the crystal, we expect a localized intensity peak at about 40° scattering angle. Measure the intensity with short time counting in the electronic scaler at different positions of the detector using steps of 0.25°. Plot this immediately, and determine the center position.

d) Set the chopper wheel in motion and stabilize at the 240 Hz burst rate as before.

e) **TIME SAVING HINT: Read Appendix B and do transmission cross-section measurements as part of the next step**

f) Collect data in the MCS giving the flight time spectrum of the neutrons which are diffracted from the (002) planes in the crystal. There should now be a sharp peak at the flight times of the selected monochromatic neutrons. You may also see a lower intensity peak characteristic of $\lambda/2$ in second order diffraction from the same planes. Collect enough MCS data for print-out. If you see second order

peaks in the MCS display, collect enough data to determine their flight time as well as for the first order.

g) Repeat for other selected θ_B values: 30°, 25°, 20°, and 15°. In setting other θ_B positions, it is worthwhile to redetermine the counter position as in 4(c) above. An off-center detector will produce an error in the measured speed relative to that expected from the Bragg angle of the crystal. You expect the scattering angle to be close to $2\theta_B$ in each case. Remember that the θ_B value read on the more accurate goniometer is the primary angle quantity and the counter position is not of use in the later analysis. You want only to have the counter in the central part of the diffracted beam. Once you have determined this central part for each angle and measured the spectrum at that angle, you should also take a second spectrum through the boron absorber (pyrex beaker-bottom) for each angle. You will use these data for checking the $1/v$ dependence of the cross-section for boron in Section 4.

h) You cannot safely access the containment area to measure the flight path distance from the chopper wheel to the counter center; it is different than in Section 3. Use the following values:

- from the chopper to the crystal is 33.63 ± 0.06 inches

- The distance from the crystal to the detector is 20.00 ± 0.06 inches.

4.2.   Analysis of Crystal Data

Graph the time spectrum data obtained at the various θ_B selections—only the peaks plus their nearby background are of interest here, including any small $\lambda/2$ ones. Notice that the channel widths of these are essentially the same as your resolution width determined in Section 3. Establish the centers of these peaks (use the steep sides of the peak in this), and correct for the neutron time origin C_0 determined in (h) above.

Calculate the wavelength and corresponding neutron speed (with significant figures consistent with the measurement precision) for the various monochromatic beam observations. Tabulate your data and graph v vs. $1/\lambda$ with scales including the origin. According to the De Broglie relation, your data points should fall on a straight line with slope h/m which passes through the origin. On your graph, draw the expected line using accepted values for h and m. This is an ideal case for applying a least-squares treatment of the line fitting (anchor the fitted line at $v = 0 = 1/\lambda$ since the De Broglie Law requires this).

Analyze the possible contributing errors that enter into your observations and establish the uncertainty in the slope of your linear fit. Is this consistent with the difference between your result and that expected from established constants? Typical runs show agreement to 1.0% or so.

Analyze the 2θ scans that you made in establishing the centered detector position in the Bragg reflection. Considering the ray geometry falling on the crystal and the angular width of the detector opening, this can tell you something about the perfection of the copper crystal.

5.   Part III: Additional Crystal Diffraction Observations and Uses of Crystal Monochromated Neutrons

There are a number of other experiments that you can perform with the simple one-axis spectrometer (more elaborate, sophisticated spectrometers sometimes involve three axes of scattering in research studies). You will have time in the scheduling to do at least one of the following. The monochromatic diffracted beams from the copper crystal are of low intensity (unlike the hot, direct white beam), and are safe to experiment with.

5.1.   Transmission of Slow Neutrons Through Materials

Most materials are relatively transparent to slow neutrons. This arises because neutrons carry no Coulombic charge (experiments have shown this to be less than 10^{-22} electron charges!), and thus they don't interact with the charge distribution in atoms by means of the long-range Coulombic interaction. They do interact with the nuclei of atoms through the short-range nuclear force interaction, and this is conveniently quantified by a nuclear scattering cross section (σ_S) and a nuclear absorption cross section (σ_A). Scattering cross sections do not vary very much from nucleus to nucleus and have values of a few barns (10^{-24} cm^2). On the other hand, capture or absorption cross sections vary widely depending upon the distribution of nuclear energy levels and thus nuclear resonance effects may be encountered. In illustration of this, we may note that the absorption cross section of carbon for thermal neutrons is only about 0.0034 barns, whereas for some exotic rare-earth nuclei this becomes as large as several million barns. Absorption cross sections invariably are sensitive to neutron energy (the $1/v$ law mentioned earlier is a mild example of this) and resonance behavior is not uncommon.

You can study some of these cross sections by using the monochromatic, Bragg diffracted beam from the copper crystal and establishing the transmission (T) of a piece of material for this beam, as illustrated in Figure 11.

By definition,

$$T = \frac{I \text{ (intensity passed through the sample)}}{I_0 \text{ (intensity incident on the sample)}}. \quad (5.1)$$
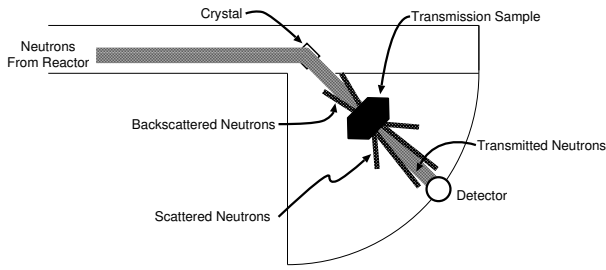
FIG. 11: Plan view of the experimental setup for measuring the attenuation of monoenergetic neutrons in a sample.

study. For Fe and Al, the transmission is dominated by the scattering process (hence it is relatively insensitive to neutron energy), whereas for Cd and B, absorption dominates with significant dependence upon neutron energy. You will want generally to spend longer periods collecting intensity data through the sample than without...see Appendix A notes on transmission measurements. Study all samples at fixed wavelength corresponding to $\theta_B = 20°$ and, as well, the boron sample at several wavelengths (energies).

This can be shown to be

$$T = \frac{I}{I_0} = \exp\left[-\sum_i M_i \sigma_{iT}\right] \quad (5.2)$$

with the index i symbolizing different nuclear species in a composite sample, σ_{iT} the transmission cross section (the sum of both σ_S and σ_A) per nucleus of the i-th species, and

$$M = \text{areal density of nuclei}$$
$$= \text{number of nuclei/cm}^2 \text{ sample}$$
$$= \text{volume density of nuclei} \cdot \text{sample thickness.}$$

Plate samples of Fe, Al, Cd, and boron-containing Pyrex glass are available for transmission cross section

The intensities to be used in obtaining T are best established from the MCS flight time spectral print-out. By summing the intensity in all channels over the monochromatic peak (corrected for background of course), you obtain the integrated intensity in the Bragg reflection. Normalize these to a common data-collection time interval in getting T. With the Pyrex plate, the strong absorption cross section of B dominates, and you can establish the $1/v$ law for this by measuring the transmission over a range of neutron velocities. Compare the established values for the cross sections with what you determine from experiment. Perhaps you have something else to place in the neutron beam whose transparency to neutrons you would like to assess. For instance, a thin plate of plastic (containing lots of hydrogen) will attenuate the neutron beam about as much as the thick iron plate!

[1] B. B. Clifford Shull, *Nobel prize lecture*, Nobel Prize Lecture (1994).
[2] A. Foster and R. Wright, *Basic Nuclear Engineering* (Allyn and Bacon, Boston, MA, 1977), tK9145.F754 ScienceLibrary Stacks.
[3] A. Henry, *Nuclear Reactor Analysis* (MIT Press, Cambridge, MA, 1975), qC786.5.H46 Science Library Stacks.
[4] A. Nero, *Guidebook to Nuclear Reactors* (U.C. Press, Berkeley, CA, 1979), tK9202.N45 Science Library Stacks.
[5] C. Kittel and H. Kroemer, *Thermal Physics* (W.H. Freeman, New York, 1980), qC311.5.K62 Physics Department Reading Room.
[6] F. Reif, *Fundamentals of Statistical and Thermal Physics* (McGraw-Hill, New York, 1965), qC175.R361 Physics Department Reading Room.
[7] W. H. Bragg and W. L. Bragg, *Analysis of crystal structure by means of x-rays*, Nobel Prize Lecture (1915).
[8] P. Tipler, *Foundations of Modern Physics* (Worth Publishers, Inc., 1969), qC21.T595 Science Library Stacks.
[9] J. McGervey, *Introduction to Modern Physics* (Academic Press, New York, 1971), qC21.2.M145 Physics Department Reading Room.
[10] B. Rossi, *Optics* (Addison Wesley, Reading, 1957), qC355.R831 Physics Department Reading Room.

APPENDIX A: TRANSMISSION CROSS-SECTION MEASUREMENT

As illustrated schematically in Figure 12, one measures the diminution in the beam intensity caused by the insertion of a given absorber between the beam and the detector. The data consist of the total numbers of neutrons detected per unit time, N_0 and N, integrated over the time-of flight spectrum, with correction for background (baseline), and with and without the sample in the monochromatic neutron beam. One then calculates the transmission T and finally the effective cross sectional area s of the scattering-absorption center according to the relation

$$T = \frac{I}{I_0} = \frac{N}{N_0} = e^{-M\sigma} \quad (A1)$$

Question (1): What is the uncertainty $\Delta\sigma$ in the σ value?

Answer: From the theory of propagating errors we have the equation

$$\left(\frac{\Delta T}{T}\right)^2 = \left(\frac{\Delta N}{N}\right)^2 + \left(\frac{\Delta N_0}{N_0}\right)^2, \quad (A2)$$
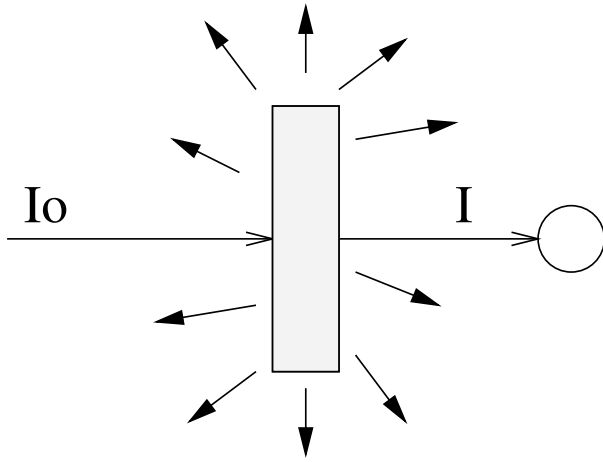
FIG. 12: Schematic diagram of an attenuation measurement.

i.e. the fractional error in T is the square root of the sum of the squares of the fractional errors in the the intensity values. Since $\Delta N = \sqrt{N}$ for a statistically random collection of N events, it follows that

$$\frac{\Delta T}{T} = -M\Delta\sigma = \left(\frac{1}{N} + \frac{1}{N_0}\right)^{1/2}. \qquad \text{(A3)}$$

Question (2): If we want to spend a total collection time t_0 distributed between sample collection time t_s and incident beam collection time t_B, what is the optimum distribution of collection time so as to minimize ΔT and $\Delta\sigma$?

Answer: $N_0 = \alpha t_B$ and $N = T\alpha t_s$, where α is the collection rate of incident beam intensity and $t_s = t_0 - t_B$. It follows that

$$\frac{\Delta T}{T} = \left(\frac{1}{T\alpha t_s} + \frac{1}{\alpha t_B}\right)^{1/2}. \qquad \text{(A4)}$$

For minimization of ΔT, we want

$$\frac{d(\Delta T)}{dt_B} = 0. \qquad \text{(A5)}$$

This is satisfied when

$$\frac{1}{T(t_0 - t_B)^2} - \frac{1}{t_B^2} = 0 \qquad \text{(A6)}$$

(check this out) which, when solved for t_B, yields the expressions

$$t_B = t_0 \frac{\sqrt{T} - T}{1 - T} \qquad \text{and} \qquad t_s = t_0 - t_B = t_0 \frac{1}{1 + \sqrt{T}} \qquad \text{(A7)}$$

and the ratio of collection times

$$t_s/t_B = T^{-1/2}. \qquad \text{(A8)}$$

Thus for high T (i.e. $T \approx 1$) we want equal collection times. On the other hand, for small T, we want to distribute the time so that more time is spent collecting neutrons through the sample. For example, if $T = 0.1$ for a sample, you will attain highest precision in the calculated value for σ if the sample collection time is about three times longer than the open beam collection time. Of course, increasing the total collection time t_0 also improves the precision. In estimating how you should best distribute the collection time, you can get a preliminary estimate of T for a sample by looking at the rate of intensity build-up on the MCS scope and comparing this with that obtained with the open beam.

A good sequence procedure for studying the different samples at fixed $\theta_B = 20°$ position is: (1) Open beam, (2) Al, (3) Fe, (4) B, (5) Cd, and (6) Open beam. Hopefully your start-end "Open beam" results are the same and you can average them. Time all collection runs so that they can be normalized.

In placing samples along the beam line, remember that we do not want to count any of the scattered intensity. This means that we want scattering samples to be well away from the detector so that the detector solid angle as seen from the sample is small compared to total 4π steradians.

FIG. 13: Plot of the ratio of collection times against transmission.

FIG. 14: Schematic of geometry necessary to calculate the neutron flux and neutron density.

APPENDIX B: CALCULATION OF NEUTRON FLUX AND NEUTRON DENSITY IN REACTOR

The neutron density n (neutrons cm^{-3} irrespective of speed or direction of travel) and the neutron flux $\phi_0 = nv$ (neutrons cm^{-2}sec) inside the reactor may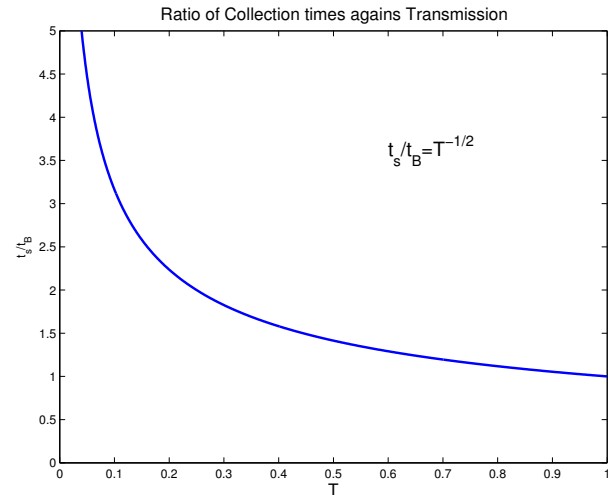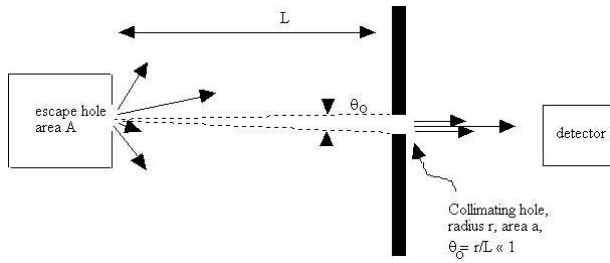 be calculated from your intensity measurement obtained in Section 3.4 item 7. We can model this problem as being similar to that found in many textbooks of statistical mechanics or thermodynamics (in particular see Sections 7.9–7.12 in Reference [6]).

Consider a gas of density n in thermal equilibrium inside a container surrounded by vacuum. A small hole is present in the container wall so that gas atoms of all speeds traveling in all directions escape out through the hole.

An additional collimating hole is placed at a large distance L from the container wall along a line perpendicular to the container wall so that a collimated beam of atoms of all speeds will pass through the collimating hole and be detected by a detector placed behind the hole. Thus following Reif eq. 7.11.9, the collimated current I (atoms/second) passing through the collimating hole would be expressed as

$$
\begin{aligned}
I &= A \int_{v_x > 0} v^3 f(v)dv \int_0^{\theta_0} \sin\theta \cos\theta d\theta \int_0^{2\pi} d\phi \\
&= \pi A \,\theta_0^2 \int_0^\infty v^3 f(v)dv \\
&= \frac{1}{4} A \,\theta_0^2 \, n\bar{v} \\
&= A \frac{a}{4\pi L^2} n\bar{v},
\end{aligned} \tag{B1}
$$

where as in Reif, $\bar{v}$ is the average speed of the Maxwell-Boltzmann speed distribution. The average speed is related to our most probable speed v_0 (see Equation 3.1) as

$$
\bar{v} = \frac{2}{\sqrt{\pi}} v_0 \tag{B2}
$$

which you have evaluated in the Maxwell-Boltzmann spectrum analysis.

For our neutron case, neutrons are delivered to a low efficiency detector ($e = 0.010$ averaged over the spectrum) behind the chopper area ($a = 2.4$ mm^2) by a long, converging, tapered collimator tube. The dimensions of this collimator tube are such that each point of the exit area sees a source area of 2.0 cm^2 on the front surface of the oversize insert tube extending through the D$_2$O reflector to the center line below the reactor volume. The distance from the exit area (the chopper slit) to the front surface source is 310 cm. Using these numerical parameters and your measured intensity you can calculate $n\bar{v}$ (commonly called the reactor flux) and n. It is to be recognized that these values are approximate (within a small factor of order unity) because our assembly does not match the features of the model exactly. We do not have a sharp containment wall for the neutrons and the void volume of the insert tube can perturb the local flux. This flux value would scale with the reactor operating power level.

APPENDIX C: EQUIPMENT LIST

Manufacturer	Description	URL
MIT	Research Reactor	
LND	He-3 Detector	lnd.com
LND	BF$_3$ Detector	lnd.com
Canberra	Proportional Counter preamp	canberra.com
Canberra	Amplifier	canberra.com
Ortec	Multi-Channel Scaler	ortec-online.com

APPENDIX D: TIME OF FLIGHT DATA ANALYSIS

The following analysis was created and provided by Prof. David Litster.

1.   Analysis

This is a brief discussion of how to analyze the TOF data for thermal neutrons.

The flux of neutrons with speeds between v and $v + dv$ will be proportional to

$$
j(v)dv = n\sqrt{\frac{2}{\pi}} \left(\frac{v}{v_0}\right)^3 e^{-(v/v_0)^2} dv \tag{D1}
$$

where

$$
v_0 = \sqrt{2k_B T/m} \approx 2300 \text{ ms}^{-1}. \tag{D2}
$$

If the detector efficiency is proportional to $1/v$ we might expect a neutron counting rate for neutrons with speeds

between v and $v + dv$ to be proportional to

$$\left(\frac{v}{v_0}\right)^2 e^{-(v/v_0)^2} dv \qquad (D3)$$

However, the chopper passes neutrons for a finite period of time every time it opens. Thus the time of flight of the neutrons from the chopper to the detector varies and the counts in each channel of the MCS represent neutrons that have a range of speeds. When the detector is close to the chopper, that does not matter much as neutrons of all speeds present in the beam will arrive at the detector at the same time (on the scale of the time resolution for the chopper) and the counts in the MCS will just measure the transmission of the chopper as a function of time. That function will be the convolution of two slits each 1.0 mm wide and will therefore be triangular in shape. The chopper wheel spins at 1800 rpm and the slits are at a radius of 54.5 mm. From this, it is easy to calculate that the triangular transmission function of the chopper should have a half-width at the base of 95 μs. This was verified by fitting the TOF spectrum obtained when the BF$_3$ detector was 3.25 in from the chopper. I will use the variable t_H to represent the 95 μs half-width of the chopper transmission. I will also use ℓ to be the distance from the chopper to the BF$_3$ detector and consider the neutrons counted into channel m of the MCS. The sweep of the MCS is triggered by a light pulse some time before the chopper opens. I assume that the MCS is counting into channel n_0 when the chopper transmission is maximum.

Now let's consider channel m of the MCS. It will represent a time $t_m = t_D(m - n_0)$ with respect to the time the chopper was maximally open. Note that t_m may be negative. If $t_m \leq -t_H$ no neutrons will have had time to reach the detector. For $t_m > -t_H$, there are three time regions to consider when calculating the neutron speeds that will be counted into channel m. They are $-t_H < t_m \leq 0$, $0 < t_m \leq t_H$ and $t_m > t_H$.

The easiest way to do the calculations is to consider the travel time t of the neutrons from the chopper to the detector. When integrating over the range of speeds for neutrons that will be counted into channel m, it will be necessary to include a factor that represents the triangular transmission function of the chopper. It will also be useful to introduce a new variable $y = v/v_0 = \ell/(v_o t)$ which means $t = \ell/(v_0 y)$ and $dt = -(\ell/v_0)(1/y^2)dy$.

What we want to integrate over these three time regions is the number of neutrons whose travel time lies between t and $t + dt$. As the number whose speed is between v and $v + dv$ is proportional to $y^2 e^{-y^2} dv$ and $t = \ell/v$, the number whose travel time is between t and $t + dt$ will be proportional to $y^4 e^{-y^2} dt$.

Some useful integrals will be:

$$\int_{y_1}^{y_2} e^{-y^2} dy = \frac{\sqrt{\pi}}{2}[\Phi(y_2) - \Phi(y_1)]$$

$$\text{where } \Phi(x) = \frac{2}{\sqrt{\pi}} \int_0^x e^{-t^2} dt, \qquad (D4)$$

$$\int_{y_1}^{y_2} y e^{-y^2} dy = -\frac{1}{2}\int_{y_1^2}^{y_2^2} e^{-z} dz = \frac{1}{2}\left(e^{-y_1^2} - e^{-y_2^2}\right) ,$$

$$\int y^2 e^{-y^2} dy = -\frac{1}{2} y e^{-y^2} + \frac{1}{2}\int e^{-y^2} dy .$$

The calculations are given below. The neutron count rate will be proportional to $\mathcal{R}(m)$ and the factor $1/t_H$ is included to make the result dimensionless.

$\underline{-\mathbf{t_H} < \mathbf{t_m} \leq \mathbf{0}}$

$$
\begin{aligned}
\mathcal{R}(m) &= \frac{1}{t_H}\int_0^{t_H + t_m}\left(\frac{t_H + t_m - t}{t_H}\right) y(t)^4 e^{-y(t)^2} dt \\
&= \frac{\ell}{v_0 t_H}\int_{y_1}^{\infty}\left[\left(1 + \frac{t_m}{t_H}\right) y^2 - \frac{\ell}{v_0 t_H} y\right] e^{-y^2} dy \text{ where } y_1 = \frac{\ell}{v_0(t_m + t_H)} \\
&= \frac{1}{2}\frac{\ell}{v_0 t_H}\left(1 + \frac{t_m}{t_H}\right)\left(\frac{\sqrt{\pi}}{2}[1 - \Phi(y_1)] + y_1 e^{-y_1^2}\right) - \frac{1}{2}\left(\frac{\ell}{v_0 t_H}\right)^2 e^{-y_1^2}
\end{aligned}
$$

$\underline{\mathbf{0} < \mathbf{t_m} \leq \mathbf{t_H}}$

$$
\begin{aligned}
\mathcal{R}(m) &= \frac{1}{t_H}\int_0^{t_m}\left(\frac{t_H - t_m + t}{t_H}\right)y(t)^4 e^{-y(t)^2}dt + \frac{1}{t_H}\int_{t_m}^{t_H+t_m}\left(\frac{t_H + t_m - t}{t_H}\right)y(t)^4 e^{-y(t)^2}dt \\
&= \frac{\ell}{v_0 t_H}\int_{y_1}^{y_m}\left[\left(1+\frac{t_m}{t_H}\right)y^2 - \frac{\ell}{v_0 t_H}y\right]e^{-y^2}dy + \frac{\ell}{v_0 t_H}\int_{y_m}^{\infty}\left[\left(1-\frac{t_m}{t_H}\right)y^2 + \frac{\ell}{v_0 t_H}y\right]e^{-y^2}dy \\
&= \frac{1}{2}\frac{\ell}{v_0 t_H}\left\{\frac{\sqrt{\pi}}{2}[1-\Phi(y_1)] + y_1 e^{-y_1^2} - \frac{t_m}{t_H}\left[\frac{\sqrt{\pi}}{2}[1+\Phi(y_1)-2\Phi(y_m)] + 2y_m e^{-y_m^2} - y_1 e^{-y_1^2}\right]\right\} \\
&\quad + \frac{1}{2}\left(\frac{\ell}{v_0 t_H}\right)^2\left[e^{-y_1^2} - 2e^{-y_m^2}\right] \quad\text{where } y_m = \frac{\ell}{v_0 t_m} .
\end{aligned}
$$

$\underline{t_m > t_H}$

$$
\begin{aligned}
\mathcal{R}(m) &= \frac{1}{t_H}\int_{t_m-t_H}^{t_m}\left(\frac{t_H - t_m + t}{t_H}\right)y(t)^4 e^{-y(t)^2}dt + \frac{1}{t_H}\int_{t_m}^{t_H+t_m}\left(\frac{t_H + t_m - t}{t_H}\right)y(t)^4 e^{-y(t)^2}dt \\
&= \frac{\ell}{v_0 t_H}\int_{y_1}^{y_m}\left[\left(1+\frac{t_m}{t_H}\right)y^2 - \frac{\ell}{v_0 t_H}y\right]e^{-y^2}dy + \frac{\ell}{v_0 t_H}\int_{y_m}^{y_2}\left[\left(1-\frac{t_m}{t_H}\right)y^2 + \frac{\ell}{v_0 t_H}y\right]e^{-y^2}dy \\
&= \frac{1}{2}\frac{\ell}{v_0 t_H}\left\{\Gamma(\tfrac{3}{2},y_1^2) - \Gamma(\tfrac{3}{2},y_2^2) + \frac{t_m}{t_H}[\Gamma(\tfrac{3}{2},y_1^2) + \Gamma(\tfrac{3}{2},y_2^2) - 2\Gamma(\tfrac{3}{2},y_m^2)]\right\} \\
&\quad + \frac{1}{2}\left(\frac{\ell}{v_0 t_H}\right)^2\left[e^{-y_1^2} + e^{-y_2^2} - 2e^{-y_m^2}\right] \quad\text{where } y_2 = \frac{\ell}{v_0(t_m - t_H)}.
\end{aligned}
$$

Thus $\mathcal{R}(m)$ has exponentials along with error functions. These should not be too hard to evaluate numerically for fitting purposes. Most compiler libraries provide them. The Gnu Scientific Library (http://www.gnu.org/software/gsl/) has routines for both of these functions. The exponential function goes rapidly to zero for large x and can lead to floating point underflows. I used code provided in the GSL library to deal with that.

When writing the fitting code, it is easy to measure time in MCS channel number units and use the dwell time to convert to μs after the fit. Section 2 list the model function code that I used. It is written in C and there are some global variables: `NO` is n_0, `X` is the channel number so that `m = X - NO` is t_m, `HW` is t_H, `PK - NO` is ℓ/v_0, all expressed in channel number units. The quantities `NO`, `PK`, `HW`, `BG` and `SF` are all the parameters that may be varied in the fit. Once `HW` and `NO` have been found from fitting data taken with the detector close to the chopper, they are then held fixed. (The value of `HW` found from the fit should, of course, agree with the calculated value from the chopper and slit dimensions and chopper rotation speed.)

My code was written for a nice fitting/plotting package called *C-Plot*, available from Certified Scientific Software (http://www.certif.com/). You could use it as pseudocode to guide code you write for *Matlab* or some other package.

Necessity:

How necessary is this correction for the finite opening time of the chopper? As you might expect, it depends on how t_H compares to the time for the neutrons to travel to the detector. The graph below shows some calculated fits with $t_H = 25$ channels (close to the 95 μs calculated value for the chopper) and $t_H = 1$ channel, essentially no correction for chopper open time. I used $n_0 = 100$ channels, which is close to correct for the apparatus. The plots are for thermal spectra with $\ell/v_0 = 10$ channels and $\ell/v_0 = 100$ channels; the latter is about what one expects for $t_D = 4\mu$s and thermal neutrons when $\ell = 1$m.

TOF: effect of t_H
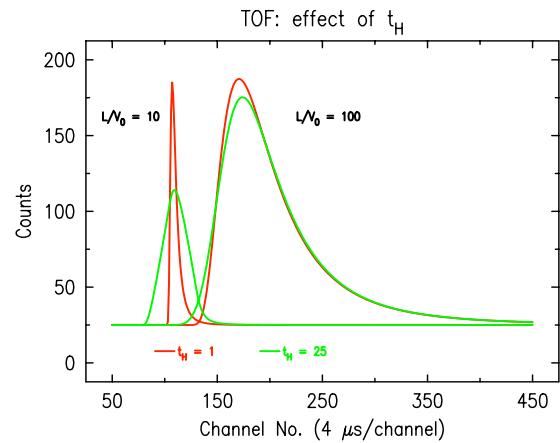
The correction is not important for thermal neutrons at $\ell = 1$ m, but it matters close to the chopper and for the epithermal peak seen in the spectrum at $\ell = 1$ m.

The fast peak above has a speed about 2.5×10^4 ms^{-1}, obtained from the peak position shift of about 45 μs as the detector was moved 1.0 m. As the plot shows, a Maxwell-Boltzmann distribution with this v_0 would rise and fall so rapidly that the fit function is essentially the triangular transmission of the chopper. (The same must be true for whatever is the actual speed distribution of the fast neutrons.) This v_0 would correspond to a thermal distribution for $T \approx 3 \times 10^4$K. The epithermal neutrons are moving so fast and their speed distribution is sufficiently narrow that even after they have travelled 1 m we cannot determine it with a chopper whose time resolution is given by $t_H \simeq 100\mu$s. However it is very unlikely to be thermal.

Fits of the thermal functions to my data are shown on the next page; the fits and plots were made with *C-Plot*.

TOF at Z = 3.25

Total TOF at Z = 42.62
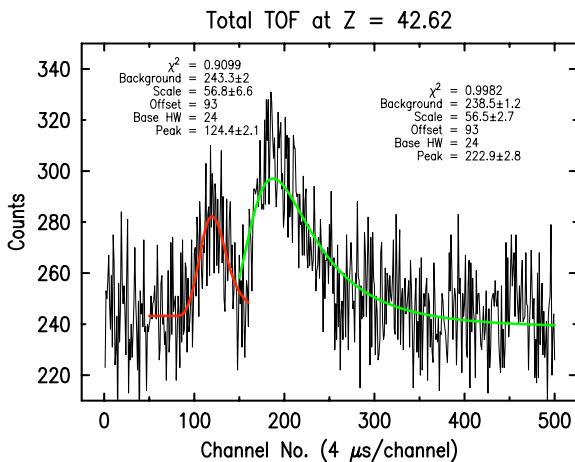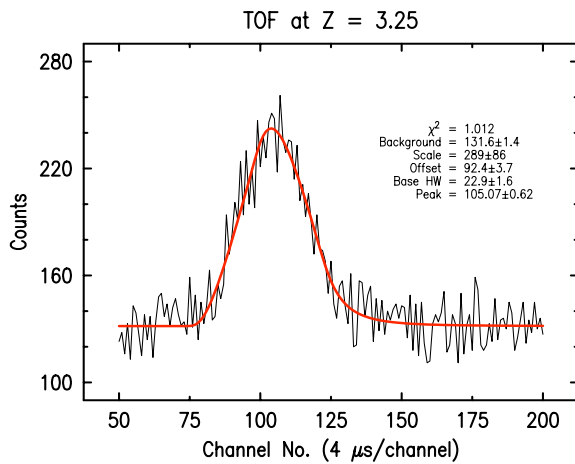
After 1 m, the scan appears to separate into two peaks. Each was fit individually to a thermal spectrum. One seems to have v_0 about 12 times the other.

Finally, the fit obtained to the fast peak portion of the scan was subtracted (with zero background) from the total data. This should, in principle, leave only the background and the neutron counts from the slow (thermal) neutrons. The data that resulted are shown in the plot below along with the fit to all of the data.

Slow Peak TOF at Z = 42.62
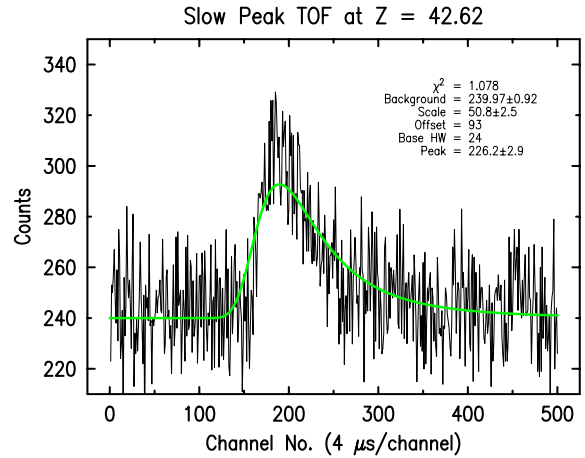
The result agrees with that otained only by fitting data in channels above number 150. The value of v_0 obtained from the fit is about 2000 m/s. The value obtained using the peak shift from $Z = 3.25$ to $Z = 42.62$ ($\Delta \ell = 1.00$ m) would be 2100 m/s. The fast peak shift suggests a speed about 13000 m/s, while the average speed obtained from the fit of the $Z = 3.25$ data to a thermal spectrum (unreliable, in my view) would be $v_0 \simeq 20000 m/s$.

This suggests to me that 93 is too low for the offset channel number and a better value would be somewhere from 95 to 100. If the angle the chopper wheel has to rotate after the light pulse until the first slit is fully open were to be measured, then the offset channel number n_0 could be calculated.

2.   *C-Plot Code*

Below is the *C-Plot* model function code used to perform the analysis described in Section 1.

```
#define RP 0.88622693        /* \sqrt{\pi}/2 */

double   model(deriv_flag)
int          deriv_flag;
{
```

```
double m, p, yfit;
double y1, y2, ym, r;
double ey1, ey2, eym;       /* exponentials */
double py1, py2, pym;       /* error functions */


m = X - NO;
p = PK - NO;
if (p < 1.0) p = 1.0;
if (m <= (-HW)) {
  r = 0;
}
else if (m <= 0) {
   y1 = p/(m+HW);
   py1 = gs1_sf_erf(y1);
   status = gsl_sf_exp_e(y1*y1, &result);
   if (status) {
      ey1 = 0.0;
      if (status != GSL_EUNDRFLW)
      printf("exp(-y1*y1) m=%g %s\n", m, gsl_strerror(status));
   }
   else ey1 = result.val;
   r = (p/HW)*( RP*(1.0 - py1) + y1*ey1
     + (m/HW)*( RP*(1.0 - py1) + y1*ey1 ) - (p/HW)*ey1 );
 }
 else if (m <= HW) {
    y1 = p/(m+HW);
    py1 = gsl_sf_erf(y1);
    status = gsl_sf_exp_e(y1*y1, &result);
    if (status) {
       ey1 = 0.0;
       if (status != GSL_EUNDRFLW)
       printf("exp(-y1*y1) m=%g %s\n", m, gsl_strerror(status));
    }
    ym = p/m;
    pym = gsl_sf_erf(ym);
    status = gsl_sf_exp_e(ym*ym, &result);
    if (status) {
       eym = 0.0;
       if (status != GSL_EUNDRFLW)
       printf("exp(-ym*ym) m=%g %s\n", m, gsl_strerror(status));
    }
    else eym = result.val;
    r = (p/HW)*( RP*(1.0 - py1) + y1*ey1
      + (m/HW)*( RP*(2.0*pym - py1 - 1.0) - 2.0*ym*eym + y1*ey1 )
      + (p/HW)*(2.0*eym - ey1) );
   }
   else { /* m > HW */
      y1 = p/(m+HW);
      py1 = gsl_sf_erf(y1);
      status = gsl_sf_exp_e(y1*y1, &result);
      if (status) {
         ey1 = 0.0;
         if (status != GSL_EUNDRFLW)
         printf("exp(-y1*y1) m=%g %s\n", m, gsl_strerror(status));
      }
      else ey1 = result.val;
      ym = p/m;
      pym = gsl_sf_erf(ym);
```

```
    status = gsl_sf_exp_e(ym*ym, &result);
    if (status) {
        eym = 0.0;
        if (status != GSL_EUNDRFLW)
        printf("exp(-ym*ym) m=%g %s\n", m, gsl_strerror(status));
    }
    else eym = result.val;
    y2 = p/(m-HW);
    py2 = gsl_sf_erf(y2);
    status = gsl_sf_exp_e(y2*y2, &result);
    if (status) {
        ey2 = 0.0;
        if (status != GSL_EUNDRFLW)
        printf("exp(-y2*y2) m=%g %s\n", m, gsl_strerror(status));
    }
    else ey2 = result.val;
    r = (p/HW)*( RP*((py2 - py1) + y1*ey1 - y2*ey2
      + (m/HW)*( RP*(2.0*pym - py1 - py2)) - 2.0*ym*eym + y1*ey1 + y2*ey2 )
      + (p/HW)*(2.0*eym - ey1 - ey2) );
    }
    yfit = BG +SF * r;
    if (deriv_flag) {
        if (fBG) dBG = 1;
        if (fSF) dSF = r;
    }
    return(yfit);
}
```
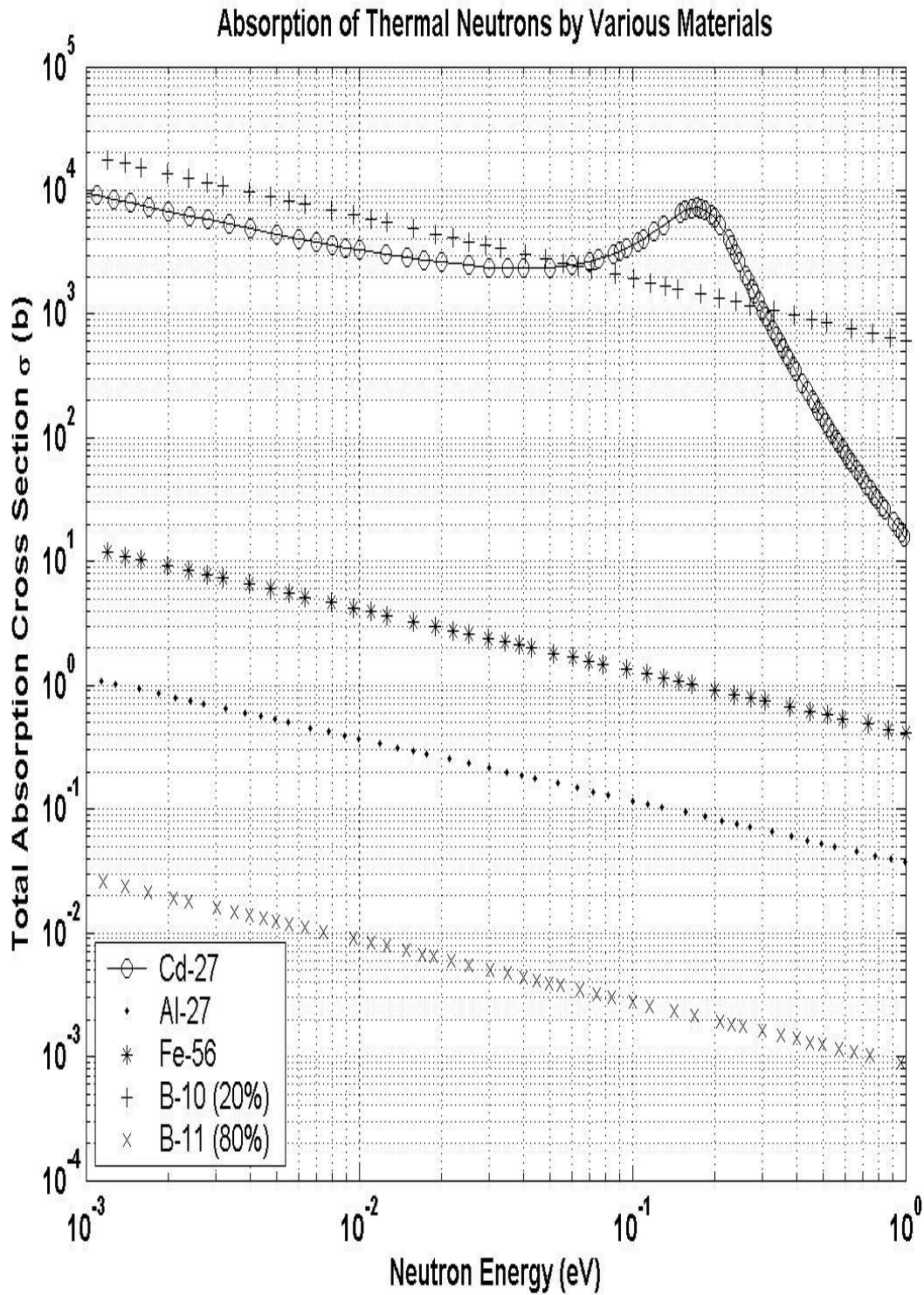
FIG. 15: Total absorption cross-sections for neutrons as a function of energy for B, Cd, Fe, and Al. Data from atom.kaeri.re.kr/ton. The percentages next to the Boron isotopes indicate their relative natural abundances.

Johnson Noise and Shot Noise

MIT Department of Physics
(Dated: September 5, 2011)

In electronic measurements, one observes "signals," which must be distinctly above the "noise." Noise induced from outside sources may be reduced by shielding and proper "grounding." Less noise means greater sensitivity with signal/noise as the figure of merit. However, there exist fundamental sources of noise which no clever circuit can avoid. The intrinsic noise is a result of the thermal jitter of the charge carriers and the quantization of charge. The purpose of this experiment is to measure these two limiting electrical noises. From the measurements, values of the Boltzmann constant, k, and the charge of the electron, e, will be derived.

1. PREPARATORY QUESTIONS

1. Define the following terms: Johnson noise, shot noise, RMS voltage, thermal equilibrium, temperature, Kelvin and centigrade temperature scales, entropy, dB.

2. What is the physical basis of the Nyquist theory [?] of Johnson noise? Give an estimate for the RMS voltage acros a 50kΩ resistor at 100°C with a frequency range of 100 to 10,000Hz.

3. What is the mean square of the fluctuating component of the current in a photodiode when its average current is I_{av} ?

4. Your measurement of the noise at a frequency $f \pm \delta f$ is inaccurate at the following level: $N = N_f \pm 2N_f$. How many additional measurements are needed to get a result accurate to 5%.

The goals of the present experiment are:

1. To measure the properties of Johnson noise in a variety of conductors and over a substantial range of temperature and to compare the results with the Nyquist theory.

2. To establish the relation between the Kelvin and centigrade temperature scales.

3. To determine from the data, values for the Boltzmann constant, k, and the centigrade temperature of absolute zero.

2. INTRODUCTION

2.1. Microscopic Quantization

"Thermal physics connects the world of everyday objects, of astronomical objects, and of chemical and biological processes with the world of molecular, atomic, and electronic systems. It unites the two parts of our world, the microscopic and the macroscopic."[?]

By the end of the 19th century, the accumulated evidence from chemistry, crystallography, and the kinetic theory of gases left little doubt about the validity of the atomic theory of matter, though a few reputable scientists still argued strongly against it on the grounds that there was no "direct" evidence of the reality of atoms. In fact there was no precise measurement yet available of the quantitative relation between atoms and the objects of direct scientific experience such as weights, meter sticks, clocks, and ammeters.

To illustrate the dilemma faced by physicists in 1900, consider the highly successful kinetic theory of gases based on the atomic hypothesis and the principles of statistical mechanics from which one can derive the equipartition theorem. The theory showed that the well-measured gas constant R_g in the equation of state of a mole of a gas at low density,

$$PV = R_g T \qquad (2.1)$$

is related to the number of degrees of freedom of the system, $3N$, by the equation

$$R_g = \frac{k(3N)}{3} = kN \qquad (2.2)$$

where N is the number of molecules in one mole (Avogadro's number), and k is the Boltzmann constant defined so that the mean energy per translational degree of freedom of the molecules in a quantity of gas in thermal equilibrium at absolute temperature T is $kT/2$. At the turn of the century, nobody knew how to measure precisely either k or N. What was required was either some delicate scheme in which the fundamental granularity of atomic phenomena could be detected and precisely measured above the smoothness that results from the huge number of atoms in even the tiniest directly observable object, or a thermodynamic system with a measurable analog of gas pressure and a countable number of degrees of freedom.

The Millikan oil drop experiment of 1910 was a delicate scheme by which the quantum of charge was accurately measured. It compared the electrical and gravitational forces on individual charged oil droplets so tiny that the effect of a change in charge by one or a few elementary charges could be directly seen and measured through a

microscope. The result was a precise determination of e which could be combined with the accurately known values of various combinations of the atomic quantities such as the Faraday (N_e), e/m, atomic weights, and the gas constant (kN), to obtain precise values of N, k, and other atomic quantities. Therefore, a current will not be continuous in the mathematical sense, it should exhibit a "noise" due to the granularity of charges.

Twenty years later Johnson discovered an analog of gas pressure in an electrical system, namely, the mean square "noise" voltage across a conductor due to thermal agitation of the electrical modes of oscillation which are coupled to the thermal environment by the charge carriers. Nyquist showed how to relate that mean square voltage to the countable number of degrees of freedom of electrical oscillations in a transmission line. The only atomic constant that occurs in Nyquist's theoretical expression for the Johnson noise voltage is the Boltzmann constant k. A measurement of Johnson noise therefore yields directly an experimental determination of k.

In classical statistical mechanics, $k/2$ is the constant of proportionality between the Kelvin temperature of a system in thermal equilibrium and the average energy per dynamical degree of freedom of the system. Its ultimate quantum physical significance emerged only with the development of quantum statistics after 1920 [?]. A summary of the modern view is given below (see reference [?], Kittel and Kroemer, for a lucid and complete exposition).

2.2.   Entropy and Temperature

A closed system of many particles exists in a number of distinct quantum states consistent with conservation constraints of the total energy of the system and the total number of particles. For a system with g accessible states, the fundamental entropy σ is defined by

$$\sigma = \ln g \qquad (2.3)$$

With the addition of heat, the number of states accessible within the limits of energy conservation rises, and the entropy increases. An exact enumeration of the quantum states accessible to a system composed of many non-interacting particles in a box and having some definite energy can be derived from an analysis based on the solutions of the Schrödinger equation (Ref. [?], p 77). It shows that for one mole of a gas at standard temperature and pressure (273K, 760 mm Hg) σ is of the order of 10^{25}. The corresponding value of g is of the order of the huge number $e^{10^{25}}$!

Suppose that the total energy U of the system is increased slightly by ΔU, perhaps by the addition of heat, while the volume V and number of particles N are held constant. With the increase in energy more quantum states become accessible to the system so the entropy is increased by $\Delta \sigma$. The fundamental temperature is defined by

$$\frac{1}{\tau} \equiv \left(\frac{\partial \sigma}{\partial U} \right)_{N,V} \qquad (2.4)$$

The units of τ are evidently the same as those of energy. Since an increase in the energy of one mole of gas by one joule causes a very large increment in σ, the magnitude of τ in common circumstances like room temperature must be much less than 1. In practical thermometry, the Kelvin temperature T is proportional to τ, but its scale is set by defining the Kelvin temperature of the triple point of water to be exactly 273.16 K. This puts the ice point of water at 273.15 K and the boiling point 100 K higher at 373.15 K. The constant of proportionality between fundamental and Kelvin temperatures is the Boltzmann constant, i.e.

$$\tau = kT \qquad (2.5)$$

where $k = 1.38066 \times 10^{-23} JK^{-1}$. By a quantum statistical analysis, based on the Schrödinger equation, of N particles in a box in thermal equilibrium at temperature T, one can then show that the mean energy per translational degree of freedom of a free particle is $\tau/2$ so the total energy of the particles is $\frac{3}{2}N\tau = \frac{3}{2}NkT$ (see [?], p. 72).

Given the quantum statistical definition of τ, the definition of T in terms of τ and the triple point of water, one could, in principle, compute k in terms of the atomic constants such as e, m_e, and h if one could solve the Schrödinger equation for water at its triple point in all its terrible complexity. But that is a hopeless task, so one must turn to empirical determinations of the proportionality constant based on experiments that link the macroscopic and microscopic aspects of the world.

A link between the microscopic and macroscopic was reported by Johnson in 1928 [?] in a paper paired in the Physical Review with one by H. Nyquist [?] that provided a rigorous theoretical explanation based on the principles of classical thermal physics. Johnson had demonstrated experimentally that **the mean square of the voltage across a conductor is proportional to the resistance and absolute temperature of the conductor and does not depend on any other chemical or physical property of the conductor.** At first thought, one might expect that the magnitude of Johnson noise must depend in some way on the number and nature of the charge carriers. In fact Nyquist's theory involves neither e nor N. It yields a result in agreement with Johnson noise observations and a formula for the mean square of the noise voltage which relates the value of the Boltzmann constant to quantities that can be readily measured by electronic methods and thermometry.

3. NYQUIST's THEORY OF JOHNSON NOISE

Two fundamental principles of thermal physics are used:

1. The second law of thermodynamics, which implies that between two bodies in thermal equilibrium at the same temperature, in contact with one another but isolated from outside influences, there can be no net flow of heat;

2. The equipartition theorem of statistical mechanics [?], which can be stated as follows:

   > Whenever the Hamiltonian of a system is homogeneous of degree 2 in a canonical momentum component, the thermal average kinetic energy associated with that momentum is $kT/2$, where T is the Kelvin temperature and k is Boltzmann's constant. Further, if the Hamiltonian is homogeneous of degree 2 in a position coordinate component, the thermal average potential energy associated with that coordinate will also be $kT/2$.

   If the system includes the electromagnetic field, then the Hamiltonian includes the term $(E^2 + B^2)/8\pi$ in which E and B are canonical variables corresponding to the q and p of a harmonic oscillator for which (with p and q in appropriate units) the Hamiltonian, is $(q^2 + p^2)/2$.

Nyquist's original presentation of his theory [?] is magnificent; please see the Junior Lab e-library for a copy.

Nyquist invoked the second law of thermodynamics to replace the apparently intractable problem of adding up the average thermal energies in the modes of the electromagnetic field around a conductor of arbitrary shape and composition with an equivalent problem of adding up the average thermal energies of the readily enumerated modes of electrical oscillation of a transmission line shorted at both ends. Each mode is a degree of freedom of the dynamical system consisting of the electromagnetic field constrained by the boundary conditions imposed by the transmission line. According to the equipartition theorem, the average energy of each mode is kT, half electric and half magnetic. The Nyquist formula for the differential contribution dV_j^2 (j for Johnson) to the mean square voltage across a resistor, R, in the frequency interval df due to the fluctuating emfs corresponding to the energies of the modes in that interval is

$$dV_j^2 = 4RkTdf \qquad (3.1)$$

To measure this quantity, or rather its integral over the frequency range of the pass band in the experiment, one must connect the resistor to the measurement device by means of cables that have a certain capacitance C. This
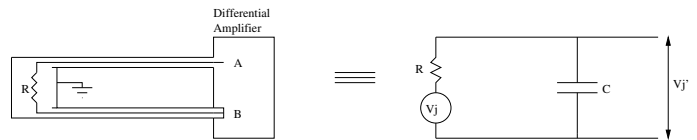
FIG. 1: Equivalent circuit of the thermal emf across a conductor of resistance R connected to a measuring device with cables having a capacitance C

shunts (short circuits) a portion of the signal, thereby reducing its RMS voltage. The equivalent circuit is shown in Figure 1. The differential contribution dV^2 to the signal presented to the input of the measuring device (in our case the A–input of a low-noise differential preamplifier) is a fluctuating voltage with a mean square value

$$dV^2 = 4R_f kTdf \qquad (3.2)$$

where

$$R_f = \frac{R}{1 + (2\pi fCR)^2} \qquad (3.3)$$

This equation results from AC circuit theory; see B8 in Appendix B.

Attention was drawn earlier to an analogy between the mean square of the Johnson noise voltage across a conductor and the pressure of a gas on the walls of a container. Both are proportional to kT and the number of degrees of freedom of the system. The big difference between the two situations is that the number of translational degrees of freedom per mole of gas is the "unknown" quantity $3N$, while the number of oscillation modes within a specified frequency interval in the transmission line invoked by Nyquist in his theory is readily calculated from the laws of classical electromagnetism.

Since the Boltzmann constant is related to the number of accessible quantum states, one might well ask:

> Where is Planck's constant, h, which fixes the actual number of accessible states?

The answer is that the Nyquist theorem in its original form, like the classical Rayleigh-Jeans formula for the spectral distribution of blackbody radiation, is valid only in the range of frequencies where $hf << kT$, in other words, at frequencies sufficiently low that the minimum excitation energy of the oscillations is small compared to kT. At 300K and 100 kHz, $kT = 4 \times 10^{-14}$ ergs (0.04 eV) and $hf = 6 \times 10^{-22}$ ergs. Thus at room temperature kT is $\sim 10^8$ times the minimum energy of an oscillation mode with a frequency near 100 kHz. The exact quantum expression for the mean energy ϵ of each oscillation mode, noted by Nyquist in his paper, is

$$\epsilon = \frac{hf}{e^{hf/kT} - 1} \qquad (3.4)$$

which reduces to $\epsilon = kT$ for $hf << kT$ over the range of frequencies and temperatures encountered in this experiment. An example of where this simplification does not

hold true is in the measurement of the cosmic microwave background. In these measurements, a radio telescope is operated at liquid helium temperatures for measurement of the $\sim 2.7K$ cosmic background radiation. The peak of this black body spectrum is around 10^{11} Hz and therefore hf is not much less than kT.

4.   EXPERIMENT

In the present experiment you will actually measure an amplified version of a portion of the Johnson noise power spectrum. The portion is defined by the "pass band" of the measurement chain which is determined by a combination of the gain characteristics of the amplifier and the frequency transmission characteristics of the low-pass/high-pass filters that are included in the measurement chain. The filters provide an adjustable and sharp control of the pass band. The combined effects of amplification and filtration on any given input signal can be described by a function of frequency called the effective gain and defined by

$$g(f) = \frac{V_0(f)}{V_i(f)} \qquad (4.1)$$

where the right side is the ratio of the RMS voltage V_0 out of the band-pass filter to the RMS voltage V_i of a pure sinusoidal signal of frequency f fed into the amplifier. **A critical task in the present experiment is to measure the effective gain as a function of frequency of the apparatus used to measure Johnson noise.**

When the input of the measurement chain is connected across the resistor, R, under study, the contribution dV^2 to the total mean square voltage out of the band-pass filter in a differential frequency interval is

$$dV_{meas}^2 = [g(f)]^2 \; dV^2 \qquad (4.2)$$

We obtain an expression for the measured total mean square voltage by integrating Equation 4.2 over the range of frequencies of the pass band. Thus

$$V^2 = 4RkTG \qquad (4.3)$$

where the quantity G is the gain integrated over the band-pass region and is given by

$$G \equiv \int_0^\infty \frac{[g(f)]^2}{1 + (2\pi fCR)^2} df \qquad (4.4)$$

The rationale behind this integration is that over any given time interval t, the meandering function of time that is the instantaneous noise voltage across the resistor can be represented as a Fourier series consisting of a sum of sinusoids with discrete frequencies $n/2t$, n=1, 2, 3 ...., each with a mean square amplitude equal to the value specified by the equipartition theorem. When the Fourier series is squared, the cross terms are products of sinusoids with different frequencies, and their average values are zero. Thus the expectation value of the squared voltage is the sum of the expectation values of the squared amplitudes, and in the limit of closely spaced frequencies as $t \to \infty$, the sum can be replaced by an integral.

Given the linear dependence of V^2 on T in Eq. 4.3, it is evident that one can use the Johnson noise in a resistor as a thermometer to measure absolute temperatures. A temperature scale must be calibrated against two phenomena that occur at definite and convenient temperatures such as the boiling and melting points of water, which fix the centigrade scale at $100°$ C and $0°$C, respectively. In the present experiment you will take the centigrade calibrations of the laboratory thermometers for granted, and determine the centigrade temperature of absolute zero as the zero-noise intercept on the negative temperature axis.

5.   PROCEDURE OVERVIEW

The experiment consists of the following parts:

1. Calibration of the measurement chain and measurement of $g(f)$;

2. Measurement of $V^2 = V_R^2 - V_S^2$, where $V_R =$ RMS voltage at the output of the band-pass filter with the resistor in place; and $V_S =$ RMS voltage with the resistor shorted); for various resistors and temperatures;

3. Determination of the Boltzmann constant from the data;

4. Determination of the centigrade temperature of absolute zero.

5.1.   Suggested Progress Check for end of 2nd Session

Plot the gain curve of your signal chain versus frequency and perform a back of the envelope integration to obtain a value of G. You should also have a few measurements at at least one resistor value: What is your value for k?

6.   Experimental Apparatus

Figure 3 depicts how you will calibrate your experimental apparatus. Figure 2 is a schematic diagram of the apparatus showing the **resistor** R mounted on the terminals of the aluminum box, shielded from electrical interference by an inverted metal beaker, and connected through switch SW2 to the measurement chain or the ohmmeter. Switch SW1 shorts R. The measurement chain consists of a low-noise differential amplifier, a

band-pass filter, and a digitizing oscilloscope. Sinusoidal calibration signals are provided by a function generator.

The noise you will measure is very small, typically on the order of microvolts. To minimize the problem of electrical interference in the measurement of the low-level noise signals it is essential that all cables be as short as possible. The two cables that connect the resistor to the 'A' and 'B' input connectors of the differential amplifier should be tightly twisted, as shown, to reduce the flux linkage of stray AC magnetic fields.

The cathode ray tube display in the digital oscilloscope emits a variable magnetic field from its beam-control coil which may have a devastating effect on your measurements unless you keep it far away ($\geq$ 5 feet) from the noise source. Take special care to avoid this problem when you arrange the components of the measurement chain on the bench.
The filter we use is a Krohn-Hite 3BS8TB-1k/50kg band-pass filter. This filter has fixed-frequency band-pass range of 1 kHz to 50 kHz. It has 8 poles, the equivelent of 8 simple filters in series, so the dropoff outside of the cut-off frequencies should be quite sharp. Connect the output of the amplifier to the positive input of the Krohn-Hite Filter. Then connect the output of the filter to the oscilloscope. The filter is equipped with an AC power adapter connector; make sure this is plugged in and that the green LED is lit indicating that the filter is receiving power.

7. DETAILED JOHNSON NOISE PROCEDURE

7.1. Calibrate the measurement chain

The digital oscilloscope can measure the RMS voltage of both periodic and random signals over a dynamic range of somewhat more than 10^3, from several millivolts to several volts, whereas the Johnson Noise signal is only microvolts. Thus, with the differential amplifier set to a nominal gain of 1000, the microvolt noise signals are amplified sufficiently to be measured in the millivolt range of the oscilloscope. To determine the overall amplification of the amplifier/filter combination, one feeds a sinusoidal test signal with an RMS voltage V_i in the millivolt range to the 'A' AC-Coupled (through $0.1\mu F$, shunted to ground with $100M\Omega$ and 25pF in parallel) of the SRS preamplifier (with the source set to 'A'), and measure the RMS voltage V_0 of the filter output using the digitizing oscilloscope. The gain of the system at the frequency of the test signal is $g(f) = V_0/V_i$.

IMPORTANT: Turn on transients exist - set the input coupling switches of the SRS preamplifier to GND before turning on the device and before making any connections to another device. Do not transfer from the GND settings until after all connections are completed.

At the voltage preamplifier, the maximum input signal in differential mode is 1V DC and $3V_{PP} \approx 1V_{RMS}$ AC. Do not exceed these values! Excessive common-mode

inputs can "turn on" low conduction paths at the input of the preamplifier to protect the input circuits, and thereby lower the input impedance.

The "roll-off" frequencies selectable from the front panel indicate 3dB points in a 6 dB/octave roll off curve. The output impedence of the preamplifier is 600Ω and can produce a maximum of 10V pk-pk ahead of 600Ω. Be careful about your terminations!
The SRS preamplifier has rechargable batteries which 'trickle charge' when the unit is plugged into the wall (and very much slower when the unit is in the ON position than when it is in the OFF position. You can use this feature if you want; it may reduce extraneous noise a bit. To operate from battery power, set the power switch to ON, but do not plug in the line cord. Be sure to plug in the line cord after your session is over to ensure that the next group has a fully charged set of batteries!

Measure the variation of the test signal RMS voltage and the gain of the measurement chain as a function of frequency and produce a rough plot in your lab notebook

Configure the function generator to output a sine wave with an RMS amplitude of 20mV. Use the Kay 837 attenuator with 26 dB (1/20) of attenuation to produce a sinusoid in the millivolt range. Use a BNC tee to simultaneously send this signal into the digitizing oscilloscope and into the 'A' (AC-Coupled) input of the amplifier with the source set to 'A'.

The output of the amplifier should then be fed into the band-pass filter. Before taking detailed measurements of $g(f)$, you'll want to make sure that filter is behaving in the way you expect it should. Spend a few moments varying the frequency of the function generator to observe the behavior below 1kHz, above 50 kHz and in between.

Without touching the amplitude control of the function generator, measure and record RMS voltages for both V_i (out of the attenuator) and V_0 (out of the band-pass filter) over the range that will pass the filter ($\sim$0.5kHz to $\sim$80kHz).

Plot $[g(f)]^2$ against f as you go along to check the consistency and adequacy of your data.

1. *Set the oscilloscope to display both the V_i and V_0 sinusoids. Use the oscilloscope Voltage measurement options to measure the RMS voltage of each channel. The RMS of V_i should remain essentially constant throughout the measurement of $g(f)$. However, you will want to keep an eye on it during the process of this measurement to ensure that this is the case.*

2. *Turn on the bandwidth limit on for the channel which is measuring V_i.*

3. *Make sure the inputs are set to AC coupling to eliminate any DC offset in the signals you are measuring.*
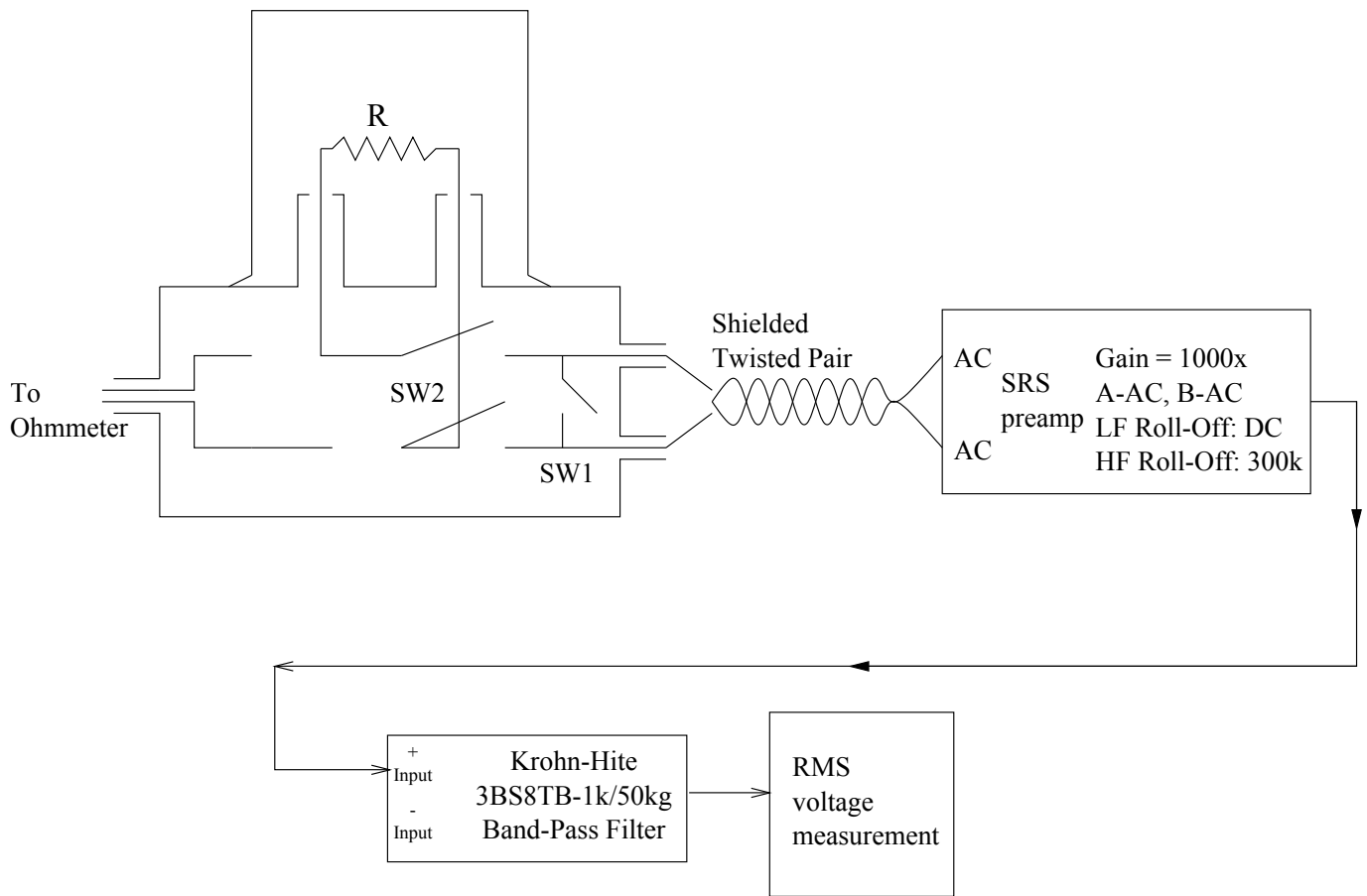
FIG. 2: Block diagram of the electronic apparatus for measuring Johnson noise.
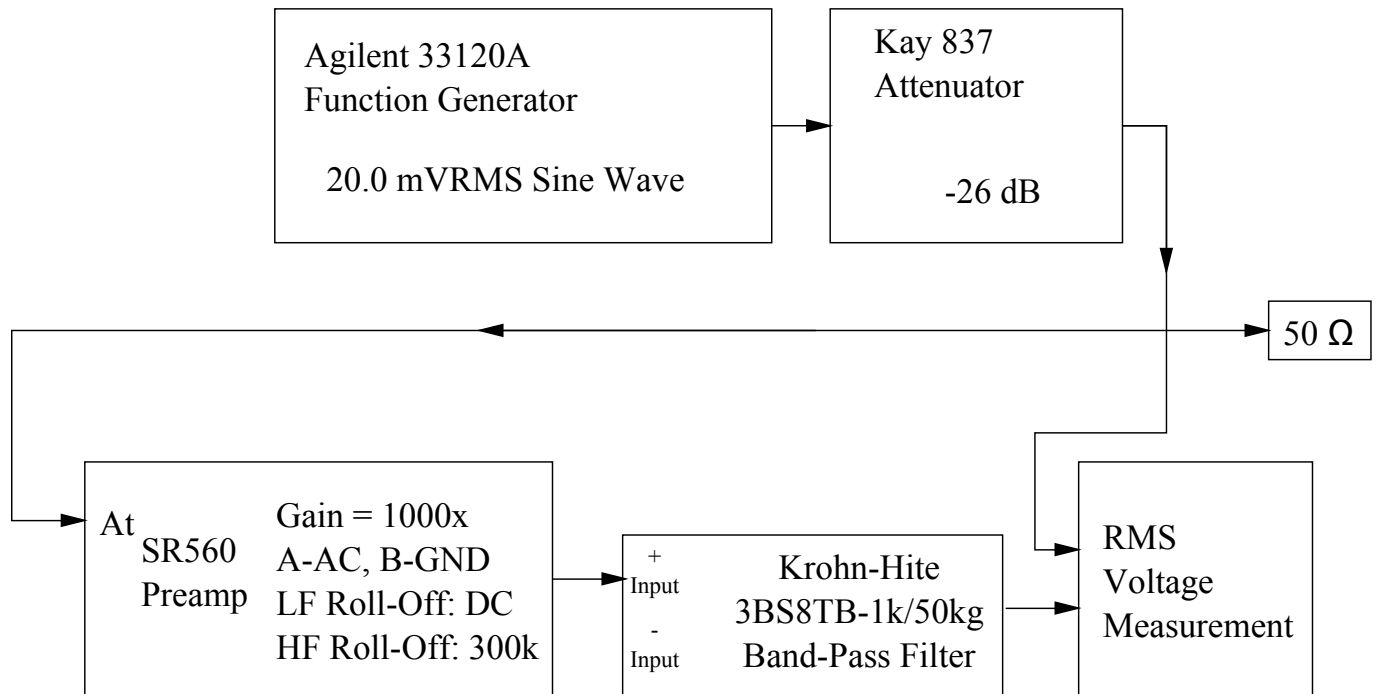
FIG. 3: Block diagram of the electronic apparatus for calibrating the Johnson Noise experiment

4. *Press 'DISPLAY', and select 'AVG 256' (Note: Later, when you take noise measurements, you must select 'normal' instead of averaging since the RMS voltage of the average of n random wave forms approaches zero as $n \to \infty$. On the other hand, the RMS voltage of the average of many wave forms consisting of a constant sinusoid plus random noise approaches the RMS voltage of the pure sinusoid.)*

5. *Adjust the digital scope amplitude and sweep-speed controls so that several ($\sim$5-10) cycles of the sinusoid appear on the screen.*

To reduce errors of measurement and obtain an error assessment, you can make repeated measurements. Record the V_{rms} and frequency displayed at the bottom of the screen; repeat n times (e.g., n=5) at each setting. For each setting, compute the mean V_{rms}, and the standard error of the mean ($= \frac{\sigma}{\sqrt{n-1}}$).

Because the oscilloscope is in averaging mode, you will want to wait several moments for transient signals to average out before taking a reading after changing the frequency or adjusting anything on the scope. Wait until you see that V_i and V_0 have leveled off in their fluctuations before pressing 'stop' to take data.

NOTE: It is very important that you keep your measurement chain in the same configuration for making both gain curve and Johnson Noise measurements. Be careful not to change any settings on the amplifier in between these two measurements (one helpful tip for making sure the gain of the amplifier is consistent between measurements taken on different days is to turn the red 'CAL' knob all the way counter-clockwise until it clicks).

7.2. Measure V^2 for a variety of resistors

When you use the apparatus to measure the Johnson Noise across a resistor, about half the RMS voltage is noise generated in the amplifier itself. Interference pickup may vary. Since all the contributions to the measured RMS voltage are **statistically uncorrelated, they add in quadrature**. To achieve accurate results it is essential to make repeated measurements with each resistor with the shorting switch across the conductor alternately opened and closed. The measure of the mean square Johnson noise is

$$V^2 = V_R^2 - V_S^2 \qquad (7.1)$$

where V_R and V_S are the RMS voltages measured with the shorting switch open and closed, respectively.

Measure the Johnson noise at room temperature in $\sim$10 metal film and/or wire-wound resistors with values from 10^4 to 10^6 ohms. Mount the resistors in the alligator clips projecting from the aluminum test box equipped with a single-pole-single-throw (SPST) shorting switch, a double-pole-double-throw (DPDT) routing switch, and

connections for a thermistor for use in the later temperature measurement. Cover the resistor and its mounts with a metal beaker to shield the input of the system from electrical interference. After each noise measurement measure the resistance of the resistor: plug a digital multimeter into the pin jacks on the aluminum box and flip the DPDT switch on the sample holder to the resistance measuring position. Before each noise measurement, be sure to disconnect the multimeter (to avoid introducing extraneous electrical noise) and flip the DPDT switch back to the noise-measurement position.

Be thoughtful about how you are using the digitizing oscilloscope to measure the RMS voltages for V_R and V_S. Again, you should use AC coupling to eliminate any DC offset. Also, you will need to be intentional about both the time and voltage scales that you choose. The range of voltages the scope is able to digitize is the range shown on the screen so you will want to fill the screen without cutting the max/min off. Be sure not to choose too small a vertical range and in the process cut off your signal!

Keep in mind, that you will want to use only one setting of the voltage scale for all your measurements of V_R and V_S for all resistors that you sample. To make sure you have an appropriate setting, you might want to look at V_R for your highest value of resistance first. As for the time axis, a setting in the range of $500\mu s$ to $5ms$ per division should work well.

A good way to determine the appropriate scale for a given resistor is to set the scope to measure V_{max}, take several readings of this value and make sure it is well contained ($\leq$75%) in the total range currently displayed. You can also do this visually by looking for the smallest scale that appears to contain all the noise fluctuations within the first three out of the four divisions above or below the baseline.

Values of V_S should remain essentially constant over all values of resistance. However, subtle changes in your experimental configuration or procedure could cause V_S to fluctuate. For instance, even the orientation of one of your cables or whether or not you are touching the cable can yield different results in your measurements. Strive to keep things as consistent as possible throughout a particular series of measurements. Additionally, it is a good idea to keep an eye on V_S and record its value each time you measure V_R.

As during your calibration measurements, you will want to repeat each measurement at least five times to reduce random errors and obtain an error assessment for your measurements.

According to equation 4.3, the value of Boltzmann's Constant, k, can be expressed in terms of measured quantities and G, which is a function of R and C:

$$k = \frac{V^2}{4RTG} \qquad (7.2)$$

So in order to calculate k from your measurements of the Johnson Noise, you will also need to measure the capacitance, C, seen by the resistor. The SRS preamplifier

has an input capacitance of 25pF. With this knowledge in hand, you will still need to determine the capacitance contributed by the switching box and the cables connecting it to the amplifier. Alternatively, you could simply measure the capacitance of all these components and the amplifier simultaneously.

A BK Precision 875A LCR Meter is provided for this purpose. First use it to measure some known capacitance by inserting a plain capacitor directly. Once you have convinced yourself that the meter is functioning properly and that you know how to read it, devise a way to measure **the same capacitance that the resistor sees.** Remember, capacitance is determined by the geometry of the conductors and dielectrics in the circuit so it is very important to have things in the exact same configuration for this measurement as you did for measurements of the Johnson Noise. Also be aware that any cables you use to connect the LCR meter to measurement chain will contribute their own capacitance.

Be sure to make an assessment of the uncertainty in your measurement of C. Calculate values of k for several values of C based on this uncertainty. You will have uncertainty associated with the the the quantities V^2, R, and C. You will need to propagate these errors in order to determine your uncertainty in k.

The factor G must be recalculated by numerical integration for each new trial value of R and C. In principle, if you use the correct value of C in your calculations of G, then the values of k obtained from Equation 7.2 should cluster around a mean value close to the value for $R \to 0$ and should not vary systematically with R. Using the best values of k and C derived in this way, you can plot experimental and theoretical curves of V^2/R against R for comparison.

Question: What happens as $R \to \infty$?

7.3. Measure Johnson noise as a function of temperature

Measure the Johnson noise in a resistor over a range of temperatures from that of liquid nitrogen (77 K) to $\sim 150°$C. Clip a resistor to the alligator clips and invert the assembly into a dewar filled with liquid nitrogen. Ask a technical instructor for help in dispensing the nitrogen and make sure to wear eye protection and gloves.

To make a high temperature measurement, invert the assembly into the cylindrical oven, heated by a variac supply set to $\sim$40 VAC. Note, it will take some time for the temperature to equilabrate and stabilize within the oven. You can take advantage of this slow process to measure the resistance, the RMS voltages of the Johnson noise and the background as the temperature rises. Try to disturb the setup as little as possible to prevent the loss of heated air and a subsequent change in the resistors temperature. Use the delicate glass immersion thermometer (range = 0-250°C) to monitor the temperature of the air bath. **Do not allow the temperature of the oven to exceed 150°C as this can damage the wire insulation within the probe.**

According to the Nyquist theory the points representing the measured values of $V^2/4RG$ plotted against T (°C degrees) should fall on a straight line with a slope equal to the Boltzmann constant, and an intercept on the temperature axis at the centigrade temperature of absolute zero. Note that if the resistance of the conductor varies significantly with temperature, then G must be evaluated separately at each temperature, i.e. the integral of Equation 4.4 must be evaluated for each significantly different value of the resistance.

1. Make a plot of $V^2/4RG$ against T (in °C degrees).

2. Derive a value and error estimate of k from the slope of the temperature curve.

3. Derive a value and error estimate of the centigrade temperature of absolute zero.

8. SHOT NOISE

A current source in which the passage of each charge carrier is a statistically independent event (rather than a steady flow of many charge carriers) necessarily delivers a "noisy" current, i.e., a current that fluctuates about an average value. Fluctuations of this kind are called "shot noise". The magnitude of such fluctuations depends on the magnitude of the charges on the individual carriers. Thus a measurement of the fluctuations should, in principle, yield a measure of the magnitude of the charges.

Consider a circuit consisting of a battery, a capacitor in the form of a photo-diode, a resistor, and an inductor, connected in series as illustrated in Figure 4a. Illumination of the photo-diode with an incoherent light source causes electrons to be ejected from the negative electrode in a random sequence of events. Each ejected photo-electron, carrying a charge of magnitude e, is accelerated to the positive electrode and, during its passage between the electrodes it induces an increasing current in the circuit, as shown in Figure 4b.

When the electron hits the positive plate the current continues briefly due to the inductance of the circuit and a damped oscillation ensues. The shape of the current pulse depends on the initial position, speed and direction of the photo-electron as well as the electrical characteristics of the circuit. The integral under the curve is evidently the charge e. If the illumination is strong enough so that many events occur during the duration of any single electron pulse, then the current will appear as in Figure 5, in which the instantaneous current $I(t)$ fluctuates about the long-term average current I_{av}.

In this part of the experiment you will measure, as a function of I_{av}, the mean square voltage of the output of an amplifier and a band-pass filter system whose input is the continuously fluctuating voltage across R_F.
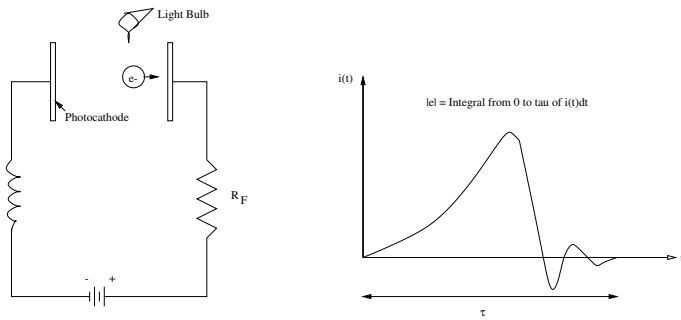
FIG. 4: (a) Schematic diagram of a circuit in which the current consists of a random sequence of pulses generated by the passage of photoelectrons between the electrodes of a photo-diode. (b) Schematic representation of the current pulse due to the passage of one photo-electron.
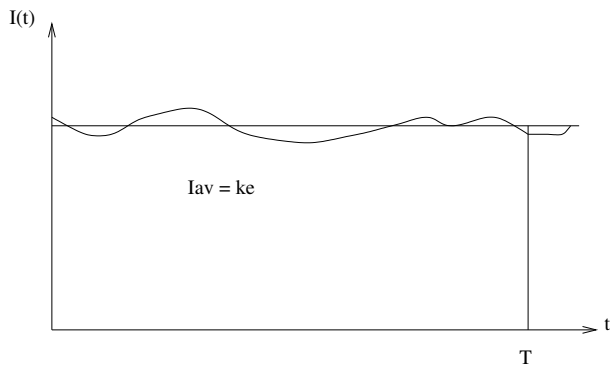
FIG. 5: Plot of a fluctuating current against time with a straight line indicating the long-term average current.

According to the theory of shot noise, a plot of this quantity against the average current should be a straight line with a slope proportional to e. The problem is to figure out what the proportionality factor is.

8.1. THEORY OF SHOT NOISE

The integral under the curve of current versus time for any given pulse due to one photo-electron event is e, the charge of the electron. If the illumination is constant and the rate of photoelectric events is very large, then the resulting current will be a superposition of many such waveforms $i_k(t)$ initiated at random times T_k with a "long term" average rate we will call K, resulting in a fluctuating current with an average value $I_{av} = Ke$, as illustrated in Figure 5. The fluctuating component of such a current was called "shot noise" by Schottky in 1919, who likened it to the acoustic noise generated by a hail of shot striking a target.

The fluctuating current is

$$I(t) = \Sigma_k i_k(t) \qquad (8.1)$$

and its mean square during the time interval T is

$$\langle I^2 \rangle = \frac{1}{T} \int_0^T [\Sigma_k i_k(t)]^2 dt \qquad (8.2)$$

The problem is to derive the relation between the measurable properties of the fluctuating current and e. Although the derivation is somewhat complicated (see Appendix C), the result is remarkably simple: within the frequency range $0 < f \ll \frac{I_{av}}{e}$, the differential contribution to the mean square of the total fluctuating current from fluctuations in the frequency interval from f to $f + df$ is (see Appendix B)

$$d\langle I^2 \rangle = 2eI_{av}df \qquad (8.3)$$

Suppose the fluctuating current flows in a resistor of resistance R_F connected across the input of an amplifier-filter combination which has a frequency-dependent gain $g(f)$. During the time interval T, the voltage developed across the resistor, IR_F, can be represented as a sum of Fourier components with frequencies $m/2T$, where $m = 1, 2, 3, ...$, plus the zero frequency (DC) component of amplitude $I_{av}R_F$. Each component emerges from the amplifier-filter with an amplitude determined by the gain of the system for that frequency. The mean square of the sum of Fourier components is the sum of the mean squares of the components (because the means of the cross terms are all zero). Thus, in the practical limit of a Fourier sum over closely spaced frequencies, we can express the mean square voltage of the fluctuating output signal from the amplifier-filter as the integral

$$V_0^2 = 2eI_{av}R_F^2 \int_0 [g(f)]^2 df + V_A^2 \qquad (8.4)$$

where V_A^2 has been added to represent the constant contributions of the amplifier noise, and Johnson Noise in R_F, to the total mean square voltage, and where the DC term is omitted because the DC gain of the amplifier-filter is zero.

To get a feel for the plausibility of the shot noise formula one can imagine that the current in the photo-diode circuit is a step function representing the amount of charge ne released in each successive equal time interval of duration τ divided by τ, i.e., the mean current in each interval $\frac{ne}{\tau}$. The expectation value of n is $\langle n \rangle = K\tau$. We assume there is no statistical correlation between the numbers of events in different intervals. According to Poisson statistics the variance of n (mean square deviation from the mean) is the mean, i.e.,

$$\langle (n - \langle n \rangle)^2 \rangle = \langle n^2 \rangle - \langle n \rangle^2 = \langle n \rangle = K\tau \qquad (8.5)$$

It follows that the mean square value of the current over

time would be

$$
\begin{aligned}
\langle I^2 \rangle &= \langle \left(\frac{ne}{\tau} \right)^2 \rangle \\
&= \left(\frac{e}{\tau} \right)^2 \langle n^2 \rangle \\
&= \left(\frac{e}{\tau} \right)^2 \left[\langle n \rangle + \langle n \rangle^2 \right] \\
&= \frac{e I_{av}}{\tau} + I_{ave}^2 \quad\quad (8.6)
\end{aligned}
$$

which shows that the fluctuating term is proportional to $e I_{av}$ as in the exact expression for the differential contribution, Equation 8.3.

Actually the current at any given instant from an illuminated photo-diode is the sum of the currents due to the photoelectrons ejected during the previous brief time interval. Thus the currents at any two instants separated in time by less than the duration of the individual pulses are not statistically independent. Moreover, the simple scheme provides no handle on the frequency spectrum of the noise which one must take into account in evaluating the response of the measurement chain. One approach to a rigorous solution is presented in Appendix B. Others are possible.

9.   SHOT NOISE EXPERIMENTAL PROCEDURE

The procedure has three parts:

1. Calibration of the gain of the measurement chain as a function of frequency;

2. Measurement of the mean square noise voltage at the output of the measurement chain as a function of the average current in the diode circuit as it is varied by changing the intensity of illumination.

3. Calculation of the charge of the photoelectrons.

9.1.   CALIBRATION OF THE MEASUREMENT CHAIN

Figure 7 is a block diagram of the electronic apparatus, and Figure 6 is a diagram of the diode circuit and preamplifier. The current $I(t)$ in the photo-diode circuit is converted to a voltage $V = I R_F$ at the point indicated in Figure 6 by the operational amplifier with precision feedback resistors in the first stage of the preamplifier inside the photodiode box. This voltage is filtered to remove frequencies <100 Hz and is fed to the second stage where it is amplified by a factor of ~ 10. The output signal is further amplified by the filtering preamp, then filtered by the 8-pole bandpass filter, before being measured by the RMS voltmeter.

There are two methods for measuring the output signal from the photo-diode box. The first is a digital oscilloscope; it gives a qualitative view of the signal, useful for debugging, and can perform signal averaging. This is useful for the calibration phase, but averaging the shot noise would be counterproductive. If you choose to measure the noise with this method, make sure to put the oscilloscope trigger to "auto" and move the trigger threshold above the signal to avoid a skewed data set. The Agilent oscilloscopes in lab have a measurement accuracy of at most 3 digits, which is a bit low. The second method uses multimeters. Multimeters allow you to select the AC or DC part of the signal. The big advantage is the number of digits given: the Agilent multimeters have $6\frac{1}{2}$ digits, giving better measurement precision. A combination of the two methods is also useful.

The photo-diode box has a test input for calibration of the overall gain of the measurement chain as a function of the frequency. The typical shot noise RMS voltage across the precision resistor R_F is of the order of 10 microvolts. Since the gain of the circuit in the photo-diode box is ~ 10, a gain of 100 in the amplifier will yield a total gain of 10^3 and bring the signal in the pass band of the filter up to the ~ 10 millivolt level that can be readily measured by the digitizing oscilloscope. As in the Johnson noise calibration, you can determine the effective gain of the amplifier-filter system as a function of frequency by feeding a millivolt sinusoid signal of measured RMS voltage from the function generator into the test input of the phototube box and measuring the RMS voltage of the signal out of the filter.

9.1.1.   Calibration

Select the sine wave output of the function generator, set the the RMS voltage to ~ 20 mV, and feed the signal directly to the digitizing oscilloscope. Without touching the amplitude control on the function generator, measure the RMS voltage for several frequencies over the range of the filter band pass and plot the result so you have a handy data base for the subsequent gain measurements.

Measure the gain of the measurement chain as a function of frequency. Make sure the photo-diode voltage is switched off so that it behaves as an open circuit with no photoelectric current. Switch on the amplifier voltage on the photo-diode box. Feed test signals of various frequencies into the 'test input' and measure the RMS voltage at the output of the bandpass filter. Experiment with the scope settings to obtain higher precision results. Plot the values of g^2 as you go along to assess where you need more or less data to define accurately the gain-squared integral.
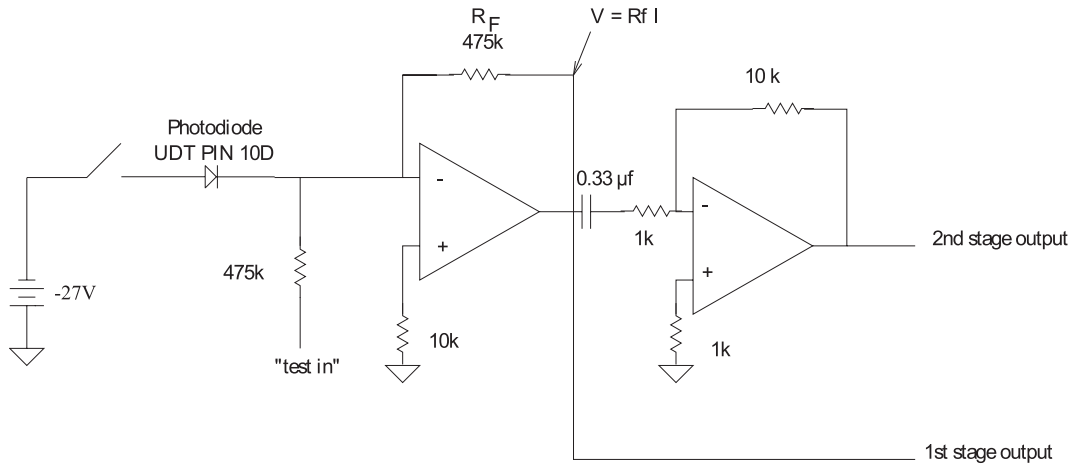
FIG. 6: Diagram of the photo-diode and preamplifier circuit.
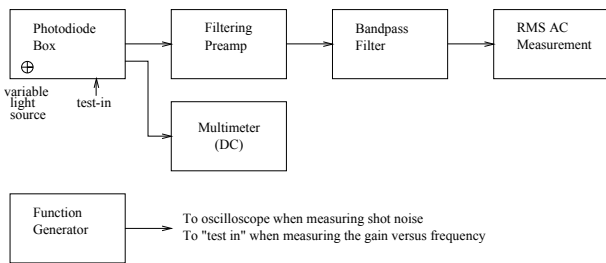
FIG. 7: Block diagram of the experimental arrangement for measuring shot noise.

9.2.   MEASUREMENT OF THE AVERAGE CURRENT AND THE CURRENT NOISE

Remove the cable from the test input and cover the input plug with the cap provided to short the input to ground. This creates a path for current to travel from ground, through the resistor, into the illuminated diode. Set the multimeter to measure DC voltage and plug it into the "first stage output" to measure the voltage $R_F I$. Leave the rest of the measurement chain just as it was when you calibrated it.

There are two banana plug ports to measure the current to the light bulb. It is a good idea to check the current before you start. The current should change as you adjust the potentiometer knob, but make sure that the current does not exceed 300 mA to avoid damaging the light bulb. If the switch is on and there isn't a change in current as you twist the knob, the light bulb or the batteries are probably dead. Once you finish with this check, it is a good idea to short the two ports to reduce extraneous noise.

Record the RMS voltage from stage 2 and the DC voltage from stage 1 for various settings of the light bulb knob. Many repeated measurements at each light intensity will beat down the random errors.

10.   ANALYSIS

Plot V_0^2 as a function of the combined quantity

$$2R_F^2 I_{av} \int_0^\infty g^2(f) df \qquad (10.1)$$

From the slope of this line determine the charge on the electron.

10.1.   Possible Theoretical Topics

- The Nyquist theorem.

- Shot noise theory

Some useful references for this lab include [? ? ? ? ?].

11.   Equipment List

Manufacturer	Description	URL
Agilent	Oscillocope and Multimeters	agilent.com
SRS	SR560 Preamplifier	thinksrs.com
Kron-Hite	8-Pole Band-Pass Filter	kron-hite.com
Kay	Precision Attenuator	

APPENDIX A: A MECHANICAL EXPERIMENT TO DETERMINE k

Before turning to a detailed consideration of the Johnson noise experiment, it is amusing to consider the possibility of a mechanical determination of k with a macroscopic system having one degree of freedom, namely a delicate torsion pendulum suspended in a room in thermal equilibrium (i.e. no drafts, etc.) at temperature T. The degree of freedom is the angular position θ with which is associated the potential energy $\frac{1}{2}\kappa\theta^2$. According to the equipartition theorem (see below), the mean thermal potential energy is

$$\frac{1}{2}\kappa\langle\theta^2\rangle = \frac{1}{2}kT \qquad (A1)$$

where κ is the torsion constant of the suspension, and $\langle\theta^2\rangle$ is the mean square angular displacement of the pendulum from the equilibrium orientation. Thus, in principle, by measuring $\langle\theta^2\rangle$ over a time long compared to the period, one can determine k. To judge what this might require in practice, imagine a torsion balance consisting of a tiny mirror (for reflecting a laser beam) suspended by a 0.5 mil tungsten wire 10 feet long. Such a suspension has a torsion constant of the order of 10^{-3} dyne cm rad^{-1}. According to Equation A1, at 300 K the value of $\langle\theta^2\rangle^{1/2}$, i.e. the RMS value of the angular deflection, would be about 1 arc second. Such an experiment might be possible, but would be exceedingly difficult.

APPENDIX B: DERIVATION OF THE RMS THERMAL VOLTAGE AT THE TERMINALS OF AN RC CIRCUIT

Figure 1 shows the circuit equivalent to the resistor and coaxial cables that are connected to the PAR preamplifier for the measurement of Johnson noise. The equivalent circuit consists of a voltage source of the fluctuating thermal emf V in series with an ideal noiseless resistor of resistance R and a capacitor of capacitance C. According to Faraday's Law, the integral of the electric field around the RC loop is zero, so

$$V = IR + \frac{Q}{C} \qquad (B1)$$

According to charge conservation (from Ampere's Law and Gauss' Law), the current into the capacitor equals the rate of change of the charge on the capacitor, so

$$I = \frac{dQ}{dt} \qquad (B2)$$

We seek an expression in terms of $d\langle V^2\rangle$, R, and C for the contribution to the RMS voltage across the terminals in a narrow frequency range, i.e.

$$d\langle V^2\rangle = d\langle Q^2\rangle/C \qquad (B3)$$

Consider one Fourier component of the fluctuating thermal emf across the resistor, and represent it by the real part of $\nu_J = \nu_0 e^{j\omega t}$, where $j = \sqrt{-1}$. The resulting current is the real part of $i = i_0 e^{j\omega t}$, the charge on the capacitor is the real part of its integral $q = -(j/\omega)i$, and the desired output voltage is the real part of $\frac{q}{C} = -(\frac{j}{\omega C}i)$. Substituting the expressions for i and q into Equation B1 and canceling the time-dependent terms, we find

$$\nu_0 = (R - \frac{j}{\omega C})i_0 \qquad (B4)$$

Solving for i_0 we obtain the relation

$$i_o = \frac{\nu_0}{R - \frac{j}{\omega C}} \qquad (B5)$$

so

$$\nu'_J = \frac{q}{C} = -(\frac{j}{\omega C})i = \frac{-j\nu_J}{\omega RC - j} \qquad (B6)$$

The statistically independent contribution which this mode gives to the measured total mean square noise voltage is the square of its amplitude which we find by multiplying ν'_J by its complex conjugate:

$$\langle\nu'^2_J\rangle = \frac{\langle\nu_J^2\rangle}{1 + (\omega RC)^2} \qquad (B7)$$

Summing all such contributions in the differential frequency range df, we obtain

$$\langle dV^2\rangle = 4R_f kT df \qquad (B8)$$

where

$$R_f = \frac{R}{1 + (2\pi f RC)^2} \qquad (B9)$$

APPENDIX C: DERIVATION OF THE SHOT NOISE EQUATION

Following is an abbreviated version of the shot noise theory given by Goldman (1948). We begin by expressing the current in the photodiode circuit due to a single event that occurs at time T_k, like that depicted in Figure 4b, as a Fourier series over a long time interval from 0 to T. Calling this current pulse $i(t - T_k)$ we represent it as a Fourier series:

$$i(t - T_k) = \frac{a_0}{2} + \sum_{n=1}^{\infty} \left(a_n \cos \frac{2\pi n t}{T} + b_n \sin \frac{2\pi n t}{T} \right) \quad (C1)$$

where

$$a_0 = \frac{2}{T} \times \int_0^T i(t - T_k) dt = \frac{2e}{T} \quad (C2)$$

$$a_n = \frac{2}{T} \times \int_0^T i(t - T_k) \cos \frac{2\pi n t}{T} dt = \frac{2e}{T} \cos \frac{2\pi n T_k}{T} \quad (C3)$$

$$b_n = \frac{2}{T} \times \int_0^T i(t - T_k) \sin \frac{2\pi n t}{T} dt = \frac{2e}{T} \sin \frac{2\pi n T_k}{T} \quad (C4)$$

with $i(t - T_k) = e\delta(t - T_k)$.

The area under the curve in Figure 4b is the charge e of one electron; it represents the "impulse" of the shot, and is accounted for in the Fourier representation by the lead term in the series whose coefficient is given by Equation C2. To justify Equations C3 and C4 in the context of the present experiment we note that the gain of the amplifier-filter system used in this measurement is different from zero only for frequencies such that $f = n/T \ll 1/\tau$. Consequently we can confine our calculation of the Fourier coefficients to those for which $n\tau \ll T$. It follows that the cos and sin factors in the integrands of equations C3 and C4 do not vary significantly over the range of t in which $i(t - T_k)$ differs from 0, and that they can therefore be taken outside their integrals with their arguments evaluated at the instant of the event. In other words, the function representing the current impulse of a single event acts like a delta-function. Substituting the expressions for a_0, a_n, and b_n from equations C2, C3, and C4 into C1 we obtain

$$i(t - T_k) = \frac{e}{T} + \frac{2e}{T} \sum_{n=1}^{\infty} \cos \left[\frac{2\pi n(t - T_k)}{T} \right]. \quad (C5)$$

We suppose now that many such events pile up to produce the total current at any given instant. We seek a way to add the currents due to the individual events to obtain the differential contribution $d\langle I_0^2 \rangle$ in the frequency interval df to the mean square of the sum. We use the well known fact that the mean square of the sum of all the Fourier components is the sum of the mean squares of the individual components (the mean values of the

cross-frequency terms in the squared Fourier series are all zero). The quantity $d\langle I_0^2 \rangle$ is therefore the sum of the mean squares of the individual contributions in the frequency range df. To evaluate it we first focus attention on the nth Fourier component which we represent by

$$c_n \cos \left(\frac{2\pi n t}{T} - \phi_n \right) \quad (C6)$$

to which the kth event contributes the quantity

$$\frac{2e}{T} \cos \left(\frac{2\pi n(t - T_k)}{T} \right) \quad (C7)$$

The mean square value of the nth component is c_n^2 so our immediate problem is to evaluate the quantity c_n^2. Since the events occur at random times from 0 to T, their contributions to the nth component have random phases which are distributed uniformly from 0 to 2π. Consequently, we must add them as vectors. To do this we first group them according to their phase. The expected number with phases between ϕ and $\phi + d\phi$ is $\frac{d\phi}{2\pi} KT$.

$$q = \frac{d\phi}{2\pi} KT \quad (C8)$$

Combining this with equations C6 and C7, we find that the average value of the sum of the contributions with phase angles in the range from ϕ to $\phi + d\phi$ for the Fourier component of frequency n/T is

$$\frac{d\phi}{2\pi} KT \frac{2e}{T} \cos \left(\frac{2\pi n t}{T} - \phi \right) = \frac{Ke}{\pi} \cos \left(\frac{2\pi n t}{T} - \phi \right) \quad (C9)$$

We now represent each one of the preliminary sums given by equation C8 by a differential vector in a two dimensional phase diagram. Added head to tail in order of increasing phase, these vectors form a closed circular polygon of many sides. If instead of the exact expected numbers of events contributing to each differential vector, we use the actual numbers q_1, q_2, ..., then, in general, the polygon will not quite close due to statistical fluctuations in these numbers. The line segment that closes the gap is the overall vector sum for this particular Fourier component. It will have a random direction and a tiny random length that represents the net effect of the fluctuations. Its x and y components will have zero expectation values, but finite variances (mean square values). Each contribution to the total x component is a number of events that obeys a Poisson distribution with a variance equal to its expectation value. By a well known theorem of statistics (used frequently in error analysis), the variance of the sum is the sum of variances. Thus the mean square of the x component of the vector representation

of the nth Fourier component is

$$\frac{4e^2}{T^2}(q_1 \cos^2 \phi_1 + q_2 \cos^2 \phi_2 + ...) =$$
$$= \frac{4e^2}{T^2} \frac{KT}{2\pi} \int_0^{2\pi} \cos^2 \phi d\phi$$
$$= \frac{2e^2 K}{T} \qquad (C10)$$

The mean square of the y components has the same value. And since the vector itself is the hypotenuse of the right triangle formed by the x and y components, the mean square of its length is the sum of the mean squares of the two components. Thus

$$\langle c_n^2 \rangle = \frac{4e^2 K}{T} \qquad (C11)$$

and it follows that the contribution of the nth Fourier component to $d\langle I_0^2 \rangle$ is $\frac{\langle C_n^2 \rangle}{2} = \frac{2e^2 K}{T}$. The frequency of the nth component is $f = n/T$, so the number of Fourier components corresponding to a frequency bandwidth df is $dn = Tdf$. Therefore the contribution to the mean square value of the sum of the Fourier components in the frequency range df is

$$d\langle I_0^2 \rangle = \frac{2e^2 K}{T} Tdf = 2e^2 Kdf \qquad (C12)$$

The average current due to the many events is $I_{av} = Ke$. Thus the final expression for the differential contribution to the mean square of the fluctuating component of the current from the differential frequency interval df is just that given by Equation 8.3 from which follows Equation 8.4, the desired formula for the relation between measured quantities and e.

APPENDIX D: ALTERNATIVE SHOT NOISE EXPLANATION - CONTRIBUTED BY SETH DORFMAN

Consider a photodiode circuit where current is produced by a light source that causes individual electrons to be emitted from the cathode. Each photoelectron will produce a current pulse whose area is the unit of electric charge. Since the total current is a superposition of currents produced by discrete events, the current produced will not be completely constant. The varying component of this current is known as shot noise. It was first cataloged by W. Schottky in a 1918 paper [?].

To derive a quantitative expression that may be used to analyze this phenomena, consider a single current pulse $G_n(t - T_n)$ produced by a single electron striking the anode. The pulse has a narrow width between $t = T_n$ and $t = T_n + \Delta t$. Following Goldman [?], the pulse may be approximated as an impulse and expanded in a Fourier series in the interval from 0 to T:

$$G_n(T - T_n) = \frac{e}{T} + \frac{2e}{T} \sum_{m=1}^{\infty} \cos \frac{2\pi m(t - T_n)}{T} \qquad (D1)$$

The first term in the expansion is the DC current for a single electron event; the series term makes up the fluctuating component. The total current from many events may also be expanded in a Fourier representation. A single frequency component of this sum is made up of a sum of contributions from the $G_{nm} = \frac{2e}{T} \cos \frac{2\pi m(t - T_n)}{T}$ term in each $G_n(t - T_n)$. However, since T_n may be anywhere in the interval from 0 to T, the phases of these components will be randomized. In other words, the components of the total current may be though of as vectors of the same magnitude, but with all possible phases.

A convenient analogy is unpolarized light passing through a linear polarizer. In that case, the randomized $\cos^2 \phi$ contribution to the intensity averages out such that the final intensity is half of the initial intensity. Similarly, the mean square of the contribution of each G_{nm} to the total current at a given frequency $\frac{m}{T}$ is:

$$\langle G_{nm}{}^2 \rangle = (\frac{2e}{T})^2 \langle cos^2 \phi_{nm} \rangle = \frac{2e^2}{T^2} \qquad (D2)$$

Now, let K equal the number of pulses $G_n(t - T_n)$ per second. The total number of pulses in the interval from 0 to T in any given time is then KT. Thus the sum of $\langle G_{nm}{}^2 \rangle$ over all pulses n is $\frac{2e^2}{T^2} KT = \frac{2e^2 K}{T}$. This is the mean square of the total current at a given frequency. Since the frequency is given by $F = \frac{m}{T}$, there are $T\Delta F$ frequencies in a given frequency band. Thus the root mean square current within a given frequency interval is given by:

$$I_{RMS}^2 = \frac{2e^2}{T^2}(KT)(T\Delta F) = 2e^2 K\Delta F \qquad (D3)$$

Here eK represents the average current. This relation will be explored further in the experiment.

The Quantum Mechanics of α-Decay

MIT Department of Physics
(Dated: September 5, 2011)

The purpose of this experiment is to explore the relation between the mean lives of alpha-active nuclides and the energies of the alpha particles they emit. You will study portions of the sequences of radioactive transformations whereby uranium is transmuted into lead. Various procedures will be used to measure the alpha-particle energies and lifetimes of five alpha-active nuclides with mean lives ranging from days to microseconds, as well as the mean lives of two beta-active nuclides.

1.   Preparatory Questions

1. With the help of Figures **??**, **??**, and **??**, in Appendix **??** and the associated reference [1], construct charts of the decay chains that start with the naturally occurring isotopes of uranium, U, and thorium, Th, terminating with a stable isotopes of lead. For each nuclide, place a box in a coordinate system with atomic number and element name on the x-axis and mass number (total number of nucleons) on the y-axis. In each box write the half life, decay mode(s) and energies, and branching probabilities. Be careful when looking up the decay energy – most sites list the *total* energy of the decay rather than just the energy of the alpha particle. For example, the energy of the alpha particle emitted in the decay of Po^{212} is 8.78 MeV, *not* 8.95 MeV. These energies can be found in reference [2].

2. *The Geiger-Nuttall Relationship.* Create a log-log plot of the expected relation between the mean lives of alpha-active nuclides and the energies of the alpha particles they emit.

3. In section 4, we analytically solve the coupled differential equations for a two-nuclide decay chain, and examine some special limiting cases. However, in the case of our experiment with decay chains consisting of dozens of nuclides, this approach becomes impractical. Today, it is much more prudent to produce a MATLAB implementation of a Bateman equation solver.

   In the liquid scintillator experiment, we employ a relatively pure source of Rn^{222} to measure the half-life of Rn^{222} and Po^{218}. Using the `bate.m` script described in Appendix **??**, the example implementation, and your answer to prepatory question 1, write a script that shows the activity of all the nuclides following Rn^{222} all the way to Pb^{206}. You should be able to figure out how much Rn^{222} there is from the information on the activity of the source in section 7.1. Make necessary approximations for multiple branchings. Plot your results, explain them, and place them in your notebook.

4. Why are there no natural nuclides with $Z > 83$ and $A = 4n + 1$?

5. Consider two counters, #1 and #2, each producing random, uncorrelated pulses at average rates of r_1 and r_2, respectively, where $r_1 \gg r_2$. What is the rate at which a pulse from #1 is succeeded by a pulse from #2 within the time interval from t to $t + dt$? What is the mean value of such time intervals (of false coincidences)? (In a measurement of the mean life of a nuclide by the method of delayed coincidences, you will have to take care that your data are not swamped by events produced by random and uncorrelated events in the two detectors.)

6. Explain how a silicon barrier solid state detector works. (see Reference[3]).

2.   Introduction

The first Nobel Prize in physics was awarded in 1901 to Wilhelm Röntgen for his discovery on November 8, 1895 that a penetrating radiation (X-rays) is emitted by the fluorescing glass of a cathode-ray tube under bombardment by cathode rays inside the tube. (Frederick Smith at Oxford missed that discovery: When he earlier noticed that films left near a cathode ray tube were darkened, he told his assistant to move the films away.) Antoine Becquerel heard Röntgen's report on January 20, 1896 at the Académie des Sciences. He immediately set about to investigate whether other fluorescent materials emitted penetrating radiations. After ten days without success he read about the fluorescent properties of uranium salts. On January 30 he sprinkled some uranyl potassium sulfate on top of a photographic plate wrapped in light-tight paper, exposed the salt to sunlight for a few hours, developed the plate, and found it darkened. He prepared to repeat the experiment on February 26 and 27, but the weather was cloudy, so he put the plate and salt away in a drawer to wait for a sunny day. On March 1 he developed the plate, "expecting to find the images very feeble. On the contrary, the silhouettes appeared with great intensity. I thought at once that the action might be able to go on in the dark." Thus Becquerel discovered the phenomena that was later dubbed *radioactivity* by Marie Curie.

Marie Sklowdowska came from Warsaw to Paris to study at the Sorbonne in 1891. A few years later she began her studies of radioactivity in collaboration with her husband, Pierre Curie. By 1898 she had discov-

ered the radioactivity of thorium and had isolated (from residues of uranium refinement) a new element, radium, and showed that its activity per gram was a million times greater than that of uranium.

Ernest Rutherford, a young New Zealander working at the Cavendish Laboratory of Cambridge University, showed that the radiation emitted by uranium is of two types distinguished by their penetrating power. In a publication, completed in 1899 after he had moved to McGill University in Montreal, Rutherford called the easily absorbed radiation "alpha rays" and the more penetrating radiation "beta rays". Becquerel discovered that the beta rays are deflected by electric and magnetic fields like charged particles with the same value of e/m as the recently discovered electrons. Then Rutherford demonstrated that alpha particles are doubly charged ions of helium, whose spectrum had been discovered first in the sun only a few years previously, and then in the gases emitted by uranium ores. Shortly thereafter, Paul Villard in France identified a third type of radiation he called "gamma", which turned out to be high energy electromagnetic radiation.

In 1900 Rutherford and Frederick Soddy found that thorium emits a short-lived radioactive gaseous element (an isotope of radon, Rn^{228}, called thoron) that is chemically inert, like argon. From measurements of its radioactivity they drew the epochal conclusion that thoron decays into other radioactive elements — the discovery of the transmutation of elements. A year later Marie Curie discovered a similar gaseous element Rn^{226} emitted by radium. In a series of papers on radioactivity Rutherford and Soddy unraveled most of the complex relations between the decay products of uranium and thorium. They discovered the exponential law of radioactive decay

$$N(t) = N_0 e^{-t/\tau} \qquad (2.1)$$

in which the "mean life" τ of the substance is a fundamental characteristic that is unaffected by heat, chemical combination, or any other condition that affects the electronic structure of the atom (except the absence of K electrons in the case of beta decay by electron capture). Also in 1903, Soddy published a calculation of the energy released by the decay of radium and wrote that it is "at least twenty-thousand times, and may be a million times, as great as the energy of any molecular change." Four years later Albert Einstein, in his discovery of the theory of relativity, deduced the equivalence of mass and energy expressed in his equation $E = mc^2$ and suggested that the energy released in radioactivity was converted mass.

Rutherford dominated experimental nuclear physics for the next thirty years. His greatest discovery was the nucleus itself which he perceived in the results of the alpha-particle scattering experiments he initiated at Manchester University in 1910. A fascinating account of this era has been written by Richard Rhodes [1986] in *The Making of the Atomic Bomb* from which the above history is taken [4].

3.   Radioactivity

Most of the natural elements with atomic numbers from 1 (hydrogen) to 82 (lead) are stable. The few exceptions include the isotope of potassium, K^{40}, which constitutes 0.01% of natural potassium and suffers beta decay with a mean life of 1.9 billion years. All the isotopes of the elements with $Z > 82$, with the possible exception of Bi^{209}, are unstable and decay with half lives ranging from microseconds to billions of years. So where, when, and how did the natural radioactive elements arise? Since the 1950s, and particularly from the work of William Fowler of Caltech and his collaborators, it has become clear that all the elements with $Z > 26$ (iron) are built up suddenly from lighter elements by absorption of neutrons in the neutron-rich region of a supernova during the first ~ 1 sec of the explosion, the so-called rapid process (r-process). Supernovas occur in our galaxy at a rate of about 2 or 3 per century. One of these probably triggered the formation of the solar system and enriched its raw material with freshly synthesized heavy elements of which all with $Z > 82$ have been decaying ever since.

Light nuclei with equal numbers of protons and neutrons (e.g., He^4, C^{12}, O^{16}) are stable. Heavier nuclei ($Z > 10$), to be stable, need a higher proportion of neutrons to provide sufficient nuclear-force binding to overcome the Coulomb-force repulsion of the protons (e.g., K^{41}, where $A = 2Z + 3$). Thus a nucleus with too few neutrons will convert a proton to a neutron by emission of a positron and an electron neutrino. On the other hand, a free neutron is slightly heavier than the proton and decays into a proton, electron, and anti-neutrino with a mean life of ~ 12 minutes. Therefore, it can be energetically favorable for a nucleus with too many neutrons to convert a neutron to a proton by emission of an electron and anti-neutrino. Thus nuclides with too few or too many neutrons transmute by electron emission toward the stable region along the bottom of the valley. A 3-D plot of neutron number (y-axis) versus proton number (x-axis) versus potential energy per nucleon (z-axis) for all the isotopes of the elements shows a steep potential energy "valley of stability" with a positive curvature in the x-y plane. The three kinds of radioactive transmutation are:

1. *Alpha decay* (ejection of a helium nucleus consisting of two neutrons and two protons) is the most common decay mode for elements above lead and near the bottom of the stability valley.

2. *Beta decay* (emission of a positive or negative electron or capture of a K-shell electron together with emission of a neutrino or anti-neutrino) generally occurs in nuclides on the valley sides and serves to correct unstable proportions of neutrons and protons.

3. *Spontaneous fission* (division into two nuclei) occurs above uranium and is a mode of rapid decay

of the artificial elements above $Z = 100$. Theoretical speculation about possible high-Z islands of stability have stimulated numerous, and so far unsuccessful, experiments to produce elements with $Z = 114$ or other so-called *magic numbers*.

A chain of radioactive decays, starting with a heavy nuclide near the bottom of the stability valley (e.g., U^{238}) and proceeding by alpha decays, produces nuclides with increasing deficiencies of neutrons and corresponding positions higher up the valley wall. The deficiency is corrected at various steps in the chain by emission of a negative electron, i.e., beta decay. The three decay chains found in nature are illustrated in Appendix **??**. The fourth doesn't exist in nature because it has no long-lived parent nuclide that could have survived in significant quantity since the creation of earth's elements. Alpha decay occurs whenever permitted by energy conservation, unless preempted by beta decay. Consider the decay process

$$Ra^{226} \longrightarrow Rn^{222} + He^4. \qquad (3.1)$$

The total mass-energy (mc^2 + kinetic energy) must be conserved. Thus, in the spontaneous alpha-decay of a radium nucleus we have,

$$Ra^{226} = Rn^{222*} + He^4 + Q, \qquad (3.2)$$

where $Q = 4.869$ MeV is the total kinetic energy of the product nuclei if they are in their ground states. (Precise values of isotopic masses are listed in the CRC nuclide table). The energy Q is shared in accordance with the conservation of momentum between the mutually repelled He^4 and Rn^{222} nuclei. However, the latter, being a complex system of many constituent particles, may be left in an excited state from which it later decays by gamma emission. Thus the kinetic energy of the remnant particles (alpha particle and Rn^{222} nucleus) just after the decay event depends on the energy of the excited state of the Rn^{222} nucleus. High resolution spectrometry of the alpha particles from Ra^{226} reveals a "fine structure" [**4.782 MeV** (94.6%), **4.599 MeV** (5.4%), **4.340 MeV** (0.0051%), **4.194 MeV** (7×10^{-4}%)], each energy corresponding to a particular excited state of the daughter nuclide Rn^{222}.

Generally, a nuclide, created in an excited state by alpha or beta decay of its parent nuclide, decays to its ground state by gamma-ray emission. In some cases it may undergo alpha decay before it has had time to settle to its ground state, thereby giving rise to a more energetic alpha particle, which is another source of fine structure in alpha spectra.

3.1.   The Geiger-Nuttall Relationship:

The Correlation Between Energy and Half Life in Alpha Decay

The principal aim of this experiment is to explore the correlation between the half lives of radioactive nuclides and the energies of the alpha particles they emit — the shorter the half life the higher the energy. The most abundant isotope of uranium, U^{238}, with a half life, of 4.5 billion years, emits alpha particles with an energy of 4.2 MeV; Po^{212} with a half life of 0.304 μs emits alpha particles with an energy of 8.785 MeV — in this case a ratio of $\sim 4 \times 10^{23}$ in half life corresponds to a factor of only ~ 2.1 in energy! The quantitative expression of this correlation, discovered early in the investigation of radioactivity, is called the Geiger-Nuttall law and is expressed by Equation 3.3,

$$\ln \lambda = a_1 \ln E_\alpha + a_2, \qquad (3.3)$$

where λ is the decay constant ($= 1/\tau$), E_α is the emitted α-particle energy and a_1 and a_2 are constants.

Then, in 1927, Rutherford observed that the scattering of 8.57 MeV alpha particles (from Po^{212}) by a thin uranium foil is exactly what is expected for elastic scattering by a perfect $1/r$ Coulomb potential down to the closest distance of approach for such particles, namely $\sim 3 \times 10^{-12}$ cm. Thus the Coulomb barrier around a uranium nucleus must be at least as high as 8.57 MeV, and any alpha particle going over the top to get out must be pushed away by Coulomb repulsion resulting in a final kinetic energy of at least that amount. And yet the energy of alpha particles emitted by uranium is only 4.2 MeV!

The explanation of these remarkable facts was an early triumph of the quantum mechanics discovered independently and in different forms by Erwin Schrödinger and Werner Heisenberg in 1926. Two years later, George Gamow, a postdoc from Russia studying with Niels Bohr at the Institute for Theoretical Physics in Copenhagen, derived the equation for quantum mechanical tunneling of alpha particles *through* the Coulomb barrier of the nucleus. Two young Americans studying in Europe, Edward Condon and Ronald Gurney, discovered the same explanation independently. Their publications, References [5, 6], on the topic are reproduced in the Junior Lab electronic library. From their barrier penetration theory is derived Equation 3.4 which is remarkably similar to the Geiger-Nuttall relationship, Equation 3.3, empirically determined many years earlier.

$$\ln \lambda = a_1 E_\alpha^{-1/2} + a_2 \qquad (3.4)$$

As mentioned earlier, radioactive decay is described by Equation 2.1 where τ is the **mean life**. The **half life**, $\tau_{1/2}$, is the solution of the equation

$$e^{-\tau_{1/2}/\tau_A} = \frac{1}{2}, \qquad (3.5)$$

which is

$$\tau_{1/2} = \tau_A \ln 2 = 0.693\tau_A. \qquad (3.6)$$

3.2. The Quantum Mechanics of Alpha-Particle Emission

A very nice and accessible introduction to this material is given in Reference [7, 8]. Nuclei consist of protons and neutrons held together by the strong, short range nuclear force which exceeds the Coulomb repulsion between the protons at distances less than of the order of 1 fermi (10^{-13} cm). The potential function (a plot of the potential energy per unit charge of a positive test particle against position) for a spherical high-Z nucleus is sketched in Figure 1. Inside the nuclear radius the potential can be approximated by a square well potential. Outside, the barrier is accurately represented by a potential proportional to $1/r$. The wave function of an alpha particle, initially localized inside the well, can be represented as a traveling wave that is partially reflected and partially transmitted at the barrier. The transmission coefficient, very small, is the probability that the alpha particle will penetrate the barrier. As it bounces back and forth inside the well the particle has multiple chances of penetrating the barrier and appearing on the outside. If it does, then the potential energy which the alpha particle had inside the nucleus is converted to kinetic energy as it slides down the outer slope of the barrier.
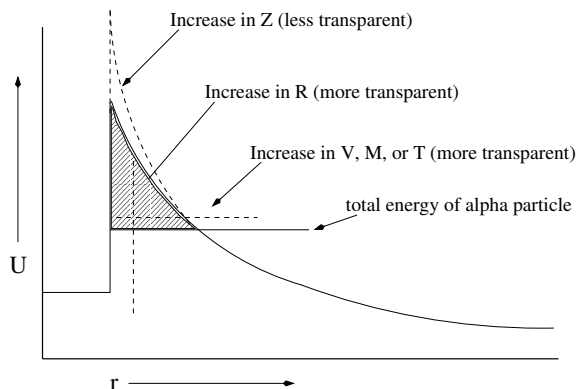
FIG. 1: Plot based on Figure 5.7 from Evans [1955] [8] illustrating the nuclear potential barrier, and the effects of changes in the nuclear parameters on the transparency of the barrier, where Z is the atomic number, R is the radius of the nucleus, V, M, T are respectively the potential energy within the nucleus, mass and bouncing period of the emitted particle.

4. Evolution of Radioactive Mixtures: The Bateman Equations

The source of radioactive nuclides in the present experiment is an ancient ($\sim 10^9$ years old) sample of the olive-green-colored mineral pitchblende containing triuranium octaoxide (U_3O_8). These rocks were borrowed from the Harvard mineral collection to which it was donated by a young rock hound who pried it out of a deposit between layers of mica in the granite shield of Maine. Some physical characteristics of U_3O_8 are a crystal density of 8.30 g cm^{-3} and a bulk (ore) density ranging from 1.5 to 4.0 g cm^{-3}. Our samples happen to be relatively enriched in U_3O_8. The specific activity of U^{238} is 3.3×10^{-7} Ci g^{-1} [1]. U_3O_8 is in soluble in water but will decompose to a solid ceramic (UO_2) material above 1300 °C. This latter form is most commonly used as fuel for nuclear reactors.

The sample is evolving in time as the various components of the decay chains are born and decay. The rates of growth and decay of radioactive isotopes in such mixed samples is governed by a set of first-order linear differential equations. Analysis of the variations of the counting rates of the various activities in light of these equations and their solutions can yield measures of the mean lives and relative abundances of the various nuclides.

A full exposition of the differential equations that describe the growth and decay of activities, the so-called Bateman equations, is given by Evans [1955], pp 470 – 510. Here we consider only the two simple cases that will be of greatest use in planning and analyzing your measurements. The fundamental law of radioactive decay is that at any instant the change, dA, in the number of atoms of any given radioactive nuclide in a time interval, dt, is proportional to the number, A, present at that particular instant times dt, i.e.,

$$dA/dt = -A/\tau_A, \qquad (4.1)$$

where τ_A is a constant characteristic of the nuclide. Integration of this equation leads immediately to the expression, previously cited, for the number at any time t, namely

$$A(t) = A_0 e^{-t/\tau_A}, \qquad (4.2)$$

where A_0 is the number present at $t = 0$. Now consider the relations between the activities (decays/second) of two radioactive isotopes, A and B, such that B arises from the decay of A. Let $A(t)$ and $B(t)$ represent the numbers of atoms of the two isotopes present at any given time, A_0 and B_0 the numbers present at $t = 0$, and τ_A and τ_B their mean lives, respectively. The rates of decay are A/τ_A and B/τ_B. As before, equation 4.1 describes

---

[1] 1 Ci = 3.7×10^{10} disintegrations s^{-1}

the change of A. The rate of change of B is the algebraic sum of the rates of build-up and decay of B,

$$dB/dt = A/\tau_A - B/\tau_B. \qquad (4.3)$$

Equations 4.1 and 4.3 are simultaneous, first-order, differential equations that must be solved subject to the initial conditions. The general solution to equation 4.1 is equation 4.2. The general solution of equation 4.3 is given by the sum of the solution of the homogeneous equation, which is identical in structure to equation 4.1 and therefore has the solution $B_h = f_h e^{-t/\tau_B}$ where f_h is any constant, and a particular solution. To find the particular solution, we use the homogeneous solution as a bootstrap and set $B_p = f_p(t)e^{-t/\tau_B}$ (this is the method of variation of parameters). Substituting B_p for B and the solution for A in equation 4.3 and rearranging, we obtain for f_p the differential equation

$$df_p/dt = (A_0/\tau_A)e^{-t(1/\tau_A - 1/\tau_B)}. \qquad (4.4)$$

Integration of equation 4.4 and imposition of the initial condition $B(t=0) = B_h(t=0) + B_p(t=0) = B_0$ yields the solution (for $\tau_B \neq \tau_A$)

$$B(t) = B_0 e^{-t/\tau_B} + A_0 \frac{\tau_B}{\tau_A - \tau_B}[e^{-t/\tau_A} - e^{-t/\tau_B}]. \quad (4.5)$$

One form of equation 4.5 is of special importance to the interpretation of data from this experiment. Suppose $B_0 = 0$, $\tau_A \gg \tau_B$ and $t \ll \tau_A$. Then the rate of decay of B is

$$r_B(t) = B(t)/\tau_B \approx [A_0/\tau_A][1 - e^{-t/\tau_B}]. \qquad (4.6)$$

Under these circumstances the decay rate of B rises from zero and approaches asymptotically the decay rate of A.

These simple analyses provide us with at least two means of determining a nuclide's lifetime:

1. One can derive an estimate of τ_B as the negative slope of a plot of $\ln[r_B(t=\infty) - r_B(t)]$ against t. The diffusion of radon out of uraninite rocks occurs at a nearly steady rate and can be considered the equivalent of production by radioactive decay of a very long-lived precursor.

2. A second way to determine τ_B is to turn off the supply of B after its decay rate has reached a respectable value. Then the B rate will simply decline according to

$$r_B = (B_0/\tau_B)e^{-t/\tau_B}. \qquad (4.7)$$

When a nuclide is third or later in a decay chain, the equation describing its decay rate is more complex, and interpretation of the variation of an observed decay rate in terms of its mean life becomes more difficult or impractical. If the mean lives of the secondary nuclides in the chain are short compared to τ_A, and if one waits for a time long compared to any of those mean lives, then a steady state is approached in which *all* of the decay rates are the same and equal to A_0/τ_A.

4.1.   Numerical Solutions to the Bateman Equations

In spite of the complexity of the analytical solution, a set of differential equations for a multi-nuclide decay chain is readily solved by numerical integration with results that can be displayed as plots of the various decay rates against time.

Expressed using matrices, the Bateman equations are

$$\frac{dN}{dt} = \mathbf{\Lambda}N, \quad \mathbf{\Lambda} = \begin{bmatrix} -\lambda_1 & & & \\ \lambda_1 & -\lambda_2 & & \\ & \lambda_2 & -\lambda_3 & \\ & & \ddots & \ddots \end{bmatrix}. \qquad (4.8)$$

N is the nuclide number row vector, with the parent nuclide the first entry. $\mathbf{\Lambda}$ is the decay constant matrix ($\lambda_i = 1/\tau_i$). The solution to this matrix differential equation, for initial conditions N_0, is analogously given by the matrix exponential,

$$N(t) = e^{\mathbf{\Lambda}t}N_0, \qquad (4.9)$$

where the matrix exponential is defined by the Taylor expansion of the exponential,

$$e^{\mathbf{\Lambda}t} = \mathbf{1} + \mathbf{\Lambda}t + \frac{(\mathbf{\Lambda}t)^2}{2!} + \frac{(\mathbf{\Lambda}t)^3}{3!} + \cdots, \qquad (4.10)$$

and we can check that it solves equation 4.8 by substitution. Although we now have an elegant solution that is similar in form to the single-nuclide solution, calculating the matrix exponential numerically is computationally intensive. Using matrix algebra, equation 4.9 can be simplified for computational purposes. Since $\mathbf{\Lambda}$ is triangular, its eigenvalues are the main diagonal elements, the negatives of the decay constants. Let $\mathbf{D} = \text{diag}\{-\lambda_i\}$ be the matrix of eigenvalues. Then $\mathbf{\Lambda}$ is diagonalized by the matrix of eigenvectors, $\mathbf{V}$, as follows[2],

----

[2] The reasoning for this theorem is easy to understand with a fundamental understanding of eigenvectors and eigenvalues. If

$$\mathbf{\Lambda V} = \mathbf{VD} \Longrightarrow \mathbf{\Lambda} = \mathbf{VDV^{-1}} \qquad (4.14)$$

Next, we express the matrix exponential $\mathrm{e}^{\mathbf{\Lambda}t}$ in terms of $\mathbf{D}^3$,

$$\mathrm{e}^{\mathbf{\Lambda}t} = \mathrm{e}^{\mathbf{VDV^{-1}}t} = \mathbf{V}\mathrm{e}^{\mathbf{D}t}\mathbf{V^{-1}}. \qquad (4.20)$$

This is a great computational improvement because the matrix exponential of a diagonal matrix is easy to calculate (this, again, can easily be seen from equation 4.10),

$$\mathrm{e}^{\mathbf{D}t} = \begin{bmatrix} e^{-\lambda_1 t} & & & \\ & e^{-\lambda_2 t} & & \\ & & e^{-\lambda_3 t} & \\ & & & \ddots \end{bmatrix} \qquad (4.21)$$

.   The new equation for $N(t)$, substituting from Eq. (4.20), is

$$N(t) = \mathbf{V}\mathrm{e}^{\mathbf{D}t}\mathbf{V^{-1}}N_0, \qquad (4.22)$$

and can easily be implemented in a program such as MATLAB. See Appendix **??** for details.

———

$\mathbf{V}$ contains the eigenvectors of $\mathbf{\Lambda}$, then $\mathbf{\Lambda V}$ is analogous to the left side of the familiar eigenvalue equation $\mathbf{A}\mathbf{x_i} = \lambda_i\mathbf{x_i}$ for each of the eigenvectors. Similarly, $\mathbf{VD}$ is analogous to $\lambda_i\mathbf{x_i}$. The following illustration may make this easier to follow:

$$\mathbf{\Lambda V} = \mathbf{VD} \qquad (4.11)$$

$$\mathbf{\Lambda} \begin{bmatrix} \vdots & \vdots & \\ \mathbf{x_1} & \mathbf{x_2} & \cdots \\ \vdots & \vdots & \end{bmatrix} = \begin{bmatrix} \vdots & \vdots & \\ \mathbf{x_1} & \mathbf{x_2} & \cdots \\ \vdots & \vdots & \end{bmatrix} \begin{bmatrix} \lambda_1 & & \\ & \lambda_2 & \\ & & \ddots \end{bmatrix} \qquad (4.12)$$

$$\mathbf{\Lambda} \begin{bmatrix} \vdots & \vdots & \\ \mathbf{x_1} & \mathbf{x_2} & \cdots \\ \vdots & \vdots & \end{bmatrix} = \begin{bmatrix} \vdots & \vdots & \\ \lambda_1\mathbf{x_1} & \lambda_2\mathbf{x_2} & \cdots \\ \vdots & \vdots & \end{bmatrix} \qquad (4.13)$$

which is merely $\mathbf{\Lambda}\mathbf{x_i} = \lambda_i\mathbf{x_i}$ i times over.

[3]   That $\mathrm{e}^{\mathbf{VDV^{-1}}t} = \mathbf{V}\mathrm{e}^{\mathbf{D}t}\mathbf{V^{-1}}$ can easily be seen from the definition of the matrix exponential in equation 4.10,

$$\mathrm{e}^{\mathbf{VDV^{-1}}t} = \mathrm{e}^{\mathbf{VD}t\mathbf{V^{-1}}} \qquad (4.15)$$

$$= \mathbf{1} + \mathbf{VD}t\mathbf{V^{-1}} + \frac{\left(\mathbf{VD}t\mathbf{V^{-1}}\right)\left(\mathbf{VD}t\mathbf{V^{-1}}\right)}{2!} + \cdots \qquad (4.16)$$

$$= \mathbf{VV^{-1}} + \mathbf{VD}t\mathbf{V^{-1}} + \frac{\mathbf{V}\left(\mathbf{D}t\right)^2\mathbf{V^{-1}}}{2!} + \cdots \qquad (4.17)$$

$$= \mathbf{V}\left(\mathbf{1} + \mathbf{D}t + \frac{\left(\mathbf{D}t\right)^2}{2!} + \cdots\right)\mathbf{V^{-1}} \qquad (4.18)$$

$$= \mathbf{V}\mathrm{e}^{\mathbf{D}t}\mathbf{V^{-1}}. \qquad (4.19)$$
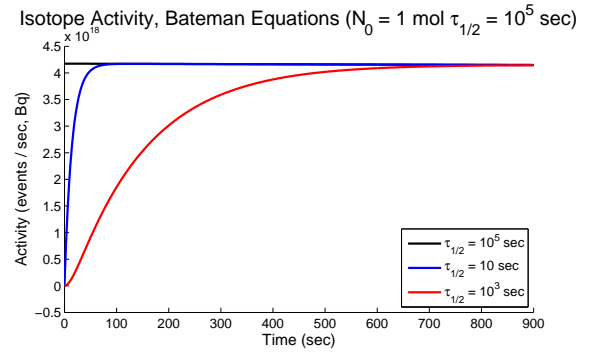
FIG. 2: Plot of the activity in becquerels (events / sec) versus time for a hypothetical decay chain consisting of isotopes with half lives $\tau_{1/2} = 10^5$ sec, 10 sec, and 10^2 sec. In time of the order of the length of the half lives, it comes to equilibrium – each isotope carries approximately the same activity. This was seen directly in equation 4.6.

5.   Experimental Overview

The Junior Lab experiment in alpha-decay consists of two different types of alpha-spectrometers:

1. *A Beckman liquid scintillation detector.* This apparatus is principally used for the determination of the lifetime of Rn^{222}, though with a certain amount of skill it can also be used to measure the much shorter lifetime of Po^{218} as well (described in Section 7.1). The lifetime of Po^{214}, heralded by the birth of a Bi^{214} atom, can be measured using delayed coincidence techniques described in Section 8.1.

2. *A Solid-State Spectrometer* based around a "Passivated Implanted Planar Silicon" or "PIPS" detector[4]. The lifetimes of all other nuclides can be measured with the PIPS based alpha-spectrometers (described in Section 6). The lifetime of Po^{212} is measured using coincidence techniques described in Section 9.3 with the assistance of a plastic scintillator to detect beta decays.

There are two sources for alpha-particle emitting isotopes in this investigation. The first is a very (chemically) stable compound called triuranium octoxide ($\mathrm{U_3O_8}$), which is the end product of the oxidation of Uraninite ($\mathrm{UO_2}$) in air (we will refer to it as uraninite for simplicity). These 'rocks' live in metal cans in the lead box in the fume hood. They should never be removed from the cans. They are used with the PIPS detectors. The other

———

[4] Canberra model A450-20AM from canberra.com

source is the tube of radium-226 salts. It emits radon-222 gas which is 'bubbled' into scintillator fluid for use in the Beckman apparatus.

5.1.   Suggested Experiment Schedule: Overview

Day 1.   1. **Section 6.3**: Seal a can containing uraninite rocks with a rubber stopper in which a certified "good" alpha particle detector is embedded. Apply a voltage ($\sim$ 450V) between the can and lab ground so as to draw to the surface of the detector *positive* ions of decay products from radon isotopes leaking out of the rocks. **Make sure the ground terminal of the floating 450V power supply is connected to earth ground using an alligator clip to the side of the NIM bin!** Record the energy spectra of the alpha particles. With the help of your charts from the preparatory questions, identify the features in the energy spectra and explain the shapes of the lines.

2. **Section 7.1**: Prepare a sealed sample of radon in liquid scintillator and initiate a measurement of the relatively long mean life of Rn^{222} and attempt to measure the short lifetime of Po^{218}. Conduct at least two runs: a "trial" run to familiarize yourself with the apparatus, and a second with all the "bugs" worked out.

Day 2.   1. **Section 6.4**: Determine the mean lives of various alpha and beta activities by measuring changes in counting rates measured with the silicon detector.

2. Measure the alpha decay activity in the liquid scintillator with the Beckman spectrometer and record the date and time.

3. **Suggested Progress Check for end of 2nd Session**: Plot an alpha particle spectrum ($\sim$ 10 minute integration) with the x-axis in calibrated units of energy. All of the peaks should be identified with energy, parent nucleus and half-lives obtained from the literature.

Day 3.   1. **Section 8.1**: Measure the short mean life of Po^{214} by the delayed coincidence method using the Beckman spectrometer coincident circuit to detect the precursor beta decays of bismuth.

2. Measure the alpha decay activity in the liquid scintillator.

Day 4.   1. **Section 9.3**: Measure the very short mean life of Po^{212} by the delayed coincidence method using the auxiliary plastic scintillation counter to detect the precursor beta decays of bismuth.

2. Refine whatever parts of the experiment need additional attention.

3. Measure the remaining alpha decay activity in the liquid scintillator.

6.   Solid-State Spectrometer Experiment

The sample of U_3O_8, consisting of a few small rocks ($\sim$ 70 g), is contained in a can which will be assigned to you for the duration of your experiment. The PIPS detectors are expensive and extremely delicate so take great care not to let anything touch the surface of the detector. The rocks leak radon gas which can be trapped in the can by sealing it with the rubber-stopper in which the detector is mounted. Jostling of the rocks within the cans has, over time, produced small quantities of dust so be careful not to spill any small particles when observing the sample. The can setup is illustrated in Figure 3.

In this experiment samples of such generically related nuclides are created on the surface of the silicon detector. Each alpha-decay process involved in a decay chain reveals itself as a distinct peak in the energy spectrum, and its rate can be measured by appropriate manipulation of the recording sequence. Thus all the necessary data for an exploration of the energy-mean life relation in alpha decay can be obtained with this one "simple" device. One can imagine that Lord Rutherford, in 1905, would have given his eyeteeth for such a detector to replace the ion chambers, cloud chambers, calorimeters, and spinthariscopes he used in his discoveries.

When a radon atom suffers alpha decay, the daughter polonium atom recoils with sufficient velocity to have several of its outer electrons stripped in collisions with air molecules. An electric field, established by application of high voltage ($\sim$ 450 VDC) between the can and the detector, draws the polonium ion to the surface of the detector where it sticks. Its subsequent decay and the decays of its daughter nuclides yield alpha and beta particles. If an alpha particle from an atom stuck on the detector surface is emitted in a direction into the detector, then nearly all of its energy will be dissipated in the sensitive volume of the silicon where the number of electrons raised to the conduction band is almost exactly proportional to the dissipated energy. The conduction electrons are swept out of the silicon by the field established by the bias voltage ($\sim$ 40 VDC) applied to the detector. The resulting charge pulse is detected by the preamplifier as a voltage pulse which is amplified and analyzed with a multichannel analyzer (MCA) card.

6.1.   Multi-Channel Analyzer

The distribution in amplitude (pulse-height spectrum) of pulses from a detector-amplifier combination or per-

haps from a Time-to-Amplitude Converter (TAC) is conveniently measured with a 2048 channel MCA card mounted in the computer. Details of the MCA operation can be found on the web in the Junior Lab E-Library and in the photocopied manual next to the experimental station. These cards allow full software control over upper and lower level discrimination voltages, have a coincidence (gated) detection mode, and offer a simple set of tools for establishing energy calibrations and determining peak statistics. With a slight amount of additional effort, the Maestro-32 control software may be programmed using simple, text-based, .job files to automate repetitive measurements with precision. This technique is outlined in appendix B.
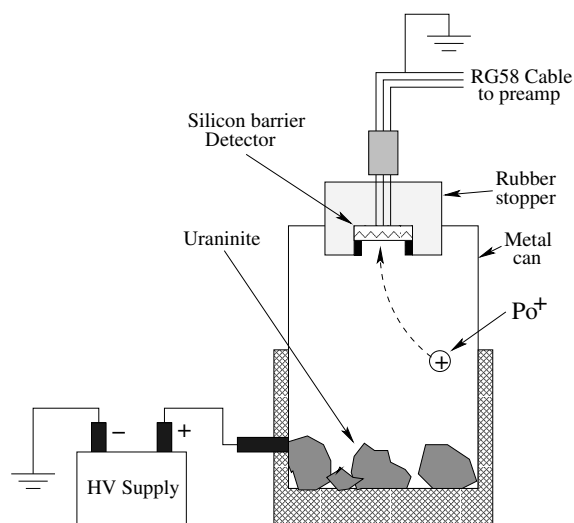

FIG. 3: Schematic diagram of the metal can containing uraninite, sealed by the rubber stopper carrying the silicon barrier detector, and attached to the high voltage supply. A polonium ion is shown as it is about to be drawn to the detector by the electric field.

You will be assigned a silicon barrier detector and a can containing a sample of uraninite rocks for your exclusive use during this experiment. The mixture of decaying nuclides stuck on the surface of the detector depends on the history of its exposure to the decay products of radon that emanates from the uraninite rocks, and on the compositions of the particular uraninite rocks. Therefore it is essential that you control the exposures for your own purposes during the two-weeks of the experiment. You will find a lot of things going on in the can and on the surface of the detector that are not explicitly mentioned in this lab guide. To figure out exactly what is going on you will have to keep a meticulous timed and dated record of your manipulations and observations.

CAUTION

Precursor nuclides of all the activities studied in this experiment are isotopes of the noble gas, radon, which diffuse at steady rates out of the rocks in the can. The nuclides drawn to the surface of the detector by the imposed electric field are the isotopes of polonium (Po^{215}, Po^{216}, and Po^{218}) which are the decay products of those radon isotopes. Therefore, to initiate a useful amount of the action that follows deposition of one of those polonium isotopes on the detector surface, there must be an adequate activity of its parent radon isotope in the gas *in the can* when you apply the high voltage, and the voltage must be left on for a time of the order of the longest-lived nuclide in the subsequent chain leading to the isotope under investigation. For example, if you want to study the rapid decay of Po^{212}, you must accumulate its 10.64-hour precursor Pb^{212} on the surface of the detector for a day or more with the high voltage on.

To study the decay of Po^{218}, you will need to keep the can sealed for a couple of days to accumulate the long lived precursor Rn^{222} gas that leaks from the rocks. Its activity will build toward its equilibrium value in proportion to the function $1 - e^{-t/\tau}$ where τ is its mean life of about 3 days. **If you open the can, the radon will escape, and you will have to wait for a time of the order of τ for the activity to build up to a useful value again.** When you have enough of the gas in the can, you can measure the meanlife of its daughter nuclide Po^{218} by turning on and off the high voltage applied to the can. In the case of Rn^{219} and Rn^{220} radon isotopes, those times are of the order of minutes and seconds. So **THINK** before you open your can.

Additional information about some of the devices can be found in Melissinos [1966] and in the equipment manuals. There are three power supplies used in this experiment. Costly damage can occur if they are inadvertently interchanged. The Ortec Model 428 Detector Bias Supply provides the low (~ 40V) voltage to the Silicon Barrier Solid State Detector. This supply should be connected to the 'HV' input on the Canberra Model 2003BT preamplifier. The second supply is housed in a black plastic box and provides ~ 425 VDC for biasing the can containing the uraninite with respect to the solid state detector, causing polonium ions to be attracted to the surface of the detector. The third supply provides high voltage to the photomultiplier of the scintillation counter used to detect beta-decay electrons emanating from the nuclides deposited on the surface of the Silicon Detector.

6.2.   Silicon Barrier Solid State Detector

When a charged particle dissipates an amount of kinetic energy, K, in the sensitive volume of a solid state detector, an average of K/ε valence electrons are raised to the conduction band and swept out by the bias field to form a pulse of negative charge. In silicon $\varepsilon \approx 3$ eV, so an alpha particle with an energy of several MeV produces a charge pulse containing so many electrons that the fluctuations are a negligible source of width of a line

in a typical alpha energy spectrum — the actual line width ΔE depends on the quality of the detector, and in a good detector it should not exceed $\Delta E \approx 0.01E$. The solid state detector is connected to a preamplifier through which the bias voltage ($<\sim 50$V!) is supplied to the detector, and in which the voltage induced by the charge pulse at the gate of an input field-effect transistor is amplified before passing to a second amplifier and on to a MCA for pulse-height analysis (the physics of solid state detectors is described in Melissinos, 1986.)

6.3. Day 1: The Energy Spectra of Alpha Particles from the Decay Products of Uraninite Emanations

The silicon detector assigned to you has probably been exposed recently to alpha emitters of which not all have decayed to negligible levels of activity. You can use the residual activity to test the detector and spectrum analysis equipment, and to adjust the gains of the system to achieve a convenient spread of the spectral lines (0 – 10 MeV) with good linearity.

Connect the detector and other components as shown in Figure 4, **except do not turn on or connect the detector bias voltage supply**. Place the detector in its rubber stopper face down on the table and cover it with a black cloth (so that room light does not strike the surface when the ~ 40 VDC bias voltage is applied). Set the MCA lower level discriminator (in software) to ~ 200 channels to eliminate detector noise (to check, make sure that the *dead time* when you're taking spectra is hovering around 0.6% and 0%).

Turn on the Ortec 428 bias supply, set it to +40 VDC and measure the voltage at the SHV connector before connecting to the preamplifier's bias voltage input (the Ortec 428 dial is a rather coarse control and you want to be sure not to exceed the manufacturer's maximum voltge recommendation at the risk of destroying the (expensive) detector.

After setting up the scope trigger and gain, adjust the spectroscopy amplifier so that the highest-energy pulses occur at ~ 8 VDC (if there is no scope, just try to make it match up to MCA channel ~ 800). Beware, you may be plagued by 80MHz rf pickup, probably from the MIT FM radio station broadcasting over the MIT 110V power line!) Record *all* the settings of *all* the components in your setup so that you can reestablish the same measurement conditions in your next lab session.

1. Record a 300 sec spectrum with the MCA memory with the detector face down on the table (and covered with a black cloth).

2. Seal your can with your stopper/detector. Record a second 300 sec spectrum with no high voltage applied to the can. Compare this spectrum with the one you obtained with the detector face down on the table.
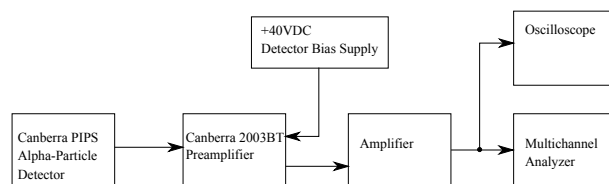
FIG. 4: Arrangement of components for measuring the energy spectra of alpha particles from nuclides deposited on the surface of the detector.

3. Connect the high voltage (~ 425 V) power supply in black plastic box between the can and lab ground and record a third 300 sec spectrum.

4. Reverse the voltage and record a fourth 300 sec spectrum.

Try to understand everything you see in these four spectra. Ask for advice if there are mysteries you can't solve. Record a 30-minute spectrum with ~ 425 V applied to the can with the polarity that produces the most action.

While you are waiting, get started on the long-term measurement of the mean life of Rn^{222} with the liquid scintillator, described in Section 7.1. You will need to get data over several days, so it's wise to start early on this measurement.

After initiating the Rn^{222} measurements, return to the silicon detector experiment and measure the channel numbers of all the peaks of the one-hour spectrum. With the aid of the chart of the nuclides (located on the wall above the experiment), your preparatory question answers and [1], identify the peaks and explain their shapes. Do you see evidence of the famous high-energy alphas from Po^{212}? If so, estimate their energies and the fraction of the decays that give rise to them.

- Try to explain any discrepancies between the spectrum of pulse heights you have observed and their expected energies (e.g. consider the effect of a thin coating of protective material or dust over the source or the detector.)

- In light of the likely age of the uranite source and the opportunity it has had to achieve equilibrium among the quantities of its radioactive decay products, try to explain the inequalities you may see in the intensities of the various alpha particle groups.

At the end of the first lab session, **keep your can sealed** with the stopper/detector and connect your high-voltage box between the can and the shield of the BNC connector with the appropriate polarity to draw the polonium ions to the detector. This will build up a supply of radioactive nuclides in the gas in the can and on the surface of the detector for analysis at your next session. Note the time in your lab notebook.

6.4.   Days 2 and 3: Determination of the Mean Lives of Several Nuclides

In preparation for your second session, devise a plan for the determination of the mean lives of as many nuclides as possible with data that you will be able to obtain from the setup used in the first session. Base your plans on the possibilities of measurement implied by equations 4.6 and 4.7 above. There are two alpha decays and two beta decays whose mean lives can be measured by appropriate manipulations with the silicon detector.

Consider:

1. Disconnecting the high voltage and measuring the decay of the nuclides stuck on the detector surface

2. Reconnecting the high voltage and measuring the build up of activities

3. Flushing the accumulated radon out of the can with nitrogen, sealing the can, and then measuring the build up of activities as radon accumulates in the gas in the can.

You may want to consult your instructor about your strategies.

Do not break the hermetic seal of your can and let the accumulated radon escape before you have extracted all the useful information from the state of things that exists after a long accumulation of radon in the can. Restore the settings of the measurement chain you established in the first session. Use the MCA to record the spectra and, for your convenience in analysis, make whatever fine adjustments of the amplification may be necessary to bring the highest energy peak into the same channel as before.

Record a 30-minute spectrum for comparison with the one you recorded in the first session.

Now proceed with the strategy you have devised to measure the mean lives of as many of the activities as you can.

7.   Liquid Scintillation Detector Experiment

The Beckman scintillation detector consists two photomultiplier tubes (PMTs) that view the flashes of light in the liquid scintillation cocktail contained in a sample vial placed between them. Particle energy dissipated in the scintillator produces a flash of blue light at a rate of about one photon per 30 eV. Some of the light is absorbed by the metallic coating on the inside of the glass window of the PMT causing emission of a burst of photoelectrons. The photoelectrons enter a series of dynode stages (electron multiplier) from which an amplified burst of electrons emerges to be measured as a pulse of charge proportional to the amount of light in the scintillation flash.

Liquid scintillation cocktails are generally xylene or other organic liquid with a small quantity of dissolved complex aromatic hydrocarbon. A liquid scintillator converts into visible light about 1% of the energy lost by an energetic electron traversing the liquid. Thus a 1 MeV electron that stops in a liquid scintillator by virtue of energy loss due to ionizing collisions with carbon and hydrogen atoms yields a flash of several thousand photons ($\sim$ 1 visible photon per 100 eV of energy loss) which is readily detected by a PMT. The liquid scintillator is also an efficient detector of alpha particles. However, the rate of energy loss along the path of a stopping alpha particle is so great that the conversion capacity of the aromatic molecules is saturated and only about 0.1% of the ionization energy is converted into optical photons. **While the commercial liquid scintillator (Ultima Gold) used in Junior Lab is not particularly dangerous, please wear gloves and note the safety precautions listed on the Material Safety Data Sheet (MSDS) posted by the hood.**

Figure 5 is a schematic diagram of the Beckman liquid scintillation spectrometer. It has a light-tight, radiation-shielded counting chamber and associated electronics to supply power and process signals. In the chamber are two PMTs that view a platform on which a sample of liquid scintillator can be lowered for counting. The platform is raised and lowered through a light-tight shutter by an electromechanical elevator. The outputs from the PMTs are amplified and fed to an addition circuit and a coincidence circuit contained in a chassis mounted by the side of the chamber. The output of the addition circuit is a *negative* $0 \sim 1$V pulse proportional to the sum of the amplitudes of the signals from the two PMTs produced by a single scintillation event. The output of the coincidence circuit is a *positive* 5V logic pulse produced whenever two pulses above a certain minimum size arrive nearly simultaneously from the two PMTs. Dark current pulses from the PMTs are random and uncorrelated, so the chances of their occurring in two PMTs within the resolving time of the circuit is small. On the other hand, a faint scintillation event that produces enough light to cause one or more photoelectrons to be ejected from each of the two photocathodes will yield pulses that are simultaneous within the decay time of the phosphor, which is on the order of 10^{-8} sec. Thus the coincidence logic signals are a very sensitive indicator of the occurrence of faint scintillation events, though they do not carry amplitude information.

You will determine the mean life of Po^{218} by measuring the rapid growth (minutes) of its radioactivity in a freshly prepared sample of Rn^{222}, and the mean life of Rn^{222} from the slow decay products. You will have to work rapidly at the beginning of this measurement in order not to miss the early stages in the build up of the Po^{218} activity (you studied how quickly in preparatory question 3). Study the following procedure before you begin. **Make up a data table in your lab notebook to record the times (starts and durations), the**
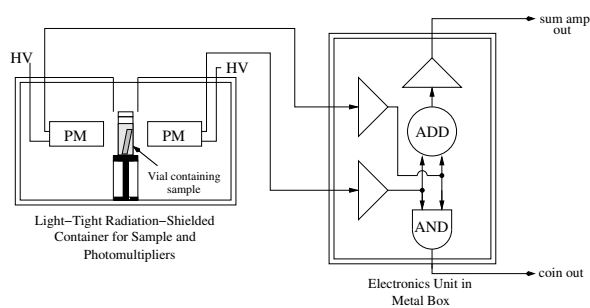
FIG. 5: Schematic diagram of the Beckman instrument for measuring the scintillations from alpha decays in the liquid scintillator.

number of counts, and your comments. You will be using the the Ortec 872 Counter / Timer to produce simple counts of activity in the vial.

7.1.   Measuring Mean Life of Rn^{222} and Po^{218}

This experiment, as explained in the overview section 5.1, should be started on the first day after setting up the "can" to begin accumulating decay products.

Radon is a closed shell atom, the heaviest in the sequence of noble gasses which begins with helium. Formed in the earth's crust by the decay of radium, radon diffuses into the atmosphere to become part of the air we breathe. Radon in the environment is now recognized as the major source of ionizing radiation to the general population. There is a concerted effort by federal and local agencies to mitigate "high" radon levels found in some homes. We place the quotes around "high" to emphasize that the adjective is appropriate only for very long term exposures to the general population. The radon intensities of concern in the environment are measured in picocuries, which is a millionth the source strength of the radioactive sources used in smoke detectors or the calibration sources we use in the laboratory. The radioactivity of the radon sources used in the present experiments are very weak and pose no health hazard.

A radon source is mounted in the back the chemical fume hood as a sealed-Pylon flow-through radium (Ra^{226}) salt cylinder which emits gaseous radon as it decays. Therefore using a series of pumps and valves the gas is safely extracted and made into a liquid scintillation cocktail. The liquid scintillation fluid used, Ultima Gold, which the radon is deposited directly into. This cocktail, or sample, will house all beta and alpha decay events that can be detect via the Beckman counter for this portion of the experiment.

Helpful Note: The maximum activity of radon atoms in equilibrium with one mole of uranium is 6.03×10^{23} $mol^{-1}/\tau_{U^{238}}$ *disintegrations* s^{-1}, *where* $\tau_{U^{238}} = 6.5 \times 10^9$ *yr is the mean life of uranium.*

7.1.1.   Liquid Scintillation Detector: Procedure for Rn^{222} and Po^{218}

Be sure to re-read your answer to prepatory question 3 so that you have a better idea of when to take spectra.

A solution of radon (Rn^{222}) in liquid scintillator will be made for use with this detector. The sample will be hermetically sealed in a glass vial in which the alpha-decay activity of Rn and its shorter-lived decay products can be assessed from time to time over the next several days with the Beckman scintillation spectrometer. To prepare a liquid scintillation sample:

1. Ensure that the radon deposition valve is completely closed (turned all the way to the right).

2. Pump 10 cc (or 10ml) of liquid scintillator from the reservoir (Ultima Gold) into glass vial.

3. Locate the mounted radon source in the back of the fume hood and open both valves (top and bottom)completely to allow for gas flow.

4. Turn on Peristaltic Pump, adjust deposition rate to be between 50-55% and begin pumping Rn gas **FORWARD , or** $>>$.

5. Place radon deposition tubing into prepared scintillation vial and open deposition valve. Bubbling should be seen in the fluid to verify gas flow!

6. Bubble for 30-45s.

7. Shut off deposition valve first then *quickly* seal vial.

8. Continue by shutting off peristaltic pump and close valves (top and bottom) on the radon source in the rear of the fume hood.

To prevent false results due to radon leaking from the vials, it is essential that they be hermetically sealed. You can improve the seal by applying vacuum grease (or vaseline) to the rim of the vial and capping it tightly so the radon does not leak out during the several days required for the measurements. Lower the vial into the counting chamber and immediately start a sequence of measurements with the Counter / Timer, appropriately spaced in time so as to define accurately the build up of the Po^{218} activity. Team work is necessary in order to start measurements in the Beckman spectrometer as soon as the sample vial is closed.

After taking the quick spectra for Po^{218}, think about your preliminary results and how you might obtain improved data on your second run. Make a practice run to familiarize yourself with the procedure and to make any needed adjustments of the electronics. Make a second run for a good set of data. Each team should attempt to get at least two good sets of data.

After you have completed the comparatively rapid series of measurements required for a determination of the Po^{218} mean life, you can turn your attention to the much

more gradual process of the decay of the parent nuclide itself, i.e. Rn^{222}. Since the mean life of radon is several days, you will have to follow the decay of your sample for several days or a week to get accurate results. Here you must overcome three problems. The first is that the beta activities of Pb^{210} and Bi^{210} and the alpha activity of Po^{214} will continue to grow for several hours before they reach the equilibrium condition of being equal to the acitivities of Rn^{222} and Po^{218}. Since you cannot isolate the counts due to Rn^{222}, any rate you measure will be influenced by these other activities. The best thing to do, therefore, is to wait until all the activities are nearly equal (a couple of hours). Then any counts will give you a rate proportional to the Rn^{222} activity from which you can determine the mean life. The other problem is the possible leakage of the radon gas from the vial.

7.1.2. Liquid Scintillation Detector: Analysis for Rn^{222} and Po^{218}

Given the follwing facts:

1. The mean life of Po^{218} is much shorter than that of Rn^{222},

2. The mean lives of the Po^{218} decay products that lead to the production of alpha-active Po^{214} are long compared to the mean life of Po^{218},

3. Some Po^{218} may be dissolved in the liquid scintillator along with Rn^{222},

one can show that the measured counting rate $r(t)$ is represented to a good approximation by a function of the form

$$r(t) = a - be^{-t/\tau} \qquad (7.1)$$

where a, b and τ are constants. Thus

$$\ln[a - r(t)] = \ln b - t/\tau \qquad (7.2)$$

The constant a is the total counting rate that is approached asymptotically by the two alpha activities at times much longer than the mean life of Po^{218}, but still much less than the mean life of Rn^{222}. It can be estimated from an examination of a plot of r vs. t. A plot of $\ln[a - r(t)]$ vs. t during the first few minutes should be nearly a straight line with a slope of $-1/\tau$ where τ is the mean life of Po^{218}. (Note: as r approaches a, statistical fluctuations will cause wild gyrations or worse in the values of $\ln[a - r]$, so the most useful information about τ must be derived from the early part of the rising curve of activity.

Additional questions:

1. Describe how the pulse height spectrum changes with time.

2. Identify the part of the pulse height spectrum due to the beta decays of Pb^{214} and Bi^{214}.

3. What is the effect of the accumulating radionuclide Po^{210} on your results?

8. Measuring Lifetimes of Short-Lived Species

A technique particularly well suited for determining the mean life of very short-lived species is to use the decay event that gives birth to a particular nuclide as a start signal for a time-to-amplitude converter (TAC), and the decay event of the nuclide as the stop signal. The distribution of time intervals between the start and stop signals is the decay curve of the nuclide. This method will be used to measure the mean lives of Po^{214} and Po^{212}. Po^{212} may be measured using the output of the Beckman's coincidence circuitry as described below.

8.1. Determination of the Mean Life of Po^{214}

Po^{214}, produced by the beta-decay of Bi^{214}, has mean life less than 300 microseconds. Its decay curve is measured with the help of the Time-to-Amplitude Converter (TAC). During the third day of the experiment, you will determine the mean life by measuring the distribution in duration of the time intervals between the scintillation pulse produced by the beta decay of a Bi^{214} nucleus into a Po^{214} and the subsequent scintillation pulse produced by the 7.6 MeV alpha particle from the decay of the Po^{214} nucleus.

8.1.1. Procedure

Use an eluted radon source that has aged sufficiently to bring the rate of Po^{214} decays up near to equilibrium with the rate of Rn^{222} decays. Set up the electronics as shown in Figure 6. An inverter is required because the TAC is wired to only trigger on negative signals.

The +5 VDC logic pulses from the coincidence output from this timing measurement offer the critically important advantage that they are produced only when pulses occur simultaneously in the two phototubes, as mentioned above. In order to detect with reasonable efficiency, the weak pulses due to the beta decays that preceded the alpha emissions, it is necessary to accept small scintillation-produced pulses, which, in the absence of a coincidence requirement, would be lost in the forest of dark current pulses created by the thermionic electrons spontaneously and randomly emitted by the photocathodes of both tubes. The inverted +5 VDC logic pulses are fed directly to both the stop input of the Ortec TAC and to the delayed gate generator. The negative pulses of the delayed gate generator are in turn fed to the start input of the TAC. The TAC range should be set to several
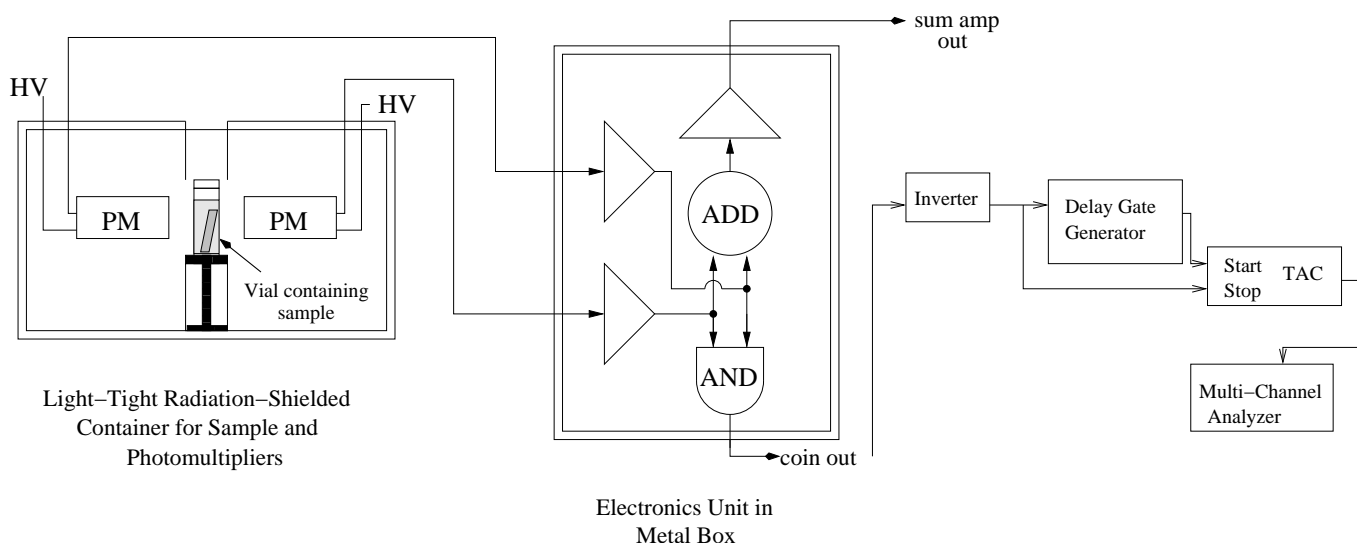
FIG. 6: Experimental arrangement for measuring the short mean life of Po^{214}. The inverter is necessary because the TAC will take only negative signals as inputs. Scintillation light from a decay event strikes both PMTs and causes simultaneous pulses that trigger the coincidence circuit.

multiples of the expected nuclide lifetime. The output of the TAC plus MCA combination records the time interval between each delayed start pulse and the next stop pulse, provided the interval is within the allowed range of the TAC. Delaying the start pulse relative to the stop pulse by several microseconds prevents the timing action of the TAC from being stopped by the same pulse that starts it. A high delay will result in the loss of events, however, so make sure you keep it suitably low. Calibrate the TAC with pulses from the Time Calibrator, though you should note that the longest range possible is only about 10% of the TAC's range. The TAC and MCA are both very linear devices however, and you can extrapolate this calibration throughout the entire range of the MCA display. In a related measurement of the mean life of Po^{212}, we employ a different detector combination to detect the birth and death of the Po^{212} nucleus. The sensitive layer of the silicon detector is too thin to yield a usable start pulse from the lightly-ionizing electrons emitted in the beta decay of the precursor bismuth nuclei. Therefore it is necessary to employ a separate detector, a plastic scintillation detector with a thin window, to detect the beta-decay electrons that signal the birth of the short-lived polonium nuclei.

9.   Measuring the Mean Life of Po^{212}

9.1.   Plastic Scintillation Counter

Beta-decay electrons emitted by the atoms plastered onto the silicon detector surface will be detected by a scintillation detector with a plastic scintillator in an arrangement shown schematically in Figure 7. The plastic scintillator is covered with a thin aluminum foil which is

readily traversed by the beta-decay electrons. Information about the wiring and operation of a photomultiplier can be found in Melissinos [3].

9.2.   Time-to-Amplitude Converter/Single Channel Analyzer (TAC/SCA)

The Ortec Model 567 Time-to-Amplitude-Converter (TAC) is used to convert the time intervals between pulses at the "start" and "stop" inputs into the amplitudes of output pulses. If a start pulse is generated in the plastic scintillator by a beta decay event heralding the birth of the radioactive nuclide Po^{212}, and the stop pulse is generated in the silicon detector by its decay, then the distribution in amplitude of the TAC output pulses will be proportional to the distribution in duration of the lifetimes of the Po^{212} atoms.

The polarity of the start and stop pulses is set using internal jumpers and the threshold for the negative and positive positions are ~ -400mV and ~ 2V respectively (it is currently set to negative and will stay that way throughout the experiment). The SCA feature of the Ortec 567 is enabled by flipping the toggle switch adjacent to the output jacks. It will inhibit the TAC output except for pulses with amplitudes that fall within the "window" set by the lower and upper discriminator dials. Within that window the TAC output remains proportional to the start-stop time intervals. For each pulse in the window, a +5 VDC logic pulse is generated at the SCA output. In this part of the experiment, it may be useful to use the SCA logic pulse to gate the MCA in an analysis of the amplitudes of pulses from the 'sum' output of the Beckman scintillation detector in order to identify which of the alpha particle groups is associated
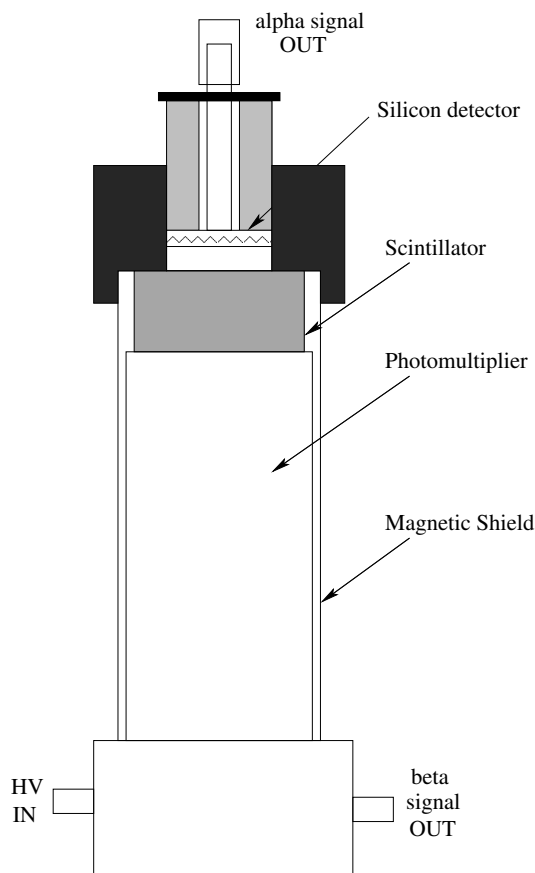
FIG. 7: Schematic diagram of the scintillation counter with the silicon detector in place.

with the very short lived ($\sim 100\mu$s) nuclide.

9.3.   Procedure

The mean-life of Po^{212} is very short. However, it can be measured by taking advantage of the fact that each birth of a Po^{212} atom is signaled by emission of an energetic electron in the beta-decay of its parent Bi^{212} nucleus. The setup employs a scintillation detector covered by a thin aluminum foil that can be penetrated by most of the decay electrons. The silicon detector must first be plated with sufficient precursors of Po^{212} by exposure to radon gas in a can with the uraninite with the plating voltage source connected ($>\sim$ 1 day). Then it is placed in the well of the scintillation counter so that electrons emitted downward in the decay of the precursor Bi nucleus will excite the scintillator. If the subsequent decay of the daughter Po nucleus produces an alpha particle going upward, the silicon detector will produce a pulse of the characteristic energy of the alpha decay. The scintillation pulse is used to start the timing sequence of the TAC, then the silicon pulse is used to stop it. The output is recorded by the MCA, from which the mean life can be determined.

The rate of accidentals during the short lifetime of Po^{212} is so small that no pulse-height selection of the alpha pulses is necessary. Thus the setup shown in Figure 8 should work.

Recommended settings:

- **Canberra 2021 Spectroscopy Amplifier**: coarse gain = 100, fine gain = 1, input polarity = +, shaping time constant = 2.0 μs, mode = ASYM, threshold = auto, output polarity = -

- **Ortec 478 Power Supply**: PMT Bias = +2000 VDC

- **Canberra 814 PAD**: coarse gain = 64, fine gain = 10, amplifier input = +, preamp = IN, input to the PREAMP IN, output from DISC OUT.

- **Ortec 567 TAC**: Set for a full scale timing range of 2μs, set the TAC inhibit = OUT

You should set the discriminator on the PAD to eliminate the triggers from the PMT due to noise.

Caution: Cover the scintillation detector with several layers of black cloth to stop light leaks.
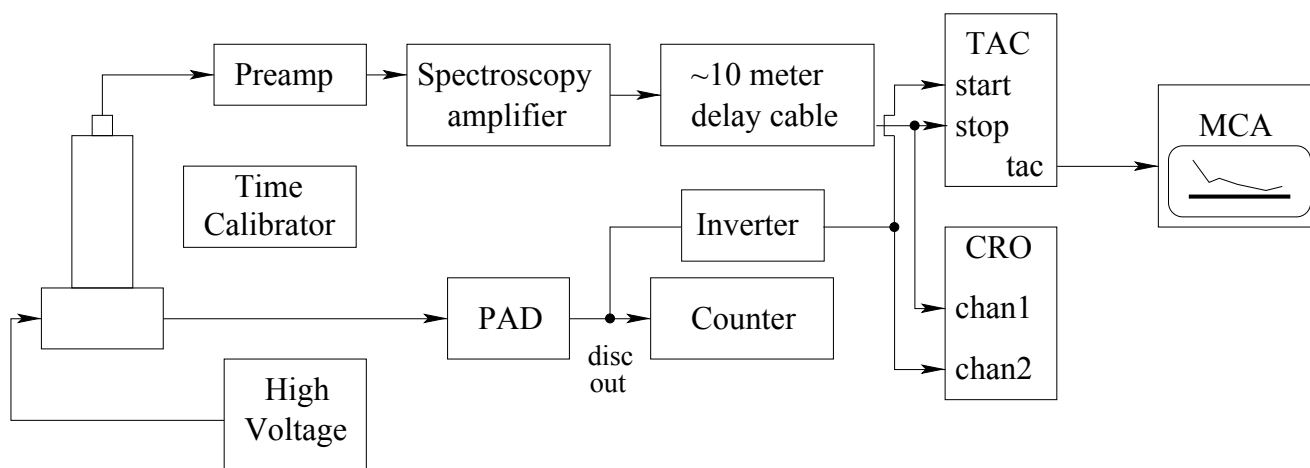
FIG. 8: Setup for measuring the decay of Po^{212}. The time calibrator puts out negative pulses so the input switch on the spectroscopy amplifier must be changed to negative for the calibration. The TAC is set to accept negative signals which should have amplitudes greater than 2 volts.

10.   Analysis

- Identify the parent nuclides in the uraninite.

- Identify all the nuclides whose alpha decays you have observed.

- Explain the shapes of the alpha peaks, especially the Po^{212} peak.

- Plot all the decay data and fitted decay curves, and estimate the mean or half-lives with errors.

11.   Determination of the Energy-Mean Life Relation

The bottom line of this experiment is in the title: The Quantum Mechanics of Alpha Decay. With the data in hand on the energies and lifetimes of four nuclides of the uranium family, you can display the energy-mean life relation and contemplate the extraordinary dependence of the decay rate on the barrier height and its explanation in terms of the quantum theory of barrier penetration. Be sure to re-read Section 3.1 when performing this analysis.

The analysis of your data on energies and mean lives should be carried out with regard for the statistical un-certainties. You should be able to determine the relative energies of the alpha particle groups from the silicon barrier detector data with uncertainties of less than 5% and the corresponding mean lives to within 10%.

Plot the log of the mean lives versus the alpha particle energies. Derive from your data a formula that expresses approximately the Geiger-Nuttall relation between mean life and energy.

Compare your experimental results with the expected relation from barrier penetration theory.

12.   Some Possible Theoretical Topics

Beyond the primary references cited earlier in the labguide, there are many references to aid you in your discussions of radioactivity, alpha and beta decay, etc. Some include: [9–13].

- Barrier penetration and alpha decay.

- The Bateman equations.

- The relation between A and Z for nuclei stable against beta decay.

- The energy loss of charged particles in matter.

[1] Tech. Rep., Nuclear Evaluation Lab and Korea Atomic Energy Research Institution and Brookhaven National Laboratory (2002), URL http://atom.kaeri.re.kr/ton/.

[2] D. R. Lide, ed., *CRC Handbook of Chemistry and Physics* (CRC, 1995), 75th ed.

[3] A. Melissinos, *Experiments in Modern Physics* (Academic Press, 2003), 2nd ed.

[4] R. Rhodes, *The Making of the Atomic Bomb* (Simon and Schuster, 1986).

[5] R. Gurney and E. Condon, Nature **122**, 439 (1928).

[6] R. Gurney and E. Condon, Physical Review **33**, 127 (1929).

[7] A. French and E. Taylor, *An Introduction to Quantum Physics* (Norton, 1978).

[8] R. Evans, *The Atomic Nucleus* (McGraw-Hill, 1955).

[9] D. Bohm, *Quantum Theory* (Prentice Hall, 1951).

[10] S. Gasiorowicz, *Quantum Physics* (Wiley, 1996), 2nd ed.

[11] R. Liboff, *Introduction to Quantum Mechanics* (Holden-Day, 1980).

[12] I. Perlman and F. Asaro, Annual Review of Nuclear Science **4**, 157 (1954).

[13] T. Kohman and N. Saito, Annual Review of Nuclear Science **4**, 401 (1954).

[14] Tech. Rep., EG&G Ortec (2003).

Acknowledgments

APPENDIX A: EQUIPMENT LIST

Manufacturer	Description	URL
Canberra	PIPS α-particle detector	canberra.com
Canberra 802	Scintillation Counter	canberra.com
Canberra 2006	Charged Particle preamp	canberra.com
Canberra	Amplifier	canberra.com
Ortec	Inverting Amplifier	ortec-online.com
	Constant Fraction Disc.	
	Coincidence Unit	
Ortec	Multi-Channel Analyzer	ortec-online.com

APPENDIX B: .JOB FILE TUTORIAL

This section attempts to summarize some of the important commands used in `.job` files to control the Ortec MCA. It summarizes what can be found in detail in the Ortec MCA manual, reference [14].

While one can manipulate the MCA manually, `.job` files are powerful tools that allow students to acquire data without constantly changing settings in the program. It is highly suggested that students take full advantage of this functionality in their studies.

1. .job File Glossary

CLEAR. Clears the data for the selected detector.

```
REM Brian A. Wilt – 8/17/2006
REM Javier Duarte – edited 11/30/2010
REM Sample .job File
```

REM <remark>. Remark (comment).

SET_BUFFER. Sets the buffer as the active detector. Equivilent to `SET_DETECTOR 0`.

SET_DETECTOR <0|13>. Chooses the active detector. The buffer detector is 0, and the alpha decay detector is 13.

SET_PRESET_CLEAR. Clears the preset values for when to stop recording. Accessed in Maestro via `Acquire` → `MCB Properties` → `Presets`.

SET_PRESET_COUNT <numcounts>. Sets the ROI number of counts. Stops taking data when the number of counts in any ROI channel reaches this value.

SET_PRESET_INTEGRAL <roiintegral>. Sets the ROI integral. Detector stops taking data when the sum of all counts in all channels marked with ROIs reaches this value.

SET_PRESET_LIVE <livetimesec>. Sets the *live time* for it to take data. Indicates amount of time the detector was available to accept another pulse (not busy). *Real time* minus *dead time*.

SET_PRESET_REAL <realtimesec>. Sets the *real time* for it to take data. Indicates elapsed time on a clock.

LOOP <numtimes> ... END_LOOP. Loops the indicated number of times.

WAIT <intervalsec>. If called immediately after `START`, waits until spectra is finished. Other intervals can be specified as an argument with units of seconds.

DESCRIBE_SAMPLE "<description>". Associates spectra with indicated description. Description should be enclosed in double quotes. ??? indicates the loop number.

SAVE "<filename>". Saves file to indicated file name. File name should be enclosed in double quotes. ??? indicates the loop number.

2. .job File Example

This `.job` file takes 30 spectra, each lasting 50 seconds, and separated by 10 seconds each. This file can be found at `labguides/45.alphadecay/pipstestrun2010.job` in the `8.13` locker, or on the local machine via `C:\User\demojob`.

```
REM Takes 30 samples for 50 seconds, separated by 10 seconds


REM LOOP for 30 minutes, taking 50 second spectra
LOOP 30
    REM Sets for the alpha decay detector
    SET_DETECTOR 1
    SET_PRESET_CLEAR

    REM Depending on how you want to measure when to
    REM   stop, you can use SET_PRESET_LIVE, SET_PRESET_REAL,
    REM   SET_PRESET_COUNT, or SET_PRESET_INTEGRAL.
    SET_PRESET_REAL 50
    CLEAR
    START

    REM WAIT by itself waits until the spectrum is finished
    WAIT 60

    REM Save in my Athena directory, the I:\
    SAVE "I:\8.13\alphadecay\data\pipstestrun\specloop_???.spe"
    CLEAR
END_LOOP
```

APPENDIX C: MATLAB IMPLEMENTATION

A helpful MATLAB script can be found as `bate.m` under the `labguides/45.alphadecay` directory in the 8.13 locker on Athena. It returns a matrix of size `[length(N0), length(t)]`. The last lines can be commented and uncommented to return either the amounts of the nuclides in atoms or the activity in Bq (events / sec):

```
function R = bate(t, lambda, N0)
% Calculates Bateman Equations
%   t: time vector
%   lambda: decay constants vector
%   N0: initial conditions vector
%      (number of each nuclide)
%
% R: size(length(N0),length(t))
%   matrix containing either activity or
%   amount for each nuclide in N0
Lambda = -diag(lambda) + ...
    diag(lambda(1:(end-1)), -1);
[V, D] = eig(Lambda);

% MATLAB trickery to make it go in t
%   step-by-step without a for loop,
%   equivalent to Vexp(Dt)V^-1 N0 for each t
Nt = V * diag(inv(V) * N0) * ...
    exp( D * repmat(t, length(N0), 1) );

% Return amount of each isotope
%   as a function of time
% R = Nt;
```

```
% Activity = Amount of isotope *
%   decay constant (in Bq, evt / sec)
R = diag(lambda) * Nt;
```

For example, to simulate a three-isotope decay chain with half lives $\tau_{1/2} = 10^5$ sec, 10 sec, and 10^2 sec, one would input:

```
% 15 minutes
t = 0 : 1 : 900;

% All the half lives, in seconds
tauHalf = [10^5; 10; 10^2];
% From half lives to decay constants
lambda = ( tauHalf / log(2) ) .^ (-1);

% Start with one mole of tau_{1/2} = 10^5
N0 = [6.0221415 * 10^23; 0; 0];
R = bate(t, lambda, N0);
```

and a plot of the output would look like figure 2. This file can also be found in that directory under `bate_ex.m`.

APPENDIX D: NATURALLY OCCURRING RADIOACTIVE CHAINS

See figures **??**, **??**, and **??** for naturally occurring radioactive chains.
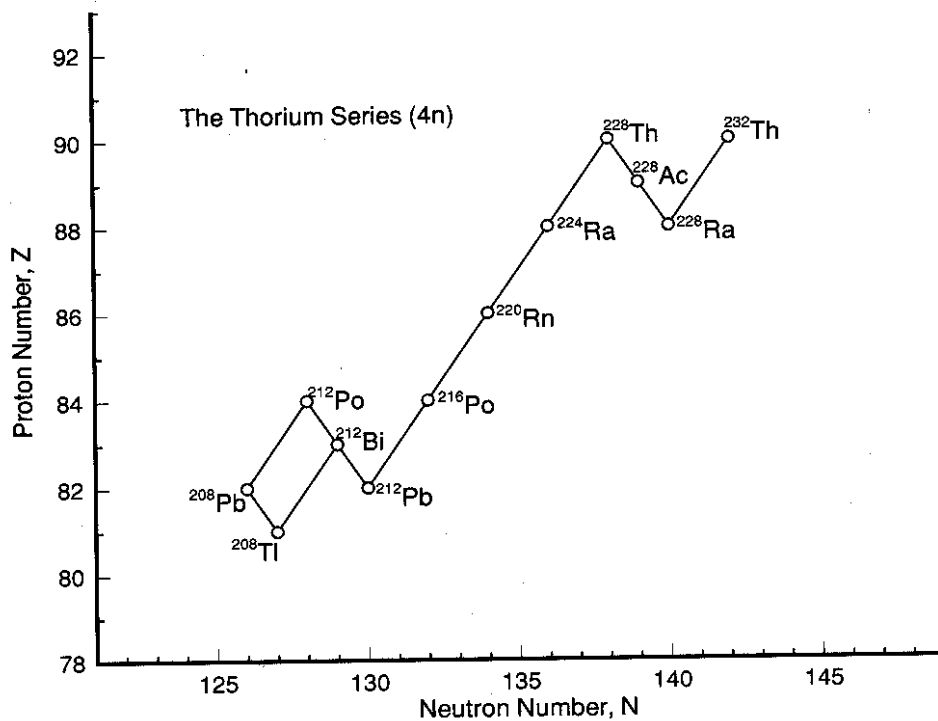
FIG. 9: The naturally occurring "Thorium" series. From "Nuclides and Isotopes, 15th Edition", Reference [1].
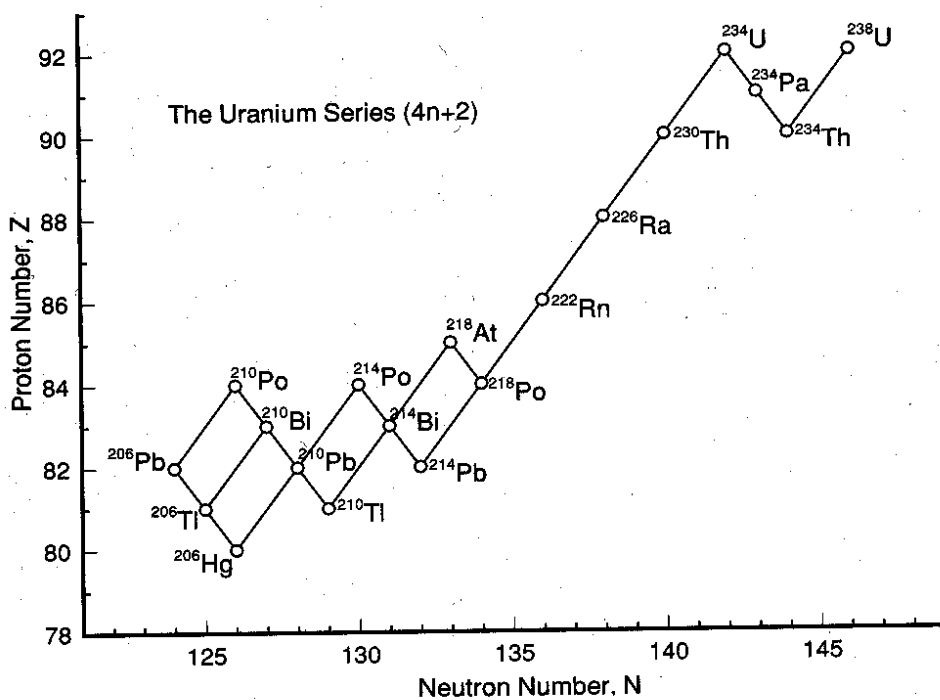

FIG. 10: The naturally occurring "Uranium" series. From "Nuclides and Isotopes, 15th Edition", Reference [1].
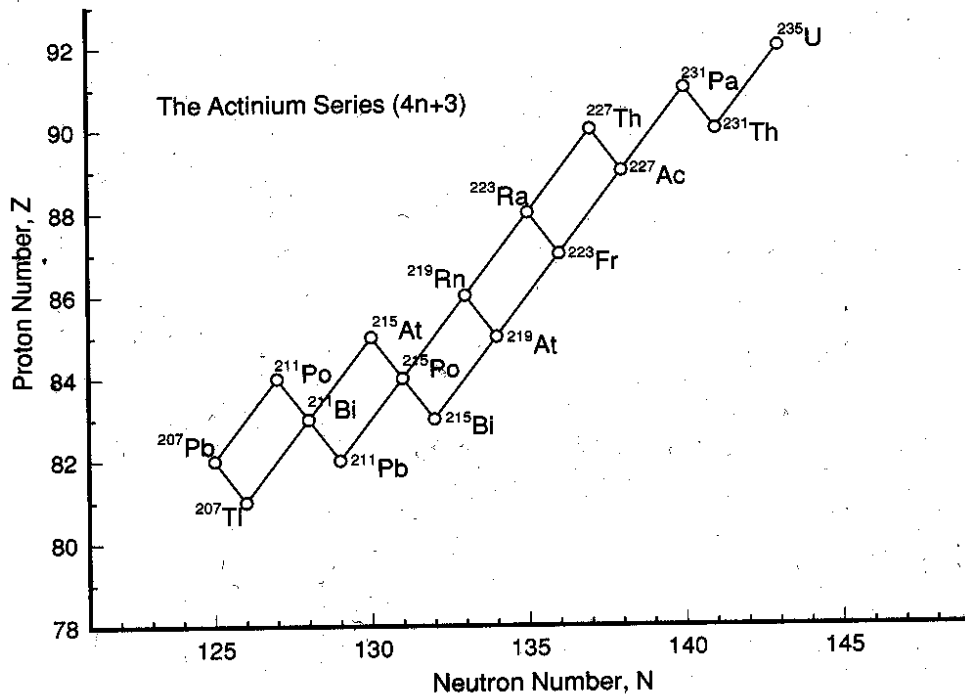
FIG. 11: The naturally occurring "Actinium" series. From "Nuclides and Isotopes, 15th Edition", Reference [1].

21-cm Radio Astrophysics

MIT Department of Physics
(Dated: September 5, 2011)

We use a computer-controlled parabolic antenna, located on the roof of Building-26 at MIT, to collect radio waves at 21 cm from the sky. In the first part of the experiment, we measure the brightness temperature of the sun at 21cm. In the second part of the experiment, we observe the Doppler spectrum of the 21-cm hyperfine line of interstellar atomic hydrogen in various directions in the plane of the Milky Way galaxy. These spectra enable us to measure the rotation-curve and deduce certain features of the spiral-arms of the Milky Way.

1.   PREPARATORY PROBLEMS

1. Explain the origin of the 21-cm line of atomic hydrogen.

2. Describe the size and shape of the Galaxy, giving our position from the center in light-years and parsecs (pc). What is the maximum Doppler shift you can expect to observe in the 21-cm line?

3. The parabolic dish antenna used in this experiment has a diameter of 7.5 feet. Suppose it is set so that a source of 21-cm radio emission drifts through its field of view. Plot the signal strength at the output of the diode detector as a function of angle from the center of the field of view.

4. Explain the 21-cm spectrum at $150°$ and $60°$ as shown in Figure 7.

5. Explain the signal chain in this experiment (e.g. how the hardware and software serve to convert the signal received by the telescope into a display of signal strength versus frequency.

2.   Progress Check for 2nd Session

What is the approximate temperature of the sun at 1420 MHz? Plot the power spectrum of galactic hydrogen at 40 degrees galactic longitude and identify all the salient characteristics of the spectrum. Does it agree with Van de Hulst's observation in Figure 7?

3.   General Structure of the Milky Way

This description of the Galaxy is a summary of the material contained in Galactic Astronomy by Mihalas and Binney [1], a very useful reference for this experiment. It also contains in Chapter 8[1] a detailed presentation of the theoretical basis for interpreting the data on galactic kinematics obtained from observations of the Doppler profile of the 21-cm line. Another very nice introduction to the structure of the Milky Way is on-line at http://cassfos02.ucsd.edu/public/tutorial/MW.html. Other useful references for this lab are [2–8].

The Sun is one among the approximately 10^{11} stars that comprise our Galaxy. From a distant vantage point this vast array of stars would appear as a rotating spiral galaxy. Detailed examination of the Milky Way reveals a spheroidal component and a concentric disk component. The spheroidal component consists mostly of small ($M < 0.8 M_\odot$), old (10-15 billion years) stars of which most are concentrated in a central "bulge" with a diameter of ~ 3 kpc and the rest are distributed in an extensive "halo" that extends to a radius of 30 kpc or more. The disk component is a thin, flat system of stars, gas and dust $\sim$200 pc thick and $\sim$30 kpc in radius. The disk stars are extremely heterogeneous, ranging in age from new-born to the age of the halo stars, and with masses from ~ 0.1 to $\sim 100 M_\odot$.

The solar system is imbedded in the disk component at a distance of 8.0±0.5 kpc from the center at which radius the circular motion of the Galaxy has a period of approximately 2×10^8 years.

Between the stars of the disk is the interstellar medium (ISM) of gas and dust comprising approximately 10% of the total mass of the disk. The gas consists primarily of hydrogen and helium with a mass density ratio of 3 to 1 and an average total number density of about 1 atom cm^{-3}. The dust is composed mostly of graphite, silicates and other compounds of the light and common elements in microscopic grains containing a small fraction of higher-Z elements, primarily iron.

Comparison of visible spectra from the stars with the line spectra of elements in the laboratory yielded information on the composition and temperature of stars, and measurement of wavelength shifts due to the Doppler effect provided determinations of radial velocities which revealed the dynamical properties of systems. Most of the interstellar medium, however, is too cold to radiate in the visible part of the spectrum and its properties remained largely unknown until fifty years ago. Then, in the midst of World War II, a young Dutch astronomer, H. van de Hulst, examined the theoretical possibilities for detecting radio waves from the ISM, which would permit

---

[1] This chapter can be found on 8.13 website.

measurements of physical conditions and radial motions like those available in the visible spectrum. He predicted that the spin-flip transition of atomic hydrogen would produce such a line at a wavelength near 21 cm, and that the unique conditions of low density and temperature in interstellar space are such as to allow time for hydrogen atoms, excited by collision to their hyperfine triplet state, to decay by radiation to the singlet ground state.

The line was observed in 1951 by Ewing and Purcell at Harvard, by Christiansen in Sydney, and by Muller and Oort in the Netherlands. Radio observations at 21 cm soon became a major tool of astronomy for exploring and measuring the structure of our Galaxy and many distant galaxies too.

Atomic hydrogen is the principal constituent of the interstellar medium, and one of the most interesting tracers of galactic structure. Whereas visible light is heavily obscured by dust in the ISM, radiation at 21 cm suffers little absorption.

Measurements of the Doppler shifts of the frequency of the 21-centimeter line determine the radial components (projections onto the line of sight) of motions of the interstellar medium. Analysis of the Doppler shifts in various directions around the galactic plane (i.e. around the Milky Way) reveal the kinematic structure of the galaxy, e.g., the tangential velocity of the matter in the Galaxy as a function of the distance from the center, and, by implication, the geometry of the spiral arms.

4.   Possible Theoretical Topics

While doing this experiment, you might find it useful to have a basic know-how about the following:

1. Hyperfine splitting of the hydrogen ground state.

2. Radiative processes in the sun.

3. Antenna theory.

4. The structure and dynamics of our Galaxy.

5. Radiative transfer.

5.   Some Jargon used in Experiment

Please look up the definitions of the following terms before you do the experiment.

1. Brightness Temperature

2. Antenna Temperature

3. Antenna Pattern or Antenna Function

4. Rotation Curve

5. Local Standard of Rest

6. Local Sidereal Time

7. Galactic Longitude

8. Azimuth and Elevation

6.   EXPERIMENTAL APPARATUS

Many details regarding the antenna, calibration and experimental procedures, and documentation for the software can be found on the Junior Lab Student Wiki and the Junior Lab Website.

6.1.   Hardware

6.1.1.   Antenna & Motors

The small radio telescope, SRT, is a 7.5 foot diameter parabolic dish and receiver designed by Haystack Observatory and sold by Cassi Corporation. Complete specifications for the antenna, mount and receiver are available under the "Antenna and Mount Information" link at the SRT website (http://www.haystack.mit.edu/edu/undergrad/srt/). It has a focal length of 85.7cm. It has a beam width of approximately 7.0 degrees.[2]. The dish is mounted on a two-axis azimuth/elevation mount. It is supported by an aluminum frame constructed from C/Ku band mesh that reflects all incident microwave energy if the surface holes are less than 1/10th of the incident wavelength. The system is controlled using a computer running a java applet that communicates with the controller, which contains a Basic-Stamp microcontroller. The microcontroller in turn controls the motor functions. A very basic block diagram of the system is shown in Fig. 1.
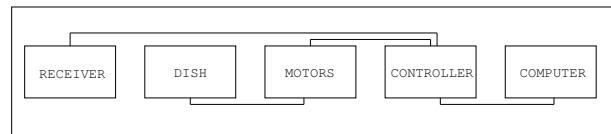

FIG. 1: A basic block diagram of the SRT

6.1.2.   Receiver

The SRT uses a phasing-type single-sideband scanning receiver. Fig. 2 shows a block diagram of the radio receiver and subsequent signal processing stages. Radio power arriving from the sky is focused by reflection to

————

[2] The first minimum of the antenna diffraction pattern is given by $1.22\lambda/d \approx 7°$.

the antenna feed horn. Signals then pass through a band pass filter, a low noise pre-amplifier and a mixer. The signal is digitized and sent back to the controlling computer over a serial RS-232 link. The central frequency of the synthesized local oscillator (LO) used in the mixer is user selectable from within the JAVA program. This permits the investigator to look at different spectral regions around 1420 MHz.

Digital Receiver for SRT   acer feb 2002   \mri\srtdig

FIG. 2: A block diagram of the SRT Receiver

FIG. 3: A picture of the antenna feedhorn

1 - L-Band probe

2 - Low Noise Amplifier

3 - Universal Male F to F Coupler

4 - Receiver mounting bracket

5 - Video Port - Analog signal

6 - Power and Communication - Digital Signal

7 - Band Pass Filter

8 - Feed Horn Extension

Signals pass from the feed horn to the low noise amplifier. The LNA provides a 24dB gain whose output passes through a 40MHz bandpass filter that prevents band signals from producing intermodulation in the image rejection mixers. Mixers are circuit elements that form the product of two analog waveforms (in NMR these elements are also called "phase detectors"). It's two inputs and output are related by the trigonometric relationship:

$$\cos \omega_1 t \cos \omega_2 t = \frac{1}{2} \cos (\omega_1 + \omega_2)t + \frac{1}{2} \cos (\omega_1 - \omega_2)t. \tag{6.1}$$

Note that both sum and difference frequencies are generated in a mixer. For our application, we band-pass filter the output and throw away the sum frequency contribution. See the "Receiver Information" link on the SRT website for more information.

6.1.3. Electronic Noise Calibration

Electronic noise calibration is performed using a noise diode, whose intensity and spectral distribution is approximately equivalent to a 115 Kelvin blackbody.

Compare this to the known signal strengths of some radio sources in the sky, shown in Figure 4.

The electronic noise calibrator is a diode (Noise/Com NC302L) connected to a small dipole antenna attached to the center of the SRT dish. A small (6mA) current is sent through a controlled bulk avalanche mechanism, resulting in a wide band of frequencies. The dipole emits the signal which is detected by the receiver. To generate the correct wavelength signal, the dipole was fabricated to be 1/2 wavelength, or approximately 10.5 cm. To minimize signal from behind the dipole, the poles are set 1/4 wavelength, or approximately 5.25 cm, above the circular plate at the center of the SRT dish.

In practice, to calibrate the telescope you just have to point the antenna at an empty part of the sky, change the frequency to the hydrogen frequency, and hit the 'Calib' button on the software interface. The software outputs a single number called T_{sys} which represents the background noise level in the device.

The software measures the ratio of the received power when the noise diode is turned on and then off again. Complete details of the SRT calibration are available at http://www.haystack.edu/edu/undergrad/srt/receiver/SRT_calibration.html and http://web.mit.edu/8.13/www/calibrator_report.pdf.

6.2. Software

The SRT control software interface is run from a computer which communicates with the ground controller in 26-630. The ground controller serves as the interface between the computer and the antenna stepper motors as well as the digital receiver located next to the antenna feed. RS-232 is used to send commands to the motors and to receive back the digitized spectral temperatures from the receiver[3]. The ground controller should be left ON so that students can remotely operate the dish from 4-361.

———

[3] Full details and schematics of the ground controller are available at http://www.haystack.edu/edu/undergrad/srt/receiver/schemgndctl2.pdf
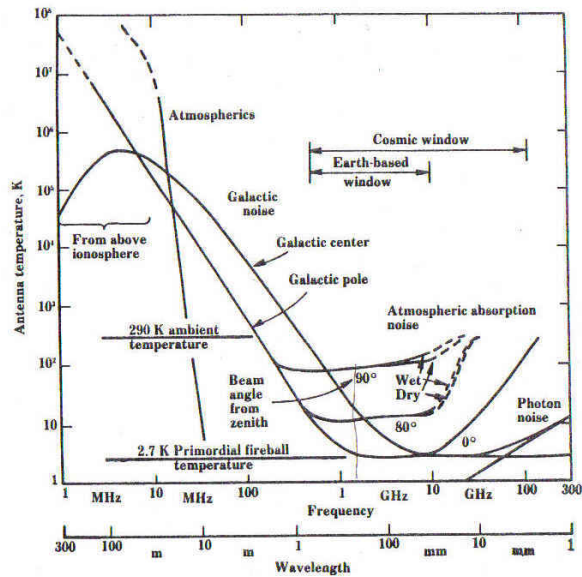
Kraus, RADIO ASTRONOMY, 2nd ed.

Fig. 8-6. Antenna sky noise temperature as a function of frequency and angle from zenith. A beam angle (HPBW) of less than a few degrees and 100 percent beam efficiency are assumed. (*After Kraus and Ko*, 1957, *cosmic noise between* 10 MHz *and* 1 GHz; *Penzias and Wilson,* 1965, *cosmic noise above* 1 GHz; *Croom*, 1964, *atmospheric noise*; *CCIR,* 1964, *atmospherics*; *and Radio Astronomy Explorer Satellite* RAE-2, *Novaco and Brown, cosmic noise below* 10 MHz.)

FIG. 4: Noise Temperature versus angle from zenith. Taken from Kraus, 2nd Edition.

A printed copy of the **SRT Manual** is located next to the computer in 4-361 and is also available online on the Junior Lab Wiki. This manual is very helpful for understanding how to work with the software.

Please take a while to look at the panel on the right-hand-side of the software window. Familiarize yourself with the information that is shown there.

The SRT is continually acquiring and processing RF signals incident upon the dish. The upper right plot in the software window shows individual power spectra updated every few seconds. The plot to the left in RED, shows an integrated power spectrum which may be cleared by pressing the "CLEAR" button.

It is convenient to check the system by generating a test signal at 1420.4 MHz. This is done with the Marconi RF synthesizer. Turn the device on, press the "RECL" button, then choose the first setting (enter '01'). This will set the generator to produce an RF signal at 710.2 MHz, which will also cause the antenna to emit the first harmonic, namely the desired 1420.4 MHz line. Press the "CARRIER ON/OFF" button to toggle the signal on and off. During this calibration, you can point the telescope at any clear part of the sky (avoid buildings – they emit and reflect all manner of infrared). Make sure that you don't leave this synthesizer on except for brief tests and system calibrations, because it will interfere with any other 21 cm experiment nearby.

You can execute commands via the toolbar located at the top of the console. Clicking on any of these but-tons either initiates an automatic response or the software waits for text input by the user.

Azimuth and elevation locations are set using the Horizon Coordinate system. Azimuth and elevation are entered in degrees. The controller moves the telescope to the required position. If "tracking mode" is on (button text is YELLOW), when the telescope reaches the position, the controller continues to move the telescope to compensate for the Earth's rotation so as to keep the telescope pointing to the specified position in the sky. To turn tracking off, simply click on the button and it should turn RED.

Try the following to get started:
Enter "180 40" in the text window and then press the Azel button. The dish should slowly move to point due south. Press STOW to return the dish to it's "parked" position at Azimuth=95°,Elevation=4°. Press the "RECORD" button to stop writing to the log file and open it up using a text editor.

It is useful to begin a log file ('.rad' file) which provides you with a continual record of your experiment. You can do this using the RECORD button. Hitting the record button again will cause the recording to stop.

Instead of using individual buttons from the toolbar, in some parts of the experiment it is useful to write a script (a '.cmd' file) and load the script to be run. Please see the SRT manual for sample scripts.

The program calculates the Local Sidereal and Universal Time based on the computer clock settings within the information sidebar on the right-hand side. **Since Universal Time = Eastern Time + 5 hours (under Standard Time) and = Eastern Time + 4 hours (under Eastern Daylight Savings Time), you must make sure the box "Automatically adjust clock for daylight savings" is checked when setting the computer's clock.** It also indicates the antenna direction in both Equatorial (RA and DEC) and Galactic ('l' and 'b').

When turning on the system, pay special attention to any error messages that may appear within the Message Board below the Total Power Chart Recorder. They may indicate that the system has failed to communicate through the coaxial cable (i.e. gnd 0 radio 1). If movement of the dish stops prematurely, "antenna drive status.." or "lost count" may appear in the Motion Status Display Area. If this occurs please turn off the control system (which in turn ends motor power) and have a technical staff member take a look at the motor drive gears. Be sure to return the dish to the stow position each time before powering down and quiting the java applet.

7. Experimental Procedure

To prepare yourself for these measurements, start by reading the Haystack 'SRT Projects' link on the SRT wesite.

First of all, set the frequency to "1420.4 4" in order to set the bandwidth as wide as possible to reduce noise variations and calibrate the system temperature T_{sys}

7.1.   The Sun's Brightness Temperature

Do an "npoint" scan of the Sun. By clicking on the "npoint" button, a series of measurements surrounding the sun in a 5×5 grid are made with the step size set by the antenna beamwidth defined in the "srt.cat" file. The default value for the beamwidth is 5°. The measured power/temperature at each of these grid points is displayed just above the text input box and at the completion of the scan, a 2-D contour plot of the grid is displayed in the graph box at the top of the page. Information about the sweep is then displayed in the information sidebar. The telescope offsets are also adjusted so as to point the dish to the maximum observed signal within the sampled region.

The "npoint" scan is also useful for verifying the targeting accuracy of the system. If the computer clock is set incorrectly or the local latitude and longitude have been inadvertently changed, the sun will NOT appear well centered in this gridded scan. See for example, Figure 5.
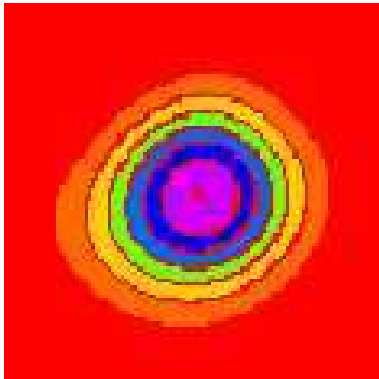

FIG. 5: Typical result from an "npoint" scan. The contour plot is generated from a 5×5 series of measurements spaced by 1/2 the antenna beamwidth as specified in the srt.cat text file within the CassiSRT folder.

The "npoint" scan will focus the dish at the maximum temperature location for the sun when completed. Pointing corrections should be set to the location of peak intensity before continuing the observation session.

To manually specify offsets, enter the offset in the command text area.

```
enter azimuth(degrees) elevation(degrees)
Press ''offset'' button
```

If you enter -5 -5, the effect is that the npoint plot will move right and up.

Do an azimuth scan and an elevation scan of the Sun. For this, you will need to write a .cmd file specifying the various offsets from the Sun that you want to take data. For example, these offsets may range from $-30°$ to $30°$ in steps of 2°. Your antenna temperature vs. angular offset curve should resemble Figure 6.

You can also use the "drift" button to cause the dish to be pointed "ahead in time" and then stopped. This will permit the sun, or any object, to drift through the antenna beam.

This data will enable you to derive an empirical value for the half-power beamwidth (HPBW) of the antenna, which can be compared to the theoretical value.

Measurement of the beam pattern can help the user discover problems with optical alignment or aid in the determination of antenna focus.

What is the convolution of a finite source with the radiation pattern of the antenna beam? Can you model this? An interesting comparison can be made by comparing your results with the solar flux measured by other antennas around the world, see http://web.haystack.mit.edu/SRT/solar.html.
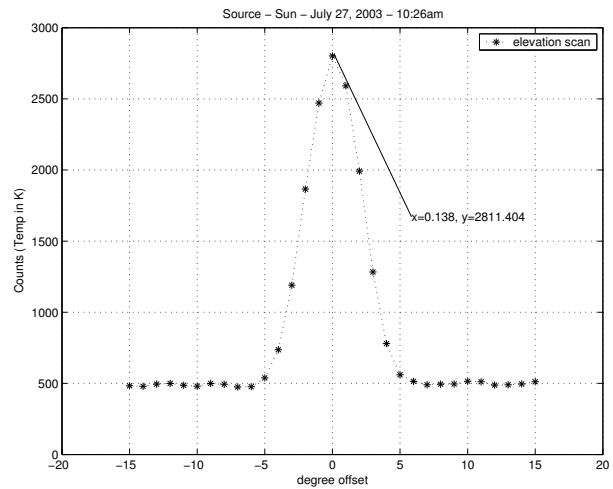

FIG. 6: A typical Azimuth or Elevation scan of the sun.

7.2.   Rotation Curve of the Milky Way

To measure the rotation curve of the Milky Way, you will need to record hydrogen line profiles at a known set of galactic coordinates.

Your first job is to figure out at which coordinates to point the telescope. Use the software to determine when these regions of the galaxy will be visible to the telescope. Since the visible portion of the galaxy varies with time, you may find it necessary to share observation time with student pairs from other sections.

Derive the Galactic rotation curve, and estimate the mass of the Galaxy interior to the circle tangent to the lines of sight.

Observe the non-uniformities in the hydrogen distribution revealed by the doppler-induced structures of the

line profiles. The multiple-component line profiles are evidence of the spiral-arm structure of the Galaxy.

8.   Analysis

1. Compare your plot of the angular response function of the antenna obtained in the scans of the sun with the theoretical diffraction pattern of a circular aperture.

2. Derive an estimate of the brightness temperature

of the sun at 21 cm from your measurements.

3. Using your Galactic data and with the help of the discussions presented in Mihalas and Binney[1] and by Shu[2], derive a plot of the velocity curve of the Galaxy as a function of radius. Why are you only able to do so for locations interior to the radial position of our solar system?

4. Optional. Using the Galactic data, construct some features of spiral-arm structure of the Milky Way.

[1] D. Mihalas and J. Binney, *Galactic Astronomy* (San Francisco, 1968).
[2] F. H. Shu, *The Physical Universe - Chapter 12* (University Science Books, Mill Valley, CA, 1982), this reference gives a clear description of the interpretation of 21cm spectra in terms of the rotation curve of the Galaxy.
[3] K. Rohlfs and T. L. Wilson, *Radio Astronomy, 2nd. ed.* (Springer, 1996), a modern handbook of radio astronomy techniques. Section 5.5 describes the relationship between antenna temperature and brightness temperature.[4] Chapter 6 provides a useful discussion of antenna theory.
[4] e. a. H. C. van de Hulst, *Bull. of the Astron.*, vol. XII, 117 (Institutes of the Netherlands, 1954).
[5] P. Duffett-Smith, *Practical Astronomy With Your Calculator* (Cambridge, 1988), 3rd ed.
[6] I. S. Shklovski, *Cosmic Radio Waves* (Cambridge; Harvard University Press, 1960).
[7] H. Horowitz and W. Hill, *The Art of Electronics, 2nd Edition* (Cambridge University Press, 1989).
[8] F. J. Kerr, Ann. Rev. Astron. Astroph. **Vol.7**, 39 (1969).

---

[4] Note, however, the following errors in Section 5.5: The equation between equation (5.59) and equation (5.60) should read $I_\nu = 2kT/\lambda^2$. Equation (5.62) should read $W = \frac{1}{2} A_e \int \int \frac{2kT_b(\theta,\phi)}{\lambda^2} P_n(\theta,\phi) d\Omega$.
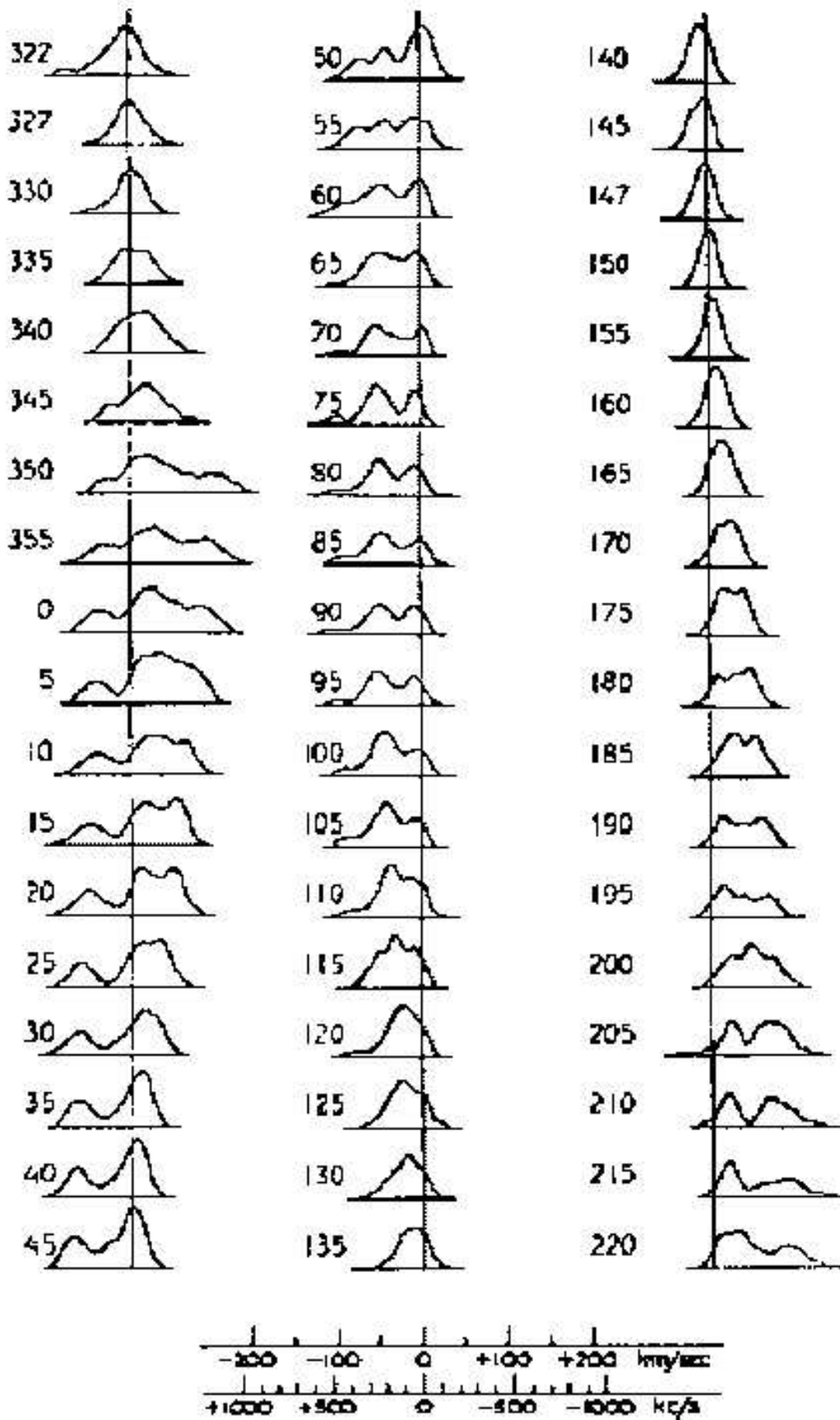
FIG. 7: Survey of hydrogen line profiles at various galactic longitudes. (from H.C. van de Hulst et. al., Bull. of the Astron. Inst. of the Netherlands, XII, 117, May 14, 1954) Note: Pictures are reversed from our images and longitude is given in the old system (l^I, b^I). $l^{II} = l^I + 32.31°$

APPENDIX A: THE SRT.CAT FILE

The text file srt.cat, located in SRTCassi, is the primary configuration file for the SRT java interface program that is used to control the telescope.

The srt.cat file may be updated, but upon doing so, please stow the telescope, shut down the control program, and restart it so that it recognizes any updates made to the srt.cat control file.

The srt.cat file contains keywords which are case sensitive. Lines that are preceded by a "*" are ignored. Blank lines are ignored.

Keywords:
AXISTILT* - Use to set the azimuth and elevation axis tilt. Default is 0 0
AZEL* - Allows user to catalog a fixed catalog location by name.
AZLIMITS - This may be set to allow movement in a clockwise position from stow from 90° to 270°. At the midpoint the telescope will face due south. Degree limits should be set slightly below the physical limitations of the telescope. It is recommended to use 95° and 265°. The telescope movement is clockwise as seen from above through increasing degree.
BEAMWIDTH* - Antenna beamwidth in degrees, default is 7.0°.
CALCONS* - Gain correction constant. This is the ratio of temperature (K) per count. Change this during calibration (should be 1 to 1 ratio). Default is 1.0. This will be changed by software after calibration occurs and value will be available in the status bar.
COMM* - Communication port, default 1, use 0 for linux.
COUNTPERSTEP* - Counts per step for stepped antenna motion. The default is no stepped motion.
CURVATURE* - Optional correction for curvature in spectrum. The default is 0.
DIGITAL - Indicates that a digital receiver is being used. Comment out if using the analog receiver (set via jumper removal).
ELBACKLASH* - Optional correction for elevation backlash to improve pointing in flipped mode. The default is 0.
ELLIMITS - This may be set to allow movement in a clockwise position from stow from 0° to 180°. At the midpoint the telescope will face up. Degree limits should be set slightly below the physical limitations of the telescope. It is recommended to use 10° and 175°. The telescope movement is clockwise as seen from above through increasing degree.
GALACTIC - Set a galactic coordinate by location and name.
MANCAL* - Calibrates vane. 0 indicates auto-calibration, 1 indicates manual calibration. Is not a requirement of the digital setup.
Moon - Add the Moon to the catalog.
NOISECAL - Calibration temperature of the noise diode located at center of dish. Temperature is in K.
RECORDFORM* - Adds tabs to separate columns in output file. The default is space delimited. "VLSR" adds vlsr and "DAY" forces a file change at each new day.
SOU - Set a source in the catalog by location and name. For negative declination us "-" in from of dd.
SSAT* - Satellite ID and location (satellite name then longitude west).
STATION - Used to set latitude (in degrees), longitude (in degrees), and station name.
Sun - Add the Sun to the catalog.
TLOAD* - Load temperature. Default is 300K.
TOLERANCE* - Counts of error which can accumulate before command to drive stow occurs. Default value is 1.
TSPILL* - Antenna spill over temperature in K. Default is 20K.

File Format:
STATION deg(latitude) deg(longitude) name
AZLIMITS deg(lower limit) deg(upperlimit)
ELLIMITS deg(lower limit) deg(upper limit)
CALCONS value
TLOAD value(in temp K - default 300K)
MANCAL value(0 or 1 - default is 0)
TSPILL value(in temp K - default 20K)
BEAMWIDTH value(in degrees - default 7)
AXISTILT deg(azimuth axis tilt - default 0) deg(elevation axis tilt - default 0)
SSAT deg
AZEL deg(azimuth) deg(elevation) name
GALACTIC deg(longitude) deg(latitude) name
SOU ra(hh mm ss) dec(dd mm ss) name [epoc]
SUN
MOON
DIGITAL
NOISECAL value(in temp K)
TOLERANCE value(in counts)
COUNTPERSTEP value(in counts)
ELBACKLASH value(default 0)
CURVATURE value(default 0)
RECORDFORM value(i.e. "TAB", "—", default is " ")

* - represents required fields or fields that should be set by user

[ ] - represents optional field

APPENDIX B: COORDINATE SYSTEMS

This material is taken in part from Duffett-Smith's book "Practical Astronomy With Your Calculator, 3rd Edition 1988, Cambridge Press". It contains many useful algorithms and is worth checking out of the library or purchasing. There are several coordinate systems which you may meet in astronomy and astrophysical work and here we shall be concerned with four of them: the horizon system (Figure 8), the equatorial system (Figure 10), the ecliptic system (Figure 13) and the galactic system (Figure 9).

Horizon Coordinates "Az" and "El" The horizon system, using Azimuth and Altitude (Elevation) is the system under which the SRT is operated.
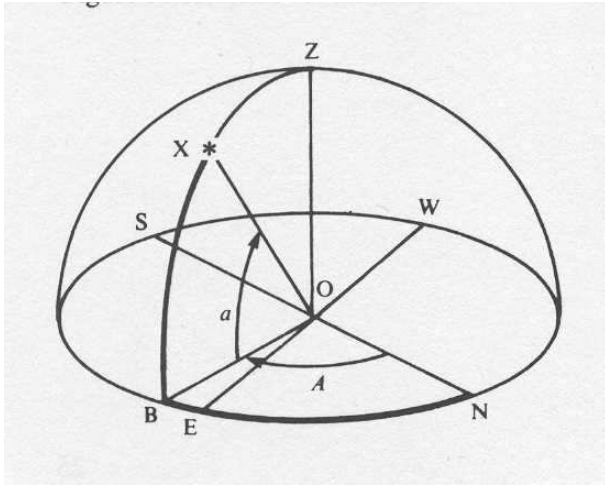

FIG. 8: Diagram of the Horizon coordinate system. Imagine an observer at point 'O'; then her horizon is the circle 'NESW' where North is the direction of the north pole on the Earth's rotation axis and not the magnetic north pole. **Azimuth** increases from 0° (north) through 360°. The **altitude** or **elevation** is 'how far up' in degrees (negative if below the horizon).

Galactic Coordinates, "l" and "b" When describing the relations between stars and other celestial objects within our own Galaxy, it is convenient to use the galactic coordinate system. The fundamental plane is the plane of the Galaxy and the fundamental directions the line joining our Sun to the center of the Galaxy as depicted in Figure 9.

Equatorial or Celestial Coordinates, "RA" and "DEC" are the spherical coordinates used to specify the location of a celestial object (Figures 10, 11 and 12). The north celestial pole (NCP) is the direction of the Earth's rotation axis, and the celestial equator is the projection onto the sky of the plane of the Earth's equator.

Right ascension (RA) is the celestial analog of geographic longitude. RA is measured eastward along the celestial equator from the vernal equinox ("V" in Figures 11 and 12) which is the ascending node of the plane
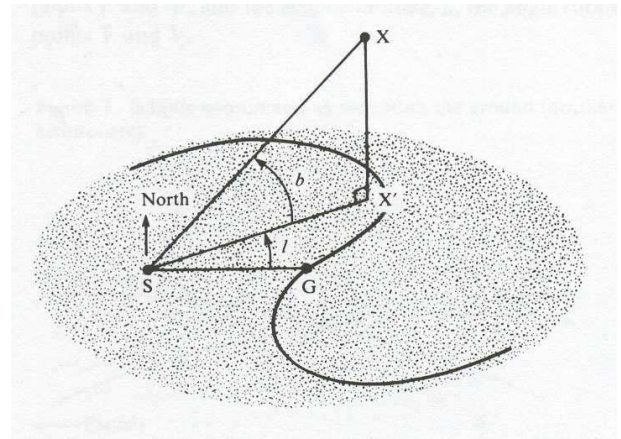

FIG. 9: Diagram of the Galactic coordinate system. The point marked "S" represents the Sun, "G" is the center of the Galaxy and "X" is a star which does not lie in the galactic plane.

defined by the sun's apparent motion (caused by the orbital motion of the Earth around the sun) and the celestial equator. In catalogs of celestial objects RA is generally specified in units of hours, minutes and seconds from 0 to 24 hours, but it is often more conveniently specified in degrees from 0° to 360° with a decimal fraction. Declination (DEC) is the celestial analog of geographic latitude. DEC is measured north from the celestial equator along a celestial meridian which is a great circle of constant RA. In catalogs DEC is generally specified in degrees, arc minutes (') and arc seconds ("), but it is also often more conveniently specified in degrees from -90° to +90° with a decimal fraction. (1 hour of RA at constant DEC corresponds to an angle of 15°*cos(DEC) degrees subtended at the origin).

The **ecliptic** is the intersection of the Earth's orbital plane with the celestial sphere. To an observer on Earth the sun appears to move relative to the background stars along the ecliptic with an angular velocity of about 1° per day. The angular velocity is not exactly constant due to the eccentricity of the Earth's orbit (e=0.016722). The period of the Earth's orbit is 365.256 days. The **inclination** (ie) of the Earth's equator to the ecliptic is 23° 27'. The **ascending node** of the ecliptic with respect to the celestial equator is the intersection of the ecliptic and the celestial equator (the vernal equinox) where the sun in its apparent motion crosses from south to north declinations on March 21. **Precession of the equinoxes** is the motion of the equinoxes along the ecliptic due to precession of the Earth's rotational angular momentum about the ecliptic pole. The precession is caused by the torque of the gravitational attractions between the sun and moon and the Earth's equatorial bulge. The period of the precession is approximately 25,000 years.

Ecliptic coordinates (Figures 14 and 13) are generally used to specify the positions and orientations of objects in the solar system. **Ecliptic longitude** (elon)

FIG. 10: Diagram of the Equatorial coordinate system

FIG. 12: Diagram of the celestial sphere, showing the celestial north pole (NCP), the celestial equator, the north ecliptic pole (NEP) and the ecliptic. The points labeled V, S, A, and W are, respectively, the vernal equinox, summer solstice, autumnal equinox, and winter solstice corresponding to the directions of the sun on March 21, June 21, September 21, and December 21. The point labeled "sun" is the direction of the sun on approximately April 21.

FIG. 11: Diagram of the celestial coordinate system

FIG. 13: Diagram of the Ecliptic coordinate system

Similarly, the orientation of a planet's rotation or the rotation of the sun itself, as illustrated in Figure 14, is specified by the ecliptic longitude (ELON) of the ascending node of its equator and the inclination (INCL) of the equator to the ecliptic.

is measured along the ecliptic eastward from the vernal equinox. **Ecliptic latitude** (elat) is measured along a great circle northward from the ecliptic.

The orientation of the orbit of a planet is specified by 1) the ecliptic longitude of the ascending node of the orbital plane and 2) the inclination of the orbit to the ecliptic.
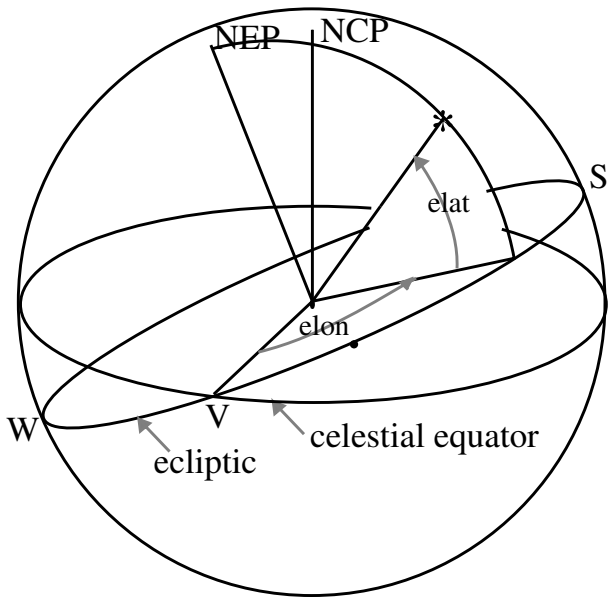
FIG. 14: Diagram showing the relation between the
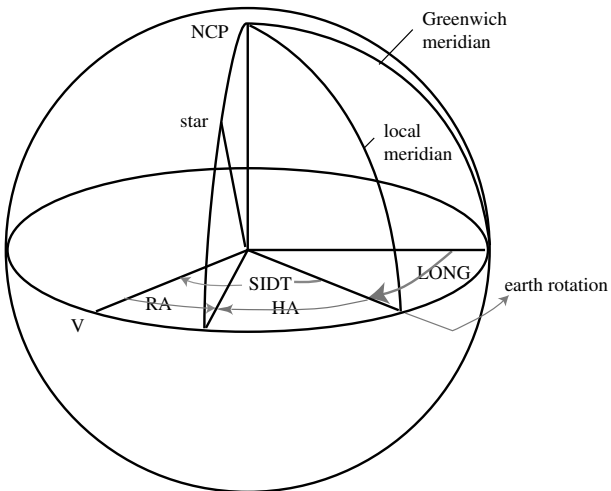ecliptic and celestial coordinate systems

FIG. 15: Diagram of the relations between the
quantities involved in setting the position of the
telescope about the polar (HA or RA) axis

APPENDIX C: SIGNAL PROCESSING IN 21-CM RADIO ASTROPHYSICS

For a voltage $v(t)$ measured in the time domain we can compute the Fourier transform $V(\nu)$:

$$V(\nu) = \int v(t)e^{-2\pi i \nu t}dt \qquad (C1)$$

Note that $V(\nu)$ is *complex*, giving us an amplitude and a phase for each frequency component. In our experiment we are not interested in the phase information. Taking the square modulus of the Fourier transform gives us the voltage power spectrum:

$$S(\nu) = [V(\nu)]^2 \qquad (C2)$$

$S(\nu)$ is the quantity plotted by the data acquisition software. For the voltage power spectrum, the units are volts^2 (rms), and a sine wave with amplitude $V_o$rms will produce a signal of amplitude $V_o$rms/4, which becomes $V_o$rms/2 in the one-sided spectrum that is displayed (see below). The spectrum displayed on the Junior Lab computer screen has units dBm, which is power expressed in dB referred to one milliwatt. The spectrum values are converted to milliwatt units by taking into account the characteristic impedance of the transmission line, $Z_o = 50 \, \Omega$. This is done according to $dBm = 10log\frac{Vrms^2}{.2236^2}$ where the 50 Ω's in the numerator and denominator have canceled. The power you measure $\frac{V_{rms}^2}{Z_0}$ is the power going down the cable to the A/D converter, related to, but not equal to, the power received at the antenna.

The above expression for the Fourier Transform, refer to a continuous signal measured for an infinite length of time. In practice, instead of $v(t)$, we in fact measure $v_i(t)$, discrete samples separated by a time interval δt, over a period of time Δt. Thus the number of points measured is $N = \Delta t/\delta t$. Our Fourier transform is now the sum

$$V_j(\nu) = \sum_{i=1}^{N} v_i(t)e^{-2\pi i \nu_j t}\delta t \qquad (C3)$$

This differs from the ideal $V(\nu)$ computed above in some important ways. We have to consider the effects of *sampling* and *windowing*. We also note that the power spectrum has the property of *symmetry about zero frequency*.

Sampling: We sample the signal at a rate $1/\delta t$, which means that only signals with frequency $2/\delta t$ or smaller can be reconstructed. In a properly designed spectrometer the sampling range and the *anti-aliasing filter* are chosen with this in mind. This is the reason for the 3 MHz bandpass filter (see Figure 2) and the sampling rate of just over 6 MHz. A strong signal with frequency larger than 6 MHz that "leaks" through the filter will appear in our power spectrum at an *aliased* frequency with the 0-3 MHz band. Thus, strong interference signals can corrupt your spectra, even though they are outside the bandpass.

Because we use the Fast Fourier Transform (FFT) algorithm to compute the Fourier transform, the spectra are also sampled with values known only at certain values of the frequency. Our frequency "channels" are centered at these values and are separated by

$$\delta\nu = \frac{1}{N\delta t} \qquad (C4)$$

Windowing: Because the time series is truncated (i.e., we only measure the voltage signal for a finite period of time), the features in the frequency domain are broadened. In other words, a pure harmonic signal, which in principle would appear as a delta function in the frequency domain, in fact appears as a feature with nonzero width. We can express this effect of the limited time span by multiplying by a "window function" $w(t)$ in the time domain:

$$v_m(t) = w(t)v(t) \qquad (C5)$$

For the simplest window function with no weighting, $w(t)$ is unity during the times of the measurements and zero otherwise:

$$w(t) = 1 \text{ for } -\frac{\Delta t}{2} \leq t \leq \frac{\Delta t}{2} \qquad (C6)$$

By the convolution theorem, the Fourier transform of $v_m(t)$ is the convolution of the Fourier transforms of $v(t)$ and $w(t)$:

$$V_m = W(\nu) * V(\nu) \qquad (C7)$$

The Fourier transform of the uniform $w(t)$ function above is a sinc function in the frequency domain (see Figure 1):

$$W(\nu) = \frac{\sin \pi\nu\Delta t}{\pi\nu} \qquad (C8)$$

The width of the sinc function is proportional to Δt. For example, the half width at the first null (HWFN) is $1/\Delta t$. Thus, each frequency "spike" in the frequency domain is broaden into a feature shaped like a sinc function with a width determined by the length of the data stream. Note that that the spacing between the nulls is equal to $1/\Delta t$ and that this is also the channel spacing. The spectral line is also characterized by "sidelobes," a sort of ringing that can extend far from the main spectral feature. For this choice of window and sampling, the width and sidelobes do not appear in the sampled values of the spectrum if the spectral line is at the center of a channel.

The uniform window is only one possible weighting scheme that can be applied to the data. By changing the weights, we can change the shape of the spectral line
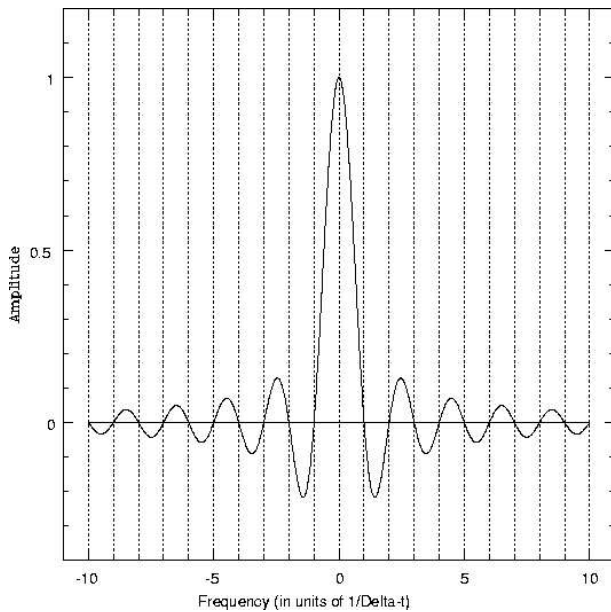
FIG. 16: The Fourier transform of a uniform window of width Δt. The vertical dotted lines show the centers of the frequency channels in the sampled power spectrum, assuming the spectral line is exactly at the center of one channel (which it may not be).

in the frequency domain. The choice should be based on considerations of the expected properties of the spectrum. For example, if we were interested in resolving two closely spaced spectral features, we would choose a weighting scheme that would produce a narrow spectral peak. If we were concerned about interfering signals, it would be prudent to choose a weighting function that produces small sidelobes, even at the cost of a broader spectral peak.

Symmetry About Zero Frequency It can be shown that the Fourier transform of a real function is symmetric about zero frequency. For nonzero frequency components, the power is equally divided between $\pm\nu$. When we display the spectrum, we just sum the frequency components at $\pm\nu$ and present a "one-sided" spectrum. Thus, the first frequency bin is at $\nu = 0$, and the last frequency bin is at $\nu = \delta\nu(\frac{N}{2} - 1)$.

1. Fourier Transform Spectroscopy

The radio astrophysics data acquisition program presents you with choices of:

- Blocks to average $= N_{\text{blocks}}$

- 2 Sided PS bins $= N_{\text{bins}}$ (corresponds to "n" above)

- Window

From these quantities the duty cycle and the frequency channel spacing are computed and displayed.

Blocks to average Each "block" of data consists of $2^{19} = 524288$ samples collected in the time domain (taking approximately 79msec at a sampling rate of 6.67Msamples/sec). This is the minimum amount of data the program can take. After collecting a block of data, the computer is occupied for some time calculating the power spectrum from $n\delta t$ segments of the data, applying any user selected windowing function and converting to dBm. A power spectrum is calculated for each block of data, and these spectra are averaged. The fraction of time that the computer is collecting data (as opposed to processing it) is the "duty cycle" that is displayed on the screen. As computers get faster and faster, this duty cycle should approach unity.

2 Sided PS bins The signal we measure is real, so the power spectrum we compute is symmetric about zero frequency. The spectrum presented on the PC screen has been "folded" so that the channels at plus and minus the same frequency have been summed. The channel spacing, $\delta\nu$, displayed on the screen is

$$\delta\nu = \frac{1}{N_{\text{bins}}\delta t} = \frac{6.67 \text{ MHz}}{N_{\text{bins}}}$$

Optical Trapping

MIT Department of Physics
(Dated: September 5, 2011)

An optical trap or "optical tweezers" is a device used to apply piconewton sized forces on micron sized objects under a microscope using a highly focused light beam. It can be created by applying a precisely focused laser onto a dielectric material. It allows very detailed manipulations and measurements on several interesting systems in the fields of molecular and cell biology and thus acts as a major tool in biophysics. They are used in biological experiments ranging from cell sorting to the unzipping of DNA. Similar principles are also used in physical applications such as atom cooling. In this experiment, you will measure the Brownian motion of a silica microsphere in aqueous solution, both testing the theory of statistical mechanics and calibrating the "spring constant" of the trap. Then, using the calibrated trap, you will measure forces in biological systems, such as the actin-myosin molecular motors of vesicle transport in onion cells, the *E. coli* flagellar motor, or the restoring force of a stretched DNA molecule.

Notice:

This labguide is still under active development. To provide an outline of the full labguide, only the preamble information and the section headings (with some filler text necessary for page breaking to work properly) are given here. For access (MIT only) to the complete working draft, please visit https://jlab.mit.edu/wiki/51._Optical_Trapping

PREPARATORY PROBLEMS

1. In the limit of ray optics, the trapping force on a dielectric sphere can be understood as arising as a reaction force the change in linear momentum experience by a deflected light ray. To better understand how the scattering and gradient forces — and the trap's stability — vary with bead displacement both vertically and horizontally, spend some time exploring this Java applet simulator developed by the lab of Roberto Di Leonardo, CNR-IPCF Dipartimento di Fiscica, Universita di Roma Sapienza in Italy: http://glass.phys.uniroma1.it/dileonardo/Applet.php?applet=TrapForcesApplet. Describe and qualitatively sketch how a bead slightly displaced from the center of a stable trap experiences a restoring force. Is the center of the trap at the same location as the focus of the light? Explain why high numerical aperture optics are used in this experiment. Finally, given the wavelength of laser and sizes of objects to be trapped in this experiment, do you trust the ray optics simulation to be quantitatively accurate?

2. Estimate the time and distance required for a mobile bacteria of typical bacterial speed in an aqueous environment to come to a halt under viscous drag. See [**?**], for example. How do these time and length scales compare to biologically relevant scales? How does ma compare to the force needed to keep the bacteria moving at its initial constant speed (before it stopped), where a is the average deceleration of the bacteria, and m is its mass?

3. What are the principle safety hazards you could encounter in this experiment? How do you avoid danger from these hazards?

Suggested Schedule

Day 1 Familiarize yourself with the apparatus and trap a bead. Make detailed notes on the effects of each control knob.

Day 2 Calibrate QPD voltage to stage position using stuck bead sample. Measure PSD noise on free bead, to obtain data for equipartition analysis. Obtain a first estimate of Boltzmann's constant and trap stiffness.

Day 3 Make onion cell sample and trap a vesicle.

Day 4 Finish onion cell experiment. Optionally do Stokes drag measurement — to refine Boltzmann's constant — or further biological experiments. Note that biological samples may take days to prepare, so you must plan ahead and communicate with your instructors.

The experimental goals are:

1. Measure Boltzmann's constant using equipartition theorem and Brownian PSD

2. Calibrate optical trap stiffness versus laser supply current

3. Estimate force and speed of molecular motors transporting vesicles in onion cells

1. Introduction

"Is this the Region, this the Soil, the Clime,"

1.1. What is an Optical Trap?

Said then the lost Arch-Angel, "this the seat

1.2. The Physics Behind Trapping

That we must change for Heav'n, this mournful gloom

1.3. Boltzmann's Constant and the Equipartition Theorem

For that celestial light? Be it so, since he

1.4. Brownian motion and the power spectral distribution (PSD) function

Who now is Sovran can dispose and bid

1.5. Molecular Motors and Forces in Microbiology

What shall be right: fardest from him is best

2. Apparatus

Whom reason hath equald, force hath made supream

2.1. Light Sources

Above his equals. Farewel happy Fields

2.1.1. Laser and laser beam path

Where Joy for ever dwells: Hail horrours, hail

2.1.2. White light LED and sample visualization

Infernal world, and thou profoundest Hell

2.2. Inverted oil immersion microscope

Receive thy new Possessor: One who brings

2.3. Position measurement

A mind not to be chang'd by Place or Time.

2.3.1. Quadrant photodetector (QPD)

The mind is its own place, and in it self

2.3.2. Microscope stage

Can make a Heav'n of Hell, a Hell of Heav'n.

2.4. Control system and electronics

What matter where, if I be still the same,

3. Samples

And what I should be, all but less then he

3.1. Sample geometry (flow channel)

Whom Thunder hath made greater? Here at least

3.2. Fixed microsphere samples

We shall be free; th' Almighty hath not built

3.3. Floating microsphere samples

Here for his envy, will not drive us hence:

3.4. Biological samples

Here we may reign secure, and in my choyce

4. Operating Instructions

To reign is worth ambition though in Hell:

4.1. Safety

Better to reign in Hell, then serve in Heav'n.

4.1.1. Laser Safety

But wherefore let we then our faithful friends,

4.1.2.   Biosharp Safety

Th' associates and copartners of our loss

4.2.   Microscope operation

Lye thus astonisht on th' oblivious Pool,

4.3.   OTKB user interface

And call them not to share with us their part

4.3.1.   Position monitor

In this unhappy Mansion, or once more

4.3.2.   X/Y scan

With rallied Arms to try what may be yet

5.   Experimental Procedure: Calibration and Statistical Mechanics Measurements

Regaind in Heav'n, or what more lost in Hell?"

5.1.   Equipartition and (optional) Stokes Drag

5.2.   Stuck bead calibration of QPD voltage

5.3.   Analysis

5.3.1.   Boltzmann's constant from equipartition data

5.3.2.   PSD method of measuring Boltzmann's constant

6.   Experimental Procedure: Biological measurements

6.1.   Strength of the actin-myosin molecular motor and intracellular transport of vesicles in onion cells

6.2.   Other measurements

6.2.1.   Strength and speed of the E. coli flaggelar motor

6.2.2.   DNA spring constant

7.   Suggested theoretical topics

- Motion at low Reynolds number

- Statistics of Brownian motion [Einstein, 1905; Wang and Uhlenbeck, 1945]
- Electrodynamic fields in matter
- Physics of diode lasers
- Energetics of molecular motors
- Worm-like chain model of DNA (enthalpy and entropy)

APPENDIX A: SAMPLE PREPARATION PROCEDURES

1. **Silica microspheres**

2. **Onion cells**